

PRESSURE BROADENING OF INFRARED
ABSORPTION LINES AT MODERATE DENSITIES

by

JODA CORNELIUS WORMHOUDT

B.S., University of Iowa

1972

Submitted in Partial Fulfillment
of the Requirements for the
Degree of Doctor of Philosophy

at the

Massachusetts Institute of Technology

September, 1976

Signature redacted

Signature of Author.....

Department of Chemistry,
September 3, 1976

Signature redacted

Signature redacted

Certified by.....

/ Thesis Supervisor

Signature redacted

Accepted by.....

Chairman, Departmental Committee



This doctoral thesis has been examined by a Committee
of the Department of Chemistry as follows:

Professor James L. Kinsey

Signature redacted

Chairman

Professor Jeffrey I. Steinfeld

Signature redacted

Co-Thesis Supervisor

Professor Irwin Oppenheim

Signature redacted

Co-Thesis Supervisor

PRESSURE BROADENING OF INFRARED
ABSORPTION LINES AT MODERATE DENSITIES

by

JODA CORNELIUS WORMHOUDT

Submitted to the Department of Chemistry on
September 3, 1976 in partial fulfillment of the
requirements for the degree of Doctor of Philosophy

ABSTRACT

The pressure broadening of several infrared vibration-rotation lines of HF and HCl by 15 to 140 atm of argon has been studied using a tunable optical parametric oscillator spectrometer. To compare with these experiments, estimates have been made of a formal theory for the density expansion of the pressure broadened lineshape.

Comparison is made in second order in density, between the theory, the experiments described in this work, and other experiments on the absorption coefficient and on the diffusion coefficient. Also, comment is made on the difficulty of finding third order (logarithmic) density terms, especially with regard to preliminary experiments with a tunable diode laser.

Thesis Supervisors: Jeffrey I. Steinfeld and Irwin Oppenheim

Titles: Associate Professor of Chemistry and Professor of
Chemistry

To the reader, if there ever
is one, in whose honor it is written
in the first person plural.

ACKNOWLEDGEMENTS

I wish to thank Professors Jeffrey I. Steinfeld and Irwin Oppenheim, without whom I would never have thought of doing any of this.

TABLE OF CONTENTS

	<u>Page</u>
TITLE PAGE	1
EXAMINATION PAGE	2
ABSTRACT	3
DEDICATION	4
ACKNOWLEDGEMENTS	5
TABLE OF CONTENTS	6
LIST OF FIGURES	8
LIST OF TABLES	11
I. OPTICAL PARAMETRIC OSCILLATOR EXPERIMENTS	12
A. Introduction	12
B. General Description of Experiment	16
C. Precision of Frequency and Amplitude Measurements	24
D. HF Low Density Linewidth Results	57
E. HCl Low Density Linewidth Results	70
II. THEORY, AND DISCUSSION OF EXPERIMENTAL RESULTS	91
A. Summary of Formal Theory	91
B. The Low Density Limit	106
C. The Triple Collision Contribution to the Linewidth	114
D. The Statistical Contribution to the Linewidth	124
E. Discussion	131
III. APPENDICES	157
A. The Chromatix Laser and Parametric Oscillator	157
B. The Sample Cell and High Pressure System	171
C. The Operational-Amplifier Integrator	179

D. Computer Programs	194
E. The Tunable Diode Laser	254
F. The Binary Collision Operator and Widths and Shifts	275
G. Determination of k_0 for a Square Well Potential	280
H. The Jacobian between p''_{13} and p''_{12}	282
REFERENCES	286
BIOGRAPHICAL NOTE	296

LIST OF FIGURES

<u>Figure</u>	<u>Page</u>
1. Tunable Laser Absorption Spectrometer	18
2. Gated Operational-Amplifier Integrator	21
3. Laser and Optical Parametric Oscillator Pulses	26
4. Parametric Oscillator Lineshapes	30
5. Deconvolution Example	32
6. Deconvolution Correction Plot	33
7. Individual Instrument Functions	36
8. Typical Detector Scatter Plots	39
9. Green and Red Light Scatter Plots	41
10. Single Detector Scatter Plot	42
11. Scattering versus Direct Detection Scatter Plot	44
12. Atypical Detector Scatter Plot	48
13. Baseline with Lines	50
14. Lineshape Traces Before Averaging	55
15. Sample HF Absorption Line	59
16. Sample High Pressure HF Absorption Line	60
17. HF P(2) Linewidth Plot	64
18. HF P(3) Linewidth Plot	65
19. HF P(4) Linewidth Plot	66
20. HCl Isotopic Doublet Trace	72
21. High Pressure HCl Trace	74
22. High Pressure HCl Trace with Low Pressure Lines	76
23. HCl R(1) Linewidth Plot	79
24. HCl R(2) Linewidth Plot	80

<u>Figure</u>	<u>Page</u>
25. HCl R(3) Linewidth Plot	82
26. HCl R(4) Linewidth Plot	83
27. HCl R(5) Linewidth Plot	84
28. HCl R(6) Linewidth Plot	85
29. Schematic Three Body Recollision	102
30. Kr-Ar Diffusion Cross Section Plot	136
31. Kr-Kr and Kr-N ₂ Diffusion Cross Section Plot	137
32. Ar-Ar Diffusion Cross Section Plot	139
33. CO ₂ -CO ₂ Diffusion Cross Section Plot	140
34. Effective Cross Section Plot for HF P(2)	147
35. Effective Cross Section Plot for HF P(3)	148
36. Effective Cross Section Plot for HF P(4)	149
37. Optical Parametric Oscillator Tuning Curve	164
38. Spectrum Analyzer Alignment Oscilloscope Traces	170
39. Sample Cell Flange Sketch	174
40. High Pressure System Diagram	175
41. Integrator Box Panels	182
42. Operational-Amplifier Integrator Circuit	183
43. Switch Trigger Circuit	184
44. Physical Placement of Integrator Components	186
45. Detector Circuit Diagram	188
46. Power Supply Circuit Diagrams	189
47. Ratio Averager Program Flow Chart	196
48. Sample Ratio Averager Dialog	222
49. Diode Laser Monochromator Scans	256

<u>Figure</u>	<u>Page</u>
50. Diode Laser Monochromator Scans	257
51. Diode Laser Monochromator Scans	258
52. Diode Laser Tuning Graph	260
53. Diode Laser Absorption Line Overlaps	263
54. Ammonia Lines in the Doppler Limit	265
55. Ammonia Self-Broadened Lineshapes	266
56. Ammonia Self-Broadened Lineshapes with Etalon Scan	267
57. Ammonia Air-Broadened Lineshapes	269
58. Anomalous Air-Broadened Ammonia Lineshapes	272
59. Repeated Ammonia Line Scans	273

LIST OF TABLES

<u>Table</u>	<u>Page</u>
1. HF Linear Linewidth Results	62
2. HF Linear Linewidths Compared with Theory	68
3. HCl Linear Linewidth Results	77
4. HCl Linear Linewidths Compared with Theory	88
5. Diffusion Coefficient Effective Cross Sections	133
6. Virial Coefficient Data Example	143
7. HF Linewidth Effective Cross Sections	150
8. Linewidth Second Density Estimates for This Work	151
9. Linewidth Second Density Estimates for Other Work	152
10. Parts List for Monel Sample Cell	176
11. Parts List for High Pressure System	177
12. Trigger Circuit Potentiometers and Capacitors	190

I OPTICAL PARAMETRIC OSCILLATOR EXPERIMENTS

A. Introduction

This thesis contains both experimental and theoretical results on the shapes of infrared absorption lines broadened by moderate densities of foreign gas. Part I of the thesis reports on the broadening of HCl and HF vibration-rotation lines by 15 to 140 atmospheres of argon, studied with a tunable laser spectrometer. The second part attempts the numerical estimation of a formal theory of the density dependence of transport coefficients. It also discusses the agreement of these estimates with experiment, especially with the line broadening data of Part I.

Line broadening has been studied for a number of reasons, most often to gain information on intermolecular potentials through the application of scattering theory to the effective cross sections obtained from linewidths. But here we wish chiefly to compare observations at moderate densities with a statistical mechanical theory approximated in such a fashion that cross sections are not calculated but taken from low density measurements.

The original reason for undertaking this study was to investigate the theoretical prediction of a logarithmic term in the density expansions of transport coefficients. The physical origin of this term, and the considerable theoretical speculation and several experimental searches it has

occasioned are discussed in Section II A. These previous studies of viscosity and thermal conductivity experiments have been inconclusive as to the existence of a logarithmic term because the relevant properties are difficult to measure and the data exhibits considerable random scatter. Yet the statistical mechanical calculation of the absorption coefficient is similar to that of these more familiar transport coefficients, and it has been predicted that at the zero density resonance frequency, its density expansion should also contain a logarithmic term. It was hoped that spectroscopic measurements could be made with greater precision. Such is indeed often the case, but here the spectrometer, based on a tunable optical parametric oscillator, was only able to measure linewidths with the precision on the order of that of the best transport coefficient measurements.

Since the logarithmic term is to appear in third order in density, it seemed unlikely that parametric oscillator experiments would ever attain the required precision to find it. But effects of second order in the density have long been seen in transport coefficient experiments. It is this study of second density effects on the linewidth that occupies the bulk of this thesis. Their size and theoretical estimates of what is expected could be used to predict the size of possible logarithmic terms. This will not be attempted here, but since, as

we will find in Section II D, the observed second density effects if they exist at all are almost within the noise level of the data, we can conclude that effects on the linewidth of higher order in the density, such as logarithmic terms, could not be found with the present parametric oscillator spectrometer. (As discussed in Section II A the logarithmic term may also manifest itself in the shape of the line, but again the parametric oscillator data has too much noise for there to be any chance of finding it. Although no experiments were done using a tunable diode laser, the possibility that its different properties might make it more appropriate for such studies is discussed in Appendix E.)

In addition to the interest in agreement between theory and experiment, there are other, practical reasons for this research. The design of high pressure gas lasers requires knowledge of the pressure broadened linewidth, and some laser systems operate at pressures where higher density effects might be expected to show up. However, the conclusion to be drawn from this work is that as an engineering approximation linewidths vary linearly with density up to the range of 100 atmospheres.

Another reason for this project is that since absorption profile measurements require accurate knowledge of both relative intensity and frequency, they make an excellent first test of a new tunable laser system. Indeed the

development of the parametric oscillator as a spectrometer together with the assumption that higher density effects are small make it a useful system for measuring low density linewidths, as we shall see in Sections I D and I E.

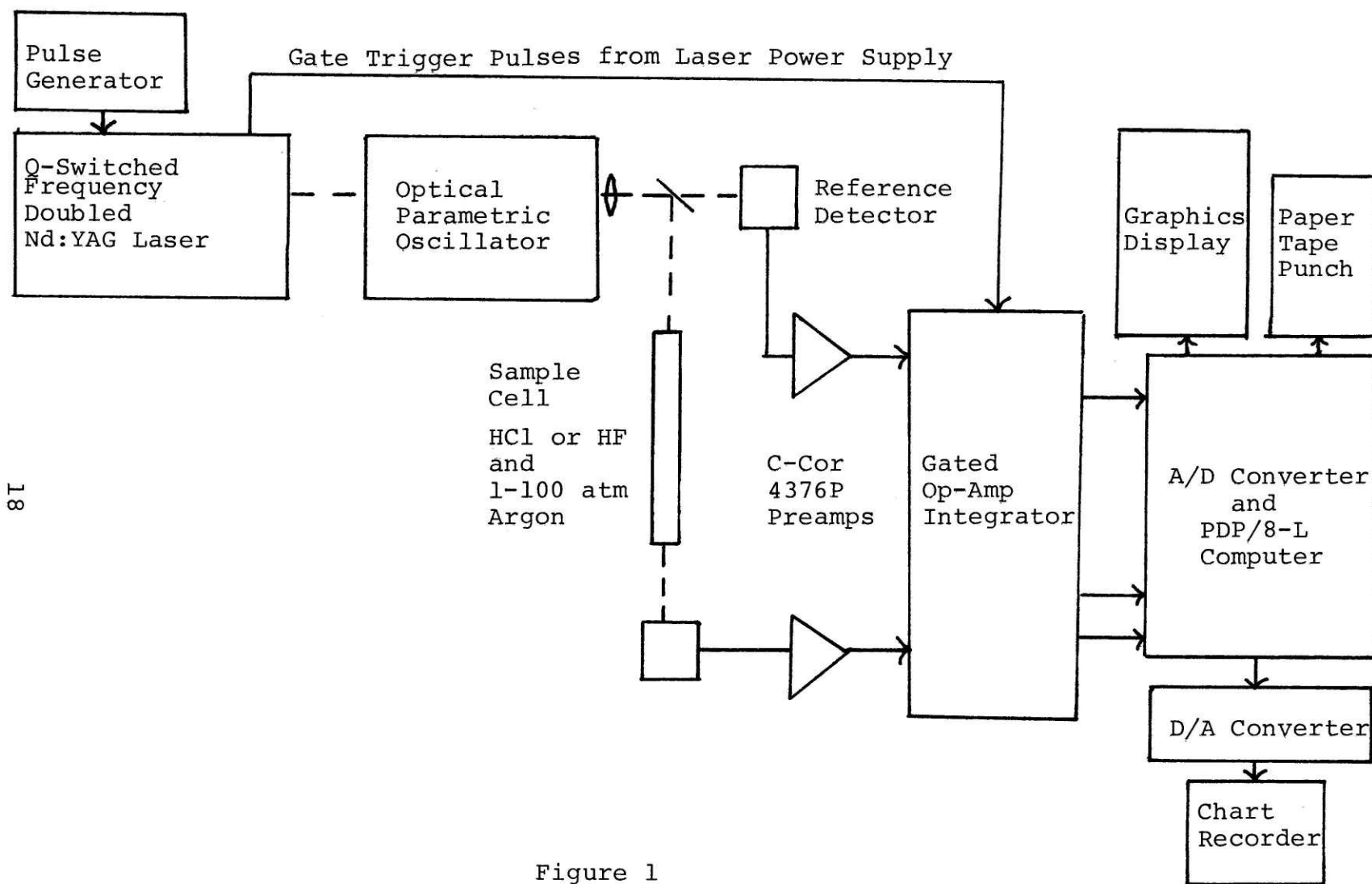
B. General Description of Experiment

Absorption measurements were made using the tunable infrared radiation from a Chromatix optical parametric oscillator, in the wavelength region of 2.55 to 2.65 microns for the HF P branch and from 3.3 to 3.4 microns for the R branches of HCl and DF. A block diagram of the apparatus is presented in Figure 1.

The parametric oscillator is pumped by the .532 micron green line of a Chromatix Q-switched frequency-doubled Nd:YAG laser. The laser is externally pulsed at 30 Hz using a General Radio model 1217-A pulse generator. Operation and maintenance of the Chromatix system are discussed in Appendix A.

The infrared beam passes through a quartz lens, which makes it less divergent, to a germanium beamsplitter. The beamsplitter has one side anti-reflection coated and has a (Valpey) coating on the other side such that 90 per cent of the infrared is reflected through the sample cell to an infrared detector, and 10 per cent is transmitted to a reference detector. (However, germanium with only the anti-reflection coating could also be used, giving about half transmitted and half reflected, by compensating with detector amplification.) The design of the monel high pressure sample cell, as well as the details of the vacuum and high pressure system and pressure measurement may be found in Appendix B.

Figure 1: Tunable laser absorption spectrometer block diagram.



18

Figure 1

Appendix C includes the biasing circuit for the infrared detectors. They were photoconductive, usually Mullard RPY77 InSb detectors operated at room temperature with the laser focused directly onto the face of the detector by a two inch focal length, quartz, anti-reflection coated lens. Some data was also taken using laser light scattered onto Ge:Au liquid nitrogen cooled detectors, in an attempt to alleviate the intensity measurement problems discussed in Section I C. However, the quality of the data turned out to be the same for both sets of detectors.

The voltage pulses from the detectors are less than 200 nsec in width. They are attenuated using a selection of terminators ranging from 50 to 1000 ohms, and then amplified by C-Cor 4376P pulse amplifiers. The preamplifiers are operated with a nominal gain of ten, although the actual gain factor is a little over twenty. Terminators are selected so that the amplifier output has about one volt peak height, since the amplifiers saturate for pulses much above this value.

The voltage pulses from the cell and reference detectors are integrated by an operational-amplifier integrator circuit, a block diagram of which is shown in Figure 2. Because the laser pulse is immediately preceded by a large amount of electrical noise, a FET switch controlled by trigger pulses from the laser power supply is used to gate the input so that only the laser pulse is integrated. Integration produces

Figure 2: Gated operational-amplifier integrator block diagram, showing input and output waveforms as they appear in oscilloscope traces.

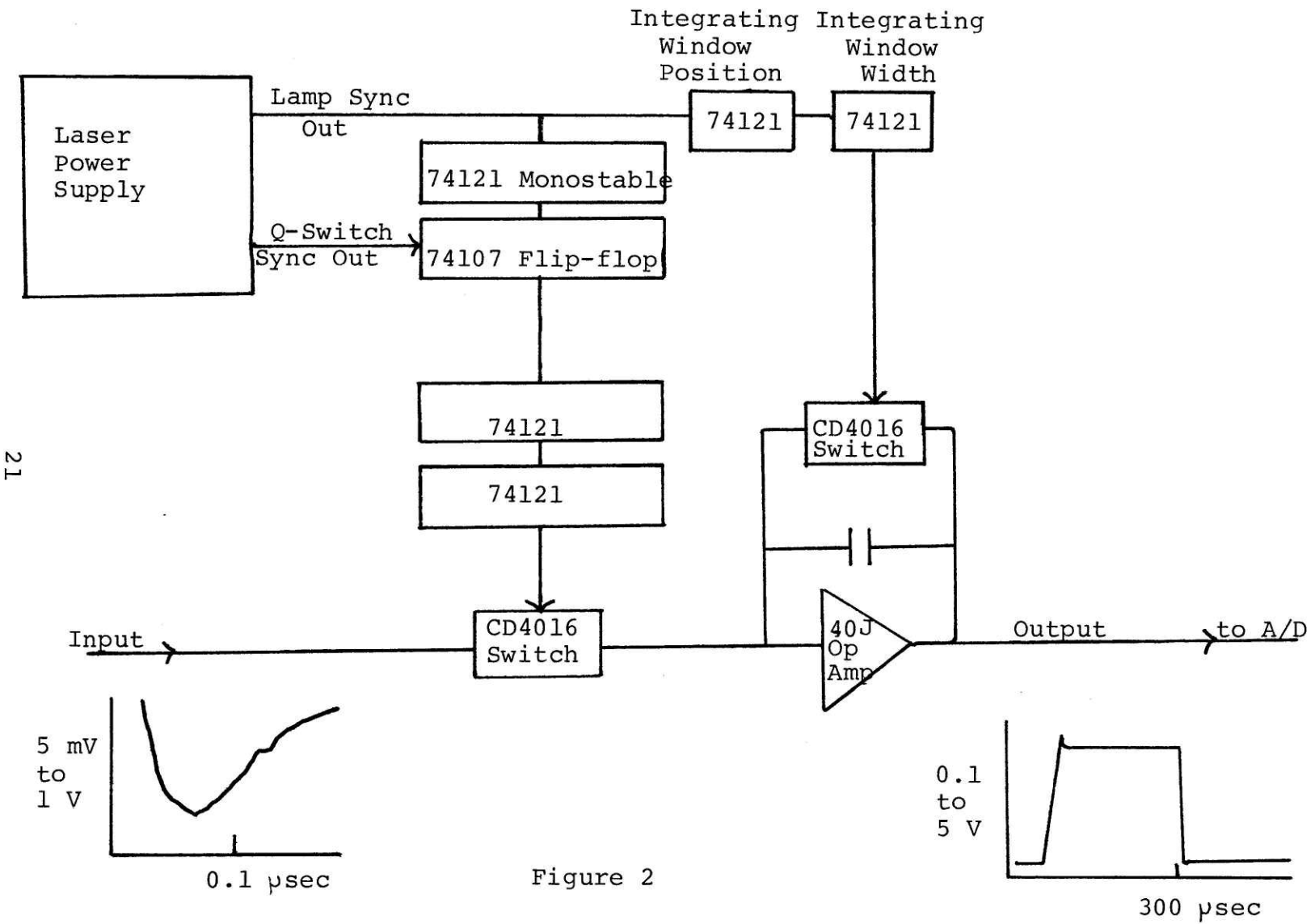


Figure 2

essentially a DC level which is read by the analog to digital converter interfaced to the PDP-8/L minicomputer, after which the integrator level is returned to its initial value by a second switch. The parametric oscillator pulses from the infrared detectors with peak values of 1 to 2 volts produce integrated levels of 5 to 10 volts. More detailed schematics, specifications, and operating instructions for the gated op-amp integrator are contained in Appendix C.

The computer averages the ratio of reference to cell pulse areas and outputs this at intervals onto a Heath strip chart recorder, and onto punched tape, so that several scans may be later averaged. Since the laser is externally pulsed, a certain number of pulses has a fixed relation to a certain amount of parametric oscillator scanning time, and therefore to a frequency increment.

The computer can also output the value for single pulses from the reference and cell detectors as the x and y coordinates of a point on the ARDS graphics display terminal, as discussed in Section I C to look at random errors in intensity measurement. The machine language programs used in acquiring the data are listed and commented on in Appendix D. In addition, FOCAL programs used in reading the punched tapes of absorption data, processing and plotting out absorption curves, and generating Lorentzian fits to experimental data are given in Appendix D. An example of the treatment of a set of tapes to produce an averaged lineshape and a fit to a sum of

Lorentzians is given is Section I C.

C. Precision of Frequency and Amplitude Measurements

Absorption lineshape measurements are among the most difficult that can be attempted using laser spectroscopy, since one needs accurate measurement of both relative intensity and frequency. In particular, an optical parametric oscillator (OPO) is difficult to work with since it has a finite frequency bandwidth of around 0.4 cm^{-1} and instability in pulse amplitude over all time scales. Parametric oscillation involves the generation of infrared and red light amplified out of quantum noise by the action of the green Nd:YAG laser light on a crystal possessing a nonlinear optical susceptibility. (The theory of the optical parametric oscillator is discussed further in References 1-6.)

The fact that these nonlinear susceptibilities are small means that when the pump laser is operated at maximum available power its 30 and 40 per cent variations are reflected in the output of the parametric oscillator, while at any lower power the same fluctuations in laser power are translated into OPO pulses which range from a maximum amplitude all the way to zero. Figure 3 shows oscilloscope displays of the laser and OPO pulses.

Another property of parametric oscillation is that generation can occur anywhere under a gain envelope of about 1 cm^{-1} in width, an instability which is magnified when the frequency is being scanned. This and other aspects of

Figure 3a: Oscilloscope traces of Nd:YAG laser and optical parametric oscillator pulses. In the upper trace, the green laser light scattered off a white screen is detected by a PIN photodiode with 100Ω termination. The laser was operating at 380 V lamp voltage and 30 Hz repetition rate, and gave an average power of 19 mW. In the lower trace is shown the OPO infrared pulse from an InSb detector with a 330Ω terminator and 10x amplification. The laser is focused directly onto the face of the detector, and the OPO is operating at 415°C with P1 mirrors. For all traces the horizontal scale is 100 nsec/cm, and the vertical scale is 1.0 V/cm.

Figure 3b: Same as 3a except at higher laser power, so that now fluctuations in OPO output are those of the Nd:YAG laser, rather than going all the way to zero.

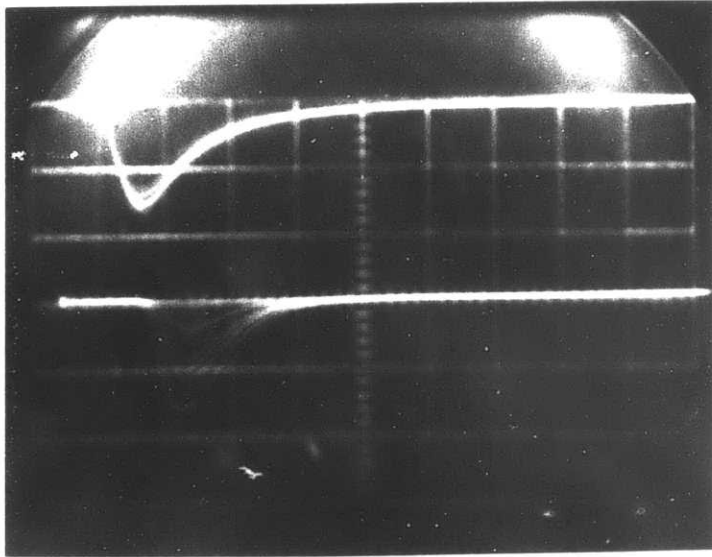


Figure 3a

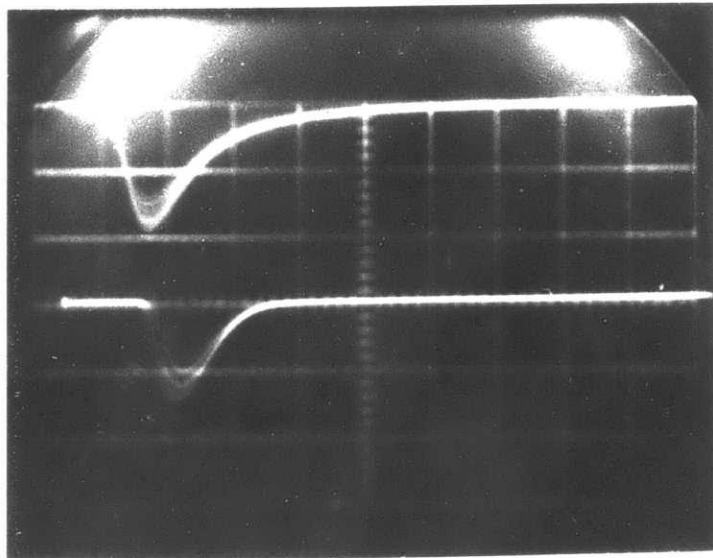


Figure 3b

the frequency and amplitude characteristics of the OPO will be discussed in this section, as well as an example of the treatment of experimental data.

The frequency characteristics of the OPO introduce both a systematic and random error into the measurement of linewidths, which we discuss in turn. The finite laser linewidth produces additional broadening of the observed absorption line, like the instrumental broadening due to the finite slit width of conventional spectrometers. In that case, the observed lineshape is a convolution of the true lineshape and the instrument function, defined as

$\int_{-\infty}^{\infty} d\omega' g(\omega-\omega') \gamma(\omega')$ where $g(\omega-\omega')$ is the true lineshape and $\gamma(\omega')$ is the instrument function.

A number of schemes have been devised to deconvolute observed absorption profiles to obtain true lineshapes. A classic iterative method first convolutes the observed data with an assumed instrument function, and then uses the difference between the original shape and the deconvolution to obtain a first approximation to a deconvolution.⁷ Here we use a method which uses the ratio instead of the difference as a correction, giving the procedure better mathematical properties as described in Reference 8. The deconvolution program is listed in Appendix D. It was originally designed to address the analogous problem of deconvoluting out the effect of velocity selector "shutter function" on molecular

beam scattering results, although Reference 8 cites work in which the ratio method has been applied to incompletely resolved spectra.

Our instrument function, the optical parametric oscillator lineshape, is found by making absorption scans using only a few torr of HF, so that on the scale of the laser linewidth the absorption line is infinitely narrow. One set of eight measurements on around 5 torr of HF was used to obtain the laser line information used to deconvolute the data. The lineshape, shown in Figure 4a, was obtained after averaging the traces and then averaging around the line center to produce a symmetric shape. This last was done because the deconvolution program only took symmetric instrument functions, and seemed to fail for asymmetric lineshapes. Besides, there was no evidence that the OPO lineshape was not on the average symmetric.

This laser lineshape was used to deconvolute a number of sample Lorentzians. An example of the two initial line profiles and the resulting deconvoluted lineshape is given in Figure 5. These samples are used to construct a plot of the amount by which the linewidth is reduced as a function of the initial linewidth, which appears in Figure 6. Its form can be understood by considering that while an infinitely narrow line is broadened by the full amount, an infinitely broad line would not be instrumentally broadened at all.

This procedure of deconvoluting computer generated

Figure 4: Averaged optical parametric oscillator lineshapes, from absorption scans of low pressure HF lines. An average of eight measurements on around 5 torr of HF is shown in (a), while (b), taken a year later but having almost the same width, is an average of 13 traces of about 8 torr of HF.

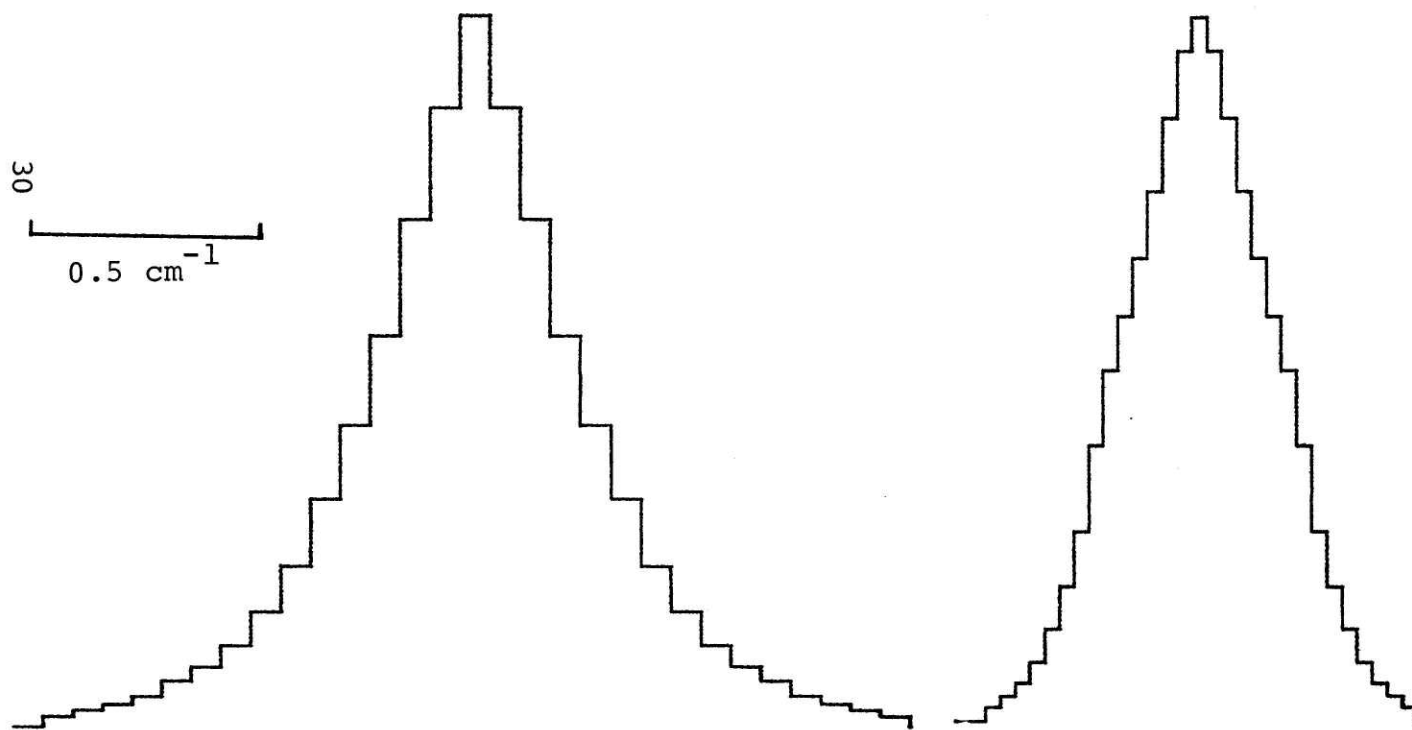


Figure 4a

Figure 4b

Figure 5: Initial (a) and deconvoluted (b) lineshapes, and parametric oscillator instrument function (c). The Lorentzian initially had a halfwidth of 1.44 cm^{-1} and went to 1.28 cm^{-1} after deconvolution. The instrument function is the same as that in Figure 4a, but averaged into larger boxes. Note that even choosing the initial line to be slightly off center introduces asymmetry into the deconvoluted lineshape.

Figure 6: Deconvolution correction plot.

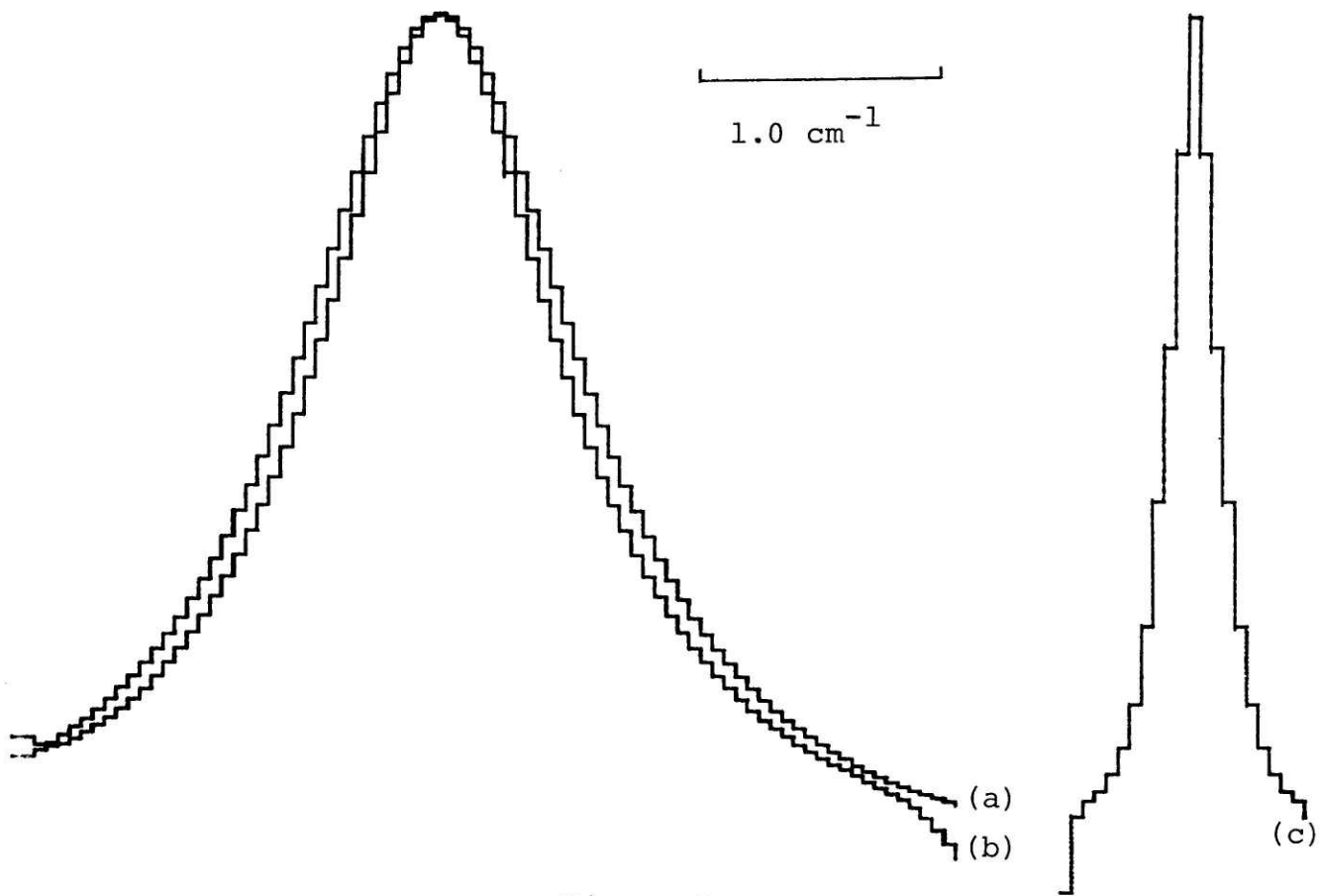


Figure 5

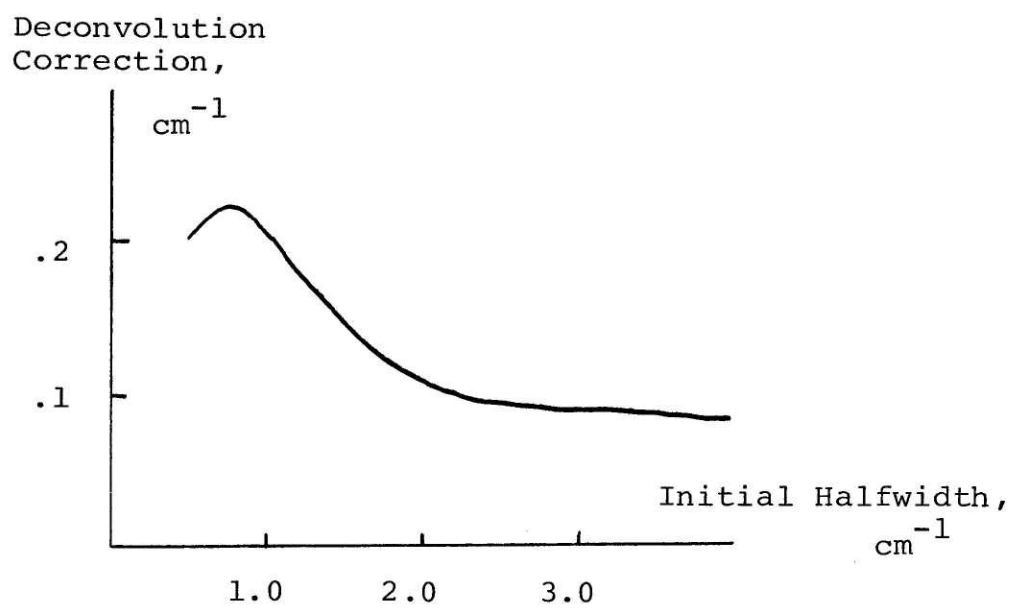


Figure 6

Lorentzian functions was used rather than individual deconvolution of each experimental profile for two reasons. First, deconvolution is time-consuming, and more importantly, the procedure, or at least the method used here, seems to magnify any irregularity or asymmetry in the initial lineshape. Since the amount to be subtracted is small and random fluctuations in linewidth and lineshape are large, it was felt that no more sophisticated procedure was justified.

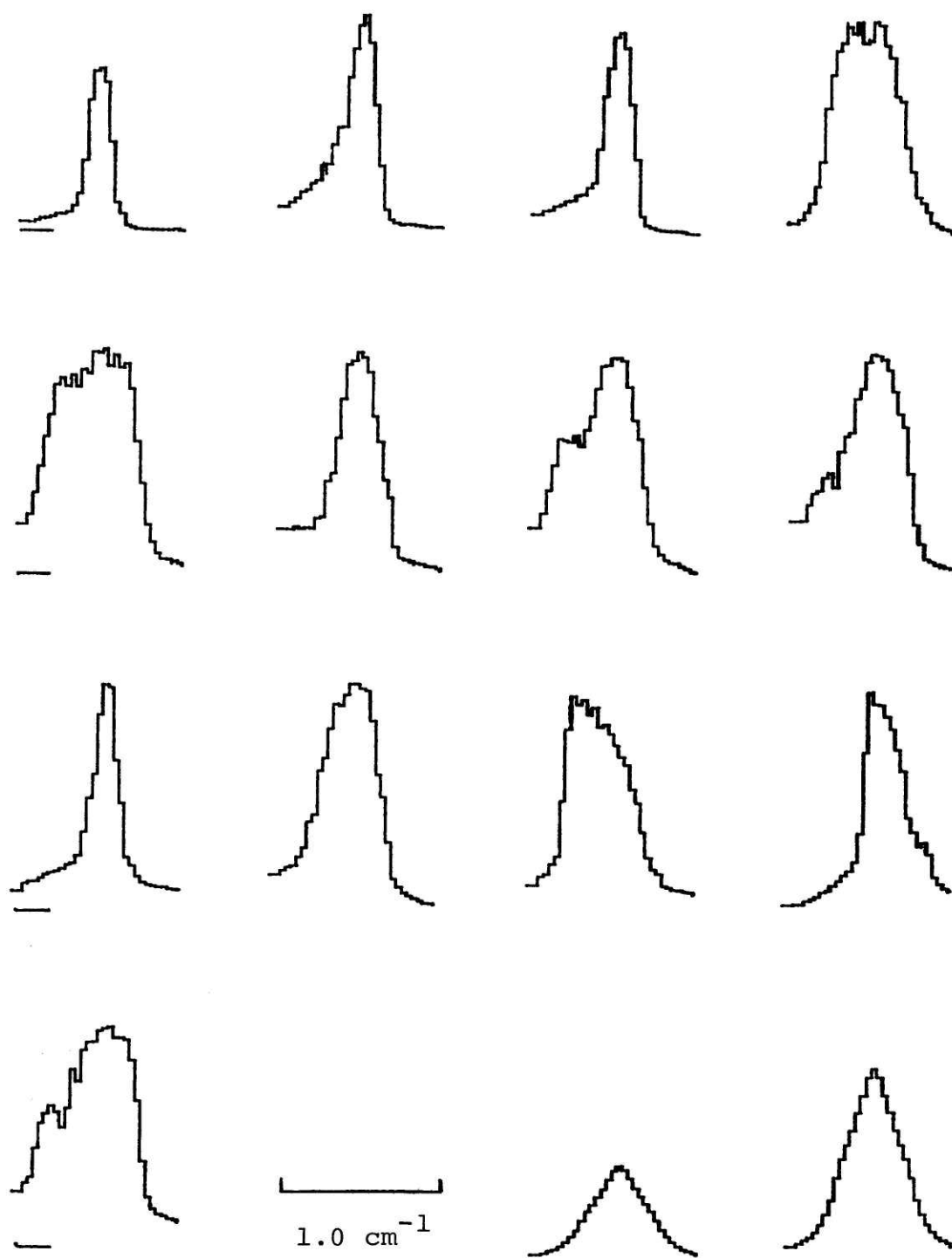
One could also least squares fit to each lineshape, using a simple Lorentzian or a Lorentzian convoluted with an assumed instrument function,⁹ but again it was felt that the accuracy of the data did not warrant such care.

A year after the first laser lineshape study was done a second set of measurements were made on around 8 torr of HF, the result of which appears in Figure 4b. The laser linewidth here is less than 10 per cent smaller than the earlier line. Figure 7 shows the individual lines before averaging and symmetrizing gave the resulting OPO profile. This figure brings us to the other effect of fluctuating laser linewidth and position, that of generating random errors in absorption and so linewidth during scanning.

This effect should be more noticeable for narrower lines, since the steeper slopes give a larger change in absorption for a given frequency, reaching a maximum for these essentially delta-function low density absorption lines. For the lines in Figure 7, the root-mean-square deviation around the average

Figure 7: Individual low pressure absorption traces before averaging into the instrument function of Figure 4b, shown in the two traces at bottom right. The line under each trace in the leftmost column denotes the position of the baseline for that row.

Figure 7



width of 0.33 cm^{-1} is 0.13 cm^{-1} . In general we find that variations of several tenths of a wavenumber in widths in scans of the same absorption line are common. Since averaged lineshapes never include more than ten experimental traces, and sometimes in early work as few as three or four, we can expect this random error to remain to the extent of 0.1 to 0.2 cm^{-1} .

We can also see another source of systematic error, in that the width of the averaged OPO line, 0.4 cm^{-1} , is larger than the average of the individual widths. This sort of broadening due to errors in superimposing lines during averaging will also occur to roughly the same extent for the experimental lineshapes. Thus it is proper that it be included in the instrument function and be deconvoluted out.

There is another problem which contributes to random noise in the lineshape scans, whose cause is unknown and which has gone unsolved. It is that the ratio of the integrated energy of single pulses seen by the cell and reference detectors fluctuates randomly from pulse to pulse. This can be shown clearly by a modification of the data acquisition program described in Appendix D which plots a point on the ARDS graphics display terminal whose x and y coordinates are the integrated outputs of the two detectors. A perfect detection system would produce a straight line plot passing through zero, indicating a constant ratio between the two detectors, while a scattered plot indicates random variations in the ratio.

Figure 8: (a) Two Ge:Au detectors receiving scattered infrared give the x and y coordinates of the points. Cell detector has 200Ω termination, reference has 100Ω , and both have 10x amplification. (b) Upper scatter plot is infrared straight on to a Ge:Au detector versus red light scattered onto a PIN photodiode. Lower plot of two PIN diodes looking at red OPO light. In both photographs the x and y scales are 8 volts maximum.

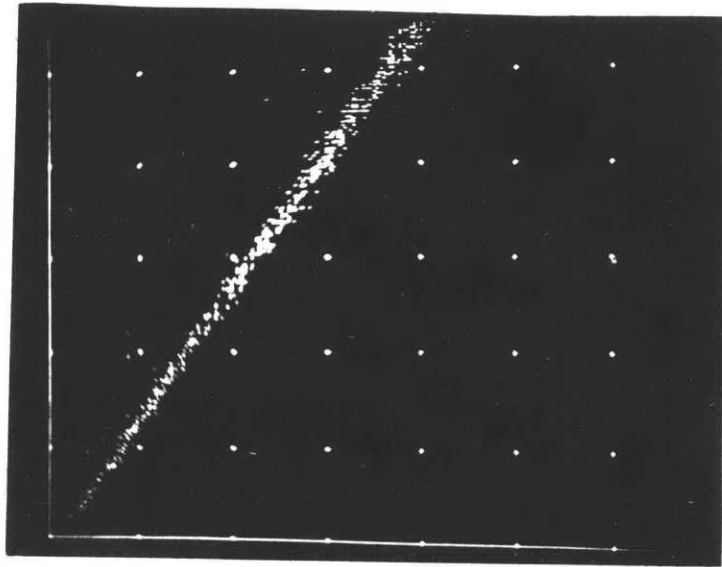


Figure 8a



Figure 8b

Figure 9: (a) Two separate PIN photodiodes looking at scattered green Nd:YAG laser light.

(b) Two separate PIN photodiodes looking at scattered red OPO light. The OPO was at 370^oC and the scales were 8 volts maximum.

Figure 10: Infrared pulse from reference InSb detector put into both integrators- so absence of scatter is not surprising.

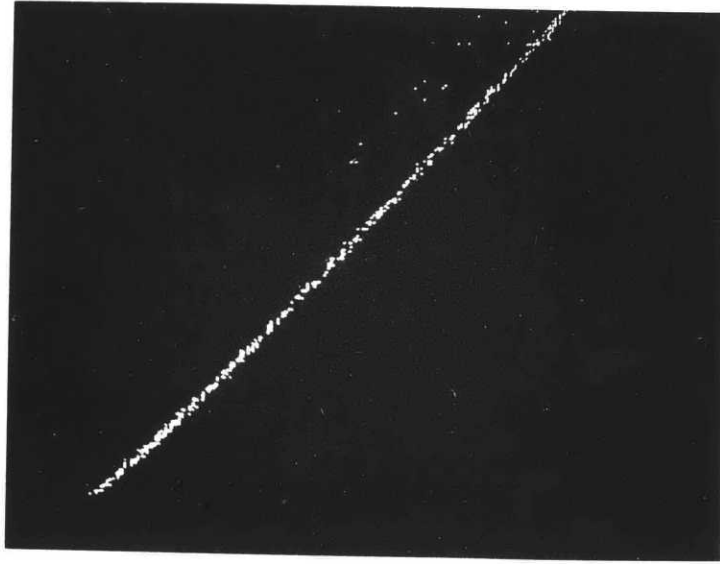


Figure 9a

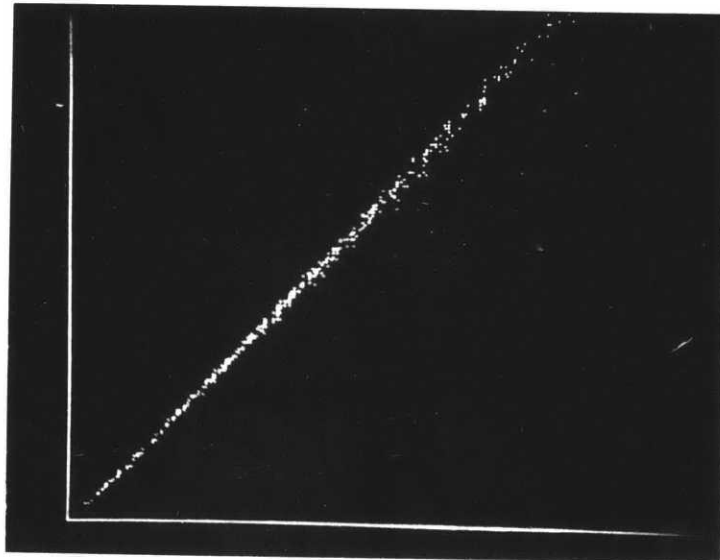


Figure 9b

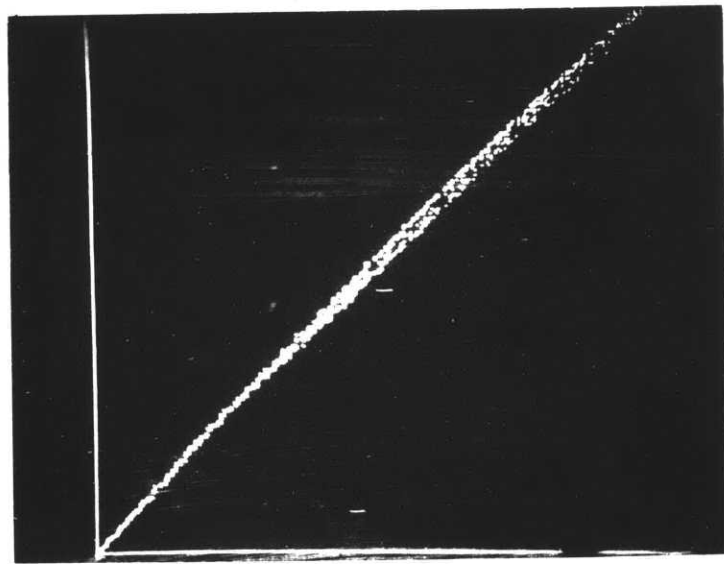


Figure 10

Figure 11: (a) Upper plot is infrared scattered onto a Ge:Au detector (100Ω terminator, 10x amplification) versus red light scattered onto a PIN photodiode (100Ω , 10x). Lower plot is infrared directed onto a Ge:Au detector (connected directly to integrator) using a mirror, versus red light scattered onto a PIN diode (200Ω , 10x). (b) Infrared pulses from two InSb detectors. Spots focused through collimating lens (and for cell detector, through a 2 inch focal length lens at about 2.5 inches from detector). Cell detector has 200Ω termination, reference 100Ω , and both have 10x amplification. Plots are 8 volts full scale.

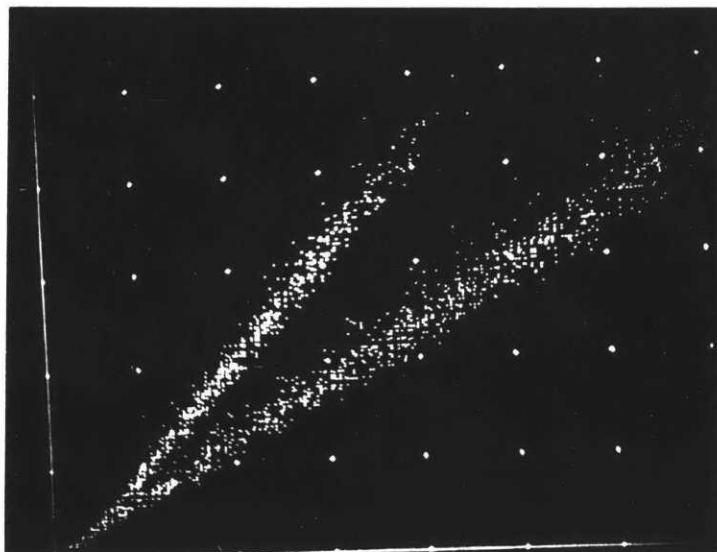


Figure 11a

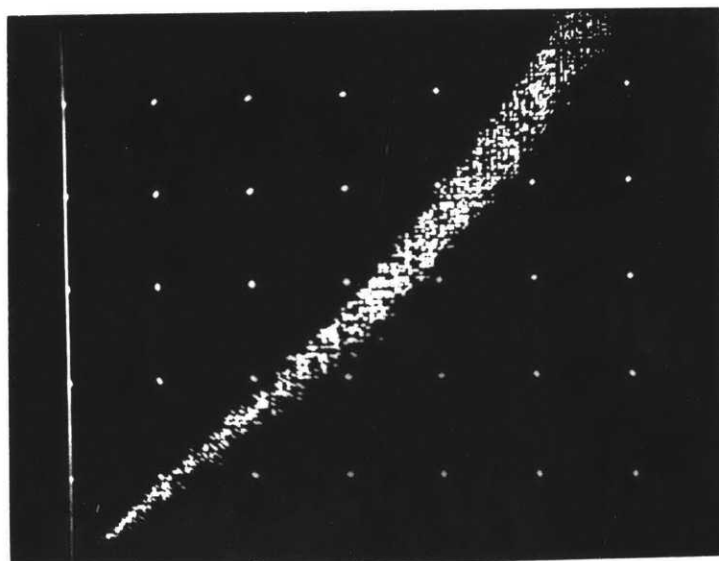


Figure 11b

Examples of this sort of this sort of random variation are shown in Figure 8.

That the fault seems not to be with the integrator or any of the electronics after the detectors can be seen in Figure 9 in which the outputs of two separate PIN photodiodes looking at scattered green laser or red OPO light pulses give a linear plot. But infrared pulses plotted as a function of the corresponding red pulses show both a random scatter and often a systematic dropping off of infrared amplitude for large pulses, as shown in Figure 8b. And it is not a property of the infrared pulse alone, as shown by Figure 10 of the same infrared detector pulse put into both integrator channels.

It was thought that the problem might be caused by the laser pulse falling off the surface of one detector more than the other, depending on the intensity and direction of the OPO beam. Therefore much of the experimental data and Figure 8a were taken by scattering the infrared from a white card onto liquid nitrogen cooled Ge:Au detectors (chosen since they were more responsive). However, Figure 11a compares scattered and direct methods of detection and shows little difference. So most data was taken by the simpler method of focusing a partially collimated OPO beam directly onto the face of room temperature InSb detectors. One example of the scatter plot resulting from this is given in Figure 11b. But with all methods of detection the amount of scatter seems to be

somehow dependent on the exact physical adjustment of the detectors or some other unknown parameter, so that at times the pulse to pulse fluctuations in ratio can be small, as in Figure 12.

Although this problem contributes to the short term fluctuations, noise on the scale of one data point (0.03 cm^{-1}), the frequency fluctuations mentioned above, on the scale of 0.1 to 0.2 cm^{-1} are a considerably larger problem. (But when attempts were made to use the internal etalon to select out one OPO cavity mode, this intensity measurement problem was aggravated by the lower power and larger fluctuations of the OPO output. Indeed with the etalons available to us, in the 3.5 micron wavelength region where the OPO operation is poor anyway, it was impossible to tell when we were on an absorption line and when we were not.)

Before we can obtain Lorentzian linewidths from experimental data we must know the tuning rate of the OPO in $\text{cm}^{-1}/\text{min}$, and the baseline, or ratio of reference to cell intensity when the cell is evacuated. An estimate of both quantities can be obtained from absorption traces like the one in Figure 13, of about 6 torr of HF. The upper trace is the region from P(2) to P(3) and the lower from P(3) to P(4). Measuring the distance between lines P(3) and P(4) on the chart paper and converting by the recorder speed we find that the lines are separated by 42.25 minutes of scanning time. Then taking the line spacing¹⁰ as 45.47 cm^{-1} we get a tuning

Figure 12: A particularly felicitous scatter plot due to infrared pulses from two InSb detectors. The cell detector had 200Ω termination, the reference detector had 100Ω , and both had 10x amplification. Full scale on this plot is 9 volts, and the minimum voltage read was 0.4 volts.

Figure 12

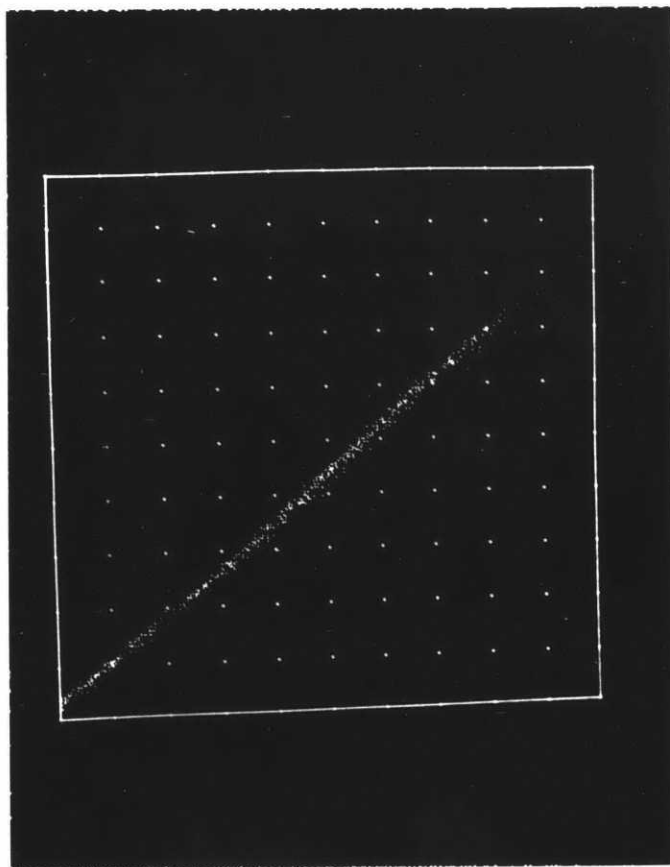
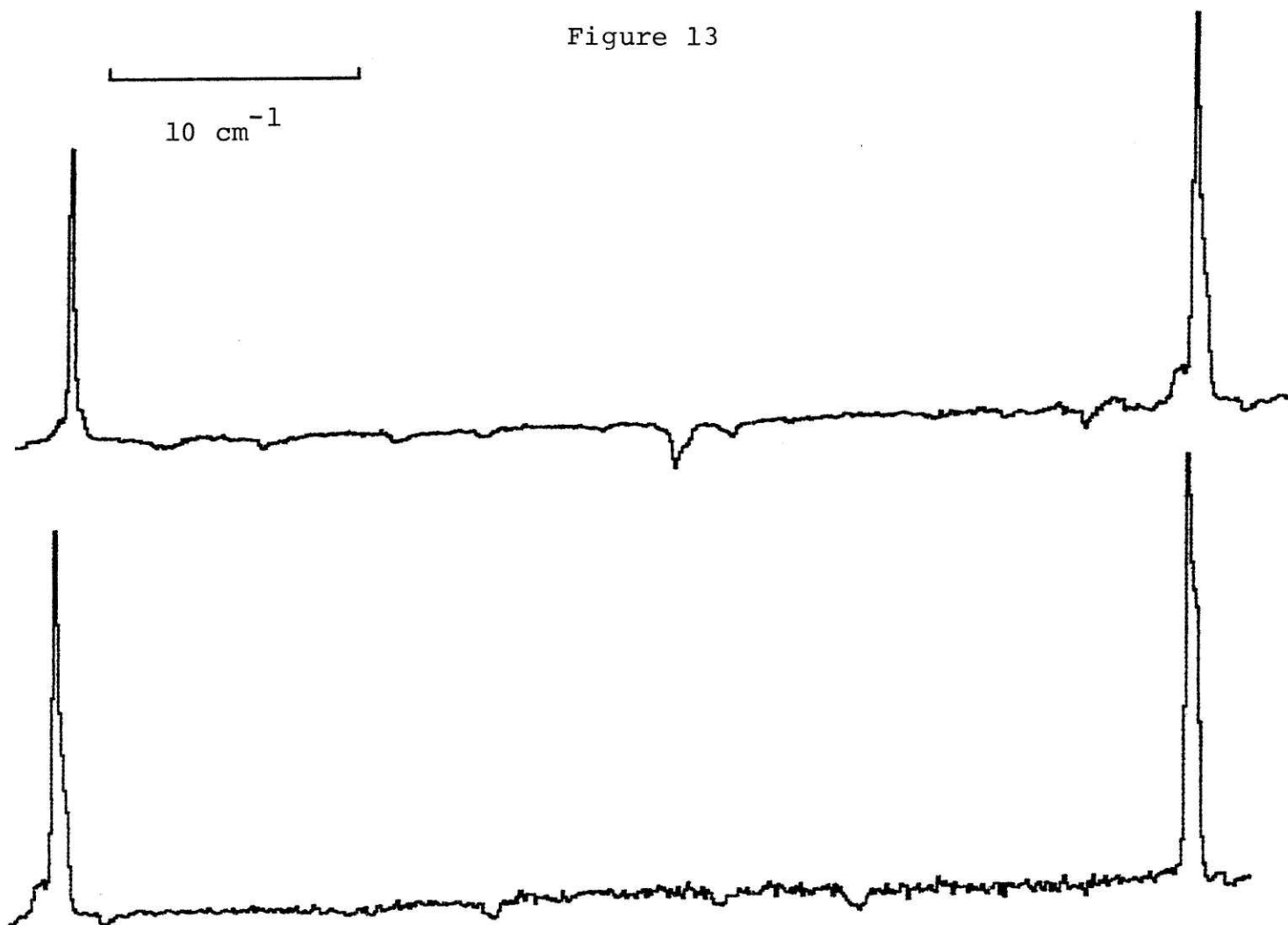


Figure 13: An absorption scan of about 6 torr of HF only, useful in choosing baselines for high pressure absorption traces and in calculating the frequency scan rate from the distances between lines. Upper trace is the region between P(2) and P(3), and the lower trace is the region between P(3) and P(4).

Figure 13



rate of $1.07 \text{ cm}^{-1}/\text{min}$. (Reference 11 gives line frequency distances up to 0.2 cm^{-1} different than those of Reference 10 even though both measure to 0.01 cm^{-1} .) Another scan taken just before the one shown in Figure 13 gave $1.08 \text{ cm}^{-1}/\text{min}$, while one taken the day before gave $1.07 \text{ cm}^{-1}/\text{min}$, which was used to process the data which we will discuss below.

The P(2)-P(3) distance in Figure 13 gives $1.05 \text{ cm}^{-1}/\text{min}$, the trace immediately before it gave $1.06 \text{ cm}^{-1}/\text{min}$, while the trace from the day before gave 1.03 cm^{-1} . One can also use frequency differences obtained from pressure broadened lines. Although pressure shifts are large at high densities, they are all very close to the same size.^{12,13,19,24} So for example the distance between the first P(4) line in Figure 14 and the P(3) line on the same tape, both broadened by 130.5 atm of argon, gives a factor of $1.07 \text{ cm}^{-1}/\text{min}$.

The two or three per cent fluctuations in tuning rate in different measurements are common and another source of error. However, the differences in tuning rate as a function of frequency are consistently observed. Tuning rates at the longest wavelength, 3.5 microns, are as large as $1.20 \text{ cm}^{-1}/\text{min}$, obtained using the HCl line spacings of Reference 14. This trend can be understood if we assume there is a direct relationship between temperature and scanning time, and note that in Figure 37 in Appendix A that the slope of the wavelength versus temperature graph increases with higher temperature.

The small-scale noise in the baseline portion of Figure 13

is due to the intensity detection problem discussed above. We see this especially near P(4) , toward the end of the OPO mirror tuning range and where the OPO output is more erratic. The larger dips, though, are associated with a large drop in intensity of both cell and reference signals. These are presumably due to absorption by atmospheric water vapor and a slight difference in path lengths to cell and reference detectors. However, attempts to assign water vapor lines using literature spectra¹⁵ were unsuccessful.

The average value of the reference to cell ratio for a small region between the P(3) and P(4) lines in Figure 13 is 1.07. In the trace immediately preceding it, however, it was 1.11 for the same region. These sorts of fluctuations are also commonly observed, so for most of the data baselines were actually chosen by the best fit to a Lorentzian. For the P(4) line measured just before the vacuum trace in Figure 13, the best fit baseline was indeed 1.07.

Figure 13 also shows that this baseline ratio is not constant, although its variation is slow enough over the range of interest to be approximated by a line. This slope is also chosen by the best fit to a Lorentzian. Of course, the double-beam experimental setup was designed to eliminate both short and long term variations in ratio when all other conditions remain unchanged. It is possible, but not proven, that this slow variation has the same origin as the pulse to pulse fluctuations.

As an example of the treatment of experimental data, and of the sort of experimental errors encountered, we present the treatment of data taken on the same day as the low pressure scan of Figure 13. We consider the measurements of the HF P(4) line broadened by 130.5 atmospheres of argon, recorded on tapes 450 through 453 and on the end of tape 443. These five traces are shown in Figure 14.

To average them, the original traces on chart paper are superimposed, and the amount of each scan to be discarded so that all scans will line up is measured off the chart, then converted into the number of data points. With the present choice of pulse rate (30 Hz) and number of pulses which are averaged to give one data point (48), there are 33 data points output per minute. Then the tapes are added by computer, (using programs in Appendix D), and the initial and final values of the ratio in the wings are sampled, to get an estimate of the initial baseline and its slope. The averaged initial ratio was 1.15, although individual values at the same point were 1.18, 1.12, 1.14, 1.17, and 1.16. The baseline found to best fit a Lorentzian was 1.07 and its slope was a positive .00023 ratio per data point.

The fits are made visually, by generating Lorentzian lineshapes and superimposing them on the experimental traces. Sometimes several iterations of the process of choosing baselines and slopes and generating Lorentzians are needed to obtain a good fit. The final averaged line plotted on an

Figure 14: Five individual absorption traces of HF P(4) broadened by 130.5 atmospheres of argon. Their average is shown in Figure 16.

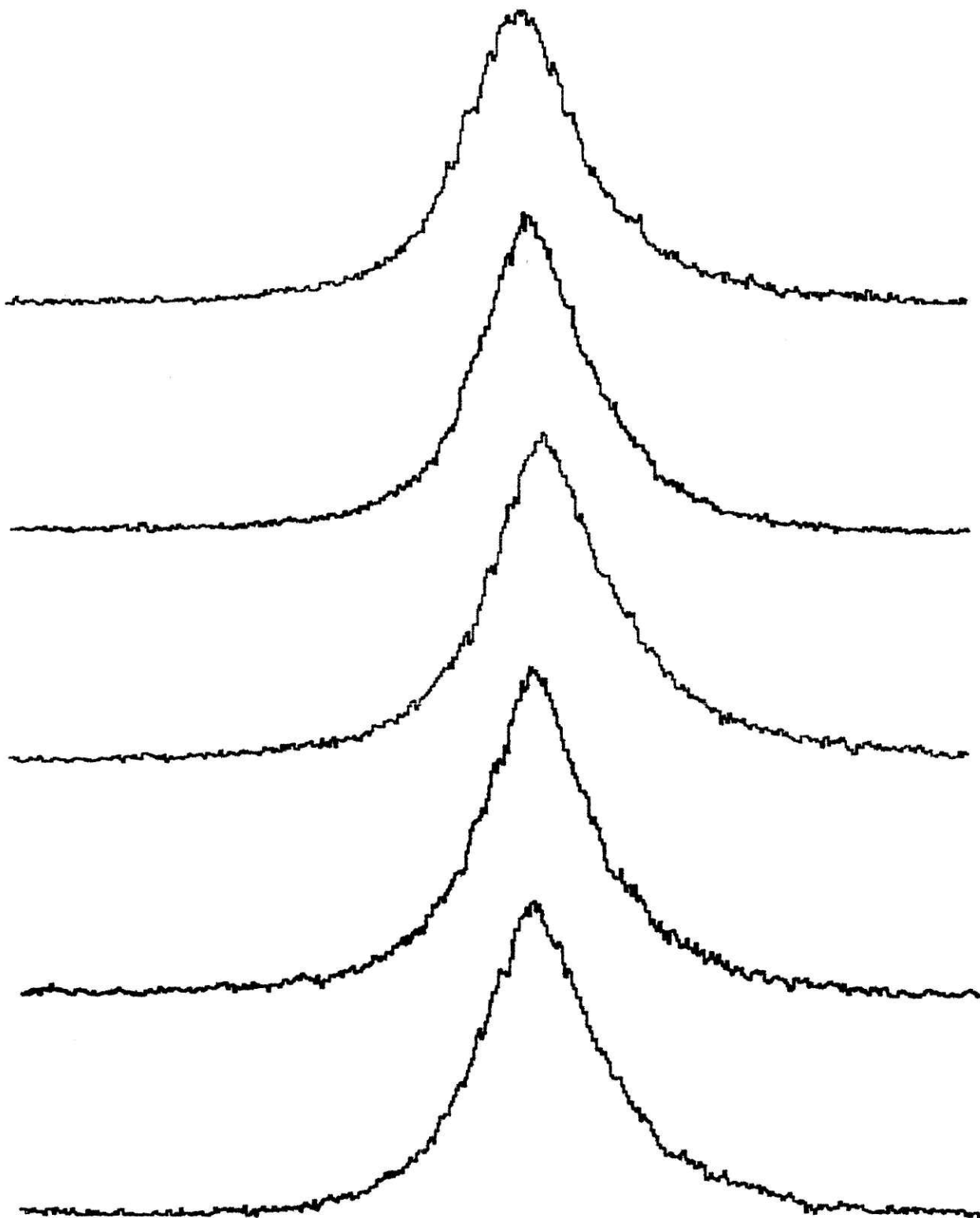


Figure 14

x-y recorder and the Lorentzian fit are shown in Figure 16 in Section I D. The halfwidths of the five individual lines were 2.68, 2.78, 2.88, 2.72 and 2.92 cm^{-1} , giving an average halfwidth of 2.78 cm^{-1} with a root-mean-square deviation of 0.1 cm^{-1} . The width of the averaged line before deconvolution was 2.82 cm^{-1} , so here 0.04 cm^{-1} was added by averaging.

To fit a Lorentzian to the experimental trace using the program in Appendix D, we must calculate the scaling factor SC in cm^{-1} per x-y recorder point. In this case this is given by $SC = 3/6.4$ data points / x point times 1/33 minutes per data point times 1.07 $\text{cm}^{-1}/\text{min}$, or .0152 $\text{cm}^{-1}/\text{x point}$. These factors can be used to estimate values for the width and center point of the experimental curve. Then these parameters and the peak height and initial value and slope of the baseline are varied to obtain the best visual fit. When several lines are used in the Lorentzian fit, the relative intensities are taken from the peak absorption values for HF in Reference 16, or from the line strengths for HCl of Reference 17. The ratios of the low density widths of neighboring lines to that of the line being fit are used to pick linewidths for the fit. But the effect of these neighboring lines on the linewidth is usually small, except for the case of the HCl isotopic doublet.

D. HF Low Density Linewidth Results

In this section we present the measurements of widths of HF vibration-rotation lines broadened by argon. We will also fit the lower density data to obtain a linewidth linear in density which may be compared with previous measurements of the pressure broadening coefficient done at low pressures. Discussion of possible second order density dependence will be left to Section II E.

The HF lines studied were P(2), P(3), and P(4), measured at room temperature and over an argon pressure range of 10 to 140 atmospheres. The linewidths were obtained by fitting a Lorentzian (or at the very highest densities a sum of Lorentzians) to the experimental trace, as detailed in the previous section. From Figures 15 and 16 we can see that the lineshape is indeed a Lorentzian function out to many halfwidths from line center, to within the accuracy of the experimental trace. In Figure 16 we also see that HF lines overlap very little even at the highest densities. This makes them easier to fit than HCl, discussed in the next section, whose lines overlap even at low densities.

Figures 17 through 19 are plots of the half width at half maximum after deconvolution as a function of the density of the perturbing argon. The deconvolution procedure has been described in Section I C. It assumes a laser full width of less than 0.5 cm^{-1} , so that the corrections are around 0.2 cm^{-1} or less. The densities are expressed in amagats, units of the

Figure 15: Sample trace of HF P(2) broadened by 51.5 atmospheres of argon. The experimental trace is the average of five data tapes. The Lorentzian fit has a halfwidth of 1.45 cm^{-1} .

Figure 16: Sample trace of HF P(4) broadened by 130.5 atmospheres of argon. The experimental trace is the average of five data tapes. The Lorentzian fit is composed of a central peak with a halfwidth of 2.75 cm^{-1} and two neighboring lines (off each side of the figure) with appropriately scaled widths.

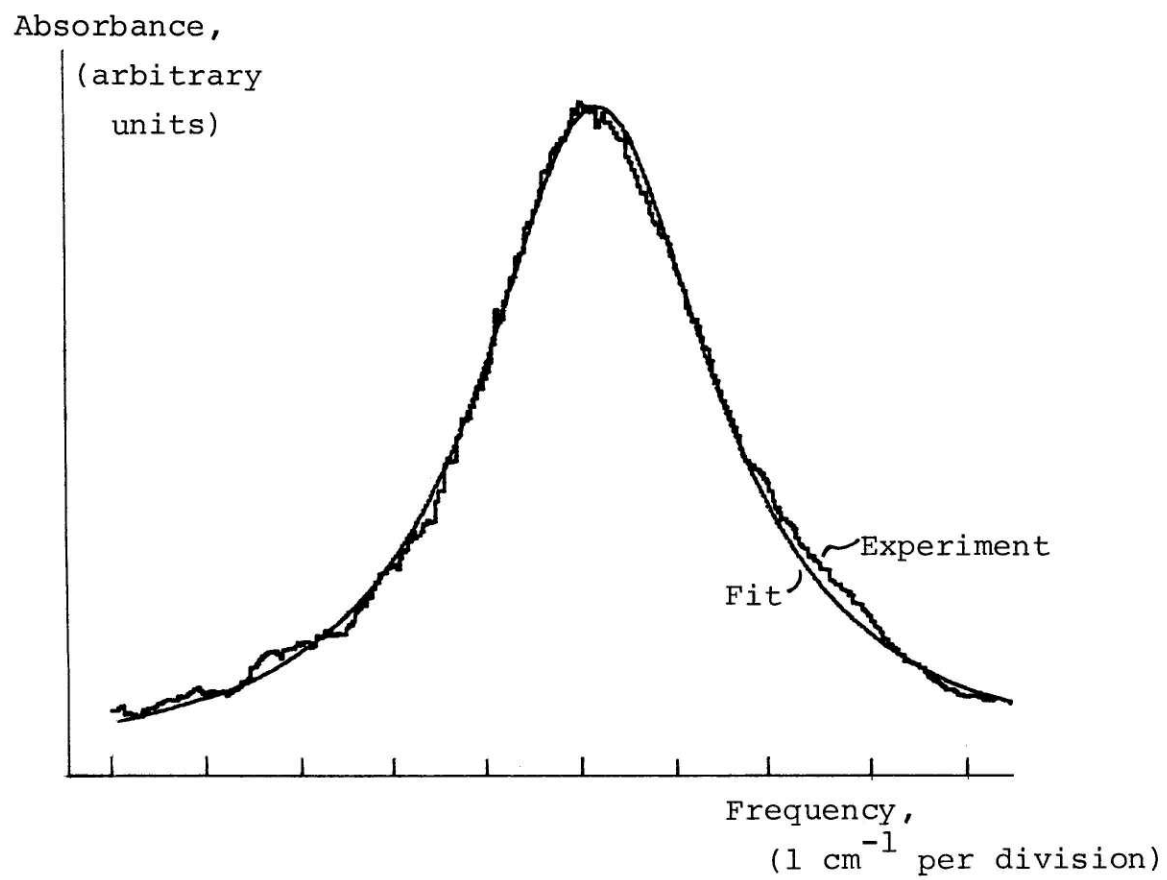


Figure 15

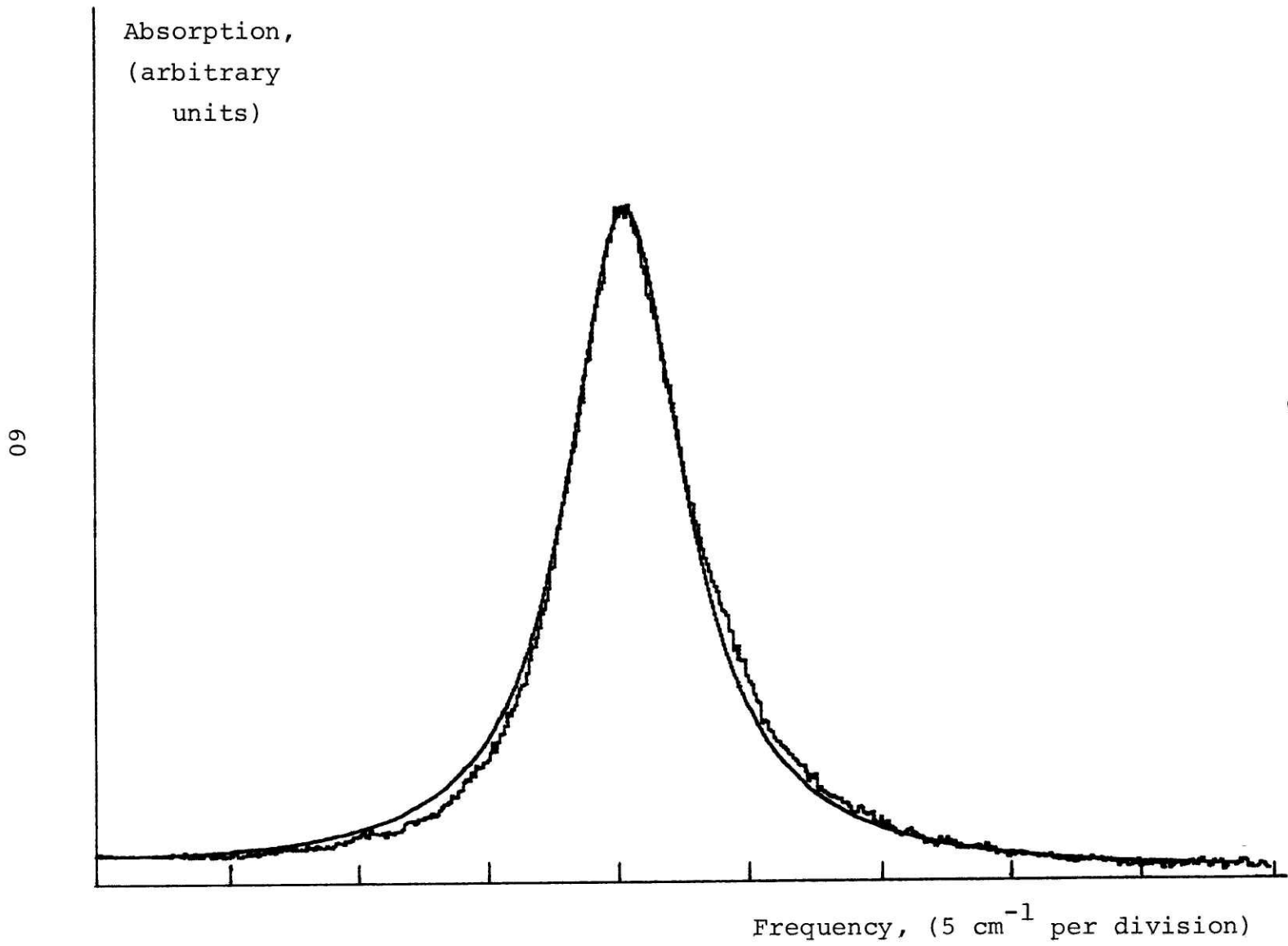


Figure 16

of a perfect gas at 0° C, and are obtained assuming a second virial coefficient of $-16 \text{ cm}^3/\text{mole}$ for argon at 298° K.¹⁸ (Throughout most of the density range studied here, the effects of the nonideality of the gas and conversion to standard temperature partially cancel. For low densities only the substantial temperature factor remains. In Section I E we will see that one must be careful on this account when comparing literature values.) Also plotted in Figures 17 through 19 are the linear extrapolations of the low density measurements of Wiggins and coworkers,¹⁹ and the least squares line fit through the experimental points and constrained to pass through zero. (Of course, as the density goes to zero, there remains a contribution to the linewidth due to Doppler broadening. However in this spectral region the Doppler width is less than 0.01 cm^{-1} and can be neglected.)

Table 1 gives linear pressure broadening coefficients determined by fitting the experimental points up to 100 amagats. (Somewhat lower densities can also be used for upper limits without changing the values obtained.) Also listed is the standard deviation in the slope calculated from the least squares fit. This is not necessarily a good measure of the error, since the average deviation per point for the fit is considerably smaller than the experimental error estimate, discussed in Section I C. Also listed are the values of Wiggins and coworkers¹⁹ and

Table 1 : Linear Pressure Broadening Coefficients for HF

<u>Line</u>	<u>This Work</u>	<u>Reference 19</u>
P(2)	.029 \pm .001 cm ⁻¹ /am	.036 \pm .001 cm ⁻¹ /am
P(3)	.023 \pm .001	.031 \pm .001
P(4)	.020 \pm .001	.024 ₅ \pm .001

Figure 17: Plot of half width at half maximum of the P(2) line of HF as a function of the perturbing argon density. In this and the following two figures, the squares are experimental points, the solid line is the least squares fit through them constrained to pass through the origin, and the dashed line is the linear extrapolation of the low density results of Reference 19.

Figure 18: Plot of linewidth of HF P(3) versus argon density.

Figure 19: Plot of linewidth of HF P(4) versus argon density.

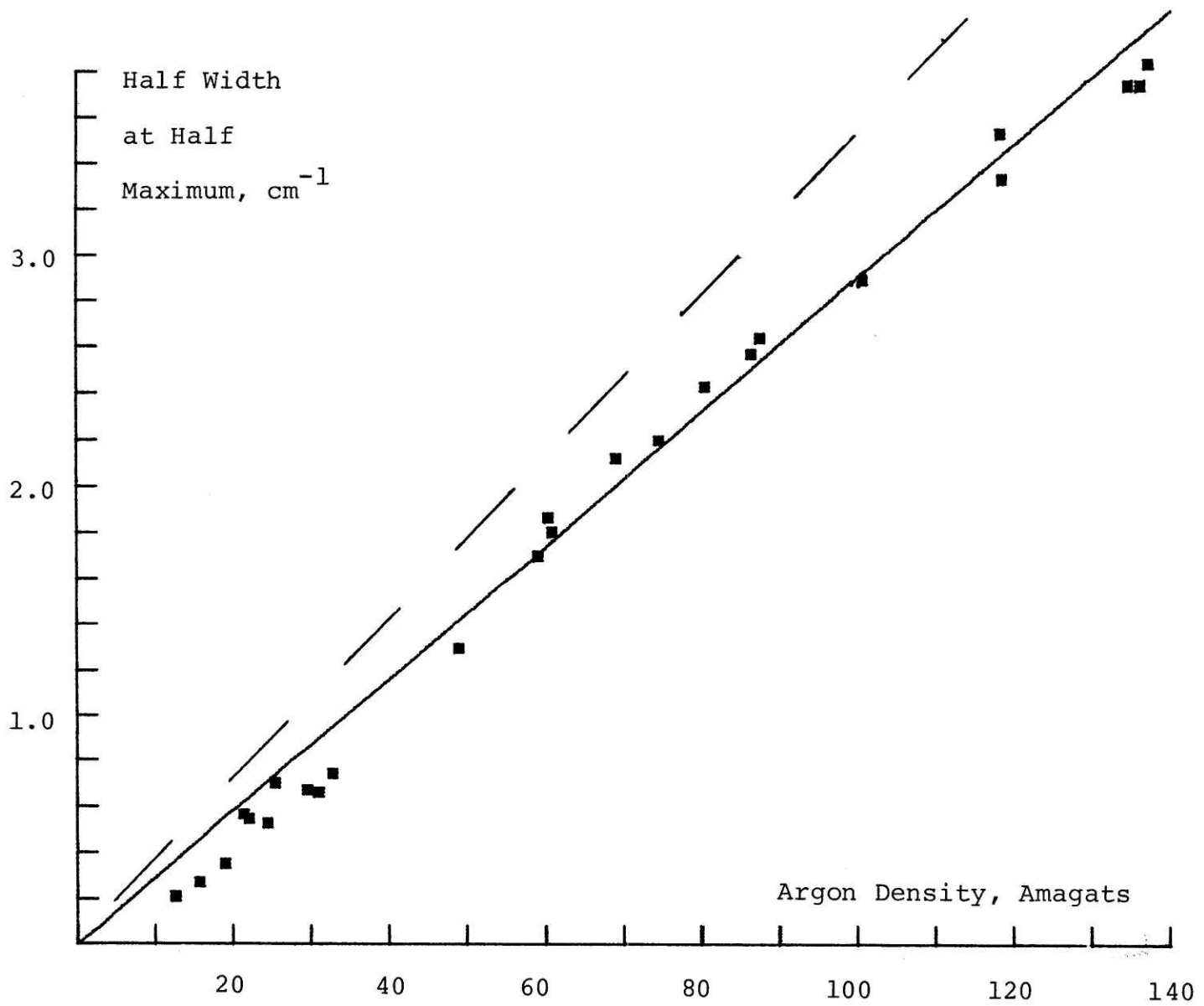


Figure 17

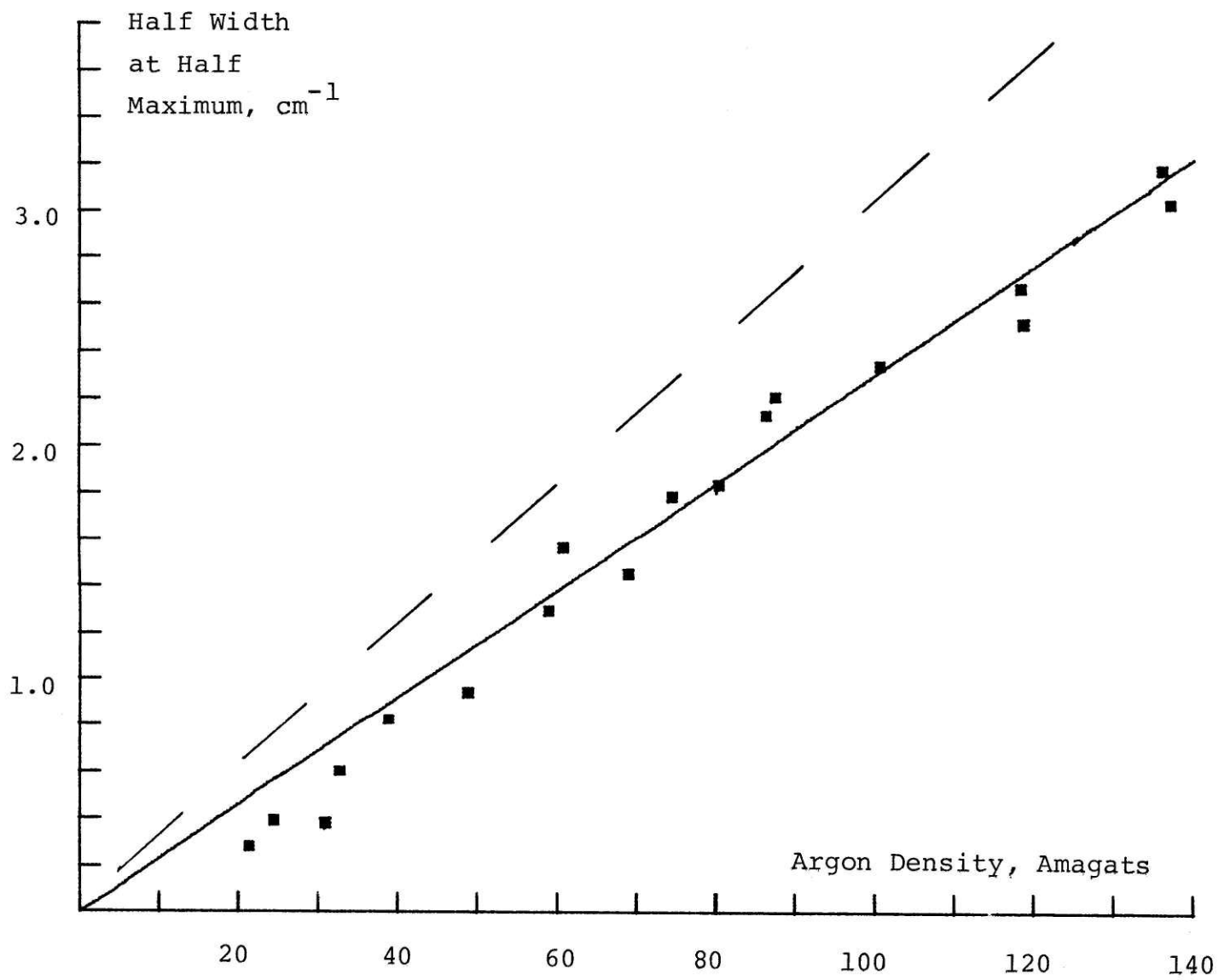


Figure 18

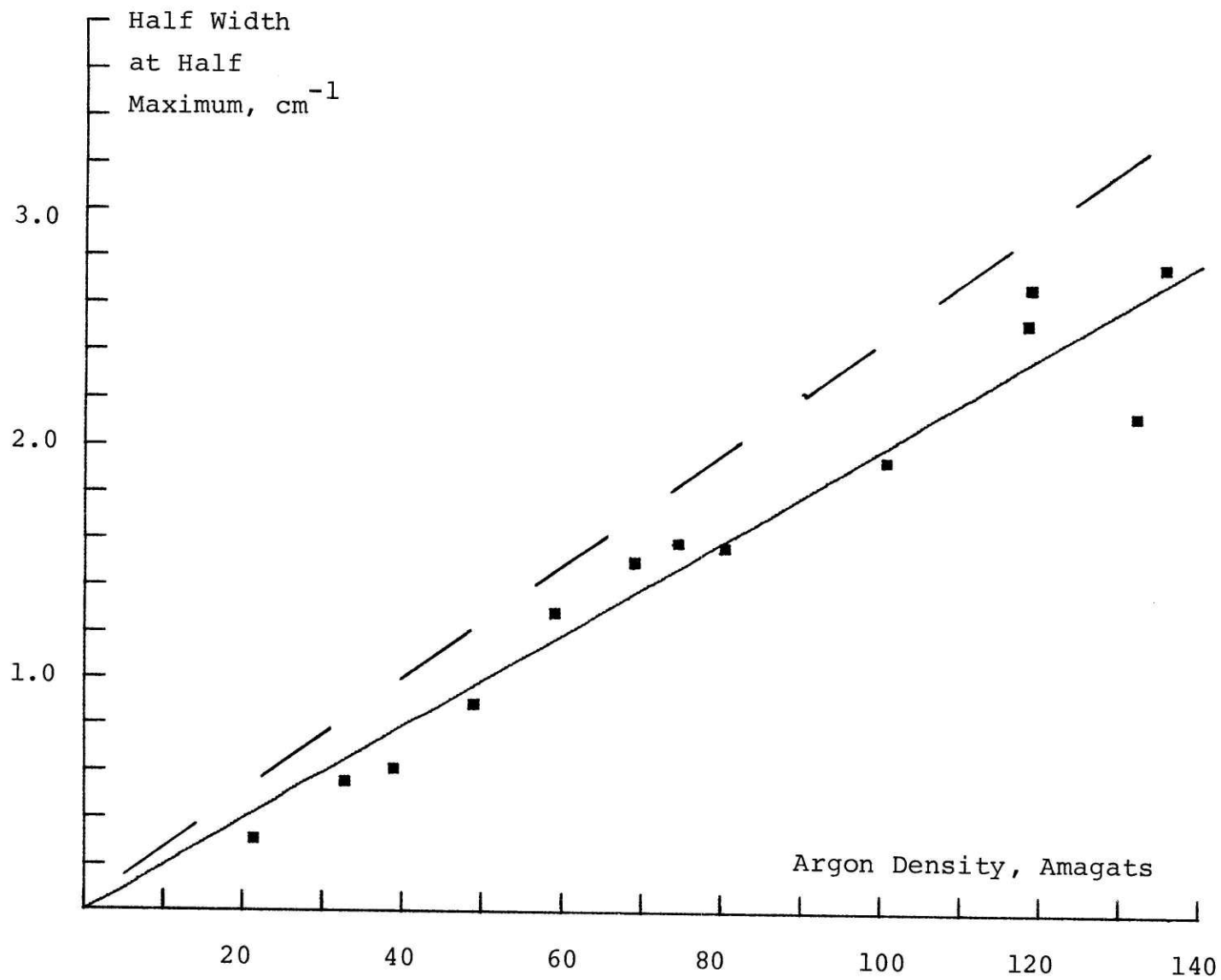


Figure 19

their error estimate. We note that the linewidths reported by Wiggins and coworkers are significantly larger than ours. This will be discussed further in Section I E, where we will find that the HCl linewidths measured by Rank and Wiggins and coworkers are systematically larger than those obtained in later work on the same system.^{25,26}

The decrease of linewidth with increasing J is commonly observed, and can be explained by simple models. For instance, one can argue that rotational energy levels are spaced farther apart at high J so that inelastic collisions become less probable.^{20,27} Or, in another way of thinking, fast rotation tends to average out angle dependent forces which give rise to reorientation contributions to line broadening.²⁸

In Table 2 we present some theoretical calculations of the broadening by argon of the three HF lines studied here. The recent calculation by Jarecki and Herman²⁰ uses a form of the theory of Baranger, in which isotropic effects represented by a phase shift are included to all orders in the interaction potential, and inelastic contributions are calculated to second order. Bachet²¹ uses standard Anderson theory, to calculate pure rotational linewidths.

We also include results of several different experiments, the pure rotation widths measured by Bachet,²¹ the R branch values of Oksengorn,²² and the first overtone measurements of Atwood and Vu.²³ These values should all be somewhat different, but they are at least interesting for comparison.

Table 2 : Comparison with Theory and Related Experiments on HF Linewidths

In the first column we repeat the results of the present work. We identify the succeeding columns by the number of the reference, as discussed in the text. All values are in $\text{cm}^{-1}/\text{amagat}$. The values from Reference 22 are actually for the lines R(1) through R(3), and those of Reference 21 marked Pure Rot. are for the pure rotational lines J $1 \rightarrow 2$, $2 \rightarrow 3$, and $3 \rightarrow 4$. See Table 1 for comparison with experiments on the same lines.

89

<u>Line</u>	<u>This</u>	<u>Theory</u>		<u>Ref. 22</u>	<u>Ref. 21</u>	<u>Ref. 23</u>
	<u>Work</u>	<u>Ref. 20</u>	<u>Ref. 21</u>	<u>R-Branch</u>	<u>Pure Rot.</u>	
P(2)	.029	.034	.0339	.051	.037	.063 ₅
P(3)	.023	.019	.0269	.043	.025	.038
P(4)	.020	.015	.0236	.037	.015	

Reference 20 contains a discussion of the vibrational dependence of linewidths. The general trend is that pure rotation lines are somewhat narrower than fundamental vibration-rotation lines, while first overtone lines are broader. It also discusses differences in width for corresponding lines in the P and R branches, concluding that these are due to the differing effects of inelastic collisions. Again, in the HF-argon system these effects are relatively small.

E. HCl Low Density Linewidth Results

This section contains the same discussion for HCl lines broadened by argon as the preceding one did for HF. For HCl the lines studied were R(1) through R(6) at room temperature broadened by up to 100 atmospheres of argon. Figures 20 through 22 show some sample experimental traces. Figure 20 shows that even at low densities the two lines due to the 35 and 37 isotopes of chlorine are broadened into each other, while Figures 21 and 22 show that at high densities the gaps between rotational lines begin to fill in. Figure 22 also includes a trace of just a few torr of HCl.

The plots of linewidth versus density appear in Figures 23 through 28, and the linewidths obtained by a linear least squares fit to all the experimental points are presented in Table 3. Again, the errors quoted are the standard deviations from the least squares fit, and our estimates of experimental error are larger. Also as before the least squares fits were made giving equal weight to each experimental point, since as for the HF data, fits weighted by the quality of the lineshape gave identical results.

In the case of HCl there are three low density measurements of the same lines, one by Rank and Wiggins and coworkers²⁴ and two more recent sets of data by workers in France.^{25,26} The agreement between our data and the last two references strengthens their assumption that (at least for the higher rotational lines) the linewidth values measured by Rank and

Figure 20: Sample trace of the HCl R(4) isotopic doublet broadened by 29.5 atm of argon. The experimental trace is an average of three data tapes. The Lorentzian fit is composed of six lines, the central isotopic doublet with 0.9 cm^{-1} halfwidths and two neighboring doublets with appropriately scaled widths.

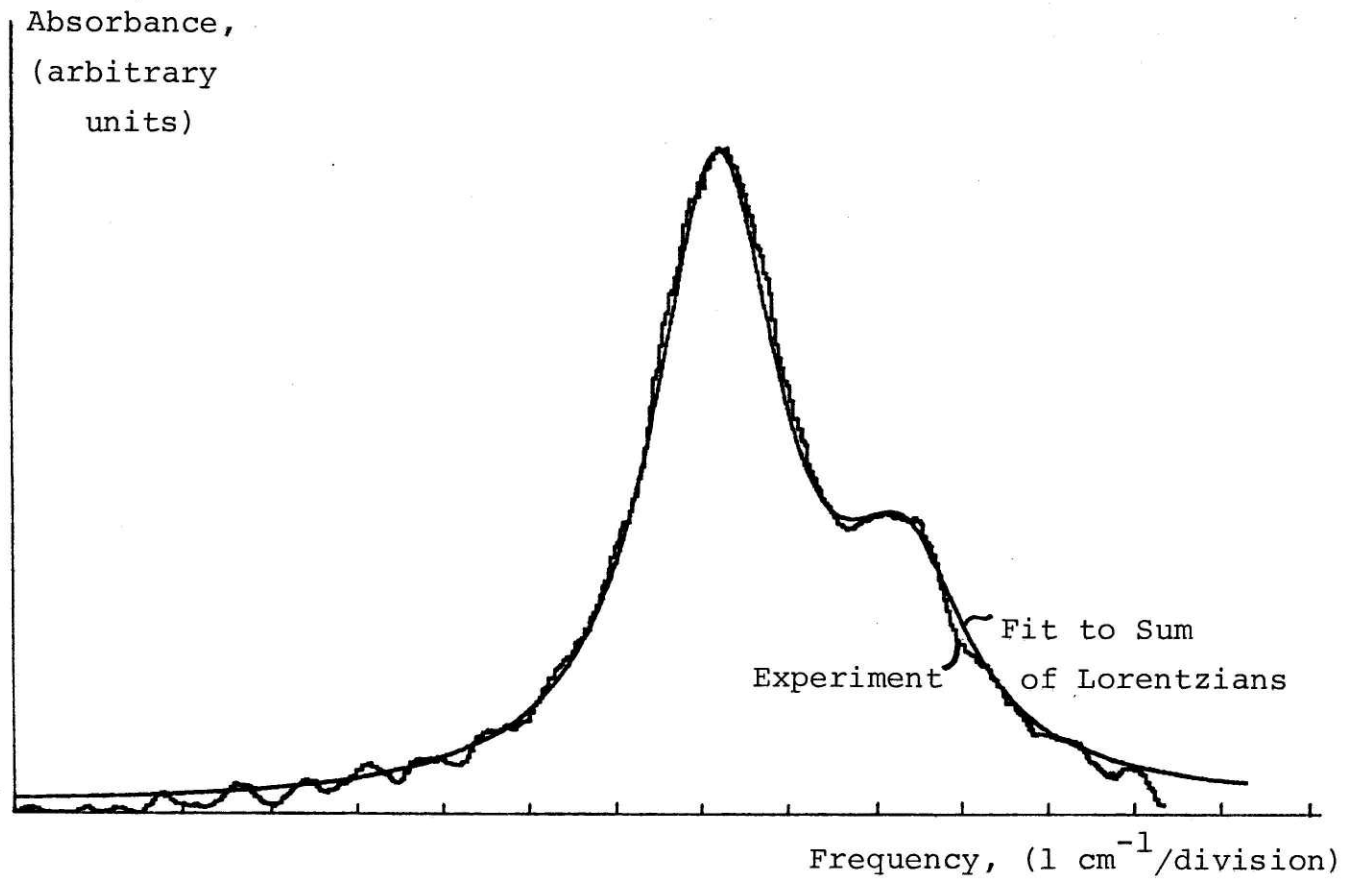


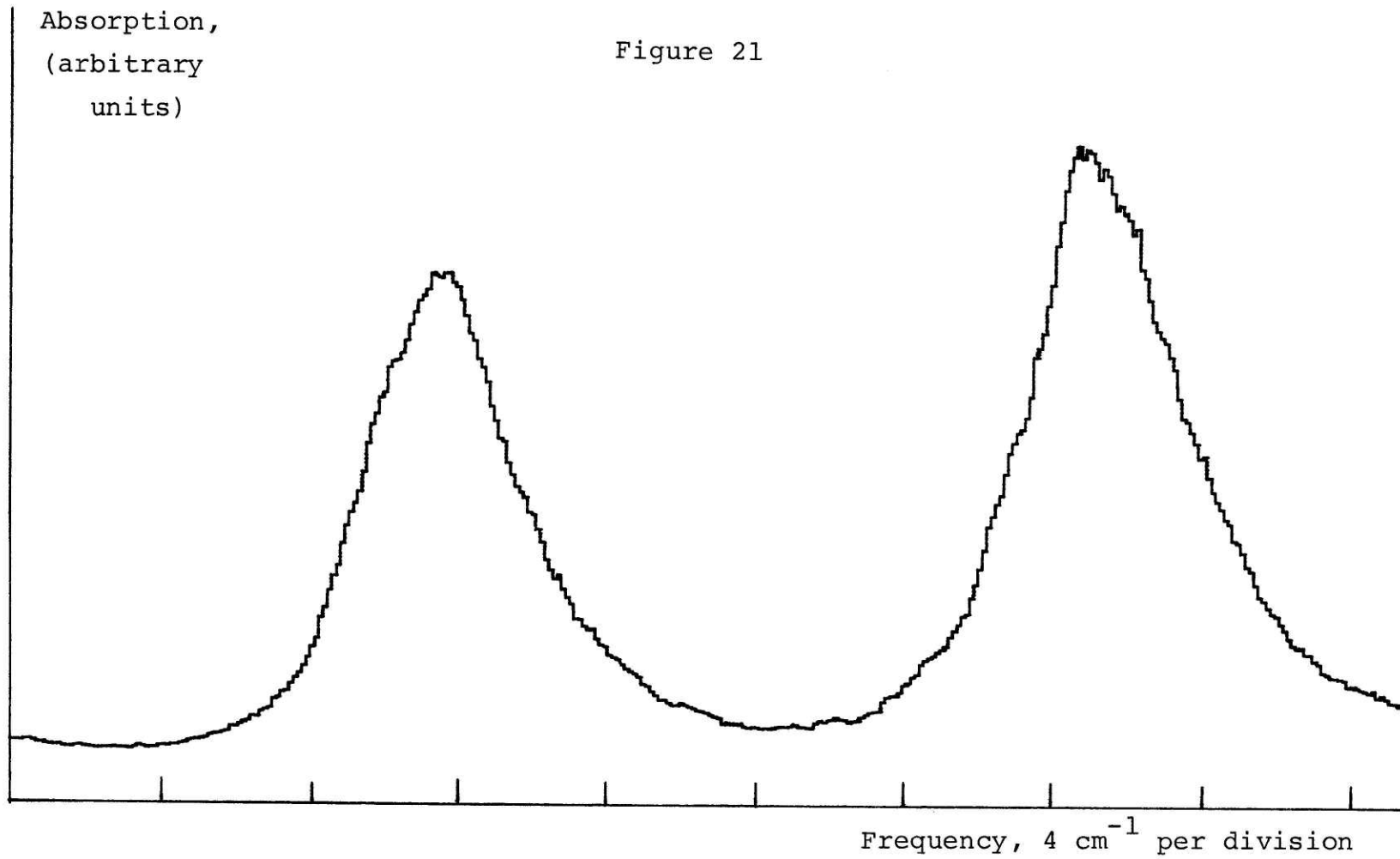
Figure 20

Figure 21: Sample trace of two sets of HCl lines, R(3) and R(4), broadened by 102 atmospheres of argon so that the isotopic splitting entirely disappears. This trace is the average of 7 experimental scans, and like the rest of the earliest HCl data was produced by measuring points off each chart recorder trace, averaging them, and replotting.

Absorption,
(arbitrary
units)

Figure 21

74



Frequency, 4 cm⁻¹ per division

Figure 22: Sample trace of HCl R(4) through R(1) broadened by 91 atmospheres of argon, showing that the gaps between the lines are filling in considerably at high pressures. Also shown is a trace of just a few torr of HCl, using the same baseline used for the high pressure scan.

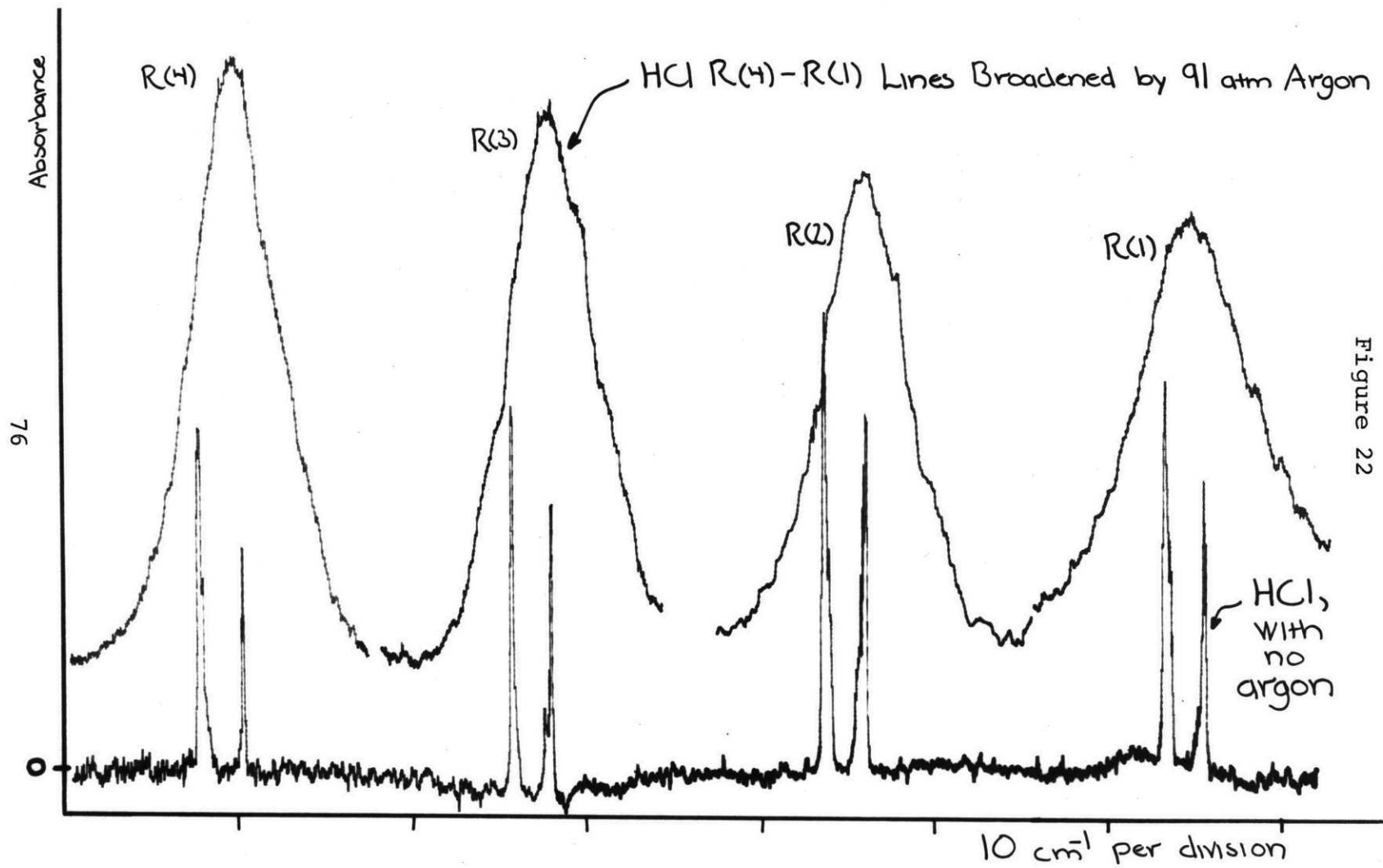


Figure 22

Table 3 : Linear Pressure Broadening Coefficients for HCl

<u>Line</u>	<u>This Work</u>		<u>Ref. 24</u>	<u>Ref. 25</u>	<u>Ref. 26</u>
R(1)	.042 \pm .001	cm ⁻¹ /am	.042 ₅	.0387	.0421
R(2)	.034 ₅ \pm .001		.044 ₅	.0336	.035
R(3)	.032 \pm .001		.039	.0315	.0306
R(4)	.028 \pm .001		.028	.0274	.0268
R(5)	.021 ₅ \pm .001		.024 ₅	.0226	.0236
R(6)	.016 \pm .001		.020	.018	

Figure 23: Plot of the half width at half maximum of the HCl R(1) line as a function of perturbing argon density. In this and the following 5 figures, the squares are experimental points, and the solid line is a least squares fit through them constrained to pass through the origin. The long dashed line is the linear extrapolation of the low density results of Reference 24, the medium dashed line the same for Reference 25, and the short dashed line for Reference 26. (Because some of the linear linewidth values are very close to each other, not all lines may be plotted on any one graph. Consult Table 3 for the values omitted.)

Figure 24: Plot of the linewidth of HCl R(2) versus argon density.

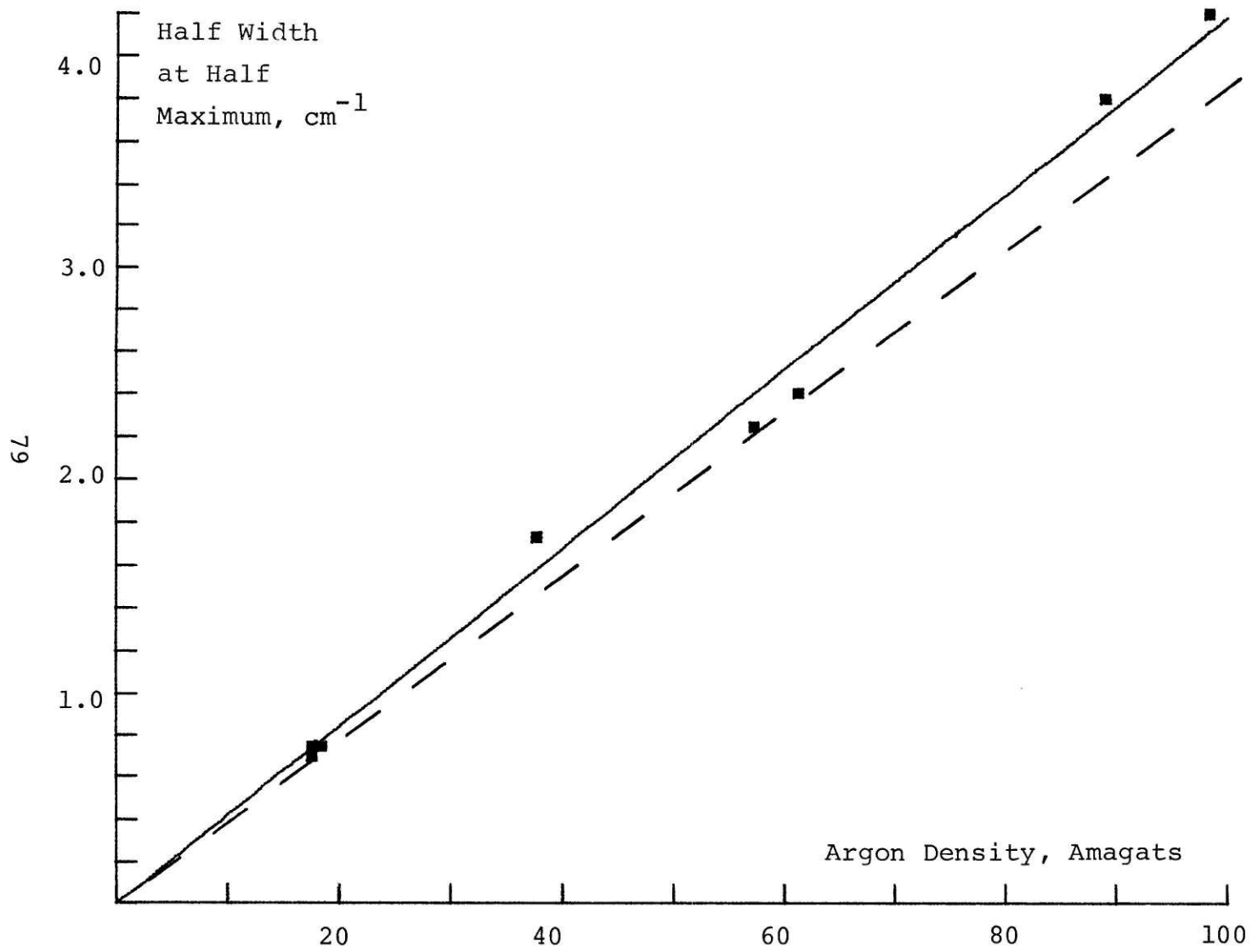


Figure 23

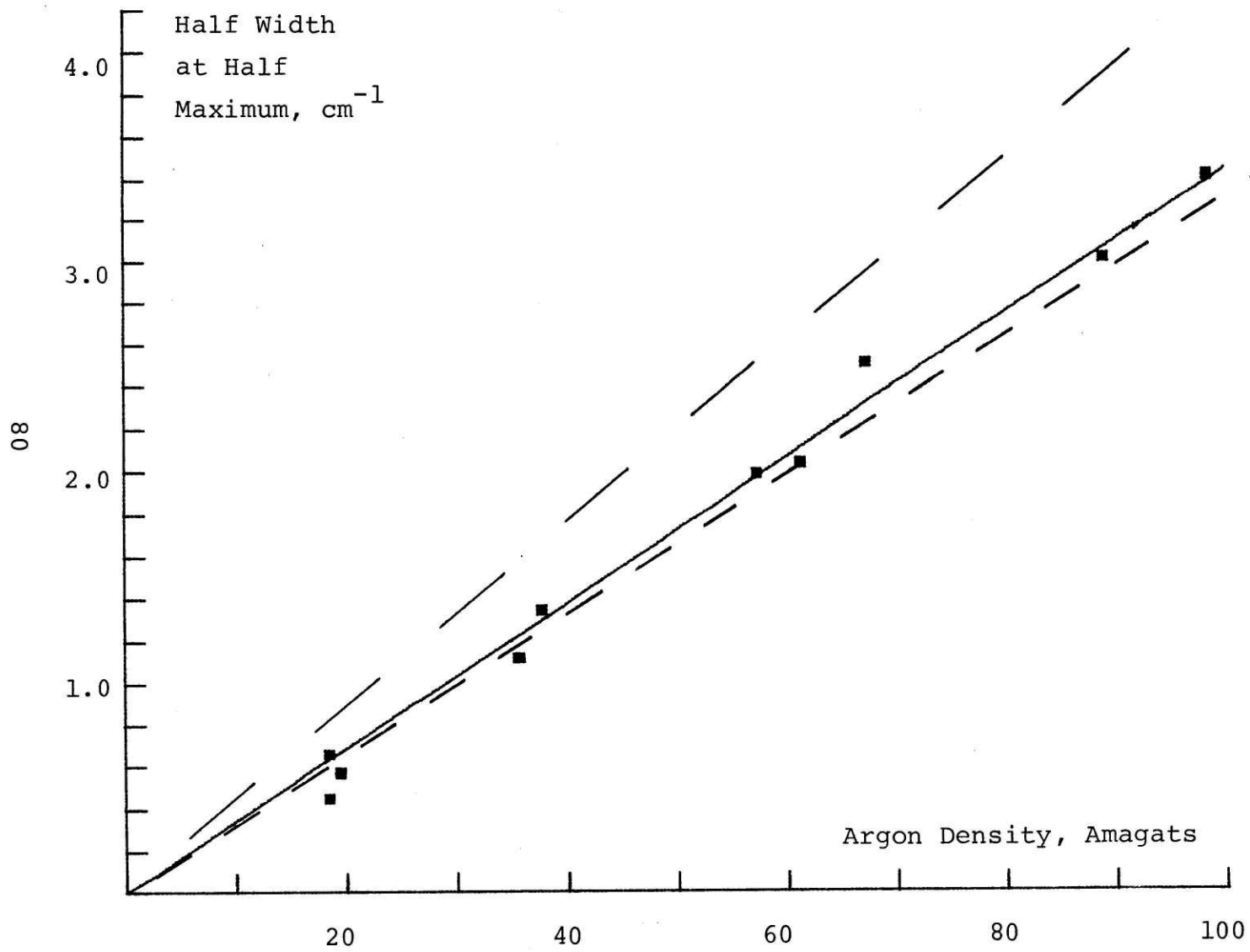


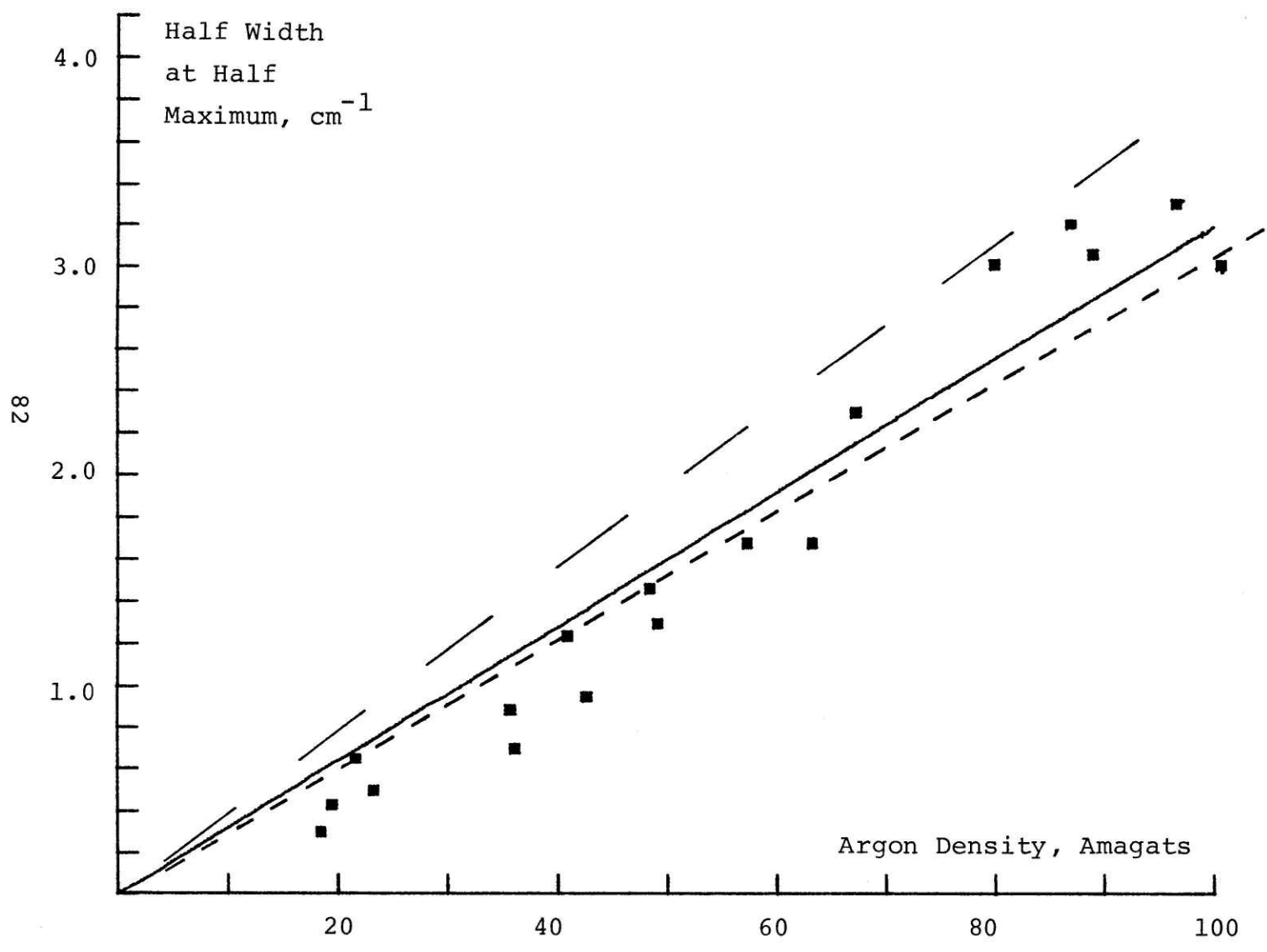
Figure 24

Figure 25: Plot of the linewidth of HCl R(3) versus argon density.

Figure 26: Plot of the linewidth of HCl R(4) versus argon density.

Figure 27: Plot of the linewidth of HCl R(5) versus argon density.

Figure 28: Plot of the linewidth of HCl R(6) versus argon density.



82

Figure 25

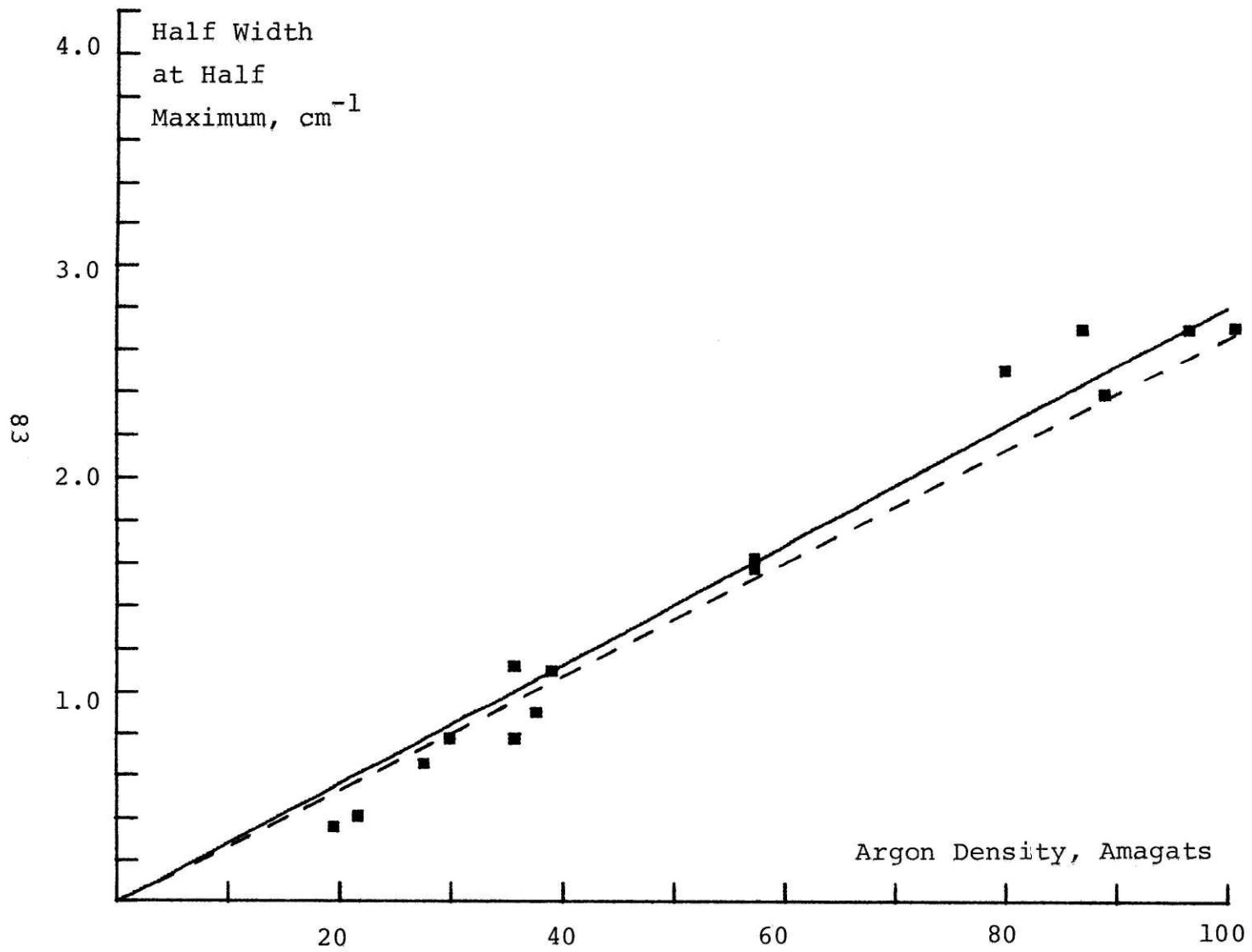


Figure 26

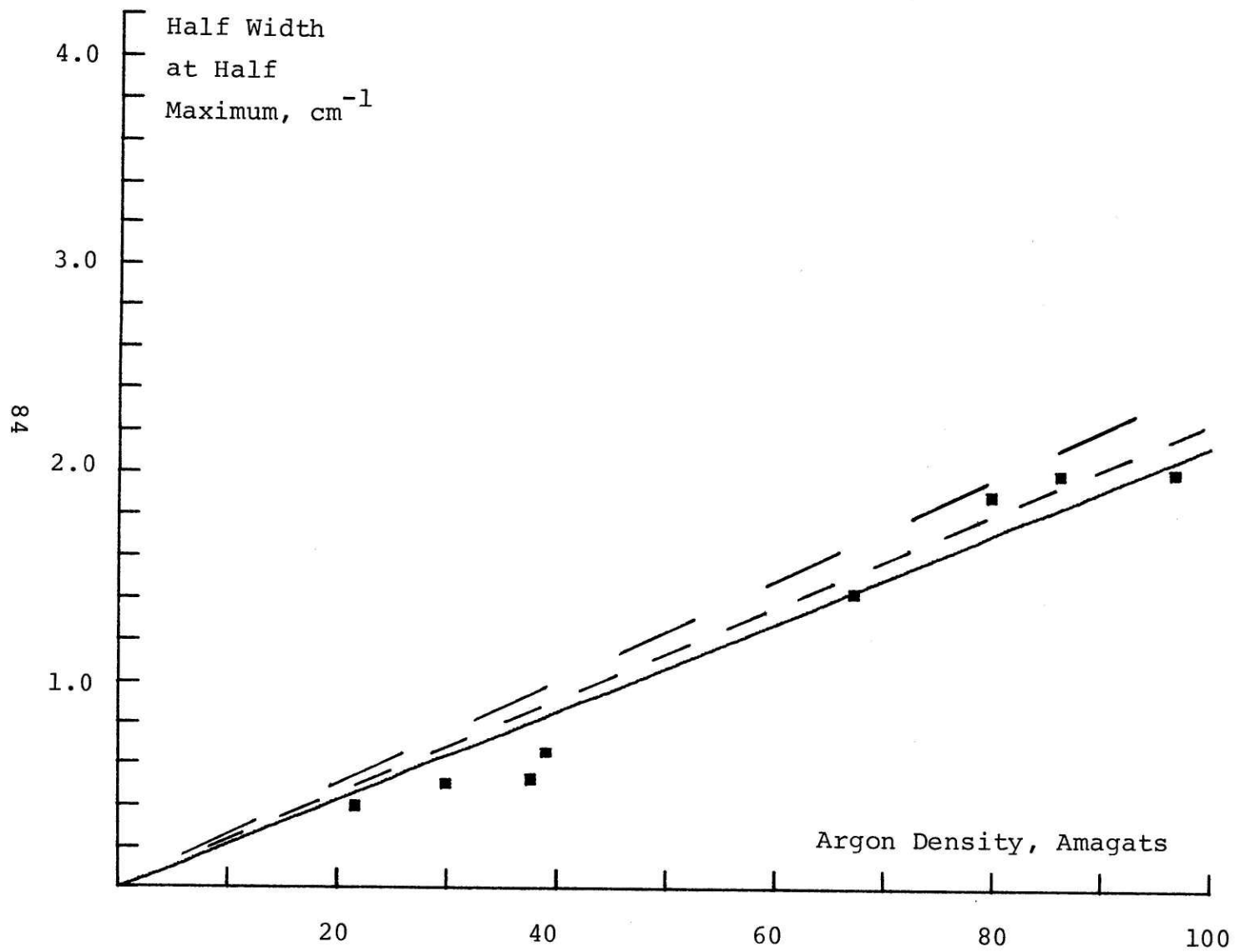


Figure 27

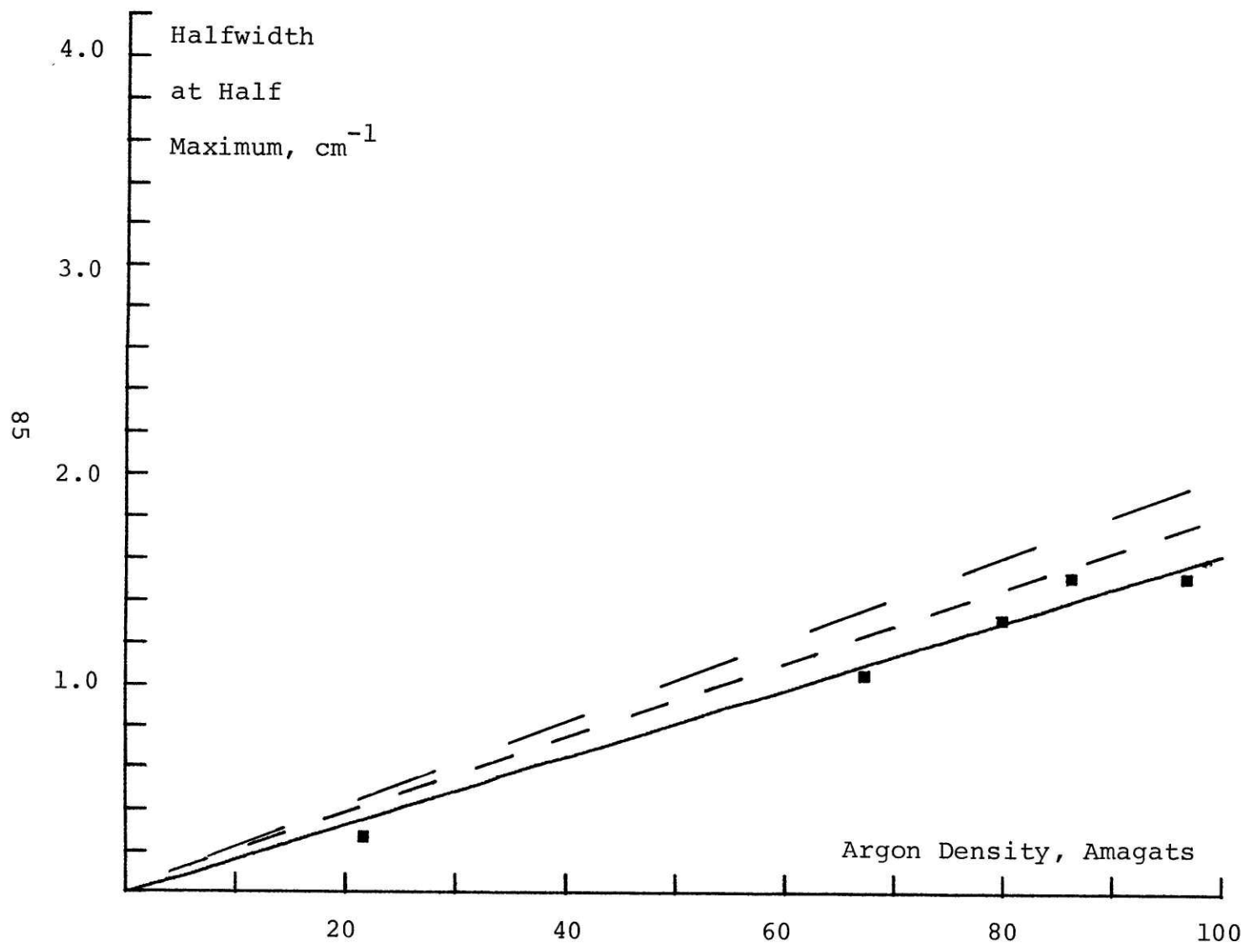


Figure 28

Wiggins are too high, and lends weight to the argument in Section I D that the HF linewidths measured by Wiggins are also too large. This conclusion is further supported by considering that our tunable laser spectrometer, with its finite linewidth and necessity for averaging by superimposing several traces, possesses systematic errors which only tend to produce observed linewidths which are too large. Yet for HF our line broadening coefficients before any deconvolution are still smaller than those of Wiggins. (We anticipate the discussion of Section II E on second order density effects to note that if it is indeed the practice of the French workers to measure linewidths at pressures of 5 to 10 atmospheres in order to reduce their instrumental error, then my estimates would say that they might actually be making a systematic error in causing their linewidths to be a few per cent too small.)

However, looking over Table 3 we conclude that the agreement between the sets of data is not too bad. Indeed, it is better than either of the French groups claims, for the following reason. Levy and coworkers²⁵ report their results in mk/bar. (A millikayser, abbreviated mk, is 0.001 cm^{-1} .) The bar is a unit of pressure equal to .9861 atm. Then since argon at 1 atmosphere is essentially a perfect gas, we need only convert to standard temperature by the rather substantial factor of $298^{\circ}\text{K}/273.15^{\circ}\text{K}$. In Reference 26 Houdeau and coworkers also made this conversion of the results of Reference 25, but further in their comparison

with Rank and Wiggins and coworkers²⁴ they assumed that units of $\text{cm}^{-1}/\text{standard atmosphere}$ meant $\text{cm}^{-1}/\text{atm}$. Yet Rank clearly states that his standard atmosphere is pressure at 0°C , and for HF Wiggins simply quotes $\text{cm}^{-1}/\text{amagat}$. So Reference 26 is in error in converting and making the values of Rank look even larger, while Reference 25 is wrong in not converting their measurements in mk/bar before comparing with Rank.

In Table 4 we again give comparisons with theory and with pure rotation measurements. The calculation of Tipping and Herman²⁹ uses the formal expression of Baranger for the linewidth, expanded to second order in the interaction potential. Although this is the same order as Anderson theory, this procedure results in some modifications. Houdeau²⁶ uses standard Anderson theory with the potential used by Tipping and Herman. Boulet, Isnard and Levy³⁰ use a modification of Anderson theory³¹ and a potential due to Buckingham, which they compare with the potential of Tipping and Herman.

The calculation of Marcus and Fitz³² uses semiclassical S-matrix theory, while that of Neilsen and Gordon³³ uses a classical path method for translation but solves the coupled equations for the quantum mechanical scattering matrix for rotational states. Gordon offers a wide variety of potentials, and here we choose the one compared by Marcus. Both calculations give no difference between corresponding

Table 4 : Comparison with Theory and Related Experiments on HCl Linewidths

In the first column we repeat the results of the present work. We identify the succeeding columns by the number of the reference, as discussed in the text. All values are in $\text{cm}^{-1}/\text{amagat}$. The values from References 32 and 34 are theoretical and experimental results for the pure rotation transition J 4 5, and the results of Reference 33 are also best compared with pure rotation experiments.

	This							
<u>Line</u>	<u>Work</u>	<u>Ref. 33</u>	<u>Ref. 32</u>	<u>Ref. 29</u>	<u>Ref. 26</u>	<u>Ref. 30</u>	<u>Ref. 34</u>	<u>Ref. 35</u>
R(1)	.042	.0438		.048 ₅	.0388	.038		.0406
R(2)	.034 ₅	.035		.046	.0351	.033		.0337
R(3)	.032	.0285		.037	.033	.032		.0237
R(4)	.028	.023	.0237	.022	.031	.027 ₅	.022	.0217
R(5)	.021 ₅	.019		.015 ₅	.0293	.022 ₅		.0216
R(6)	.016			.011 ₅		.0187		

R and P branch lines, and are best compared with pure rotation measurements. Also the results of both calculations are expressed in terms of cross sections. In comparison, conversion from linewidths to cross sections requires some care, since it is essentially an arbitrary definition. Here we will define the cross section σ in cm^2 by³¹

$$\Delta\nu_{1/2} = \tilde{N}/\tilde{V} \bar{v}_{12} \sigma/2\pi c$$

where \tilde{N} is the Avogadro number, \tilde{V} is the molar volume, \bar{v}_{12} is the thermal average relative velocity, and $\Delta\nu_{1/2}$ is the linewidth in cm^{-1}/am . (For HCl at 298°K this means multiplying the linewidth in cm^{-1}/am by 1.22 gives the cross section in A^2 .) By checking their conversion of the data of Rank, Gordon seems to use this factor, while Marcus uses a larger factor (which might be due to his again assuming that the values of Rank are expressed in $\text{cm}^{-1}/\text{atm}$ instead of $\text{cm}^{-1}/\text{amagat}$).

In addition Table 4 presents two measurements of pure rotation lines,^{34,35} which are in general expected to be smaller than the corresponding vibration-rotation linewidths. Reference 29 has a discussion of the vibrational dependence of linewidths. Also Gordon³³ quotes some unpublished pure rotational widths due to Scott and Sanderson of Ohio State.

After the studies of HCl and HF, some preliminary measurements were made on DF broadened by argon. DF is a molecule which has been little studied, but which has lately become quite interesting.³⁶ All that can be said presently is that the lines are quite narrow, at least as narrow as the

corresponding HF lines. This means that although they have roughly the same rotational spacing as HCl (and are in the same spectral region) they do not have the serious problem of overlapping rotational lines at high densities.

II THEORY, AND DISCUSSION OF EXPERIMENTS

A. Summary of Formal Theory

In this section we will present a reprise of the formal theory of Albers and Oppenheim³⁷⁻³⁹ for the density expansion of the lineshape, in order to reach our own forms of the triple collision contributions. We will also include a short discussion of the physical origin of the logarithmic divergence and density dependence, although in three dimensions this occurs in third order in the density and we shall be most interested in second order density corrections. Additional discussion of the theory in its classical mechanical form is contained in References 40 through 44.

Since we will begin our density expansion with the correlation function expression for the absorption coefficient, we should give some explanation of that form. While it can be derived from perturbation theory,^{39,45-47} there are some assumptions which have their best justification in linear response theory,⁴⁸ and we shall use that here.

To begin, we consider a total Hamiltonian $H_T(t) = H + H_1(t)$, where H describes the motion and interaction of an N particle system including an absorbing particle, and $H_1(t)$, the coupling to the outside world, will eventually be $\vec{E}(t) \cdot \vec{p}$, where \vec{p} is the dipole moment and $\vec{E}(t)$ the electric field of the light. So for foreign gas broadening we want the nonequilibrium average of a single dipole moment \vec{p} , which in quantum mechanics is $\overline{\vec{p}(t)} = \sum_n \rho_n \langle n+1 | \vec{p} | n+1 \rangle$. Instead of

time dependent energy states, $|n, t\rangle$, we use the equation

$$(1) \quad i\hbar \frac{\partial}{\partial t} |n, t\rangle = H_T(t) |n, t\rangle$$

with $|n, -\infty\rangle$ being $|n\rangle$ to introduce time development operators,

$$U(t) |n\rangle = |n, t\rangle . \quad \text{Then}$$

$$(2) \quad \overline{\vec{p}(t)} = \text{Tr} (\rho_{eq} U^\dagger(t) \vec{p} U(t))$$

where $\rho_{eq} = e^{-\beta H} / \text{Tr} e^{-\beta H} = \bar{e}^{-\beta H} / Z$ and Tr denotes a sum over diagonal matrix elements. In order that $U(-\infty) = 1$

(if $\vec{E}(t)$ is like $\vec{E}_0 \cos \omega t$) we will have to write $H_1(t)$ as

$$\lim_{\epsilon \rightarrow 0^+} \bar{e}^{\epsilon t} \vec{E}(t) \cdot \vec{p} \quad \text{to show that the disturbance was adiabatically turned on at } t = -\infty .$$

By trace invariance to order of operations, Equation (2)

becomes

$$(3) \quad \overline{\vec{p}(t)} = \text{Tr} (\rho(t) \vec{p})$$

with $\rho(t)$ given by

$$(4) \quad \rho(t) = U(t) \rho_{eq} U^\dagger(t) ,$$

whose equation of motion is

$$(5) \quad \dot{\rho}(t) = -i/\hbar [H_T, \rho(t)]$$

Now we make the linear response assumption, by saying the solution of Equation (5) is $\rho(t) = \rho_{eq} + \rho_1(t)$ If we substitute and keep only linear terms, we find

$$(6) \quad \dot{\rho}_1(t) = -i/\hbar [H_1, \rho_1(t)] - i/\hbar [H_1(t), \rho_{eq}]$$

or rewriting,

$$(7) \quad \frac{d}{dt} (e^{iHt/\hbar} \rho_1(t) e^{-iHt/\hbar}) = -i/\hbar e^{iHt/\hbar} [H_1(t), \rho_{eq}] e^{-iHt/\hbar}$$

Integrating,

$$(8) \quad \rho_1(t) = -i/\hbar \int_{-\infty}^t d\tau e^{-iH(t-\tau)/\hbar} [H_1(\tau), \rho_{eq}] e^{iH(t-\tau)/\hbar}$$

or with $H_1(t) = \vec{E}(t) \cdot \vec{p}$,

$$(9) \rho_1(t) = -i/\hbar \int_{-\infty}^t d\tau e^{-iH(t-\tau)/\hbar} [\vec{p}, \rho_{eq}] e^{iH(t-\tau)/\hbar} \cdot \vec{E}(\tau)$$

In equilibrium, $\vec{p}(t) = e^{iHt/\hbar} \vec{p} e^{-iHt/\hbar}$ so that

$$(10) \rho_1(t) = -i/\hbar \int_{-\infty}^t d\tau [\vec{p}(t-\tau), \rho_{eq}] \cdot \vec{E}(\tau)$$

Now we can write

$$(11) \overline{\vec{p}(t)} - \langle \vec{p} \rangle = \int_{-\infty}^t \vec{\chi}_{\mu\nu}(t-\tau) \cdot \vec{E}(\tau)$$

where the tensor

$$(12) \vec{\chi}_{\mu\nu}(t) = -i/\hbar \text{Tr}(\vec{p}(t) [\vec{p}, \rho_{eq}])$$

is the response function. The brackets $\langle \rangle$ denote a trace over ρ_{eq} , and here $\langle \vec{p} \rangle$, the equilibrium value of \vec{p} , is zero.

Now we assume that

$$(13) \vec{E}(t) = \lim_{\epsilon \rightarrow 0^+} \vec{E}_0 \cos \omega t e^{-\epsilon t}$$

so that Equation (11) becomes

$$(14) \overline{\vec{p}(t)} = \lim_{\epsilon \rightarrow 0^+} \text{Re} \int_{-\infty}^t \vec{\chi}_{\mu\nu}(t-\tau) e^{-\epsilon t} e^{i\omega\tau} d\tau \cdot \vec{E}_0$$

or with $s = t - \tau$,

$$(15) \overline{\vec{p}(t)} = \lim_{\epsilon \rightarrow 0^+} \text{Re} \int_0^{\infty} \vec{\chi}_{\mu\nu}(s) e^{-i\omega s} e^{-\epsilon s} \cdot \vec{E}_0 e^{i\omega t} \equiv \text{Re} \vec{\chi}(\omega) \cdot \vec{E}_0 e^{i\omega t}$$

or writing the susceptibility $\vec{\chi}$ as $\vec{\chi}' + i\vec{\chi}''$,

$$(16) \overline{\vec{p}(t)} = \vec{\chi}'(\omega) \cdot \vec{E}_0 \cos \omega t - \vec{\chi}''(\omega) \cdot \vec{E}_0 \sin \omega t$$

For one dipole the power absorbed, dU/dt , is $\overline{\vec{p}(t)} \cdot d\vec{E}/dt$.

So since $d\vec{E}/dt = -\omega \vec{E}_0 \sin \omega t$, (taking the ϵ limit here),

$$(17) dU/dt = 1/3 (-\omega \chi'(\omega) \cos \omega t \sin \omega t E_0^2 + \omega \chi''(\omega) \sin^2 \omega t E_0^2)$$

where the 1/3 comes from averaging over polarizations to take

$\vec{E}_0 \cdot \vec{\chi} \cdot \vec{E}_0$ to χE_0^2 . Now we average over one period to get the

power absorbed per unit time,

$$(18) 1/3 \omega E_0^2 \chi''(\omega) \omega/2\pi \int_0^{2\pi/\omega} \sin^2 \omega t dt = 1/3 \omega/2 E_0^2 \chi''(\omega)$$

$$= 1/3 \omega/2 E_0^2 \lim_{\epsilon \rightarrow 0^+} \text{Im} \int_0^{\infty} e^{-\epsilon t} e^{-i\omega t} i/\hbar \text{Tr}(\vec{p}(t) [\vec{p}, \rho_{eq}]) dt$$

Then $A(\omega)$, the power absorbed per unit distance, is simply

Equation (18) divided by the speed of light c and $F_0^2/2\pi$. Now, writing the trace as a sum of diagonal matrix elements, and using $\vec{p}(t) = e^{iHt/\hbar} \vec{p} e^{-iHt/\hbar}$,

$$(19) A(\omega) = \frac{1}{3\hbar c} \pi \omega \lim_{\epsilon \rightarrow 0^+} \text{Im} \int_0^\infty e^{-\epsilon t} e^{i\omega t} \sum_{mn} \langle m | e^{iE_m t/\hbar} \vec{p} e^{-iE_n t/\hbar} | n \rangle \langle n | [P, \rho_{eq}] | m \rangle$$

Now we use the definition of the δ function, and

$$\langle n | [P, \rho_{eq}] | m \rangle = \langle n | P \rho_{eq} | m \rangle - \langle n | \rho_{eq} P | m \rangle = e^{-\beta E_m} (1 - e^{-\beta(E_n - E_m)}) \rho_{nm} / Z$$

We have in $A(\omega)$

$$(20) \text{Im} \int_0^\infty \sum_{nm} 2\pi \delta(\omega - \omega_{mn}) e^{-\beta E_m} (1 - e^{-\beta \hbar \omega_{nm}}) \text{or } \text{Re} \sum_{nm} 2\pi \delta(\omega - \omega_{mn}) e^{-\beta E_m} (1 - e^{-\beta \hbar \omega})$$

Reversing,

$$(21) A(\omega) = \frac{\pi \omega}{3\hbar c} (1 - e^{-\beta \hbar \omega}) \lim_{\epsilon \rightarrow 0^+} \text{Re} \int_0^\infty e^{i\omega t} e^{-\epsilon t} \text{Tr} (P e^{iHt/\hbar} \rho_N P e^{-iHt/\hbar})$$

Following Albers, we introduce the tetradic operator L by

$$e^{-iL t} P_N P = e^{-iH t/\hbar} P_N P e^{iH t/\hbar}. \quad \text{We can now perform the time}$$

integration, and, if we define

$$(22) \int_0^\infty dt e^{-\epsilon t} e^{-i\omega t} e^{iL t} = (\epsilon + i\omega + iL)^{-1} \equiv G,$$

then

$$(23) A(\omega) = \frac{\pi \omega}{3\hbar c} (1 - e^{-\beta \hbar \omega}) \lim_{\epsilon \rightarrow 0^+} \text{Re} \langle P, G P \rangle$$

The brackets $\langle \rangle$ denote an equilibrium average which in classical mechanics is an integration over all coordinates and momenta of $N-1$ structureless particles and on absorber, weighted by the classical distribution function. In quantum mechanics, they become a trace (Tr) over all states weighted by the corresponding quantum mechanical density matrix, $\rho_N = \exp(-\beta H) / \text{Tr}(\exp(-\beta H))$, where the Hamiltonian H describes the translational motion of all N particles, the internal motion of the absorber, particle 1, and pair interactions between all N particles,

$$(24) H = H_0 + H_{int}(1) + V = \sum_i^N H_0(i) + H_{int}(1) + \sum_{i < j}^N V_{ij}$$

giving corresponding $L_0(i)$, $L_{int}(1)$ and L'_{ij} operators. We can divide the trace into Tr_1 over the translational states of particle 1, TR_1 over the internal states of 1, and Tr_{N-1} over the translational states of N-1 structureless perturbers, so that

$$(25) A(\omega) = \frac{\pi \omega}{3hc} (1 - e^{-\beta \hbar \omega}) \lim_{\epsilon \rightarrow 0^+} \text{Re} \text{Tr}_1 \text{TR}_1 \text{Tr}_{N-1} G \rho_N \rho_1$$

Now we want to expand in two particle operators, by isolating the effect of a binary collision in an operator T_{12} defined by

$$(26) G_{12} = G_0 - G_0 T_{12} G_0 \text{ or } T_{12} = -G_0^{-1} (G_{12} - G_0) G_0^{-1}$$

where $G_0 = (\epsilon + i\omega + iL_0 + iL_{int}(1))^{-1}$, $G_{12} = (\epsilon + i\omega + iL_0 + iL_{int}(1) + iL'_{12})^{-1}$

This operator is also discussed in Appendix F. By the identity

$$\frac{1}{A+B} = \frac{1}{A} - \frac{1}{A} B \frac{1}{A+B}, \text{ we have}$$

$$(27) G_{12} = G_0 - G_{12} iL'_{12} G_0 \text{ so that } G_0 T_{12} = G_{12} iL'_{12}$$

Also by the identity, (with α being all pairs of molecules)

$$(28) G = G_0 - \sum_{\alpha} G_0 iL'_{\alpha} G$$

and

$$(29) G = G_{12} - \sum_{\beta \text{ not } 12} G_{12} iL'_{\beta} G = G_{12} - \sum_{\alpha \text{ not } 12} G_0 T_{\alpha} G_{\alpha}$$

Using Equation (29) to iterate Equation (28), we obtain the binary collision expansion (BCE),

$$(30) G = G_0 - \sum_{\alpha} G_0 T_{\alpha} G_0 + \sum_{\alpha \text{ not } \beta} G_0 T_{\alpha} G_0 T_{\beta} G_0 + \dots$$

As in Albers this expansion may be generalized to include triple collisions, by defining an operator which takes into account all processes that three particles can perform other than the first two binary collision processes,

$$(31) \tau(ijk) = -G_0^{-1} G_{ijk} G_0^{-1} - \sum_{\alpha} T_{\alpha} + \sum_{\alpha \text{ not } \beta} T_{\alpha} G_0 T_{\beta}$$

where $G_{ijk} = (\epsilon + i\omega + i(L_0(i) + L_0(j) + L_0(k) + L_j^i + L_k^i + L_{jk}^i))^{-1}$

So we will use

$$(32) \quad G = G_0 + \sum_{\alpha} G_0 T_{\alpha} G_0 - \sum_{\alpha \neq \beta} G_0 T_{\alpha} G_0 T_{\beta} G_0 - \sum_{i < j < k} G_0 T(ijk) G_0$$

By restoring the time integration and explicitly writing out the trace as the sum of diagonal matrix elements, it is easy to obtain³⁷

$$(33) \quad \text{Tr}_1 G_0(1) \tilde{\rho}(1)$$

for the first term, where $G_0(1)$ is $(\epsilon + i\omega + i(L_0(1) + iL_{int}(1)))^{-1}$ and $\tilde{\rho}(1)$ is $\text{Tr}_{N-1} \rho_N$.

Since collisions not involving particle 1 do not affect its motion, only terms in $\text{Tr}_{N-1} \sum_{\alpha} G_0 T_{\alpha} G_0$ in which α is 1j are nonzero. (This can be shown using the invariance of the trace to representation.) Since the N-1 other particles are identical, and $(N-1)/V \approx N/V = \rho$, the sum over α becomes

$$(34) \quad \rho \text{Tr}_{N-1} G_0 V T_{12} G_0 \rho_N = \rho G_0 \text{Tr}_2 V T_{12} G_0 \tilde{\rho}(12)$$

Similarly, from the last two terms, Tr_{N-1} gives

$$(35) \quad \rho^2 G_0(1) \text{Tr}_{2,3} V T_{12} G_0(123) (V T_{13} + V T_{23}) G_0(123) \tilde{\rho}(123) \\ - \rho^2 G_0(1) \text{Tr}_{2,3} V^2 \tau(123) G_0(123) \tilde{\rho}(123)$$

By explicitly writing out the trace over particle 1, using the diagonality of $H_0(1)$ and H_{int} in momentum and internal energy states respectively, and the translational invariance of $\tilde{\rho}$ to reduce the matrix elements, and then restoring to trace and operator form, one finds that (again as in Reference 37)

$$(36) \quad \text{Tr}_1 \text{Tr}_{R_1} \mu_1 G_0(1) \tilde{\rho}(1) \mu_1 = \text{Tr}_1 \text{Tr}_{R_1} \mu_1 R(1) \tilde{\rho}(1) \mu_1$$

where the internal resolvent $R(1)$ is $(\epsilon + i\omega + iL_{int}(1))^{-1}$ and $\tilde{\rho}(1)$ is in the internal and translational space of particle 1.

For the second term, $\text{Tr}_1 \text{Tr}_2 \rho_1 \rho G_0 \text{Tr}_2 V T_{12} G_0 \tilde{\rho}(12)$, we can write³⁷ the reduced density matrix as a sum of correlated and uncorrelated parts,

$$(37) \quad \tilde{\rho}(12) = \tilde{\rho}(1)\tilde{\rho}(2) + \chi(12)$$

Examination of matrix elements using momentum conservation gives the resulting two terms as

$$(38) \quad \text{Tr}_1 \text{Tr}_2 \rho_1 R(1) \text{Tr}_2 V T_{12} \tilde{\rho}(2) R(1) \tilde{\rho}(1) \rho_1 + \text{Tr}_1 \text{Tr}_2 \rho_1 R(1) \text{Tr}_2 V T_{12} G_0(12) \chi(12)$$

Similarly it can be shown that to second order in the density, the trace of the last two terms is

$$(39) \quad \begin{aligned} & \text{Tr}_1 \text{Tr}_2 \rho_1 (\rho^2 R(1) \text{Tr}_{23} V T_{12} R(1) V T_{13} R(1) \tilde{\rho}(1) \tilde{\rho}(2) \tilde{\rho}(3) \\ & + \rho^2 R(1) \text{Tr}_{23} V T_{12} R(1) V T_{13} G_0(13) \tilde{\rho}(2) \chi(13) \\ & + \rho^2 R(1) \text{Tr}_{23} V^2 \tau(123) R(1) \tilde{\rho}(1) \tilde{\rho}(2) \tilde{\rho}(3)) \rho_1 \end{aligned}$$

where terms involving the trace over particles 2 and 3 of T_{23} can be shown (in Appendix A of Reference 37) to vanish because of the form of T_{23} and the fact that the translational density matrix vanishes for large momentum.

Now defining

$$\mathcal{L}(1) = \text{Tr}_2 V T_{12} \tilde{\rho}(2)$$

$$\tau_1(1) = \text{Tr}_2 V T_{12} G_0(12) \chi(12)$$

and $\tau^v(1) = \text{Tr}_{23} V^2 \tau(123) \tilde{\rho}(2) \tilde{\rho}(3)$

the six lowest order terms can be collected and written as

$$(40) \quad \begin{aligned} & \text{Tr}_1 \text{Tr}_2 \rho_1 (R(1) (1 - (\rho \mathcal{L}(1) - \rho^2 \mathcal{L}(1) R(1) \mathcal{L}(1) + \rho^2 + \tau^v(1)) R(1)) \tilde{\rho}(1) \\ & - R(1) (1 - \rho \mathcal{L}(1) R(1)) \rho \tau_1(1)) \rho_1 \end{aligned}$$

Looking at the density expansion Equation (40) we see there is an obvious problem. The ab tetradic element of $R(1) = (\epsilon + i\omega + i\eta \text{Im}\tau(1))^{-1}$, $(\epsilon + i\omega + \frac{i}{\eta} (E_a - E_b))^{-1} = (\epsilon + i(\omega - \omega_{ba}))^{-1}$

behaves like ϵ^{-1} on resonance. So in the limit of $\epsilon \rightarrow 0$ the expansion Equation (40) diverges. What we want, (as pointed out by Zwanzig, Reference 49), is a series in $R(1)^{-1}$.

If the operators in the above equation were classical, or if the full density matrix $\tilde{\rho}$ factored into single particle distribution functions, we could write a density expansion for the inverse of Equation (40), multiply the two series together and solve for the coefficients of the inverse series, which would involve only $R(1)^{-1}$, and then take the $\epsilon \rightarrow 0$ limit and reinvert. (Later, I will actually do only this.) But because $t_1(1)$ satisfies a different algebra than $\mathcal{L}(1)$, we should treat these two independently, as follows.

As is suggested by the first three terms from the binary collision expansion,

$$(R(1) - \rho R(1)\mathcal{L}(1)R(1) + \rho^2 R(1)\mathcal{L}(1)R(1)\mathcal{L}(1)R(1) \dots) \tilde{\rho}(1)$$

one can easily show that there is a general term $R(1) (-\rho \mathcal{L}(1)R(1))^n \tilde{\rho}(1)$ where n is 0 to ∞ , resulting from the term in the BCE

$$\rho^n T_{r_{n-1}} G_0 V T_{12} G_0 V T_{13} \dots G_0 V T_{1n} \tilde{\rho}(1) \tilde{\rho}(2) \dots \tilde{\rho}(n)$$

There are also general terms of the form $R(1) (-\rho^2 + r(1)R(1))^n \tilde{\rho}(1)$,

and indeed $R(1) \binom{m}{n} \frac{m!}{(m-n)!} (-\rho^2 + r(1)R(1))^n (-\rho \mathcal{L}(1)R(1))^{m-n}$ from the $m-n$ permutations of the term from the binary collision expansion

$$\rho^{m+2n} T_{r_{m+2n-1}} G_0 V^2 \tau(123) G_0 V^2 \tau(145) \dots G_0 V^2 \tau(1 2n-1 2n) G_0 V T_{1 2n+1} \\ \times \dots G_0 V T_{1 2n+m} \tilde{\rho}(1) \dots \tilde{\rho}(2n+m)$$

and finally a general term $R(1) (-\rho \mathcal{L}(1)R(1))^n \rho r_1(1)$ One can also show that all other terms are of higher order in the density for that particular process, or vanish.

Then from the identity $\sum_0^{\infty} (-x)^n = \frac{1}{(1+x)}$, where x is $R(1)(\rho L(1) + \rho^2 x^r(1))$ for the series ending with $\tilde{\rho}(1)$, and $R(1)\rho L(1)$ for the $t_1(1)$ terms, we can see that $\text{Tr}_{N-1} G \tilde{\rho}_N$ becomes

$$(R(1)^{-1} + \rho L(1) + \rho^2 x^r(1))^{-1} \tilde{\rho}(1) - (R(1)^{-1} + \rho L(1))^{-1} \rho x_1(1)$$

So if we send ϵ to zero from the positive side and denote operators in that limit by $(\)_+$, we get

$$(41) \quad A(\omega) = \pi \omega / 3\pi c (1 - e^{-\beta \hbar \omega}) \text{Re Tr}_r \text{Tr}_l \nu_1 \left((\rho(\omega + h_{int}^{(1)}) + \rho L(1) + \rho^2 x^r(1))_+^{-1} \tilde{\rho}(1) - (\rho(\omega + h_{int}^{(1)}) + \rho L(1))_+^{-1} x_1(1)_+ \right) \nu_1$$

which is Equation (3.28) of Albers.³⁷

One can also resum by using the same identity in reverse, $(1-x) = \frac{1}{\sum(x)^n}$, and taking only terms in the sum which are to the same order in density as x. Thus using the identity in either direction there is an assumption of ordering in terms of density.

To compare with observed linewidths, we really want to put all terms in one denominator. We will discuss this in Section II D.

On resonance, however, there is one more problem, coming from $x^r(1) = \text{Tr}_{2,3} V^2 \tau(123) \tilde{\rho}(2) \tilde{\rho}(3)$ where $\tau(123)$ is $-\sum_{\alpha\beta\gamma} T_\alpha G_\alpha T_\beta G_\beta T_\gamma$ plus terms involving more T operators, where the indices involve only particles 1, 2, and 3. It is most easily drawn and explained in two dimensions.

Specifically, the problem comes from terms like

$T_{12} G_\alpha T_{13} G_\beta T_{12}$ (in two dimensions) whose matrix elements can,

in either quantum mechanical or classical formulations, eventually be written to include the integral

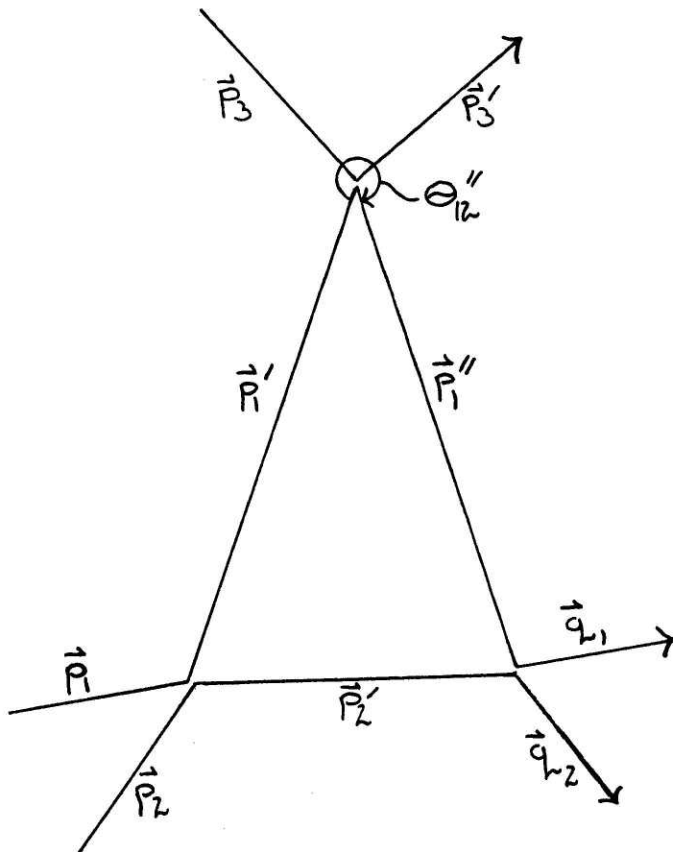
$$(42) \int d\vec{k} d\vec{v}_{12} d\vec{v}'_{12} T_{12} (\epsilon + i\vec{k} \cdot \vec{v}_{12})^{-1} T_{13} (\epsilon + i\vec{k} \cdot \vec{v}'_{12})^{-1} T_{12}$$

so that (in two dimensions) the sum over fourier components of the G_0 operators diverges (logarithmically) for small \vec{k} , or large distances, or values of the scattering angle Θ'_{12} which are close to π . Figure 29 is a schematic representation of this recollision event.

Physically, we have, through an admittedly unlikely set of initial momenta and impact parameters, the possibility that after particle 1 collides with 2 it travels a large distance, before being hit by particle 3 in just such a fashion that it returns to recollide with 2. But even though as the excursion of particle 1 between collisions with 2 becomes larger the probability of the right set of collision parameters to complete the ring decreases, still if one tries to count up all such processes, which allow particle 1 to go even as far as infinity, make a head-on collision, and return, their contribution increases slightly faster. This gives rise to a logarithmically infinite contribution, the weakest divergence, but still a serious problem.

Of course it is obvious that such events would not take place if the other particles in the system were taken into account, and introducing a cutoff k of order of an inverse mean free path would be a good guess. Since the mean free path depends on the density (approximately as $1/\rho$), this

Figure 29: A schematic drawing of a three body recollision event, showing the momenta possessed by the particles at various stages. In two dimensions, processes of this sort in which particle 1 travels a large distance before encountering particle 3, and in which the angle θ_{12}^* is close to π , give rise to the logarithmic divergence.



would give a logarithmic density dependence.

In fact, one can take into account the effect of the other particles by resumming the most likely (most divergent) terms.⁴¹ This replaces T_{13} and the intermediate G_0 by $\rho \mathcal{L}$ and by a propagator which is damped by a factor $\rho \mathcal{L}$, so that the contribution to the triple collision term is

$$\mathcal{T}_{r_2} \sqrt{\mathcal{T}_{12}} (\epsilon + i\omega + i\gamma_0(\nu) + i\gamma_{\text{int}}(\nu) + \rho \mathcal{L}(\nu))^{-1} \rho \mathcal{L}(\nu) G_0 \mathcal{T}_{12} \tilde{\rho}(\nu)$$
which permits an integration over \vec{k} which does not diverge but gives the expected logarithmic density factor.

For the case of the absorption coefficient, when we are off the resonance frequency, the singularity is damped anyway. So we might expect³⁸ that terms would become anomalously large only around 0.1 cm^{-1} from line center.

This logarithmic term has been heavily discussed.^{50,51} Its existence has been questioned,⁵² its size has been estimated,⁵³ and the density dependence of transport coefficients has been studied to find experimental evidence for it.⁵¹ Even the work here on second density effects has implications for finding logarithmic terms, which appear in three dimensions in third order in density. In three dimensions the same sort of trouble arises from certain four body collisions.⁵³ Although we cannot hope to see these directly, one might be able to infer something about their size from the size of the second order density effects discussed in this work.

We will conclude this section by giving the explicit

tetradic element expressions for the three contributions from three body collision processes, (dynamical correlations in second order in the density), $T_{12} G_0 T_{13} G_0 T_{12}$, $T_{12} G_0 T_{23} G_0 T_{12}$, and $T_{12} G_0 T_{23} G_0 T_{13}$.

First we look at $\frac{1}{\hbar^3} \text{Tr} (V^2 T_{12} G_0 T_{13} G_0 T_{12} \tilde{\rho}(2) \tilde{\rho}(3))$, which becomes (by the rules of tetradic algebra, given in References 37 and 39),

$$(43) \quad \frac{1}{\hbar^3} \sum_{\substack{\vec{p}_1, \vec{p}_1', \vec{p}_2, \vec{p}_2', \vec{p}_3, \vec{p}_3', \vec{q}_1, \vec{q}_1', \vec{q}_2, \vec{q}_2', \vec{q}_3, \vec{q}_3'}} V^2 T_{12} (a_{\vec{p}_1, \vec{p}_2} b_{\vec{p}_1', \vec{p}_2'} a_{\vec{p}_1', \vec{p}_2'} b_{\vec{p}_1, \vec{p}_2}) G_0 (a_{\vec{p}_1', \vec{p}_2'} b_{\vec{p}_1, \vec{p}_2}) \\ \times T_{13} (a_{\vec{p}_1', \vec{p}_3} b_{\vec{p}_1, \vec{p}_3} a_{\vec{q}_1', \vec{p}_3} b_{\vec{q}_1, \vec{p}_3}) G_0 (a_{\vec{q}_1', \vec{p}_3} b_{\vec{q}_1, \vec{p}_3}) \\ \times T_{12} (a_{\vec{q}_1', \vec{q}_2'} b_{\vec{q}_1, \vec{q}_2'} a_{\vec{q}_1, \vec{q}_2} b_{\vec{q}_1', \vec{q}_2}) \tilde{\rho}_{\vec{q}_2} \tilde{\rho}_{\vec{p}_3}$$

By translational invariance (see Equation (B.4) of Reference 37) the T operators contain momentum conservation conditions.

From the first T_{12} we have $\vec{p}_1 + \vec{p}_2 = \vec{p}_1' + \vec{p}_2'$ and $\vec{p}_1 + \vec{p}_2 = \vec{p}_1'' + \vec{p}_2''$, or $\vec{p}_2'' = \vec{p}_2' + (\vec{p}_1' - \vec{p}_1'')$. And from $\vec{p}_1' + \vec{p}_3 = \vec{q}_1' + \vec{p}_3'$ and $\vec{p}_1'' + \vec{p}_3 = \vec{q}_1'' + \vec{p}_3'$, by subtracting we find $\vec{p}_1' - \vec{p}_1'' = \vec{q}_1' - \vec{q}_1''$.

It is useful to define $\hbar \vec{k} = \vec{p}_1' - \vec{p}_1''$, so that when we sum over the two delta functions in \vec{p}_2' and \vec{q}_1'' we get

$$(44) \quad \frac{1}{\hbar^3} \sum_{\substack{\vec{k}, \vec{p}_1, \vec{p}_1', \vec{q}_1, \vec{q}_1', \vec{q}_2, \vec{p}_2, \vec{p}_2', \vec{p}_3, \vec{p}_3'}} V^2 T_{12} (a_{\vec{p}_1, \vec{p}_2} b_{\vec{p}_1', \vec{p}_2'} a_{\vec{p}_1', \vec{p}_2'} b_{\vec{p}_1, \vec{p}_2} - \hbar \vec{k} \cdot \vec{p}_2' + \hbar \vec{k}) G_0 (a_{\vec{p}_1', \vec{p}_2'} b_{\vec{p}_1, \vec{p}_2} - \hbar \vec{k} \cdot \vec{p}_2' + \hbar \vec{k}) \\ \times T_{13} (a_{\vec{p}_1', \vec{p}_3} b_{\vec{p}_1, \vec{p}_3} - \hbar \vec{k} \cdot \vec{p}_3 a_{\vec{q}_1', \vec{p}_3} b_{\vec{q}_1, \vec{p}_3} - \hbar \vec{k} \cdot \vec{p}_3) G_0 (a_{\vec{q}_1', \vec{p}_3} b_{\vec{q}_1, \vec{p}_3} - \hbar \vec{k} \cdot \vec{p}_3 + \hbar \vec{k}) \\ \times T_{12} (a_{\vec{q}_1', \vec{q}_2'} b_{\vec{q}_1, \vec{q}_2'} - \hbar \vec{k} \cdot \vec{p}_2' + \hbar \vec{k} a_{\vec{q}_1, \vec{q}_2} b_{\vec{q}_1', \vec{q}_2}) \tilde{\rho}_{\vec{q}_2} \tilde{\rho}_{\vec{p}_3}$$

From Equation (3.13) of Reference 37, to first order in \vec{k} , we have that

$$(45) \quad G_0 (a_{\vec{p}_1', \vec{p}_2'} b_{\vec{p}_1, \vec{p}_2} - \hbar \vec{k} \cdot \vec{p}_2' + \hbar \vec{k}) = \\ (\epsilon + i\omega + \frac{1}{\hbar} (E_0 - E_0 + E(\vec{p}_1', \vec{p}_2') - E(\vec{p}_1' - \hbar \vec{k}, \vec{p}_2' + \hbar \vec{k})))^{-1}$$

is $(\epsilon + i(\omega - \omega_{b0}) + i\vec{k} \cdot \vec{p}_{12, m})^{-1}$

For $T_{12}^G T_{23}^G T_{12}$ we have³⁹

$$(46) \quad \sum_{\vec{P}_1 \vec{P}_1'} V_{h_3} V^2 \sum_{\vec{q}_1 \vec{q}_2 \vec{q}_1'} T_{12} (a_{\vec{P}_1 \vec{P}_2} b_{\vec{P}_1 \vec{P}_2} a_{\vec{q}_1 \vec{q}_2} b_{\vec{q}_1'} (\vec{q}_2 - \vec{q}_1 + \vec{q}_1')) G_0 (a_{\vec{q}_1 \vec{q}_2} b_{\vec{q}_1'} (\vec{q}_2 - \vec{q}_1 + \vec{q}_1)) \\ \times T_{23} (q_2 P_3 (q_2 - q_1 + q_1) P_3 q_2' P_3' (q_1 + q_2 - q_1) P_3') G_0 (a_{\vec{q}_1 \vec{q}_2} b_{\vec{q}_1'} (\vec{q}_2 - \vec{q}_1 + \vec{q}_1)) \\ \times T_{12} (a_{\vec{q}_1 \vec{q}_2} b_{\vec{q}_1'} (\vec{q}_2 - \vec{q}_1 + \vec{q}_1) a_{\vec{P}_1 \vec{P}_2'} b_{\vec{P}_1 \vec{P}_2'}) \tilde{P}_{P_2'} \tilde{P}_{P_3'}$$

which becomes

$$(47) \quad \sum_{\vec{P}_1 \vec{P}_1'} V_{h_3} V^2 \sum_{\vec{q}_1 \vec{q}_2 \vec{q}_1'} T_{12} (a_{\vec{P}_1 \vec{P}_2} b_{\vec{P}_1 \vec{P}_2} a_{\vec{q}_1 \vec{q}_2} b_{\vec{q}_1'} + \hbar \vec{K} \cdot \vec{q}_2 + \hbar \vec{K}) (\epsilon + i(\omega - \omega_{ba}) + i\vec{K} \cdot \vec{P}_{12/m})^{-1} \\ \times T_{23} (\vec{q}_2 P_3 \vec{q}_2 + \hbar \vec{K} \cdot \vec{q}_3 \vec{q}_2' P_3' \vec{q}_2 + \hbar \vec{K} \cdot \vec{P}_3') (\epsilon + i(\omega - \omega_{ba}) + i\vec{K} \cdot \vec{P}_{12/m})^{-1} \\ \times T_{12} (a_{\vec{q}_1 \vec{q}_2} b_{\vec{q}_1'} + \hbar \vec{K} \cdot \vec{q}_2 + \hbar \vec{K} a_{\vec{P}_1 \vec{P}_2'} b_{\vec{P}_1 \vec{P}_2'}) \tilde{P}_{P_2'} \tilde{P}_{P_3'}$$

with $\hbar \vec{K} = \vec{q}_1 - \vec{q}_1'$, $\vec{P}_{12/m} = \vec{q}_1/m_1 - \vec{q}_2/m_2$, $\vec{P}_{12/m}' = \vec{q}_1'/m_1 - \vec{q}_2'/m_2$

And for $T_{12}^G T_{23}^G T_{13}$ we have³⁹

$$(48) \quad \sum_{\vec{P}_1 \vec{P}_1'} V_{h_3} V^2 \sum_{\vec{q}_1 \vec{q}_2 \vec{q}_1'} T_{12} (a_{\vec{P}_1 \vec{P}_2} b_{\vec{P}_1 \vec{P}_2} a_{\vec{q}_1 \vec{q}_2} b_{\vec{q}_1'} (\vec{q}_2 - \vec{q}_1')) G_0 (a_{\vec{q}_1 \vec{q}_2} b_{\vec{q}_1'} (\vec{q}_2 - \vec{q}_1)) \\ \times T_{23} (\vec{q}_2 P_3 \vec{q}_2' P_3' \vec{q}_2' P_2' \vec{q}_3' P_2' \vec{q}_3') G_0 (a_{\vec{q}_1 \vec{q}_2} b_{\vec{q}_1'} (\vec{q}_2 - \vec{q}_1)) \\ \times T_{13} (a_{\vec{q}_1 \vec{q}_2} b_{\vec{q}_1'} (\vec{q}_2 - \vec{q}_1) a_{\vec{P}_1 \vec{P}_3'} b_{\vec{P}_1 \vec{P}_3'}) \tilde{P}_{P_2'} \tilde{P}_{P_3'}$$

which with $\vec{q}_1 - \vec{q}_1' = \vec{K}$ so that $\vec{q}_2' = \vec{q}_2 + \vec{K}$ and $\vec{q}_3' = \vec{q}_3 + \vec{K}$ becomes

$$(49) \quad \sum_{\vec{P}_1 \vec{P}_1'} V_{h_3} V^2 \sum_{\vec{q}_1 \vec{q}_2 \vec{q}_1'} T_{12} (a_{\vec{P}_1 \vec{P}_2} b_{\vec{P}_1 \vec{P}_2} a_{\vec{q}_1 \vec{q}_2} b_{\vec{q}_1'} + \hbar \vec{K} \cdot \vec{q}_2 + \hbar \vec{K}) (\epsilon + i(\omega - \omega_{ba}) + i\vec{K} \cdot \vec{q}_{12/m})^{-1} \\ \times T_{23} (q_2 P_3 q_2 + \hbar \vec{K} \cdot P_3 P_2' q_3 P_2' q_3 + \hbar \vec{K}) (\epsilon + i(\omega - \omega_{ba}) + i\vec{K} \cdot \vec{q}_{13/m})^{-1} \\ \times T_{13} (a_{\vec{q}_1 \vec{q}_2} b_{\vec{q}_1'} + \hbar \vec{K} \cdot \vec{q}_2 + \hbar \vec{K} a_{\vec{P}_1 \vec{P}_3'} b_{\vec{P}_1 \vec{P}_3'}) \tilde{P}_{P_2'} \tilde{P}_{P_3'}$$

In Section II C, the results of Equations (44) and (45) will be obtained again from expressions in Reference 38, and will serve as a basis for the estimation of three body recollision corrections to the linewidth. With the approximations made there, the contributions of Equations (47) and (49) can then be estimated by analogy, without additional detailed calculations.

B. The Low Density Limit

The Lorentzian function,

$$(50) \quad \alpha(\omega) \propto \frac{\gamma}{((\omega - \omega_{ba})^2 + \gamma^2)}$$

is often used to represent lineshapes at low densities. The linewidth γ is a number often written as $\rho \bar{v} \sigma^p / 2\pi c$ in frequency units, where ρ is the density, \bar{v} an average velocity, and σ^p a pressure broadening cross section.³¹

In this section, we want to detail the approximations necessary to obtain the simple Lorentzian from the form for the absorption coefficient derived in Section A or taken from Reference 37, Equation (3.28), to lowest order in the density, so considering only binary collisions.

This is

$$(51) \quad \text{Tr}_i (\mu_i (\epsilon + i\omega + iL_{int}(i) + \rho L(i))^{-1} \mu_i \tilde{\rho}(i))$$

Writing out in matrix and tetradic elements, the trace is defined as

$$(52) \quad \sum_{\substack{a,b,c \\ \bar{a}, \bar{b}}} \mu_{ba} (\epsilon + i\omega + iL_{int}(i) + \rho L(i))^{-1} (a_{\bar{a}b} b_{\bar{c}a} a'_{\bar{c}b'} b'_{\bar{a}c'}) \tilde{\rho}^{(i)}(a'_{\bar{c}b'} c_{\bar{a}b'}) \mu_{c\bar{b}}$$

The distribution function $\tilde{\rho}^{(i)}$ should also be taken to lowest order in the density, and since we know that matrix elements

of $\langle i | \tilde{\rho}^{(i)} | i \rangle = \frac{e^{-\beta(H_0 + H_{int}(i))}}{\sum_j e^{-\beta(H_0 + H_{int}(j))}}$ will just lead to factors of $e^{-\beta P_i^2 / 2m}$ and $e^{-\beta E_{a'}}$, $\tilde{\rho}^{(i)}$ is diagonal in internal state indices.

We now write the operator identity

$$(53) \quad \frac{1}{(i\omega + iL_{int} + \rho L)} = \frac{1}{(i\omega + iL_{int})} (1 + \rho L \sum_0^{\infty} (\frac{1}{(i\omega + iL_{int})} \rho L)^n \frac{1}{(i\omega + iL_{int})})$$

and first take internal state tetradic elements,

$$(54) \quad (i\omega + iL_{int} + \rho L)^{-1}_{abcd} = \left(\frac{1}{i(\omega - \omega_{ba})} \Delta_{ab} \Delta_{cd} + \frac{1}{i(\omega - \omega_{ba})} \rho L_{abcd} \frac{1}{i(\omega - \omega_{dc})} \right) \\ + \sum_{mn} \frac{1}{i(\omega - \omega_{ba})} \rho L_{abmn} \frac{1}{i(\omega - \omega_{mn})} \rho L_{mncd} \frac{1}{i(\omega - \omega_{dc})} + \dots$$

Now if we are looking at isolated lines, which is true except at the highest densities for HCl and perhaps HF, the frequency denominators will eliminate all ω_{mn} except the ω_{ba} near the ω we observe with, because $(\omega - \omega_{mn}) \gg \mathcal{L}_{abmn}$ for all mn but ab . (For a discussion of the case of overlapping lines, see Reference 54 or 55.) So we have \mathcal{L}_{abab} , which can now appear in the denominator.

We have more difficulty in treating the momentum tetradic elements in such a fashion that Equation (52) may be replaced by an expression with a momentum dependent tetradic element of \mathcal{L} in the denominator. If we look at

$$\sum_{\vec{P}, \vec{P}'} (\mathcal{I}(\omega - \omega_{ba} + \rho \mathcal{L}(1)))^{-1} (\vec{P}, \vec{P}, \vec{P}', \vec{P}') \phi(\vec{P}') = \sum_{\vec{P}, \vec{P}'} \left(\frac{1}{\mathcal{I}(\omega - \omega_{ba})} \Delta \vec{P}, \vec{P}' \Delta \vec{P}, \vec{P}' \right. \\ \left. + \frac{1}{\mathcal{I}(\omega - \omega_{ba})} \rho \mathcal{L}(\vec{P}, \vec{P}, \vec{P}', \vec{P}') \frac{1}{\mathcal{I}(\omega - \omega_{ba})} + \sum_{\vec{P}''} \frac{1}{\mathcal{I}(\omega - \omega_{ba})} \rho \mathcal{L}(\vec{P}, \vec{P}, \vec{P}'', \vec{P}'') \frac{1}{\mathcal{I}(\omega - \omega_{ba})} \rho \mathcal{L}(\vec{P}'', \vec{P}'', \vec{P}', \vec{P}') \frac{1}{\mathcal{I}(\omega - \omega_{ba})} + \dots \right) \phi(\vec{P}') \quad (55)$$

one approximation we can make is to assume a constant change of momentum (on the average) so that $\vec{p}_1 - \vec{p}_1'' = \vec{p}_1'' - \vec{p}_1'$ and so on, and we may have $\rho \mathcal{L}(\vec{p}_1, \vec{p}_1, \vec{p}_1', \vec{p}_1')$ in the denominator.

A more drastic approximation is to assume that initial and final momenta are the same, so that $\mathcal{L}(\vec{p}_1, \vec{p}_1, \vec{p}_1, \vec{p}_1)$ may immediately appear in the denominator. This straight-line path approximation is actually useful in pressure broadening theory, because collisions which change, for instance, the orientation or speed of rotation of a diatomic molecule can involve long range forces which have little effect on the momenta.^{29, 61-64} The approximation that the momentum change of particle 1 in a collision is negligible is certainly good in the limit of

a Brownian particle, of much greater mass than the perturbers.⁶⁴

If as an extension of these series expansions in powers of $\rho \mathcal{L}$ one assumes that $\rho \mathcal{L}$, though an operator describing momentum changes during collisions, operates on its momentum eigenfunctions to give a number, not a function of momentum, one obtains the analog of the Chapman-Enskog approximation.⁵⁷⁻⁶⁰

There is yet another way of approaching this problem, variations of which have been used in treating the problem of combined Doppler and collision broadening.⁶⁵⁻⁶⁷ (We will discuss Doppler broadening at the end of this section.) As discussed in Appendix F and Section II C, the binary collision operator (and therefore $\mathcal{L} = \langle \mathcal{V}_{12} \rangle_{\mathcal{L}}$) is composed of two parts, a noninteracting part \mathcal{L}^{non} which is diagonal in momentum and an interacting part \mathcal{L}^{int} which is not. So instead of the expansion in Equation (55) we may have

$$\begin{aligned}
 (56) \quad & \sum_{\vec{R}\vec{R}'} \left(\downarrow \right. \\
 & \left. \frac{\rho \mathcal{L}^{\text{non}}}{i(\omega - \omega_{ba}) + \rho \mathcal{L}^{\text{non}}(\vec{R})} \Delta \vec{R} \vec{R}' \Delta \vec{R} \vec{R}' \phi(\vec{R}') \right) \\
 & + \left(\downarrow \right. \\
 & \left. \frac{\rho \mathcal{L}^{\text{int}}(\vec{R}\vec{R}'\vec{R}'\vec{R}')}{i(\omega - \omega_{ba}) + \rho \mathcal{L}^{\text{non}}(\vec{R})} \right) \left(\downarrow \right. \\
 & \left. \frac{\rho \mathcal{L}^{\text{non}}}{i(\omega - \omega_{ba}) + \rho \mathcal{L}^{\text{non}}(\vec{R}')} \phi(\vec{R}') \right) \\
 & + \sum_{\vec{R}''} \left(\downarrow \right. \\
 & \left. \frac{\rho \mathcal{L}^{\text{int}}(\vec{R}\vec{R}''\vec{R}'\vec{R}')}{i(\omega - \omega_{ba}) + \rho \mathcal{L}^{\text{non}}(\vec{R})} \right) \left(\downarrow \right. \\
 & \left. \frac{\rho \mathcal{L}^{\text{int}}(\vec{R}''\vec{R}''\vec{R}'\vec{R}')}{i(\omega - \omega_{ba}) + \rho \mathcal{L}^{\text{non}}(\vec{R}'')} \right) \left(\downarrow \right. \\
 & \left. \frac{\rho \mathcal{L}^{\text{non}}}{i(\omega - \omega_{ba}) + \rho \mathcal{L}^{\text{non}}(\vec{R}')} \phi(\vec{R}') + \dots \right)
 \end{aligned}$$

There are two complementary limits which may be taken in order to sum this expansion. In one, we imagine that the value of \mathcal{L}^{int} depends only on the last indices, the momentum after collision, and that each contains a Maxwellian distribution function for this last momentum, so that each term factors into powers of

$$\int \frac{\phi(\vec{p}) d\vec{p}}{i(\omega - \omega_{ba}) + \rho \mathcal{L}^{\text{non}}(\vec{p})} \rho \mathcal{L}^{\text{int}}(\vec{p})$$

and the spectrum is proportional to

$$(57) \quad \left(1 - \frac{\int \phi(p) dp \rho \mathcal{L}^{int}(p)}{\int \phi(p) dp (\nu(\omega - \omega_{ba}) + \rho \mathcal{L}^{non}(p))} \right)^{-1}$$

This is the hard collision approximation, so called because each collision is violent enough to destroy all memory of the previous momenta. It is discussed in References 68 through 71.

The alternate soft collision limit of small momentum changes with a Gaussian distribution centered around zero is based on the same assumptions that allow one to obtain the Fokker-Planck equation from the Boltzmann equation.⁷²⁻⁷⁸

Moving on to other approximations, the full expression for T_{12} and thus $\mathcal{L}(\omega)$, given in References 38 and 79, depends on ω . The assumption that the frequency difference $\omega - \omega_{ba}$ in the range of interest, of the order of $\rho \mathcal{L}_{ab}$, is negligible compared with the energies found in the definition of the t matrices, or alternatively (in Fourier transform space) that the time between collisions which change the energy by no more than a specified amount is much greater than the time of a collision, is the basis of the impact approximation.^{31,80-87}

Next, $\mathcal{L}(\omega)$ still depends on p_1 , and so in general an integration over the Maxwellian and this momentum dependent denominator has an effect on the lineshape, but it is small.⁸⁸⁻⁸⁹ Therefore the usual approximation made³¹ is to say that the integration over the Maxwell distribution has the effect of

replacing the momenta in $\mathcal{L}(\rho_i)$ by their thermal averages.

Then with the integration over the momentum part of $\tilde{\rho}^{(1)}$, the internal part, $e^{-\beta E_a}$, is just the statistical weight for the initial state, and $\rho \mathcal{L}$ is just a number which we can call γ , so indeed we have obtained the Lorentzian lineshape, Equation (50), by taking the real part of the denominator.

There is, however, yet one more approximation which we must discuss, involving the contribution of Doppler broadening. In Equations (51) and (52) we had actually made the dipole approximation⁹¹, which says that since the wavelength of light λ (or the reciprocal of the wave vector k , $k = 2\pi/\lambda$) is much larger than a molecular size, we can ignore the fact that Equation (51) should actually be

$$(58) \text{Tr}_i \rho_i e^{i\vec{k} \cdot \vec{r}_i} (\epsilon + i\omega + i\gamma_{lmr}^{(1)} + i\gamma_{l0}^{(1)} + \rho \mathcal{L}^{(1)})^{-1} \tilde{\rho}^{(1)} e^{-i\vec{k} \cdot \vec{r}_i} \rho_i$$

so that Equation (52) becomes

$$(59) \sum_{\vec{q}_1, \vec{q}_1', \vec{q}_1''} \rho_{ba} \langle \vec{p}_i | e^{i\vec{k} \cdot \vec{r}_i} | \vec{q}_1 \rangle (\epsilon + i\omega + i\gamma_{lmr}^{(1)} + i\gamma_{l0}^{(1)} + \rho \mathcal{L}^{(1)})^{-1} \langle \vec{q}_1 | \vec{p}_i \rangle \langle \vec{q}_1' | \vec{p}_i \rangle \langle \vec{q}_1'' | \vec{p}_i \rangle \times \tilde{\rho}^{(1)} \langle \vec{q}_1' | \vec{p}_i \rangle \langle \vec{q}_1'' | \vec{p}_i \rangle \rho_{cb}$$

or, quickly making some of the same approximations,

$$(60) \sum_{\vec{q}_1, \vec{q}_1'} \rho_{ba} (\epsilon + i\omega + i\gamma_{lmr}^{(1)} + i\gamma_{l0}^{(1)} + \rho \mathcal{L}^{(1)})^{-1} \langle \vec{q}_1 | \vec{p}_i \rangle \langle \vec{q}_1' | \vec{p}_i \rangle \tilde{\rho}_{ap}^{(1)} \rho_{cb}$$

In the expansion analogous to Equation (65), the tetradic element of G_0 is

$$(\epsilon + i\omega + i\gamma_{lmr}^{(1)} + i\gamma_{l0}^{(1)})^{-1} \langle \vec{q}_1 | \vec{p}_i \rangle \langle \vec{q}_1' | \vec{p}_i \rangle = \langle \epsilon + i(\omega - \omega_{ba} - i\vec{k} \cdot \vec{p}_i/m) \rangle^{-1}$$

where \vec{k} is still the wave vector of light. When $\vec{k} \cdot \vec{p}_i/m$ is large compared to $\rho \mathcal{L}_{ab}$, we need only retain the first term (G_0) in the expansion. Then integration of the denominator and the Maxwellian distribution of momenta produces a Gaussian frequency distribution, the Doppler lineshape.

We will perform this integration in two different ways, since each method has some instructive features. First, we proceed straightforwardly from Equation (60) and its following definition. If we take the \vec{k} vector to be in the p_z direction, and ignore the normalization of the Maxwell distribution and all other prefactors, we have

$$\text{Re } i \int_{-\infty}^{\infty} e^{-\beta p_z^2 / 2m} (i\epsilon - (\omega - \omega_{ba}) + K p_z / m)^{-1} dp_z$$

which is

$$\text{Re } -\pi \text{Res} (i\epsilon - (\omega - \omega_{ba}) + K p_z / m)^{-1} e^{-\beta p_z^2 / 2m}$$

evaluated at the pole $p_z = \frac{m}{K} (\omega - \omega_{ba} - i\epsilon)$. (The pole only contributes πi because as ϵ goes to zero, the pole is on the real axis and the integration path is only indented around an angle π .) So letting ϵ go to zero, taking the real part, and again ignoring constants we have the Gaussian frequency distribution of the Doppler lineshape,

$$e^{-\beta / 2m \left(\frac{(\omega - \omega_{ba})m}{K} \right)^2} = e^{-\beta m / 2 \left(\frac{(\omega - \omega_{ba})}{K} \right)^2}$$

In an alternative method we rewrite the denominator as an integration over a variable t which has the units of time, which means effectively returning to the time representation of Equation (21).

$$\int_0^{\infty} e^{-(\epsilon + i(\omega - \omega_{ba}) - iK p_z / m)t} dt$$

We then integrate over momentum and the Maxwell distribution,

now writing the normalization simply as N .

$$N \int_{-\infty}^{\infty} e^{-\beta p_z^2 / 2m} e^{-iK p_z t / m} dp_z$$

$$= N e^{-K^2 t^2 / 2m\beta} \left(\int_{-\infty}^{\infty} e^{-\beta / 2m (p_z + iKt/\beta)^2} d(p_z + iKt/\beta) \right) = e^{-K^2 t^2 / 2m\beta}$$

Having obtained this Gaussian in time, the Doppler time correlation function, we can let ϵ go to zero and do the time integration, again by completing the square in the exponent, so that

$$\begin{aligned} & \int_0^\infty e^{i(\omega - \omega_{ba})\tau} e^{-K^2\tau^2/2m\beta} d\tau \\ &= e^{-K^2/2m\beta} (m\beta/K^2(\omega - \omega_{ba}))^2 \int_0^\infty e^{-K^2/2m\beta} (\tau + i m\beta/K^2(\omega - \omega_{ba}))^2 d\tau \\ &\propto e^{-m\beta/2K^2(\omega - \omega_{ba})^2} \end{aligned}$$

The one-dimensional root-mean-square velocity, which we denote by \bar{v}_z , is $(1/\beta m)^{1/2}$. The half width at half maximum of a Gaussian e^{-x^2/a^2} is reached when x/a is $\sqrt{\ln 2}$. So the Doppler halfwidth is given by the simple formula $\sqrt{\ln 2} K \bar{v}_z$.

In the case when neither pressure broadening nor Doppler broadening is negligible, if we use one of the approximations discussed above to put the linewidth operator into the denominator, we must still integrate over a speed dependent width along with a Doppler shift. Again, the effect is small.⁹⁰ So if we ignore it we obtain a function intermediate between a Gaussian and a Lorentzian and traditionally used to describe combined Doppler and pressure broadening, the Voigt profile

$$(61) \quad \alpha(\omega) \propto \int (\gamma(\omega - \omega_{ba}) - i\vec{k} \cdot \vec{p}_i/m + p^2 \mathcal{L}_{ab})^{-1} \phi(p_i) d\vec{p}_i$$

And, of course, if $\vec{k} \cdot \vec{p}_i/m$ is much smaller than $p^2 \mathcal{L}_{ab}$, we may ignore it and again obtain a Lorentzian. This approximation is obviously good at high densities, and will be used in all that follows.

To summarize, we list approximations we found to be needed to arrive at a Lorentzian lineshape.

1. To obtain a linewidth which is linearly proportional to the density we assumed only binary collisions occur. This was done by resumming the binary collision expansion only in lowest order in the density. We also ignored correlations in the density matrices for different particles.

2. We assumed isolated lines, thus ignoring interference terms which can lead to a non-Lorentzian shape.

3. We had to adopt some approximation in regard to the momentum change in order to obtain a momentum dependent collision operator in the denominator of the linewidth expression. In pressure broadening theory this is most often the straight-line path assumption.

4. We made the impact approximation, which can be expressed as ignoring the ω dependence of the t matrices.

5. After Approximation 3, we then assumed a momentum-independent width.

6. We ignored the Doppler shift.

In Appendix F and Section II C we justify the use of the simple Anderson³¹ formula for the linewidth in terms of a cross section, $\frac{\rho \bar{v} \sigma_{pp}}{2\pi c}$. For more accurate, fully quantum-mechanical calculations one may use the formulas of Baranger⁸⁰⁻⁸² in terms of scattering amplitudes. Semiclassical approximations may be used on the quantum formulas we began with, for instance to obtain the classical Fourier integral^{92,93} or Anderson theory.⁹⁴

C. The Triple Collision Contribution to the Linewidth

We begin our discussion of the triple collision contributions with the $T_{12}G_0T_{13}G_0T_{12}$ term, whose tetradic element representation was given in Section II A. However, we will start here with a version of Equation (2.24) of Reference 38,

$$(62) \sum_{\substack{\vec{k}, \vec{p}_1, \vec{p}_2 \\ \vec{q}_1, \vec{q}_2 \\ \vec{q}'_1, \vec{q}'_2}} \frac{1}{\chi} \chi^2 T_{12}(a_{\vec{p}_1 \vec{p}_2} b_{\vec{p}_1 \vec{p}_2} a_{\vec{q}_1 \vec{q}_2} b_{\vec{q}_1 \vec{q}_2} + \hbar \vec{k} \cdot \vec{q}_2 + \hbar \vec{k}) (\epsilon + i(\omega - \omega_{ba} + i\vec{k} \cdot \vec{v}_{12})^{-1}) \\ \times T_{13}(a_{\vec{q}_1 \vec{p}_3} b_{\vec{q}_1 \vec{p}_3} + \hbar \vec{k} \cdot \vec{p}_3) a_{\vec{q}'_1 \vec{p}'_3} b_{\vec{q}'_1 \vec{p}'_3} - \hbar \vec{k} \cdot \vec{p}'_3) (\epsilon + i(\omega - \omega_{ba}) + i\vec{k} \cdot \vec{v}'_{12})^{-1} \\ \times T_{12}(a_{\vec{q}'_1 \vec{q}'_2} b_{\vec{q}'_1 \vec{q}'_2} - \hbar \vec{k} \cdot \vec{q}'_2 + \hbar \vec{k} \cdot \vec{p}'_2) \tilde{\rho}_{\vec{p}_2} \tilde{\rho}_{\vec{p}'_3}$$

This expression differs from Equation (2.24) of Reference 38 in that all momenta involved in the trace have been summed over, and the sums over intermediate internal states have been omitted since (as discussed in Section II B) vibration-rotation lines are spaced widely enough that only one G_0 denominator (here the ab element) contributes for a given frequency. (The wave vector \vec{k} is $(\vec{q}_1 - \vec{q}'_1)/\chi$ and was generated by momentum conservation conditions in the T operators, as discussed in Section II A and Reference 38. Since terms of order \vec{k}^2 are unimportant in the G_0 denominators, we can ignore the \vec{k} dependence of \vec{v}_{12} and \vec{v}'_{12} and find from Equations (2.28) and (2.29) of Reference 38 that \vec{v}_{12} is $\vec{q}_1/m_1 - \vec{q}_2/m_2$ and \vec{v}'_{12} is $\vec{q}'_1/m_1 - \vec{q}'_2/m_2$.

With approximations discussed in Appendix F, as an example the first T_{12} tetradic when expressed in terms of t matrix elements becomes (writing the volume normalization explicitly)

$$(63) \quad \frac{1}{V^2} (\frac{1}{V^2} a_{\vec{p}_1 \vec{p}_2} a_{\vec{q}_1 \vec{q}_2} \Delta_{\vec{p}_1 \vec{q}_1} \Delta_{\vec{p}_2 \vec{q}_2} + \hbar \vec{k} \Delta_{\vec{p}_2 \vec{q}_2} + \hbar \vec{k} - \frac{1}{V^2} b_{\vec{p}_1 \vec{p}_2}^* b_{\vec{q}_1 \vec{q}_2} - \hbar \vec{k} \Delta_{\vec{p}_1 \vec{q}_1} \Delta_{\vec{p}_2 \vec{q}_2} + 2\pi i \delta(E(a_{\vec{p}_1 \vec{p}_2}) - E(b_{\vec{q}_1 \vec{q}_2})) \frac{1}{V^2} a_{\vec{p}_1 \vec{p}_2} a_{\vec{q}_1 \vec{q}_2} + \frac{1}{V^2} b_{\vec{p}_1 \vec{p}_2}^* b_{\vec{q}_1 \vec{q}_2} - \hbar \vec{k} \Delta_{\vec{q}_1 \vec{q}_2} + \hbar \vec{k})$$

The first two and last terms are referred to as noninteracting, or forward scattering, and interacting terms respectively.

From Equation 63 it can be seen that both T_{12} terms contain a matrix element of the form $\frac{1}{V^2} \vec{p}_1 \vec{p}_2 + \hbar \vec{k}$, while T_{13} will give no low order \vec{k} dependence. In the classical path version of this \vec{k} vector formalism,⁹⁵ it is from these two T_{12} operators that one obtains a factor $e^{i\vec{k} \cdot \vec{\rho}}$, where $\vec{\rho}$ is a function of the parameters of the first and second 1-2 collisions. This factor seems to be necessary to show that the part of the $T_{12} G_0 T_{13} G_0 T_{12}$ term which contains the noninteracting part of the T_{13} operator is zero. Of course it is easy to see physically why that part should give no contribution, since two successive collisions between two particles cannot occur without some change in the intermediate path of at least one particle.⁹⁵⁻⁹⁷

(The fact that in the first order term, $\langle \sqrt{T_{12}} \rangle$, the contribution from the noninteracting part of T_{12} is larger and of opposite sign than that from the interacting part, while in one of the three T operators in the triple collision expression the noninteracting part gives zero will mean that the contribution from these triple collisions will be negative with respect to the first order linewidth. We will give more discussion on this point when we transform into cross sections.)

In the quantum mechanical formulation t matrix elements from the two T_{12} tetradics contain a similar factor $e^{i\vec{k}\cdot\vec{r}_{12}}$ along with some function of the (finite range) intermolecular potential $V(\vec{r}_{12})$. This will also make the contribution to the \vec{k} integral from large values of \vec{k} finite, effectively cutting off the region of integration at some upper limit k_0 . Estimates of the size of k_0 using step and square well potentials and the first Born approximation are made in Appendix G.

So with these comments we may ignore the \vec{k} dependence of the T operators, but we must retain \vec{k} in the G_0 denominators. We can write (relabeling momenta)

$$(64) \quad \frac{V_{\vec{k}}}{\hbar} \sum_{\vec{R}, \vec{R}'} \frac{V_{\vec{k}}}{\hbar} \sum_{\vec{R}''} T_{12}(a\vec{p}_1\vec{p}_2 b\vec{p}_1'\vec{p}_2' a\vec{p}_1''\vec{p}_2'' b\vec{p}_1''\vec{p}_2'') (\epsilon + i(\omega - \omega_{ba}) + i\vec{k}\cdot(\frac{\vec{p}_1 - \vec{p}_2}{m_1 m_2}))^{-1} \\ \times T_{13}(a\vec{p}_1'\vec{p}_3 b\vec{p}_1''\vec{p}_3 a\vec{p}_1''\vec{p}_3' b\vec{p}_1''\vec{p}_3') (\epsilon + i(\omega - \omega_{ba}) + i\vec{k}\cdot(\frac{\vec{p}_1'' - \vec{p}_3'}{m_1 m_2}))^{-1} \\ \times T_{12}(a\vec{p}_1''\vec{p}_2' b\vec{p}_1''\vec{p}_2' a\vec{q}_1\vec{q}_2 b\vec{q}_1\vec{q}_2) \tilde{p}_{q_2} \tilde{p}_{p_3'}$$

where \vec{p}_{12}/m and $\vec{p}_{12}'' = \vec{p}_{11}'' - \vec{p}_{22}'$ are relative velocities before and after the 1-3 collision, m being the reduced mass. We keep in mind that the sum over \vec{k} now has an upper limit.

Next we go from the matrix elements of t operators to elastic and total scattering cross sections. By Equation (19.37) of Reference 98 the scattering amplitude f is related to t by

$$(65) \quad t = -2\pi \hbar^2 / m f$$

so that

$$(66) \quad \frac{\partial \sigma_{el}}{\partial \Omega} = |f|^2 = \frac{m^2}{(2\pi)^2 \hbar^4} t t^* \approx 2\pi \frac{m^2}{\hbar} t_{aa} t_{bb}^* / (2\pi \hbar)^3$$

in three dimensions, while in two dimensions,

$$(67) \quad 2\pi m / \hbar t t^* / (2\pi \hbar)^2 = v |f(\chi)|^2 = v \partial \sigma / \partial \chi$$

where σ has units of length. And by the optical theorem, for instance Equation (19.74) of Reference 98,

$$(68) \quad v\sigma^{tot} = -2\chi''/\chi \approx i(\chi_{aa} - \chi_{bb}^*)/\chi$$

where in Equations (66) and (68) the approximations follow since the intermolecular potential for the initial and final states involved in infrared transitions are not very different.

We can transform momenta to center of mass and relative variables, for instance by

$$\vec{p}_L \rightarrow \vec{p}_{12} \quad \vec{p}_3 \rightarrow \vec{p}'_{13} = \vec{p}'_{1/m_1} - \vec{p}'_{2/m_2} \quad \vec{p}_1 \rightarrow \vec{p}'_{12} \quad \vec{p}_2 \rightarrow \vec{p}'_{12}$$

$$\vec{p}_1'' \rightarrow \vec{p}''_{13} \quad \vec{p}_3' \rightarrow \vec{p}''_{13} \quad \vec{q}_1 \rightarrow \vec{q}_{12} \quad \vec{q}_2 \rightarrow \vec{Q}_{12}$$

With \vec{k} , and \vec{p}_1 whose integration over \vec{p}_1 remains outside the lineshape expression, this accounts for all 10 momenta summed over in Equation (64). Evidently the 1-2 relative velocity after the 1-3 collision, $\vec{v}_{12}'' = \vec{p}''_{13}/m_1 - \vec{p}'_{12}/m_2$, is not an independent variable, but a function of \vec{p}'_{12} , \vec{p}'_{13} , and \vec{p}''_{13} . Yet we will want to integrate over \vec{v}_{12}'' in the second denominator, and so we introduce a Jacobian $J = \frac{\partial \Omega''_{13}}{\partial \Omega''_{12}}$. In three dimensions Ω''_{13} represents the two angles Θ''_{13} and Φ''_{13} , while in two it is Θ''_{13} . Integration over this Ω''_{13} would ordinarily change $\frac{\partial \sigma^{el}}{\partial \Omega}$ into σ^{el} , so to avoid complication we must assume that the scattering amplitude is independent of angle, and simply $\frac{\sigma^{el}}{4\pi}$ in three dimensions or $\frac{\sigma^{el}}{2\pi}$ in two dimensions.

By Equation (63) we write schematically

$$\frac{T}{\chi} \rightarrow \left(-2\chi''/\chi \frac{\Delta\Delta}{\chi^2} - 2\pi d(E-E') \frac{\chi + \chi^*}{\chi^4} \right) \rightarrow \left(\frac{v\sigma^{tot}}{\chi^2} \langle P|P' \rangle \Delta\Delta - \frac{(2\pi\chi)^3}{m^2} \frac{\sigma^{el}}{4\pi} \frac{\delta(E-E')}{\chi^4} \langle P_{12}|P'_{12} \rangle \langle P_{12}|P'_{12} \rangle \right)$$

where in the center of mass matrix elements we are still using the normalization $\langle P_{12}|P_{12} \rangle = V$. So again schematically, after

changing to an integration over momentum the interacting parts of both T_{12} operators will become

$$(69) \quad \int d\vec{p}' \frac{(2\pi\hbar)^3}{m^2} G^{el} \delta(E-E')$$

$$\rightarrow \int V d(\frac{1}{2}mv'^2) \delta(E-E') G^{el} (2\pi\hbar)^3 = (2\pi\hbar)^3 V G^{el}$$

Now we go to the continuous momentum limit, using

$$\sum_p \rightarrow \left(\frac{V}{(2\pi\hbar)^d} \right) \int d\vec{p} \quad \text{and} \quad \tilde{\rho} \rightarrow \left(\frac{(2\pi\hbar)^d}{V} \right) \phi$$

in d dimensions, where ϕ is the Maxwellian momentum distribution function. So we get factors of $\left(\frac{V}{(2\pi\hbar)^3} \right)^9$ in three dimensions from the momentum integration, since the sum over p_1 remains outside, and $\left(\frac{(2\pi\hbar)^3}{V} \right)^2$ from $\tilde{\rho}_2 \tilde{\rho}_3$ going to $\phi_2 \phi_3$. Now, for the interacting parts of the T operators we get factors of V^2 and $\left(\frac{(2\pi\hbar)^3}{V} \right)$ from the two center of mass Δ functions. That is,

$$\left(\frac{V}{(2\pi\hbar)^3} \right) \int dP'_{12} \frac{+_{R_2 P_1 P'_2} +^*_{R_2 P_1 P'_2}}{V^2} \rightarrow \left(\frac{V}{(2\pi\hbar)^3} \right) \int dP'_{12} \frac{+_{P_{12} P'_2} +^*_{R_2 P_2}}{V} \frac{\langle P_{12} | P'_{12} \rangle}{V} \frac{\langle P_{12} | P'_{12} \rangle}{V}$$

because $\frac{V}{(2\pi\hbar)^3} \int dP'_{12} \frac{(2\pi\hbar)^3}{V} \delta(P'_{12} - P_{12}) \frac{\langle P_{12} | P'_{12} \rangle}{V} = 1$

since $\frac{\langle P_{12} | P_{12} \rangle}{V} = \int \frac{d^3P_{12}}{V} = 1$.

So, including $(2\pi\hbar)^3$ from Equation 69, the fact that

$$\frac{1}{V^2} \left(\frac{V}{(2\pi\hbar)^3} \right)^9 V^6 \left(\frac{(2\pi\hbar)^3}{V} \right)^2 \left((2\pi\hbar)^3 \right)^3 \left(\frac{(2\pi\hbar)^3}{V} \right)^2 = \frac{1}{(2\pi\hbar)^3}$$

means that looking at the real collision parts of all three T operators we have shown that all volume dependence disappears, as it must.

For the noninteracting parts, $(t - t^*)$, the $V^2 \left(\frac{(2\pi\hbar)^3}{V} \right) (2\pi\hbar)^3$ from each tt^* is instead obtained from $\left(\frac{(2\pi\hbar)^3}{V} \right)^2$ from $\Delta_{P_1 P'_1} \Delta_{P_2 P'_2}$ going to $\delta(P_1 - P'_1) \delta(P_2 - P'_2)$, a factor of $\langle P_{12} | P_{12} \rangle = V$, and the absence of $1/V^2$ normalization for a second t matrix element. So again, we are left only with a factor of $\frac{1}{(2\pi\hbar)^3}$, which we associate with

the integration over the momentum $\chi_{\vec{k}}$.

Therefore, collecting the results of the above discussion, Equation (64) has become, in three dimensions,

$$(70) \quad - \int \frac{d\vec{K}}{(2\pi)^3} d\vec{P}_{12} \phi_2 d\vec{P}_{13} \phi_3 d\hat{P}_{12}' d\hat{P}_{12}'' J_{\gamma_{12}} \frac{(\epsilon^{tot} - \epsilon^{el}) \gamma_{13} \epsilon^{el}}{4\pi} \gamma_{12}'' (\epsilon^{tot} - \epsilon^{el})$$

$$(\epsilon + i(\omega - \omega_{b0}) + i\vec{K} \cdot \vec{v}_{12}') (\epsilon + i(\omega - \omega_{b0}) + i\vec{K} \cdot \vec{v}_{12}'')$$

So here $T_{\vec{P}_{12} \vec{P}_{12}}$ denotes an operator which becomes

$$\chi_{\gamma_{12}} \epsilon^{pb} = \chi_{\gamma_{12}} (\epsilon^{tot} - \epsilon^{el})$$

with ϵ^{pb} being the pressure-broadening cross section. Also, it is the fact that T_{13} has become only $-\epsilon^{el}$ that has reversed the sign of the entire term in Equation (70). In the spirit of using average values of momenta, in Equation (70) we have ignored the dependence of \vec{v}_{12}'' on \vec{P}_{13}'' , and have simply integrated over $\delta(E_{13}' - E_{13})$. We have also changed ϕ_{P_2}' and ϕ_{P_3}' to ϕ_{P_2} and ϕ_{P_3} .

In proceeding further, with integrations over momenta, it is instructive to look at the two dimensional case first. It is shown in Appendix H that in two dimensions the Jacobian $J, \partial\theta_{13}'' / \partial\theta_{12}''$, is $(\frac{m_1}{m}) \frac{\vec{P}_{12}'' \cdot \vec{P}_{13}''}{P_{13}''^2}$. So we simply consider

$$(71) \quad \int \frac{d\vec{K}}{(2\pi)^2} d\vec{P}_{12} \phi_2 d\vec{P}_{13} \phi_3 d\hat{P}_{12}' d\hat{P}_{12}'' \left(\frac{m_1}{m} \right) \frac{\vec{P}_{12}'' \cdot \vec{P}_{13}''}{P_{13}''^2} \left(-\gamma_{12} \frac{\epsilon^{pb}}{2\pi} \gamma_{13} \frac{\epsilon^{el}}{2\pi} \gamma_{12}'' \epsilon^{pb} \right)$$

$$(\epsilon + i(\omega - \omega_{b0}) + i\vec{K} \cdot \vec{v}_{12}') (\epsilon + i(\omega - \omega_{b0}) + i\vec{K} \cdot \vec{v}_{12}'')$$

We have shown in Appendix H that by momentum conservation

$$\vec{P}_{13}'' = \vec{P}_{13}' - \left(\frac{m_1}{m} \right) (\vec{P}_{12}' - \vec{P}_{12}'')$$

So in terms of θ_{13}' and θ_{12}'' , the angles of \vec{P}_{13}' and \vec{P}_{12}'' with respect to \vec{P}_{12}'' ,

$$(72) \quad \left(\frac{m_1}{m} \right) \left(\frac{m_1}{m} \right) \left(\frac{\vec{P}_{13}'' \cdot \vec{P}_{12}''}{P_{13}''^2} \right) =$$

$$\left(\frac{m_1}{m} \right) \left(\left(\frac{m_1}{m} \right) \left(P_{12}''^2 + P_{12}' P_{12}'' \cos\theta_{12}'' \right) + P_{13}' P_{12}'' \cos(\theta_{12}'' - \theta_{13}') \right)$$

$$\left(\frac{m_1}{m} \right)^2 (P_{12}'^2 + P_{12}''^2) + P_{13}'^2 + 2 \left(\frac{m_1}{m} \right)^2 P_{12}' P_{12}'' \cos\theta_{12}'' - 2 \left(\frac{m_1}{m} \right) P_{13}' P_{12}'' \cos\theta_{13}' + 2 \left(\frac{m_1}{m} \right) P_{13}' P_{12}'' \cos(\theta_{12}'' - \theta_{13}')$$

The angle Θ_{12}'' is the χ of Reference 41, where it is shown that integration over χ and Θ_{12}' , the angle of \vec{p}'_{12} with respect to \vec{k} , gives the result that $\Theta_{12}'' \rightarrow \pi$. (After integration over angles, we would obtain a k integral similar to that in Equation (13) of Reference 41.) If we take this $\Theta_{12}'' \rightarrow \pi$ limit in the Jacobian, we obtain

$$(73) \quad \begin{aligned} & \left(\frac{m_1}{m}\right)^2 p_{12}'' (p_{12}' + p_{12}'') - \left(\frac{m_1}{m}\right) p_{12}'' p_{13}' \cos \Theta_{13}' \\ & p_{13}'^2 + \left(\frac{m_1}{m}\right)^2 (p_{12}'' + p_{12}') - 2 \left(\frac{m_1}{m}\right) p_{13}' (p_{12}'' + p_{12}') \cos \Theta_{13}' \end{aligned}$$

Now the energy delta function from T_{13} said $\frac{p_{12}''}{m_1} + \frac{p_{13}''}{m_3} = \frac{p_{12}''}{m_1} + \frac{p_{13}''}{m_3}$ and using $\vec{p}' + \vec{p}_3 = \vec{p}' + \vec{p}_3'$ this means $p_{13}' = p_{13}''$. But this means that in the denominator of J ,

$$(74) \quad 2 p_{13}' \cos \Theta_{13}' - \left(\frac{m_1}{m}\right) (p_{12}' + p_{12}'') = 0$$

This equation agrees with the discussion in Reference 95, where for the case that $m_1 = m_2 = m_3$ so that $m^{1/2} = m$, and taking \hat{p}'_{12} to define the direction of the x coordinate, it is shown that $p_{12x}'' = p_{13}' \cos \Theta_{13}' - p_{12}'$ and $p_{12y}'' \approx 0$. These relations follow from Equation (74) when we realize that it is for the case $\Theta_{12}'' \rightarrow \pi$, describing a long narrow triangle between collisions. It is important to note that the integration of J over momenta should give a contribution which is less than one because p_{12x}'' is the difference of two quantities which are on the average almost equal. This should be especially true in Reference 95 where for the case of viscosity the factor of p_{12}'' enters raised to the third power.

But where Reference 95 is discussing terms in a density expansion and so can average each term over \vec{p}_1 , we wish to look

at the effect of thermal averaging on the linewidth while leaving the integral over \vec{p}_1 outside the lineshape. So we choose to integrate our modified J over Θ'_{13} ,

$$(75) \int_0^{2\pi} d\Theta'_{13} \left(\frac{m_1}{m}\right) \frac{P_{13} \cos \Theta'_{13} (P'_{13} \cos \Theta'_{13} - P'_{12})}{P'_{13}{}^2} = 2\pi$$

Equation (75) means that if we had despaired of integrating J and decided to choose a number with which to replace it, that number might as well have been 1. With this and with the results of the integrations over Θ'_{12} and Θ''_{12} as in Equation (13) of Reference 41, as well as a 2π from the free angle of \vec{k} , Equation (71) has become

$$(76) \quad - \int_0^{k_0} \frac{2\pi k dk}{(2\pi)^2} \int d\vec{p}_2 \phi_2 \int d\vec{p}'_3 \phi_3 \frac{2\pi v'_{12} \epsilon^{pb}}{2\pi} \frac{v'_{12} \epsilon^{el}}{2\pi} \frac{v''_{12} \epsilon^{pb}}{2\pi} \frac{(2\pi)^2}{v'_{12} v''_{12}}$$

$$\frac{1}{(K^2 + (\epsilon + \eta(\omega - \omega_{ba}) \frac{1}{v'_{12}})^2 + \frac{1}{\Lambda})^2} \frac{1}{(K^2 + (\epsilon + \eta(\omega - \omega_{ba}) \frac{1}{v''_{12}})^2)^2}$$

The k dependent integrand differs from that in Reference 41 in that one denominator contains a cutoff $1/\Lambda$, where Λ is of the order of a mean free path, necessary because in two dimensions the \vec{k} integral is also divergent at the lower limit. The derivation and physical interpretation of this cutoff is discussed extensively in References 38, 41, and 44, and has been touched on in Section II A. The k integral can be done as in Reference (41) to obtain

$$\ln \left((K^2 + (\epsilon + \eta(\omega - \omega_{ba}) \frac{1}{v'_{12}})^2 + \frac{1}{\Lambda})^2 \right)^{1/2} + (K^2 + (\epsilon + \eta(\omega - \omega_{ba}) \frac{1}{v''_{12}})^2)^{1/2}$$

Evaluating at k_0 and zero, and finally taking the limit $\epsilon \rightarrow 0$, this becomes (after some algebra)

$$(77) \quad \ln \frac{2k_0}{\left((2(\omega - \omega_{ba}) \frac{1}{v})^2 + K_1^2 \right)^{1/4}}$$

Being of the order of an inverse mean free path, k_1 increases

with increasing density, so that at the sort of densities at which the triple collision term becomes important, the term $(\omega - \omega_{\infty}) / \bar{v}$ with \bar{v} the average velocity, is the same size or smaller for any frequency difference of interest. So we will simply use $\ln(k_0/k_1)$ as an estimate of the logarithmic term.

We know that the cross sections do not have an important dependence on momentum.⁸⁸⁻⁹⁰ So if we carry to new depths an approximation often used in line broadening theory, and assume that the cross sections have no velocity dependence and imagine that the Maxwellians, originally ϕ'_2 and ϕ'_3 have become ϕ_2 and ϕ_3 , or alternatively if we just replace all momenta by their thermal averages, \bar{v} , we obtain for Equation (76) the estimate in two dimensions,

$$(78) \quad \bar{v} G^{pb} G^{el} G^{pb} \ln k_0/k_1$$

In three dimensions, we find, again from Appendix H, that J or $\frac{\partial \Omega_{13}''}{\partial \Omega_{12}''}$ is $(\frac{m_1}{m})^2 \frac{P_{12}''^2}{P_{13}''^2} \frac{\vec{P}_{12}'' \cdot \vec{P}_{13}''}{P_{12}'' P_{13}''}$. This is difficult to integrate accurately, so although it may mean an error of up to an order of magnitude, at the present state of calculation we perhaps do best by replacing J by one. (In Appendix H we attempt an integration which says that J might be worth 4 rather than 1, for the case that $(m_1/m)^2 = 4$. However, on physical grounds and to agree with experiment one wants J to be less than one, so we compromise.)

With this approximation, we can use $\lim_{\epsilon \rightarrow 0} (\epsilon + ix)^{-1} = \pi \delta(x) - iP'_{1/x}$ and $P \int_{-1}^1 \frac{dx}{u - u_0} = 0$ to evaluate the integrals over the angles of \vec{p}'_{12} and \vec{p}''_{12} in Equation (70), (angles measured with respect to \vec{k}),

so that $\int \sin \theta_{12}' d\theta_{12}' \sin \theta_{12}'' d\theta_{12}''$
 $(\epsilon + i(\omega - \omega_{ba}) + iKv_{12}' \cos \theta_{12}') (\epsilon + i(\omega - \omega_{ba}) + iKv_{12}'' \cos \theta_{12}'')$
 just contributes $\pi^2 / (k^2 v_{12}' v_{12}'')$. We also have factors of 2π from
 integrations over ϕ_{12}' and ϕ_{12}'' , and a factor of k_0 since $1/k^2$
 from the denominators leaves simply $4\pi \int_0^{k_0} dk$. Then using
 integration over the Maxwellians only to replace momenta by
 their averages, we approximate (70) by

$$(79) \quad -K_0 / 8 \sqrt{v} G^{pb} G^{el} G^{pb}$$

The first order linewidth coefficient $\Delta v_{1/2}$ in $\text{cm}^{-1}/\text{atm}$ is
 $v G^{pb} / 2\pi c$, so to convert one G^{pb} to $\text{sec}^{-1}/\text{atm}$, we multiply by
 $2\pi c$. The term $T_{12} G_O T_{23} G_O T_{12}$ ought to behave precisely as
 $T_{12} G_O T_{13} G_O T_{12}$ except for the small difference between the 13
 and 23 cross sections. However, the third term, $T_{12} G_O T_{23} G_O T_{13}$,
 also has a contribution from the noninteracting part of the
 T_{23} operator, which is of opposite sign (and of the same sign
 as $\Delta v_{1/2}$), and which for this estimate may be taken to be about
 double the interacting part. In other words, for an estimate
 of triple collision contributions in three dimensions it suffices
 to take

$$(80) \quad -2\pi c / \sqrt{v} G^{el} K_0 / 8 (\Delta v_{1/2} \text{ in } \frac{\text{cm}^{-1}}{\text{atm}})^2 \quad \text{or} \quad \approx -3/4 c / \sqrt{v} G / v_0 (\Delta v_{1/2})^2$$

If we perform a quick numerical estimate, with $r_0 = 1/k_0$
 being estimated in Appendix G, we find (with values roughly suited
 to the HF-Ar system)

$$-3/4 \quad 3 \times 10^{10} \text{ cm/sec} / 6 \times 10^4 \text{ cm/sec} \quad \frac{30 \times 10^{-16} \text{ cm}^2}{3 \times 10^{-8} \text{ cm}} \quad (.03 \frac{\text{cm}^{-1}}{\text{atm}})^2 \approx -.000035 \frac{\text{cm}^{-1}}{\text{atm}^2}$$

or around $-.35 \text{ cm}^{-1}$ at 100 atm out of 3 cm^{-1} , an observable effect,
 by itself. More estimates for various systems will be given in
 Section II E.

D. The Statistical Contribution to the Linewidth

We wish to treat the statistical corrections in second order in the density as if they appeared in the denominator of the lineshape expression and thus contributed directly to the linewidth. We begin with Equation (5.15) of Reference 40 and construct a density expansion from it by equating terms of the same order in the density ρ ,

$$(81) \quad (G_0^{-1} + \rho \mathcal{L} + \rho^2 \Gamma)^{-1} (1 + \rho a_1 + \rho^2 a_2) A = (W^0 + \rho W^1 + \rho^2 W^2) A$$

where A is an arbitrary function. The first term in the density expansion is obtained by solving $G_0^{-1} W^0 A = A$ so that $W^0 = G_0$. Similarly, $\rho a_1 A = G_0^{-1} \rho W^1 A + \rho \mathcal{L} W^0 A$ means

$$W^1 = G_0 a_1 - G_0 \mathcal{L} G_0. \quad \text{Finally}$$

$$\rho^2 a_2 A = G_0^{-1} \rho^2 W^2 A + \rho \mathcal{L} \rho W^1 A + \rho^2 \Gamma W^0 A$$

$$= G_0^{-1} \rho^2 W^2 A + \rho \mathcal{L} \rho (G_0 a_1 - G_0 \mathcal{L} G_0) A + \rho^2 \Gamma G_0 A$$

which gives $W^2 = G_0 a_2 - G_0 \mathcal{L} G_0 a_1 + G_0 \mathcal{L} G_0 \mathcal{L} G_0 - G_0 \Gamma G_0$.

Then to put everything into a denominator we solve

$$(G_0^{-1} + \rho \mathcal{L} + \rho^2 \Gamma + \rho a_1 b_1^1 + \rho^2 a_2 b_1^2 + \rho^2 a_1 b_2^1)^{-1} A = W A$$

Again equating powers of ρ , $\rho \mathcal{L} W^0 A + G_0^{-1} \rho W^1 A + \rho a_1 b_1^1 W^0 A = 0$ says

that $b_1^1 = -G_0^{-1}$. Then

$$G_0^{-1} \rho^2 W^2 A + \rho \mathcal{L} \rho W^1 A + \rho^2 \Gamma W^0 A + \rho^2 a_2 b_1^2 W^0 A + \rho^2 a_1 b_2^1 W^0 A - \rho^2 a_1 G_0^{-1} W^1 A = 0$$

or

$$a_2 - \mathcal{L} G_0 a_1 + \mathcal{L} G_0 \mathcal{L} G_0 - \Gamma G_0 + \mathcal{L} G_0 a_1 - \mathcal{L} G_0 \mathcal{L} G_0 + \Gamma G_0 - a_1^2 + a_1 G_0 \mathcal{L} + a_2 b_1^2 G_0 + a_1 b_2^1 G_0 = 0$$

so $b_1^2 = -G_0^{-1}$ and $b_2^1 = a_1 G_0^{-1} - \mathcal{L}$. So the second order statistical term in the denominator is

$$(82) \quad -G_0^{-1} a_2 + G_0^{-1} a_1^2 - \mathcal{L} a_1$$

Here we use the definitions that the two particle distribution function $\tilde{\rho}(12) = g(12) \tilde{\rho}(1) \tilde{\rho}(2)$ (or $g_{12} \tilde{\rho}_1 \tilde{\rho}_2$), and f_{12} is not $\tilde{\rho}(12) - \tilde{\rho}(1) \tilde{\rho}(2)$ as in

Reference 37, but $f_{12} = g_{12} - 1$. Also we use brackets $\langle \rangle$ to indicate the average over one particle distribution functions. The using the definitions, $G_0^{-1} a_2$ is $\langle -V T_{12} g_{12}^{(0)} f_{12} f_{23} \rangle_{23}$, which we shall show is the second order contribution from the Enskog theory of dense gases, plus other terms,

$\langle V^2 T_{12} G_0 T_{13} g_{13}^{(0)} (f_{12} + f_{23} + f_{12} f_{23}) \rangle_{23} + \langle V^2 T_{12} G_0 T_{23} g_{23}^{(0)} (f_{12} + f_{13} + f_{12} f_{13}) \rangle_{23}$
 The term $G_0^{-1} a_1^2$ could be written as $\langle -V^2 T_{12} G_0 T_{13} f_{12} f_{13} \rangle_{23}$ while $-2a_1$ is $\langle -V T_{12} G_0 T_{13} f_{13} \rangle_{23}$. We note that there are many more terms than the first Enskog correction.

We now comment on some previous methods for approximating the statistical corrections. If one expands Equations (5.15) and (5.16) of Reference 40 ignoring ϵ ,

$$\frac{1}{\rho} (1 + \rho \Gamma_{12})^{-1} (1 - \rho a_1) = \frac{1}{\rho} (1 + \rho \Gamma_{12} - \rho a_1),$$

they are indeed equivalent to order ρ^2 . However, if one includes ϵ , which in our case contains the factor $\rho(\omega - \omega_{ba})$, the expansion of Equation (5.15) is

$$\frac{1}{\epsilon} (1 - \rho \frac{a_1}{\epsilon} + \rho a_1 + \rho^2 \Gamma_{12} + \rho^2 \frac{a_1^2}{\epsilon} + \rho^2 \frac{2a_1}{\epsilon})$$

which is not equal to

$$\frac{1}{\epsilon} (1 - \rho \frac{a_1}{\epsilon} - \rho^2 \Gamma_{12} + \rho^2 \frac{2a_1}{\epsilon} + \rho^2 \frac{a_1^2}{\epsilon})$$

obtained from (5.16)

So if one went directly from an ϵ series or from the correctly summed Equation (5.15), and used the definition of the second virial coefficient $B(T) = -\frac{1}{2} \int f_{12} d\vec{r}_{12}$, one would not want to approximate the first density correction as $(1 - 2\rho B)$ multiplied times a linewidth or cross section, as Equation (5.16) might suggest, but rather to include a factor $(1 - 2B)$ in lowest order

in the density. As discussed in Reference 56, the reduced volume factor $(1-2\rho B)$ is only one of two contributions, the other being due to shielding by a third particle to reduce the probability of collisions. The entire statistical correction factor in Enskog theory comes from averaging the density expansion of the pair correlation function $g(12) = 1 + \chi(12)$. Its density expansion to second order is $\bar{e}^{(2)}(1+\rho \int \chi_{13} \chi_{23} d\vec{r}_3 + \dots)$. If $V_{12}(r_{12})$ is a hard sphere potential, the integration over \vec{r}_3 can be done⁹⁹ to obtain the original Enskog result,

$$1 + \rho^{5/2} \pi d^3, \quad d \text{ the hard sphere diameter.}$$

Given that the third virial coefficient $C(T)$ is

$$C(T) = -1/3V \int \chi_{12} \chi_{23} \chi_{13} d\vec{r}_1 d\vec{r}_2 d\vec{r}_3,$$

one might then want to approximate the first order statistical correction to the linewidth as $\rho C/B$ times the linewidth.¹⁰⁰ However, there are better approximations to the Enskog term which have been traditionally used. We will discuss one in the next section, but first we must satisfy ourselves that this term is the most important.

To gain an idea of the relative magnitudes of the statistical terms, we will write out the traces over tetradic and matrix elements. We want to look first at the Enskog term,

$$\langle V T_{12} \langle g_{(12)}^{(0)} \chi_{13} \chi_{23} \rangle_3 \rangle_2,$$

in which we shall denote the operator averaged over the coordinates and momenta of particle 3 as E_{12} .

The derivation which follows would work as well for a term

$$\langle V T_{12} g_{12} \rangle_2, \quad \text{or} \quad \langle V T_{12} \chi_{12} \rangle_2.$$

(The latter object, as if a_1 were $V f_{12}$, might indeed result from an evaluation of the term $2a_1$,

as we shall see in the next section.)

We begin with

$$(83) \quad \sum_{\vec{p}_1, \vec{p}_2, \vec{p}'_1, \vec{p}'_2} V^2 T_{\vec{p}_1, \vec{p}_2, \vec{p}'_1, \vec{p}'_2} E_{\vec{p}'_1, \vec{p}'_2} \tilde{P}_{\vec{p}_1, \vec{p}_2}$$

Summation over \vec{p}''_{12} and the momentum conservation conditions in T_{12} such that $\vec{p}'_1 + \vec{p}'_2 = \vec{p}_1 + \vec{p}_2$ generate a momentum $\vec{k} = \vec{p}'_1 - \vec{p}_1$ just as in Section II C, and give factors of $T_{\vec{p}_2, \vec{p}'_2, \vec{p}_2, \vec{p}'_2 - \vec{k}}$ and $\chi_{\vec{p}'_1, \vec{p}'_2 - \vec{k}}$. We change the remaining three momenta, \vec{p}_2, \vec{p}'_1 and \vec{p}'_2 to center of mass variables $\vec{p}_{12}, \vec{p}'_{12}$ and \vec{p}_{12} . Going to continuous momenta, center of mass delta functions give us a factor of V from E_{12} and cause $T_{\vec{p}_1}$ to go to

$$\frac{V_{12} G^{tot}}{V^2} V \left(\frac{(2\pi\hbar)^3}{V} \right)^2 \delta_{\vec{p}_2, \vec{p}'_2} \delta_{\vec{p}_{12}, \vec{p}'_{12}} - \frac{(2\pi\hbar)^3}{m^2} \delta(E-E') \frac{G^d}{4\pi} V^2 \left(\frac{(2\pi\hbar)^3}{V} \right)$$

which we call

$$\frac{1}{V} V_{12} G^{pb} \delta_{\vec{p}_2, \vec{p}'_2} \delta_{\vec{p}_{12}, \vec{p}'_{12}} \left(\frac{(2\pi\hbar)^3}{V} \right)^2$$

With explicit volume normalization, we have

$$(84) \quad \left(\frac{V}{(2\pi\hbar)^3} \right)^4 \int d\vec{p}'_{12} d\vec{p}'_{12} d\vec{p}'_{12} d\vec{k} V^2 \frac{1}{V} V_{12} G^{pb} \delta_{\vec{p}_2, \vec{p}'_2} \delta_{\vec{p}_{12}, \vec{p}'_{12}} \left(\frac{(2\pi\hbar)^3}{V} \right)^2 \frac{1}{V^2} E_{\vec{p}'_1, \vec{p}'_2, \vec{p}'_2 - \vec{k}} \frac{V}{V} \frac{(2\pi\hbar)^3}{V} \frac{(2\pi\hbar)^3}{V}$$

The last factor of $\left(\frac{(2\pi\hbar)^3}{V} \right)$ comes about because one can argue that $E_{\vec{p}'_1, \vec{p}'_2, \vec{p}'_2 - \vec{k}}$, being approximately $\int d\vec{r}_{12} E_{12} e^{i\vec{k} \cdot \vec{r}_{12} / \hbar}$, should be

$$\int d\vec{r}_{12} E_{12} \left(\frac{(2\pi\hbar)^3}{V} \right) \delta(\vec{r}) \text{ since } \int d\vec{r}_{12} e^{i\vec{k} \cdot \vec{r}_{12} / \hbar} = V \left(\frac{(2\pi\hbar)^3}{V} \right) \delta(\vec{k}) = \int d\vec{r}_{12} E_{12} \left(\frac{(2\pi\hbar)^3}{V} \right) \delta(\vec{k})$$

(Similarly, f_{12} can be approximated by $B \left(\frac{(2\pi\hbar)^3}{V} \right) \delta(\vec{k})$) Actually

E_{12} (and f_{12}), being of finite range in \vec{r}_{12} , can be approximated by a square well, and will lead to a cutoff k_0 as discussed in Appendix G. But this k_0 is much less than a thermal average momentum, and, in contrast to the denominators discussed in Section II C, here appears only added to the relative momentum.

If we use the average over the Maxwellian to simply substitute in average momenta, Equation (84) simplifies to $\bar{V} G^{pb} E$ (where from above E for hard spheres was $\frac{5}{12} \pi d^3$).

Next we look at $\langle V^2 T_{12} G_0 T_{13} g_{13}^{(0)} f_{13} \rangle_{23}$, from $\mathcal{L} a_1$. We begin with

$$(85) \quad \sum_{\vec{p}_2, \vec{p}'_2, \vec{p}_3, \vec{q}_1, \vec{k}, \vec{q}_3, \vec{k}'} T_{12} (\vec{p}_2, \vec{p}'_2, \vec{p}_2 - \vec{k}) T_{13} (\vec{p}'_3, \vec{p}_3, \vec{q}'_3, \vec{q}_3 - \vec{k}') \times G_0(\vec{q}_3, \vec{q}_3 - \vec{k}') (g_{13}^{(0)} f_{13}) (\vec{q}_3, \vec{q}_3 - \vec{k}') \tilde{p}_2 \tilde{p}_3$$

Actually, the second \vec{p}'_1 in T_{13} is $\vec{p}'_1 - \vec{k}$, and the $\vec{q}'_3 - \vec{k}$ index is really composed of $\vec{q}'_1 = \vec{q}_1 - \vec{k}'$ and $\vec{q}'_3 = \vec{q}_3 + \vec{k}' - \vec{k}$. But this \vec{k} momentum index is really zero because there are no more particle 2 operators in the expression, and therefore with this definition of \vec{k} and \vec{k}' we have not only $\vec{q}_1 + \vec{q}_3 = \vec{q}'_1 + \vec{q}'_3 - \vec{k}$ from T_{13} but also $\vec{q}_1 + \vec{q}_3 = \vec{q}'_1 + \vec{q}'_3$ from the momentum conservation condition in f_{13} .

Changing to integrations over center of mass momenta, we obtain

$$(86) \quad \left(\frac{V}{(2\pi\hbar)^3} \right)^8 \int d\vec{p}_2 d\vec{p}'_2 d\vec{p}_3 d\vec{q}_1 d\vec{k} d\vec{q}_3 d\vec{k}' V^2 \frac{1}{V} \frac{V_{12} G^{pb}}{4\pi} \int d\vec{p}_2 d\vec{p}'_2 \int d\vec{p}_2 d\vec{p}'_2 \left(\frac{(2\pi\hbar)^3}{V} \right)^2 G_0(\vec{k}') \times \frac{1}{V} \frac{V_{13} G^{pb}}{4\pi} \int d\vec{p}'_3 d\vec{p}_3 \int d\vec{q}_3 d\vec{q}'_3 \left(\frac{(2\pi\hbar)^3}{V} \right)^2 g_{13}^{(0)} f_{13} (2\pi\hbar)^3 \delta(\vec{k}) \phi_2 \phi_3 \left(\frac{(2\pi\hbar)^3}{V} \right)^2$$

We can simplify Equation (86) by again using $\lim_{\epsilon \rightarrow 0} (\epsilon + |x|)^{-1} = \pi \delta(x) - i P' \frac{1}{x}$ on G_0 to do the integration over the angles of \vec{k}' . Cancellation leaves one factor of $\frac{1}{(2\pi\hbar)^3}$, which we incorporate into \vec{k}' to make it a wave vector. Then we include a cutoff wave vector k'_0 as an upper limit (which can be determined by the estimation methods in Appendix G, perhaps using $\int_0^\infty V(k') k' dk' = \frac{k'^2_0}{2} \sqrt{V(0)} r_{12}^2 dr_{12}$). We argue that the result of the radial integration, $\pi^2 k'^2_0 / \bar{V}_{13}$, approximately cancels the $\bar{V}_{13} G_{13}$ resulting from T_{13} , since we

choose k'_0 to be of the order of a molecular diameter. Then substituting in average momenta, and taking $g_{13}^{(0)}$ to be one, we can approximate Equation (86) by $-2B \frac{V_6}{(2\pi)^3}$, since neglecting \vec{k} in the matrix element of f_{13} it is approximately $\int f_{13} d\vec{r}_{13} = -2B$.

Terms like $\langle V^2 T_{12} G_0 T_{13} g_{13}^{(0)} f_{12} \rangle_{23}$ go in much the same fashion, so we look at only one more, $\langle V^2 T_{12} G_0 T_{13} g_{13}^{(0)} f_{12} f_{13} \rangle_{23}$, which if we immediately take $g_{13}^{(0)}$ as one becomes

$$(87) \quad \left(\frac{V}{(2\pi\hbar)^3}\right)^8 \int d\vec{p}_2 d\vec{p}'_1 d\vec{p}'_2 d\vec{k} d\vec{p}_3 d\vec{q}_1 d\vec{q}_2 d\vec{k}'$$

$$\times V^2 \left(\frac{1}{V} \frac{V_{12} G^{pb}}{4\pi} \int_{P_{12} P'_{12}} \int_{P_{12} P'_{12}} \left(\frac{2\pi\hbar}{V}\right)^3 \right)^2 (i\epsilon - \vec{k} \cdot \vec{q}_2 - \vec{k}' \cdot \vec{q}_{13})^{-1}$$

$$\times \left(\frac{1}{V} \frac{V_{13} G^{pb}}{4\pi} \int_{P_{13} P'_{13}} \int_{P_{13} P'_{13}} \left(\frac{2\pi\hbar}{V}\right)^3 \right)^2 \frac{f_{12}}{V^2} \int d(\vec{k}) \frac{f_{23}}{V^2} \int d(\vec{k}') \phi_2 \phi_3 \left(\frac{2\pi\hbar}{V}\right)^2$$

Here two factors of $\frac{1}{(2\pi\hbar)^3}$ survive and are incorporated into integrals over \vec{k} and \vec{k}' . So again cancelling $T_{13} G_0$ as above and breaking averages over momenta Equation (87) could be crudely approximated by $\frac{V_6 4B^2}{(2\pi)^6} \frac{4\pi k_0^3}{3}$. We will find ourselves in desperate need of this factor of $\frac{1}{(2\pi)^6}$ when we estimate the relative sizes of the statistical terms, which we now proceed to do.

If we first, only for an order of magnitude estimate, use the hard sphere Enskog expression, we find $\frac{5}{12} \pi d^3$ to be $1.2 \times 10^{-3}/\text{atm}$ for d , the hard sphere diameter, taken as 3.2 Å. Interestingly, B for an attractive potential like that for argon-argon is around $-16 \text{ cm}^3/\text{mole}^{18}$ so that $-2B$ is $1.4 \times 10^{-3}/\text{atm}$. Therefore from our estimate of Equation (86), terms like $\langle V^2 T_{12} G_0 T_{13} g_{13}^{(0)} f_{13} \rangle_{23}$ might be of the same size as the Enskog term, were it not for the factor of $\frac{1}{(2\pi)^3}$, left over from a k integration which the

Enskog term did not have. Similarly, if we estimate (87) by again cancelling the integration over $G_0(k)$ with T_{13} , and approximating $\langle \epsilon_{13} \epsilon_{23} \rangle$ by $4B^2$, we find multiplying times $4\pi k_0^3/\lambda^3$ gives about 8 times the $2B$ found in the above f_{13} correction. But fortunately, $1/(2\pi)^6$ is $1/61529$ so this contribution is also negligible.

So we need consider only the Enskog type term out of all the statistical corrections in second order in the density. For further discussion of this term see References 100-106. We will actually not use the hard sphere Enskog theory, but will discuss in the next section a commonly used method of approximating the Enskog term for real potentials.

E. Discussion of Theory and Experiment

We begin this section comparing theory and experiment by exhibiting the results of a number of other workers on the density dependence of the diffusion coefficient. We do this because the diffusion coefficient and the effective cross section derived from it are in closest analogy of all transport coefficients to the absorption coefficient and the cross section obtained from the linewidth.

This is so because the higher density contributions to both the absorption and diffusion coefficients arise only from the increased local density around the particle of interest described by the statistical terms of Section II D and from the triple collision events of Section II C. In the case of other transport processes, like viscosity and thermal conductivity which involve transfer of momentum or kinetic energy over a given boundary, the transport can occur due to collisions at the imaginary boundary, in addition to transport due to crossing the boundary. In the hard sphere Enskog theory for dense gases⁵⁶ this effect is shown to be larger than the statistical, collision frequency correction from the radial distribution function, χ in the Enskog theory. Diffusion and absorption of radiation involve properties, the mass of the molecule and the dipole moment, which cannot be transferred by collision, so the Enskog relation for the diffusion constant

D in terms of its low density limit D_0 is just $D=D_0/\chi$.

For purposes of comparison, all diffusion coefficients were reduced to density dependent effective cross sections σ using the relation from simple kinetic theory,¹⁰⁷

$$(88) \quad D = \frac{3}{8} \left(\frac{kT}{\pi m} \right)^{1/2} \frac{1}{\rho \sigma}$$

This cross section would be constant if diffusion involved only binary collisions. A linear least squares fit of the effective cross section as a function of density gives a low density limiting value for the cross section as an intercept and a second density correction as a slope. These parameters for a number of systems are presented in Table 5.

In Figures 30 through 33 we give some examples of this sort of cross section plot. The general trend of all the data, as shown in the least squares fits, is for the effective cross section to decrease with increasing pressure, as is the effective collision frequency were increasing at a less than linear rate. The plots are useful to show that while there are some excellent measurements in which the second density effect is clearly visible, many sets of data contain such random error as to cast doubt on the exact size if not the existence of this effect. It is the well known difficulty in making transport coefficient measurements precisely which led us to look for density effects in lineshapes. When the linewidth data of the present work is put into the same format of a plot of effective cross section against density, we will find that the scatter in the data compares favorably with much

Table 5 : Density Dependent Effective Cross Sections from Diffusion Coefficients

This table gives the low density cross section (ϵ) and first density correction in A^2/amagat (in the column marked Slope) obtained from a linear least squares fit to diffusion coefficient data. The first three columns give the system studied, the temperature for the measurements (seen to have a noticeable effect on ϵ), and the literature reference. The column labeled MET is the estimate of the modified Enskog theory for the first density correction in A^2/am , and the column labeled Eq. (79) is the estimate of the contribution to the same property from recollisions.

To compute this last, we need the average relative velocity \bar{v} , here listed in units of 10^4 cm/sec, and a cutoff radius r_0 , here in A. Also listed is the linewidth equivalent of the diffusion cross section, $\bar{v}\epsilon/2\pi c$, given in cm^{-1} .

<u>System</u>	<u>Temp.</u>	<u>Ref.</u>	<u>ϵ</u>	<u>Slope</u>	<u>MET</u>	<u>\bar{v}</u>	<u>r_0</u>	<u>$\bar{v}\epsilon/2\pi c$</u>	<u>Eq. 79</u>
Kr-He	35°C	109	25.1 A^2	-.016	0	13.0	2.5	.046	-.018
Ar-Ar	49.4	108	39.1	-.01	-.007	5.6	3	.033	-.06
CO ₂ -H ₂	35	114	41.2	-.004	-.002	18.5	3.2	.11	-.007
	100		44.3	-.0095	-.01	20.4		.13	-.009
Kr-Ar	35	109	41.9	-.032	-.007	4.9	3.3	.03	-.076
	-25		43.0	-.027	-.011	4.4		.03	-.09

133

Table 5 : (continued)

System	Temp.	Ref.	\bar{G}	Slope	MET	\bar{v}	r_0	$\bar{v}_G/2\pi C$	Eq. 79
Kr-N ₂	35	109	42.8	-.024	-.022	5.6	3.3	.03	-.057
	-25		43.4	-.027	-.027	5.0			-.073
CO ₂ -Ar	75	113	43.1	-.014	-.012	5.9	3.3	.03	-.052
	50		44.2	-.016	-.006	5.7		.03	-.055
	25		44.0	-.018	-.005	5.5		.03	-.060
Kr-Kr	35	109	47.7	-.026	-.009	3.9	3.4	.027	-.10
	0	111,	51.1	-.043	-.0003	3.7	3.6	.027	-.12
	-53	112	57.3	-.042	-.004	3.3	3.8	.027	-.15
Kr-CO ₂ CO ₂ -CO ₂	35	109	49.3	-.070	-.005	4.75	3.5	.033	-.10
	100	115	51.3	-.017	-.013	6.0	3.6	.044	-.12
	75	116	52.0	-.038	-.008	5.8	3.6	.043	-.12
	50	116	53.2	-.026	-.003	5.6	3.6	.042	-.13
	45	110	57.2	-.060	-.003	5.55	3.8	.045	-.20
	35	115	56.5	-.013	-.002	5.45	3.8	.044	-.15
	25	116	54.8	-.019	-.0026	5.35	3.7	.042	-.14
	25	110,117	59.7	-.078	-.0029	5.35	3.9	.046	-.17
	20	118	59.6	-.027	-.004	5.3	3.9	.045	-.17

134

Figure 30: A plot of effective cross section for Kr-Ar derived from diffusion coefficient data using Equation (88), as a function of Ar density. Data taken from Reference 109.

Figure 31: Effective cross section plot for Kr diffusing through Kr (squares) and N_2 (triangles). Data from Reference 109.

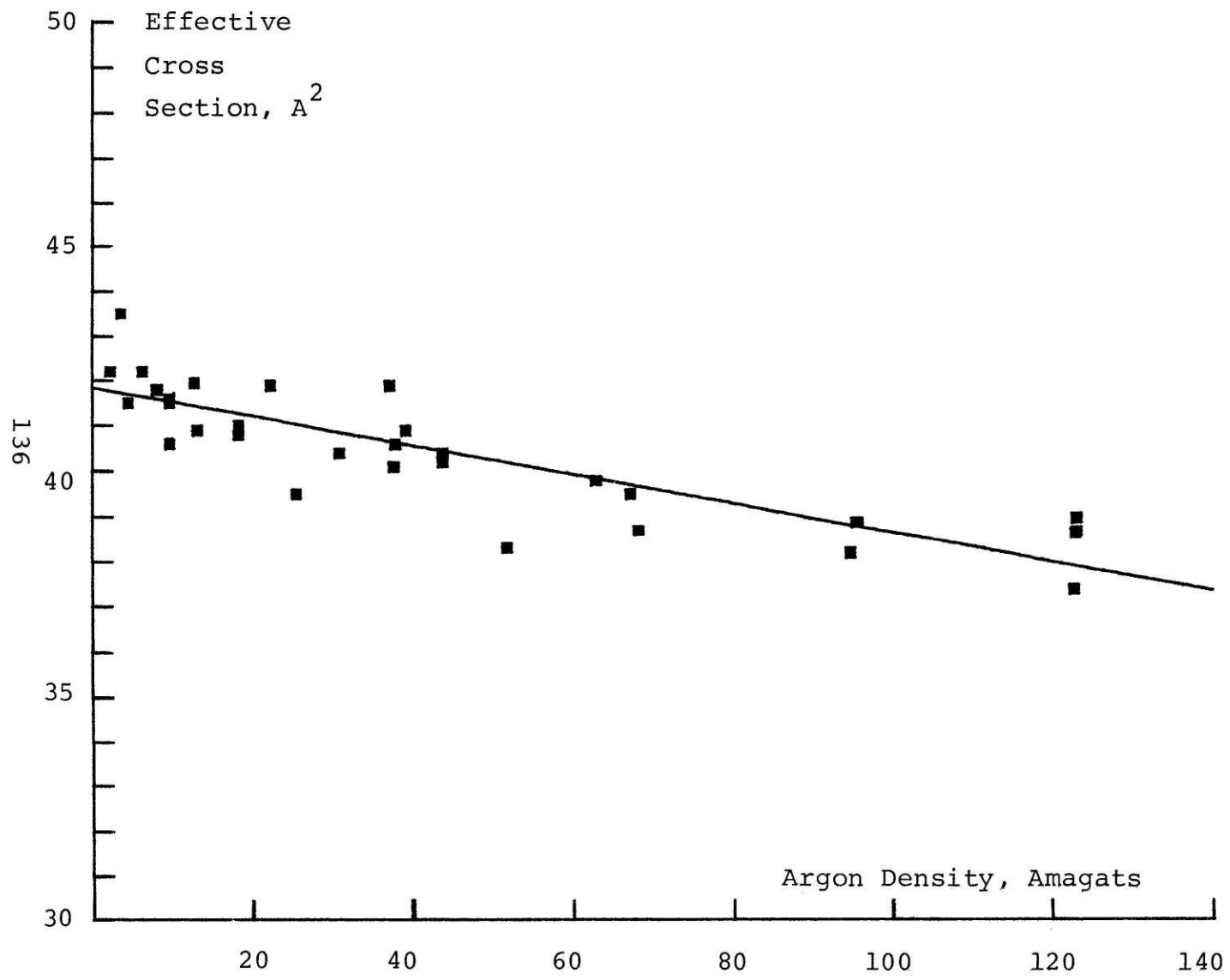


Figure 30

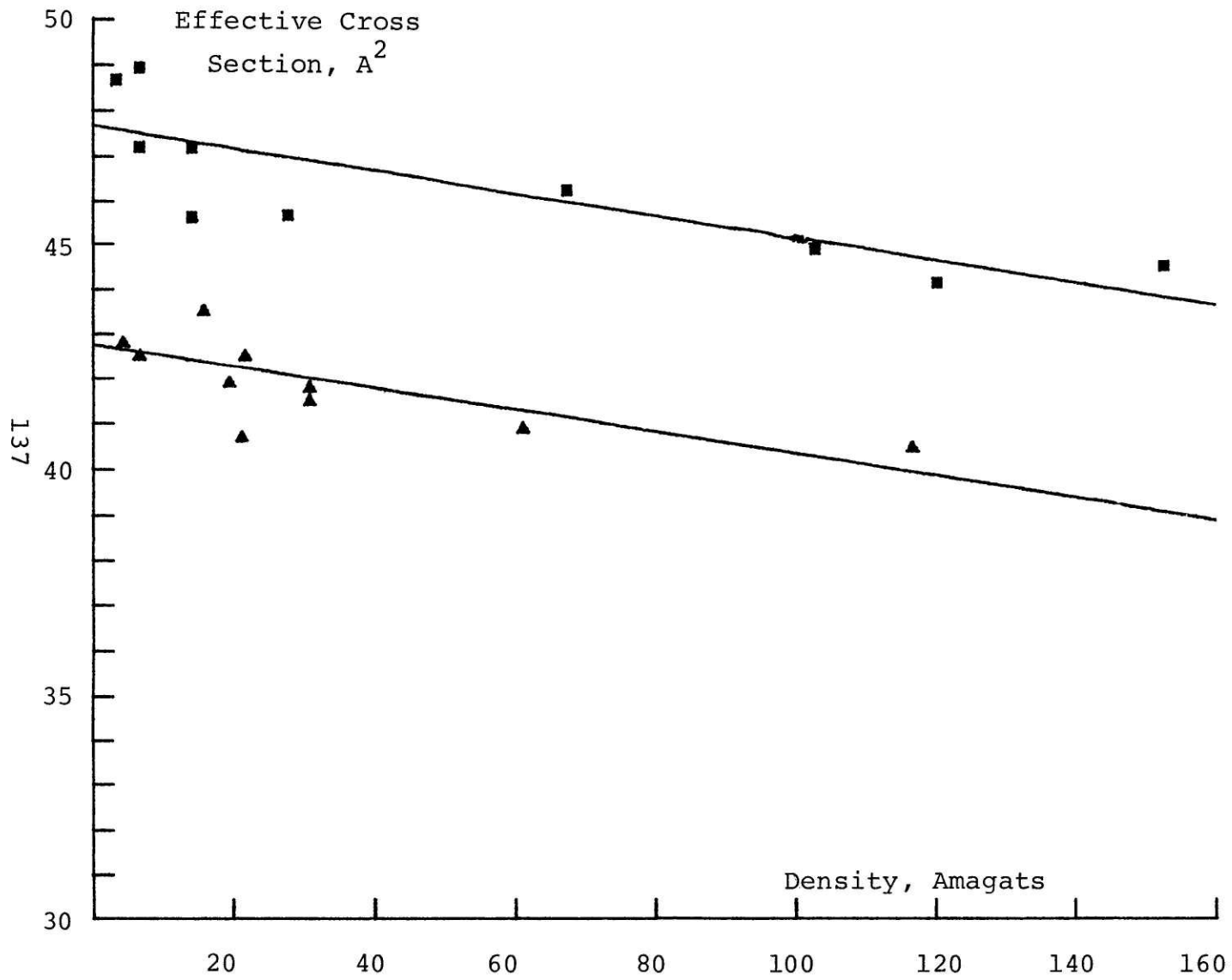


Figure 31

Figure 32: A plot of effective cross section derived from Ar self diffusion as a function of Ar density. Data from Reference 108.

Figure 33: A plot of effective cross section derived from CO₂ self diffusion as a function of CO₂ density. References 110 and 117 gave the data.

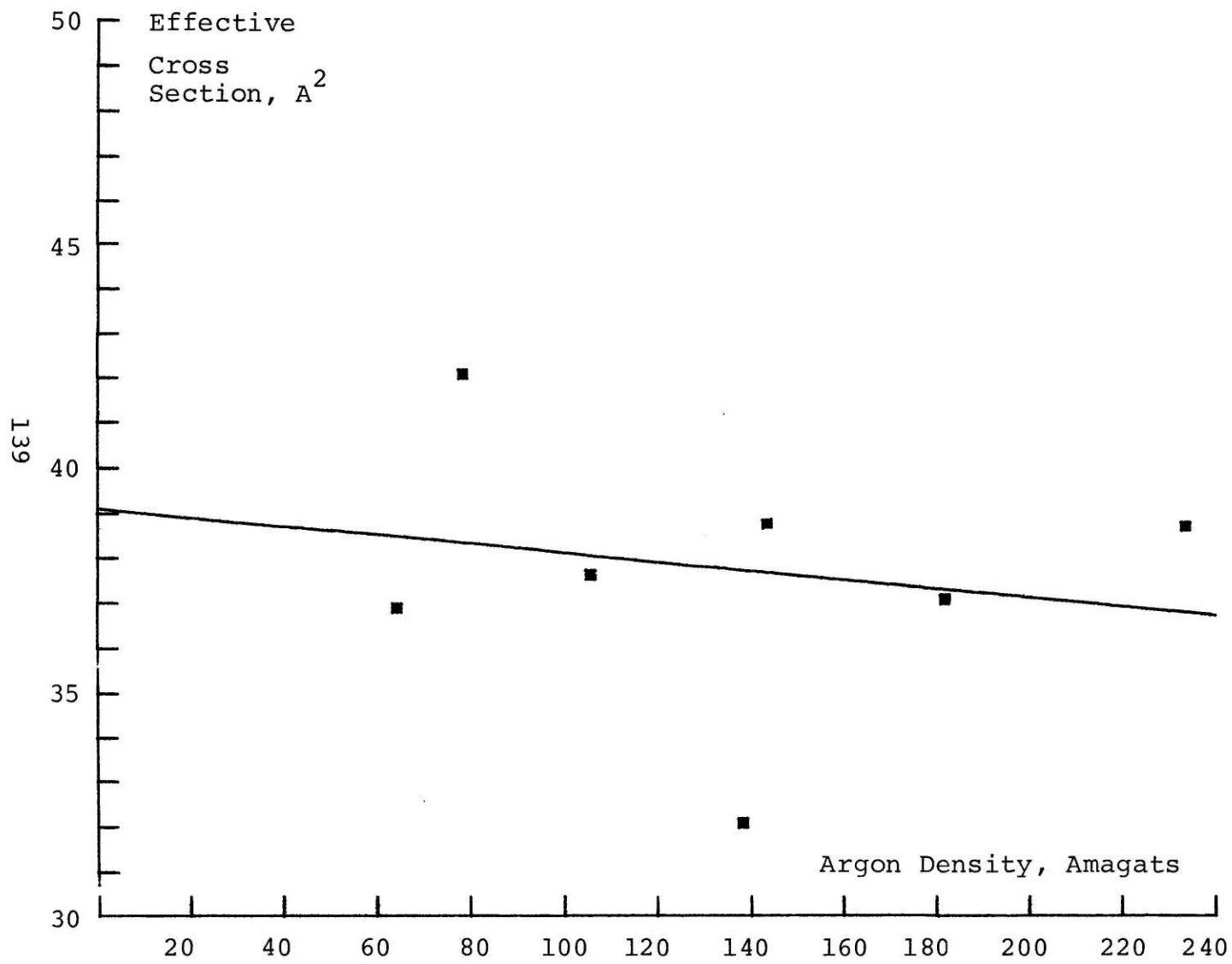


Figure 32

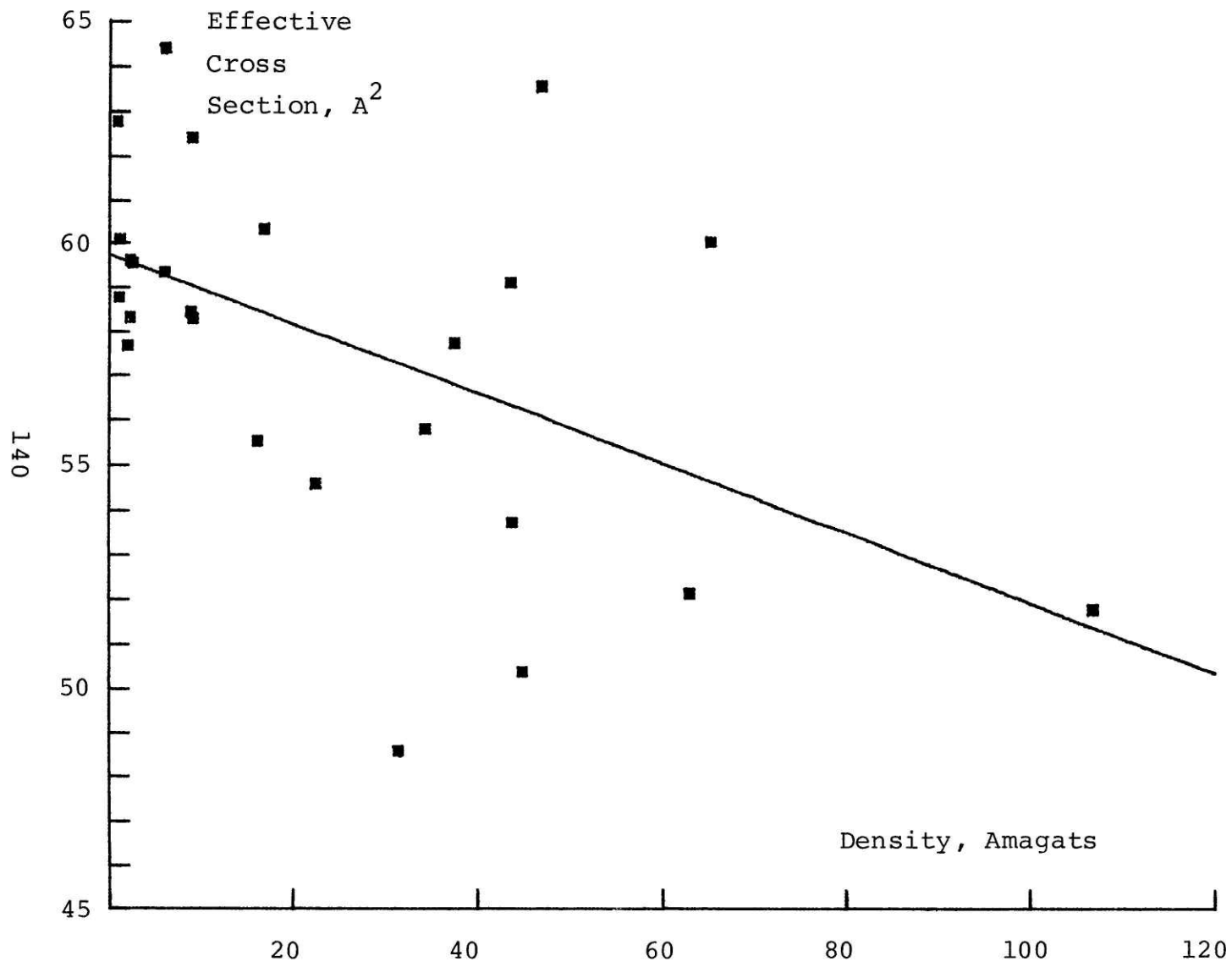


Figure 33

of the diffusion coefficient data, at least at high enough densities that the absorption linewidth is considerably larger than the laser linewidth.

Before we can compare estimates of triple collision contributions to experiment, we must find a reliable way of estimating the statistical correction discussed in Section II D. We will use a method first suggested by Enskog, of incorporating experimental compressibility data (and therefore properties of real gases), now known as modified Enskog theory (MET).¹⁰⁶ The pair correlation function appearing in our formulation of the statistical term becomes for the case of hard spheres the expression found in the Enskog equation of state,

$$(89) \quad PV/RT = 1 + b\rho\chi$$

where $\chi = (1 + 5/8 b\rho + \dots)$ and $b = 2/3\pi d^3$ with d being the hard sphere diameter. In other words, we have an effective $1/b\rho (PV/RT - 1)$ in the denominator multiplying the low density cross section.

It was the suggestion of Enskog that, first, the pressure P be replaced by the "thermal pressure" $T (\partial P / \partial T)_V$.¹⁰⁶ (Or as in Reference 56, since P becomes $P + a\rho^2$ in the Van der Waals equation of state, we should have P go to $T (\partial P / \partial T)_V$. Then, one can use experimental compressibility data in the form of a virial expansion, $(PV/RT = 1 + B\rho + C\rho^2 + \dots)$, to obtain

$$b\rho\chi = 1/R (\partial PV / \partial T)_V - 1 = T \partial / \partial T (PV/RT)_V + PV/RT - 1$$

Then we substitute in the virial expansion, and insist that

$\chi \rightarrow 1$ as $\rho \rightarrow 0$ so that we identify $b = B + T \frac{dB}{dT}$, we have

$$(90) \quad \chi = 1 + \rho \frac{(C + T \frac{dC}{dT})}{(B + T \frac{dB}{dT})} + \dots$$

in $D = D_0/\chi$.

So, to compute second order density corrections to the effective cross section or collision frequency we need not only the second virial coefficient but the third, as well as their temperature dependences.

For purposes of this estimation, we will take our virial coefficient data from the compilation given in Reference 119. Of course, virial data are not known perfectly, and in particular the third virial coefficient and its temperature derivative may be more inaccurate than even the second order density dependence we wish to compare them to. However, all the estimates display the properties of the following example, for Kr-Ar.

At 35°C, virial coefficient data from Reference 119 is given in Table 6. The third row of the table is calculated by assuming that the virial coefficients are functions of hard sphere diameters, and that these diameters obey the addition rule. In other words, we take $B_{12} = \frac{1}{2} (B_1^{1/2} + B_2^{1/2})^2$ and $C_{12} = \frac{1}{2} (C_1^{1/4} + C_2^{1/4})^4$. Note that the temperature derivatives in both cases are larger than and of opposite sign to the virial coefficients. So with both signs reversed, the ratio remains negative, thus giving a decrease in effective cross section with increasing density. However, the difference $C + T \frac{dC}{dT}$ is

Table 6 : Example of Virial Coefficient Data

<u>System</u>	<u>B</u>	<u>$T \frac{dB}{dT}$</u>	<u>C</u>	<u>$T \frac{dC}{dT}$</u>
Ar	-14.2 cm ³ /mole	59 cm ³ /mole	1130 ($\frac{\text{cm}^3}{\text{mole}}$) ²	-1330 ($\frac{\text{cm}^3}{\text{mole}}$) ²
Kr	-48	114	2420	-2640
Ar-Kr	-28.6	84	1685	-1900

now smaller than C alone. So continuing our example we have $-215/55 = -3.9 \text{ cm}^3/\text{mole}$. Dividing by $22414 \text{ cm}^3\text{atm}/\text{mole}$ gives a fractional contribution of $-1.7 \times 10^{-4} / \text{am}$, and multiplying by the cross section, 41.9 A^2 , our estimate of the second density contribution is $-.007 \text{ A}^2/\text{am}$, while the observed value was $-.032 \text{ A}^2/\text{amagat}$.

And indeed, looking down the column labeled MET in Table 5, where we list the first density corrections obtained by Equation (90), we conclude that by this method of estimation the Enskog term seems too small to explain the observations for the diffusion coefficients by itself.

Using the simple expression for the linewidth, and the conversion from density in mole/cm³ to amagats, $3.72 \times 10^{-20} \text{ atm cm}^3$, we can also convert our observed line broadening coefficients to effective cross sections, and produce the same sort of plots we used to show second density dependence in the diffusion coefficient. (An amusing coincidence is that for HF-Ar the factor $\sqrt{2\pi}(3.72 \times 10^{-20})$ is precisely 0.001×10^{16} at 310°K , so that anywhere around room temperature cross sections in A^2 and linewidths in thousandths of wavenumbers (millikaysers) per amagat are numerically equal.)

Only our data for HF broadened by argon is sufficiently reliable and goes to high enough densities that there is any hope of finding believable second density affects. Also, the data at low densities, where the linewidth is of the same size

as the width of the laser line, is too unruly to include in any fit. Therefore, the plots of effective cross section versus density in Figures 34 through 36 and the results of the least squares fit given in Table 7 are based on data above 50 amagats. (Choosing other nearby points at which to begin the fit will change these numbers by around 20 per cent. And certainly for the smaller lines the magnitude of the effect is very much in doubt. But it seems clear that at high densities there is a second order density effect, very similar to that seen in the diffusion coefficient.)

Table 8 presents the observed second density terms for the HF-Ar system, together with the calculation of my estimate of the triple collision contribution derived in Section II C, Equation 80,

$$-3/4 \cdot c/\bar{v} \cdot \sigma/r_0 \cdot (\Delta\nu_{1/2})^2$$

where v is the average velocity, σ is the elastic cross section, $1/r_0$ is a cutoff wave vector, and $\Delta\nu_{1/2}$ is the observed line broadening coefficient. This is at best an order of magnitude estimate, and the close agreement is fortuitous. Also in the table we present these estimates for the HCl-Ar and DF-Ar systems, although the quality of the data does not allow obtaining experimental values. (We note however that the total second density terms for the low J HCl lines cannot possibly be as large as my triple collision estimate, since otherwise they would be seen.)

Table 9 reports the results of some linewidth measurements

Figure 34: A plot of effective cross sections derived from HF P(2) linewidths by assuming the linewidth is given by $\rho \bar{v} \sigma^{p_0} / 4\pi c$, plotted as a function of argon density.

Figure 35: A plot of effective cross sections from HF P(3) linewidths.

Figure 36: A plot of effective cross sections from HF P(4) linewidths.

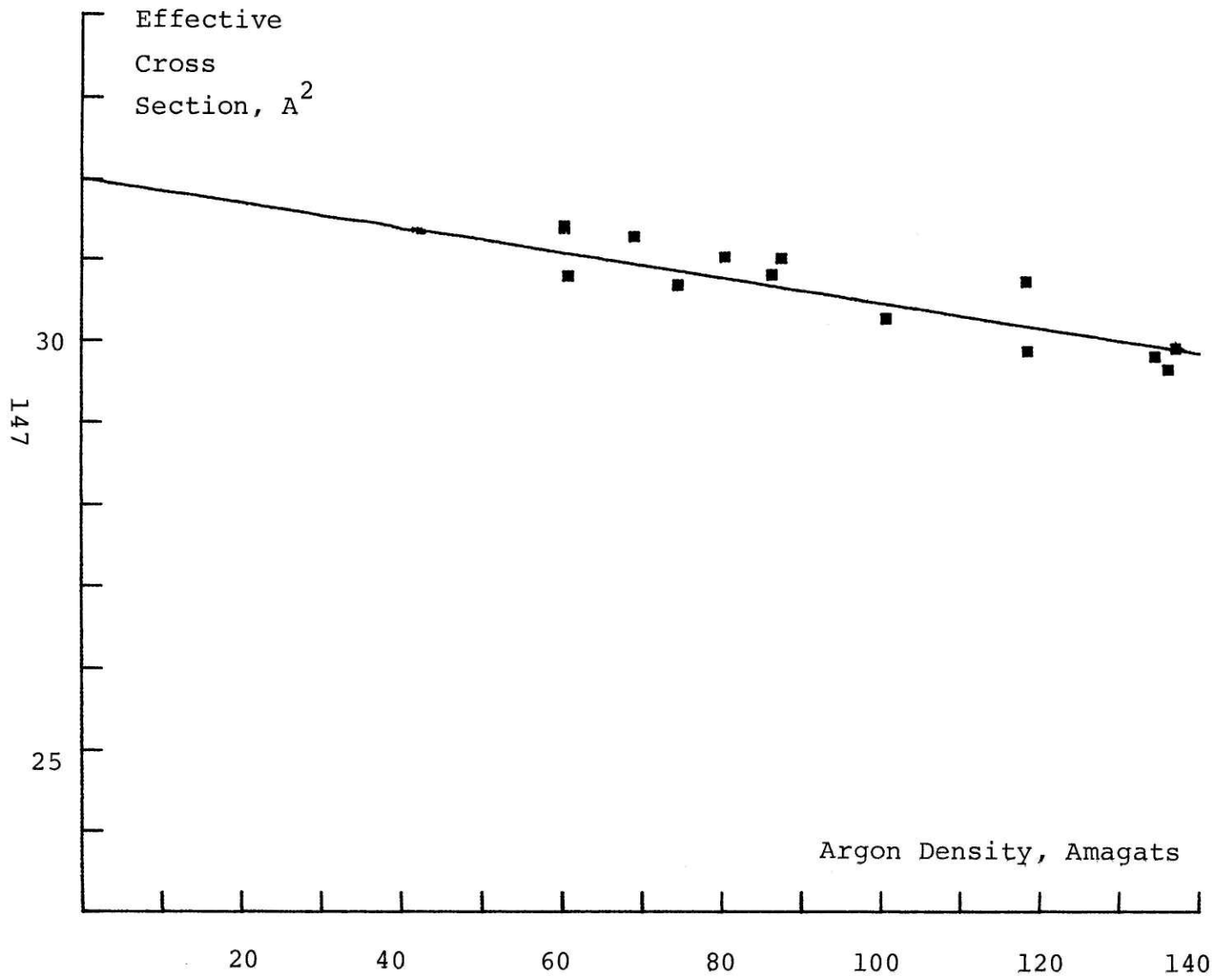


Figure 34

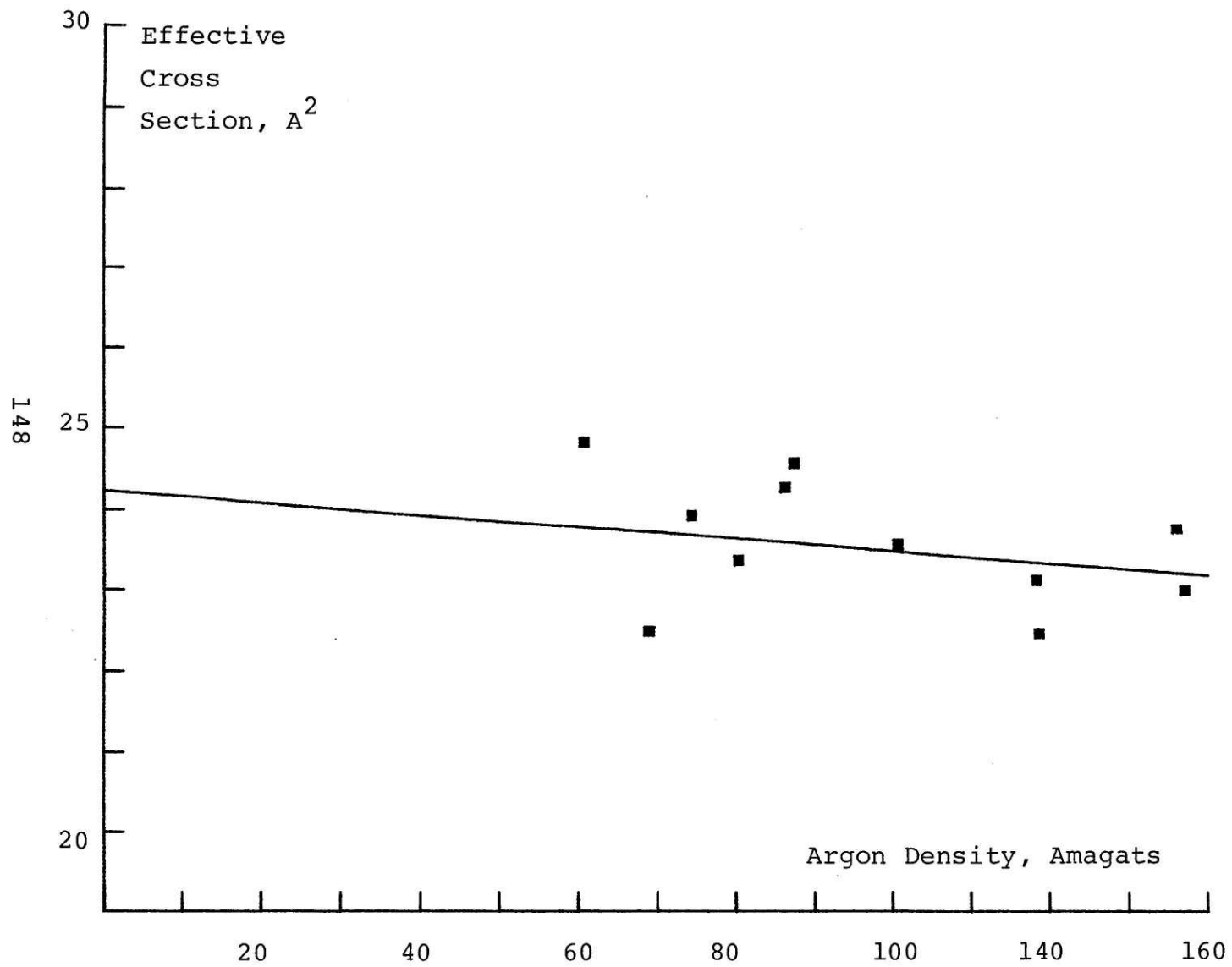


Figure 35

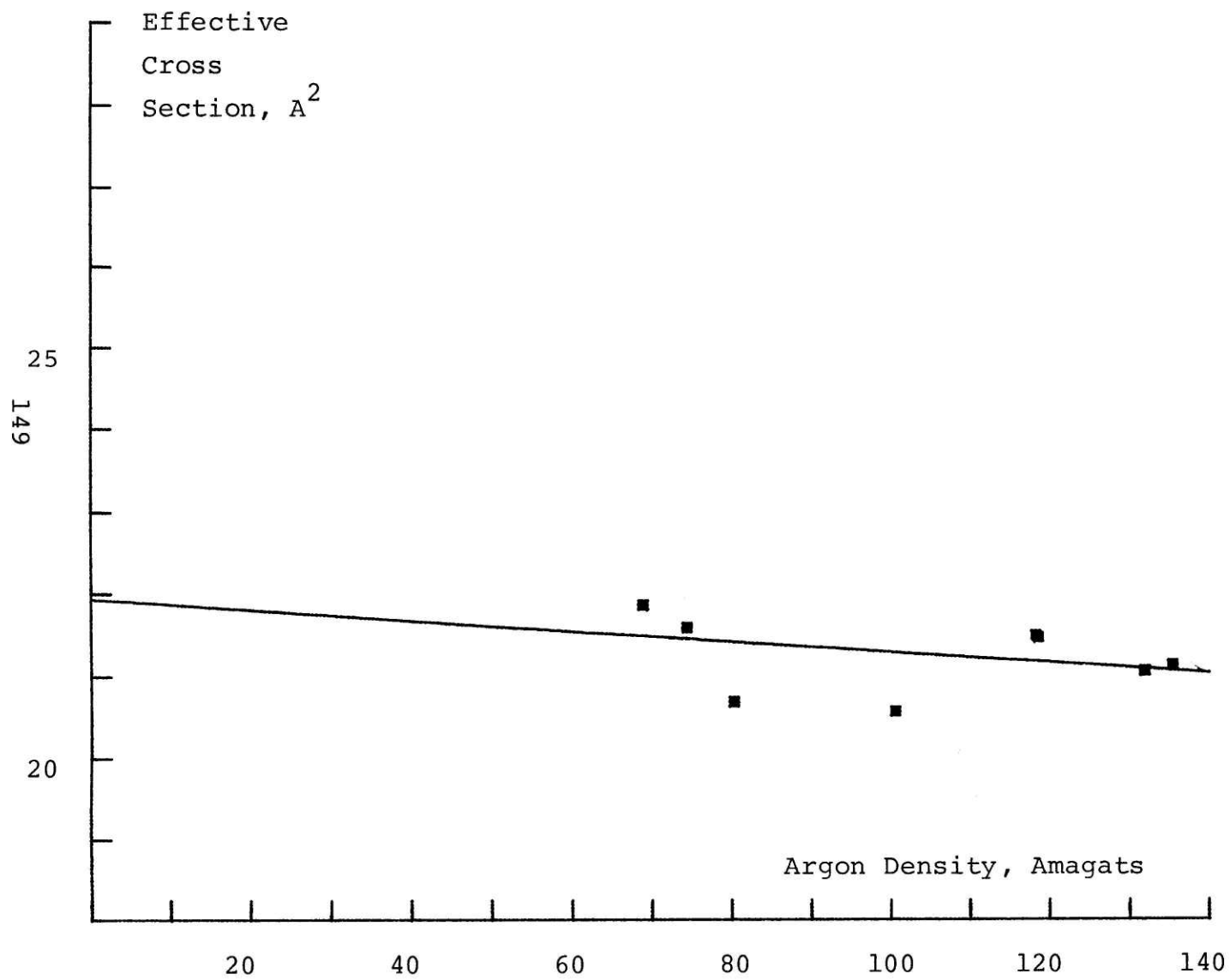


Figure 36

Table 7 : HF Linewidth Second Order Density Effects

This table reports the results of a linear least squares fit to a plot of effective cross section derived from HF linewidths as a function of density. The column marked Intercept gives the low density limit of the effective cross section, and that labeled Slope gives the second density correction. Both values are listed with the standard deviations obtained from the fit.

<u>Line</u>	<u>Intercept</u>	<u>Slope</u>
P(2)	32.0 \pm .6 A ²	-.031 \pm .006 A ² /am
P(3)	24.5 \pm 1.5	-.015 \pm .015
P(4)	21.8 \pm 1.0	-.012 \pm .01

Table 8 : Estimates of Triple Collision Contributions to Linewidths

For use in estimating triple collision terms, this table includes columns of the average velocity \bar{v} listed in units of 10^4 cm/sec, the cutoff r_0 in Å, the elastic cross section σ (obtained from rare gas values) in Å², and the line broadening coefficient $\Delta\nu_{\nu_L}$ from this work in cm⁻¹/am. The last two columns give the observed second density term and its estimate using Equation (80).

<u>System</u>	<u>\bar{v}</u>	<u>r_0</u>	<u>σ</u>	<u>$\Delta\nu_{\nu_L}$</u>	<u>Observed</u>	<u>Equation (80)</u>	
151 HF-Ar	P(2)	6.9	3	31	.029	-.000031 $\frac{\text{cm}^{-1}}{\text{am}^2}$	-.000028 $\frac{\text{cm}^{-1}}{\text{am}^2}$
	P(3)				.023	-.000015 $\frac{\text{cm}^{-1}}{\text{am}^2}$	-.000018 $\frac{\text{cm}^{-1}}{\text{am}^2}$
	P(4)				.020	-.000013	-.000012
HCl-Ar	R(1)	5.8	3.25	36.3	.042		-.000076
	R(2)				.034 ₅		-.00005
	R(3)				.032		-.000044
	R(4)				.028		-.000034
	R(5)				.021 ₅		-.00002
	R(6)				.016		-.000011
DF-Ar	R(2)				(.023)		-.000018
	R(4)				(.016)		-.000009

Table 9 : Estimates of Triple Collision Contributions to Other Linewidths

The numbers listed in the first few columns of this table are explained in Table 8. The line broadening coefficients were taken from the same reference as the density dependence. In contrast to the previous table, the last two columns give the observed deviation from the linear linewidth at the highest pressure studied.

<u>System</u>	\bar{v}	r_0	G	$\Delta\nu_L$	<u>Observed</u>	<u>Equation (80)</u>	
152 HCl-Ar 0-2, Ref. 120	P(1)	5.8	3.5	35	.063	-.11 cm ⁻¹ at 10 atm	-.015cm ⁻¹ at 10 atm
	P(3)				.047	-.065	-.008
	R(5)				.033	-.047	-.004
HCl-HCl 0-2, Ref. 121	R(8)	6	3.5	34	.115	-.039 cm ⁻¹ at 5 atm	-.012 cm ⁻¹ at 5 atm
	R(5)				.178	-.056	-.029
	R(4)				.208	-.05	-.039
	P(3)				.23	-.074	-.048
HCl-Xe 0-2, Ref. 25	P(1)	4.3	3.6	52	.077	0 at 9 atm	-.01
	R(6)				.054	0	-.005

Table 9: (continued)

<u>System</u>		$\bar{\nu}$	r_0	σ	$\Delta\nu_{v_2}$	<u>Observed</u>	<u>Equation (80)</u>
HF-HF 0-1, Ref. 10	R(6)	8	2.5	26	.158	-.03 cm ⁻¹ at 5 atm	-.018 cm ⁻¹ at 5 atm
	R(5)				.238	-.06	-.06
	R(4)				.354	-.24	-.09
	R(3)				.446	-.31	-.14
	R(2)				.537	-.715	-.20
	R(1)				.496	-.615	-.17
	R(0)				.453	-.405	-.14
	P(4)				.453	-.465	-.14
	P(5)				.295	0	-.06
P(6)				.174	+.35	-.02	
HCl-Ar Pure Rot. Ref 34	J 0-1	5.8	3.5	35	.06	0 at 15 atm	-.03
	1-2				.037	0	-.01
	2-3				.026	0	-.006
	3-4				.025	0	-.006

153

from the literature in which second order density effects on the linewidth had at least some chance of being observed. Of course there is no guarantee that deviations from a linear behavior for the linewidth are not due to some other trouble with the experiment. Indeed, for some experiments, both those which show an effect and those which see nothing, the experimental data consists of only two points.

In Table 5 we present a column (marked Eq. 79) of my estimates of the triple collision contribution to the diffusion coefficient. This simply assumes that the collision frequency correction Equation (79) $(-k_0/8 \bar{v}^3)$ in $\text{sec}^{-1}\text{am}^{-2}$ is the average velocity \bar{v} times a cross section correction in cm^2/am .

These estimates are obviously too large. But this is not surprising considering our discussion in Section II C showing that transport coefficients, in which the collision operator operates on functions of momentum, have reduced triple collision terms due to constraints on the angles of the relative momenta. Exactly what factor should be used to reduce the estimates is a matter for detailed calculation which will not be attempted here.

In order to finish our discussion of the second density effects on the linewidth, we should compute estimates for their Enskog contribution. We might like to simply conclude that the contributions will have the same characteristics as the MET estimates for systems studied by diffusion, that is, having the same sign and order of magnitude but not being

large enough to explain the observed effect by themselves.

If we wish to do better, however, repeating the MET calculations for systems like HF-Ar and HCl-Ar is difficult. There exist some compressibility data for HCl^{122,123} and HF¹²⁴, and even some indication that the third virial coefficients are of the same order of magnitude as those previously encountered¹²² and decrease with increasing temperature¹²³. But even if the data for the individual virial coefficients were trustworthy, which is not, the procedure of using combining rules to obtain virial coefficients for an HCl-Ar mixture is probably not justified.

Another possible approach is to use the expressions for B and C and their temperature derivatives for a Lennard-Jones 6-12 potential from Reference 125. For instance, for the isotropic HCl-Ar potential used by Gordon³³ (originally from Reference 126) the r_0 is 3.39 Å and the well depth is 205°K so that $T^* = kT/\epsilon$ is 1.45. From Reference 125, with $B^* = B/b_0$, $C^* = C/b_0^2$, and $b_0 = \frac{2}{3}\pi N_0 \sigma^3$, at $T^* = 1.45$ we have $C^* = .556$, $TdC^*/dT = -.364$, $B^* = -1.28$, and $TdB^*/dT = 2.53$. With b_0 being 46.9 cm³/mole, this means a MET second density contribution of + 7.2 cm³/mole is obtained, which is larger and of opposite sign to those from experimental virial coefficients.

So perhaps we indeed do best by assuming that the statistical corrections are of the order of the MET estimates made for the diffusion constant, and that therefore recollision

terms the size of those obtained in Section II C may be needed for agreement with experiment.

Further it seems a fair conclusion that the experiments do support the existence of a second order in density correction to the linewidth, but this term is small, almost within the experimental uncertainty. Therefore, any third order terms, logarithmic in density or not, would be very small at moderate densities, and very difficult to measure.

III APPENDICES

Appendix A : The Chromatix Laser and Parametric Oscillator

This appendix contains a discussion of the routine operation and maintainance of the Chromatix Nd:YAG laser and optical parametric oscillator (OPO), the frequency and power characteristics of the parametric oscillator and some comments on its operation with an intracavity etalon. Much of the information given here is also contained in the Chromatix manuals for the laser, parametric oscillator, and crystal oven, but like all manuals they benefit from the addition of personal experience.

We begin with the normal operation of the Nd:YAG laser as it is used to produce green pump light for the parametric oscillator. First, the power for the laser is normally kept turned off at the laboratory circuit breaker (number 8). Second, cooling water for the refrigerator heat exchanger must be flowing through the garden hose at an adequate rate or the laser refrigeration system circuit breaker will open. Assuming operation in the green region, the laser may be run without refrigeration, and indeed it seems one may obtain slightly higher power without it. On some occasions, however, the laser seems to have had better long term stability with the refrigeration on. In any case, going from one to the other changes the laser cavity and necessitates readjustment.

Only when the power and water have been turned on can the laser be turned on at the power supply. However, the flashlamp

should still not be turned on until it is verified that either the pulse rate knob is on, or the laser is being triggered externally. For these experiments, the laser was triggered by a pulse generator (General Radio model 1217-A) through the Lamp Trigger In connection, as specified in Section 1.4 of the Chromatix laser manual. When the laser is triggered externally, the pulse rate knob is set to zero, which turns on a red warning light beside the laser power knob. Turning on the power when the laser is totally untriggered will charge the capacitors well above a safe level, causing at worst a component failure and at best an unpleasant time when the flashlamp is required to discharge the overload.

Operation of the parametric oscillator requires that the Nd:YAG laser be Q-switched, and also demands close to its maximum safe power. There are four adjustments commonly used to peak the laser output. The first two, the back mirror knobs, will need readjustment almost every time the laser is turned on. The back mirror is on a triangle mount, and the knob closest to the operator (corresponding to vertical tilt if the cavity were not bent) is quite sensitive, while the far knob, with a gear arrangement, is less so. It is this knob, however, which controls the laser frequency. (If this knob is too far out of adjustment, the laser can operate on a green line at 531 nm, instead of the considerably stronger 532 nm line.) Only the back mirror should be adjusted, with the front mirror kept fixed.

Next the frequency doubler will often need alignment, but this should only be done with great care. When its green output is not maximized, the doubler crystal absorbs the infrared radiation and can be thermally damaged. Furthermore, this adjustment has an extremely narrow maximum. This maximum lies between two secondary maxima, so at times a quick check should be made to see that the knob is at the central peak. (The maximum height of the pulse from the visible monitor, an internal PIN photodiode, appears to occur at the two intermediate minima around the central laser power peak. Therefore all adjustments should be made using the power meter, a Scientech model 36-0001 1 inch Disc Calorimeter, and a sensitive voltmeter.) Often a change in the doubler angle will necessitate a change in the back mirror alignment, and one should go back and forth between the two adjustments to make sure the output has been optimized.

Finally, an adjustment which can sometimes have a sizable effect on the output is the Q-switch vernier control. This positions the window in the radio frequency field applied to the acousto-optic Q-switch over the maximum in the flashlamp pulse. For this experiment, any adjustment of the Q-switch vernier will necessitate repositioning of the integrator switch window (described in Appendix C) over the laser pulse before it can be detected. It is possible that this Q-switch vernier adjustment may contribute to the pulse to pulse stability of the laser.

Another source of instability is competition between transverse modes of the laser. The laser should operate only in the TEM_{00} mode. This can be checked by expanding the beam using a lens and projecting it onto a wall, looking for any sign of TEM_{01} or TEM_{10} modes. These can then be eliminated by closing down the diaphragm in the laser cavity.

In the best of times, a clean, well adjusted laser should produce around 16 mW average power at 370 volts across the flashlamp and 30 Hz pulse repetition rate, and 20 mW at 390 volts. However, the laser is dirty enough that these power levels are only attained at 10 or 20 volts higher lamp voltage.

If the preceding routine adjustments do not result in the desired power level, there are several items which may be checked. First, the laser water and coolant systems should be flushed every month, or every few weeks if the laser is being operated every day. The laser may show up to a five or ten per cent increase in power after a flush. Additional cleaning may be achieved by flushing with a solution of around one per cent of EDTA (in coolant system only) and Liquinox soap. However, the laser will inevitably become dirtier, and even frequent flushes can only slow this trend. The flashlamp water jacket can be swabbed out during lamp changes using a mild HCl solution and a Q-tip, which can be checked for any brown deposits. The top of the reflector cavity can even be removed to check for deposits on the laser rod. However,

removing and cleaning the rod itself is a major and difficult operation, which has only been attempted once. Preventive maintenance is advised to forestall this unpleasant task.

A second source of power loss may be a deteriorating flashlamp. Their output may show some falloff after 3 or 4 million pulses. This possibility is easy to check, using the simple lamp replacement procedure given in the laser manual.

Two other components which may be adjusted occasionally for maximum pulse stability and amplitude during Q-switched operation are the RF switch and RF oscillator. The RF switch is located in the laser head and has an impedance-matching network which can be optimized with two screwdriver adjustments. There is a BNC tee on the switch which allows observation of the Q-switch RF during these adjustments using an oscilloscope probe. The RF oscillator is a large vacuum tube located in the laser power supply next to the circuit boards. It should be optimized first. It has two very sensitive knobs, of which the upper one should be adjusted first. The object of both these adjustments is to maximize the peak-to-peak value of the Q-switch RF, but also more importantly to maximize the laser power and stability.

Now we discuss the normal operation of the optical parametric oscillator. When the parametric oscillator is already producing red and infrared light, it is customary to vary the alignment of one or both mirrors and perhaps the crystal oven and visually maximize the red output. The true

maximum in output cannot be located by more systematic methods, but "walking" the cavity is a dangerous practice and may result in straying far away from best alignment. When this happens, or when mirrors are changed so there is no output at all, it is necessary to follow the alignment procedure discussed below.

First, before the oven temperature controller is turned on, the pressure from the ultrapure oxygen cylinder should be raised to ten pounds from slightly above zero, where it is always left to keep dust away from the crystal. Second, the OPO crystal has four quadrants, with different coatings which make some difference in operation in various spectral regions. The crystal is installed so that quadrant 1 is at the top and closest to the operator. Two adjustment knobs on the oven allow the various quadrants to be moved onto the laser spot, which can be seen to become more diffuse when moving through a boundary. Quadrant 1 is used with the P1 mirrors, while quadrant 2 is used with P2 and P3 mirrors. (See Figure 37 for ranges of operation of these sets of mirrors.)

When aligning the OPO the Nd:YAG laser should not be Q-switched and should be operated near threshold lamp voltage and with the green attenuator. Also, no light should be put onto a cold crystal. The oven should be set somewhere in the wavelength region for the mirrors being aligned (near the center, if there is no output to start with).

Several measurements have been made on the power of the red light at around 6710 to 6680 Å wavelength or 335 to 340°C

Figure 37: A plot of wavelength of optical parametric oscillator output as a function of crystal oven temperature. The bars mark the regions of operation of the various mirror sets, P1 mirrors being used in the longest wavelength regions and then P2 and P3. The P2 and P3 regions overlap, while there is a small wavelength region which is not easily obtained using either P1 or P2 mirrors.

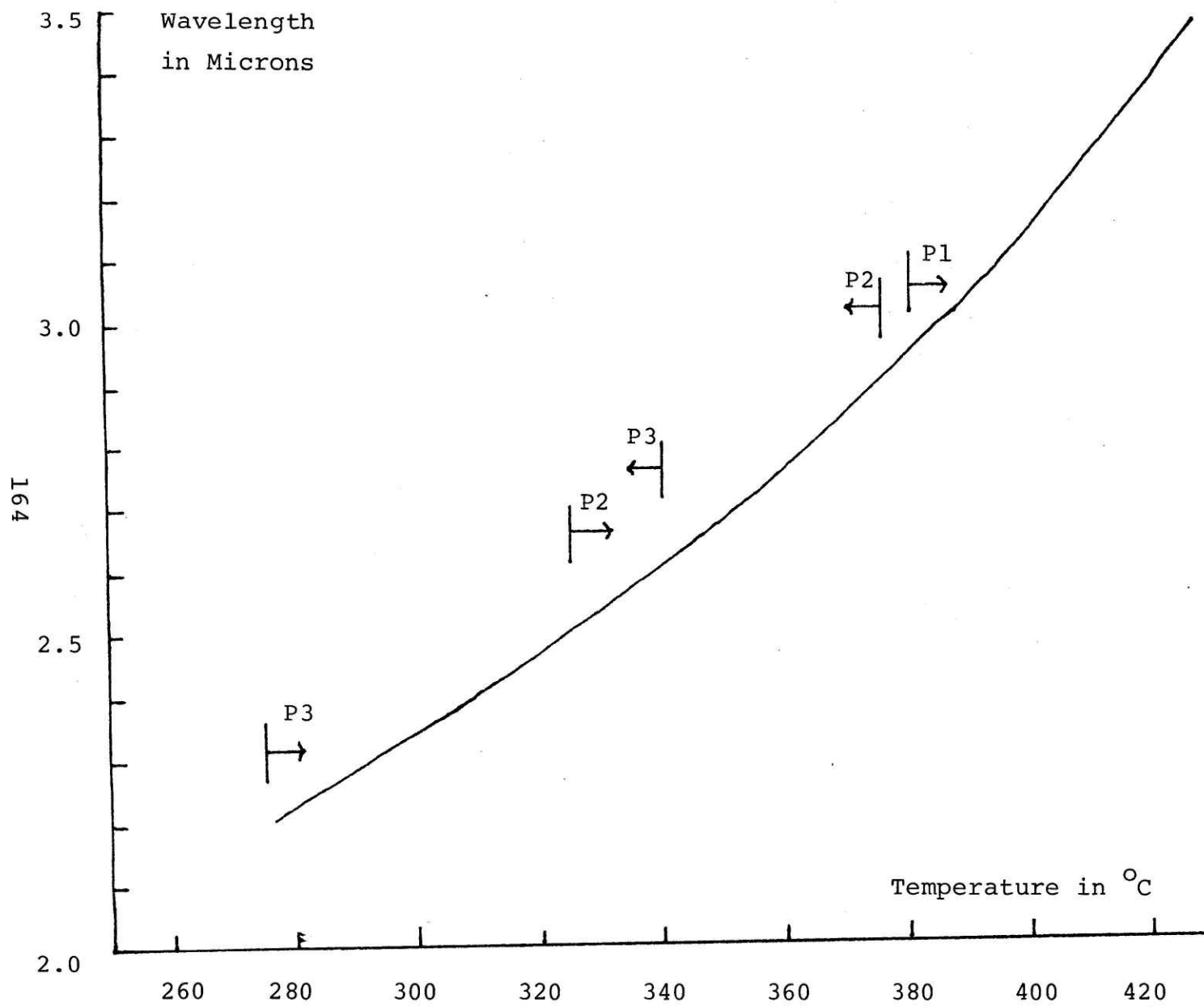


Figure 37

oven temperature. (The infrared power is too weak to be measured directly.) The results are that with a 30 Hz pulse rate, an average green pump power of 16 to 18 mW produced 2.1 to 2.3 mW red power. Assuming a pulse width of 100 nsec this translates into a peak red power of 800 watts. The corresponding infrared power levels would be about 0.5 mW average power at 30 Hz, and 200 watts peak power. These figures vary with wavelength, and would be smaller in the 3.5 micron region, at the end of the OPO gain curve.

The parametric oscillator crystal can be damaged by too high peak pump laser power. A good safe maximum is 0.75 mJ per pulse. Since this translates into about 8 kW peak power, or 22 mW average power at 30 Hz, it is also close to a safe maximum for the pump laser. The actual damage threshold may be much above these figures, according to people who have enough money to find out.

For a well adjusted parametric oscillator, 14 mW average pump laser power should be enough to produce red light in almost any spectral region, and 16 mW should be enough to give stable operation.

Although no experimental measurements were taken with the intracavity etalon and external spectrum analyzer, a good deal of time was spent in characterizing them. Here we shall simply state the progress made in finding the properties of the etalon and spectrum analyzer, and then describe their alignment procedures.

We have three intracavity Fabry-Perot etalons, numbered EY 45, 46, and 57, with finesses (free spectral range divided by bandwidth) of 4, 7, and 11 respectively. They are solid, temperature tuned etalons, all with a bandwidth of about 0.6 cm^{-1} and coated for the region of 2.7 to 3.3 microns. The etalon temperature controller also has a knob which allows matching the OPO modes to the peak of the etalon window. This is done by changing the cavity length by means of a piezoelectric transducer on the output mirror. The number of cavity modes passed by the etalon can be checked using an external etalon, or spectrum analyzer (Spectra-Physics model 422). This is also scanned by a piezoelectric transducer, controlled by a Lambda model 4 power supply.

Briefly, the following characteristics have been observed. The spectrum analyzer indicates that single mode operation can be obtained using the two highest finesse etalons, with the finesse of 4 etalon passing between 1 and 3 modes. Single mode operation can be stable in frequency for periods of 5 to 15 minutes. Using the etalon temperature control one can move from one OPO cavity mode to the next. This mode spacing is 10 to 20 etalon temperature units. This spacing, around 0.04 cm^{-1} , is also around 35 to 40 volts for the spectrum analyzer. It is also consistently about 300 volts on the OPO cavity piezoelectric control, although this shows some unpredictable behavior in between transmission peaks. The free spectral range of the etalon is on the order of 100 temperature units

on the etalon oven control, and that of the spectrum analyzer is 200 to 220 volts.

Finally, we discuss the alignment of the etalon and spectrum analyzer. In aligning the etalon, one should take the same precautions in regard to temperature and laser power as were described for mirror alignment. Three very faint spots will be seen on a scatter screen placed behind the output mirror. The two that move toward each other as the etalon is tilted are the ones to superimpose. (An equivalent procedure is to superimpose the two spots that can be seen between the OPO lens and the input mirror.)

The spectrum analyzer is aligned using a Spectra-Physics model 132 helium-neon laser, an iris to prevent reflections from interfering with the laser output, a photodiode, and the 90 volt sawtooth wave generated by an oscilloscope at a time base setting of around 10 msec/cm, used to drive the piezo-electric transducer. Alignment begins by centering the He-Ne laser spot on the input lens of the spectrum analyzer and tilting and translating until the laser comes through. Roughly align by watching the reflections off the spectrum analyzer onto the iris. When the system is well aligned, four spots are seen, one small bright spot, one small rather weak spot, one medium-sized very dim spot, and one large bright spot. The best alignment is when the second and fourth spots, and probably the third, are superimposed.

Final adjustments on the spectrum analyzer are made by

changing the mirror separation while looking at the pattern on the oscilloscope due to the transmitted light detected by the photodiode with changing ramp voltage. As shown in Figure 38, the pattern consists of repeated scans of the He-Ne laser output. The object in alignment is to maximize the sharpness of the peaks.

To allow changing mirror separation, one of the spectrum analyzer mirrors is on a screw thread mount, adjusted with a special tool. When starting from the beginning, turn the screw all the way in and slowly back it out, about two revolutions. Each time the separation is changed the tilt has to be adjusted. If the scope pattern moves to the right as the tilt is adjusted then the separation screw should be turned in, and vice versa. Alignment is achieved when the resolution of the laser peaks is maximized and when they decrease in amplitude without moving either to the right or to the left when the spectrum analyzer is tilted.

Figure 38a: Oscilloscope trace of He-Ne laser output detected through the spectrum analyzer driven by the 90 volt ramp from the scope. The x scale is 10 msec/cm and the y scale is 0.2 volts/cm. The spectrum analyzer was using the number 18 mirrors.

Figure 38b: The same, but using number 7 mirrors. These mirrors give much sharper peaks, and were used during the studies of the internal etalon in the 3.5 micron region of the infrared.

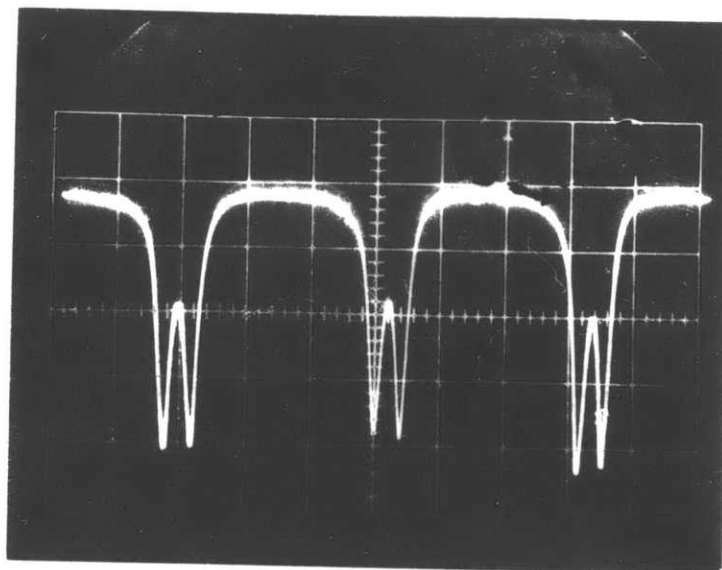


Figure 38a

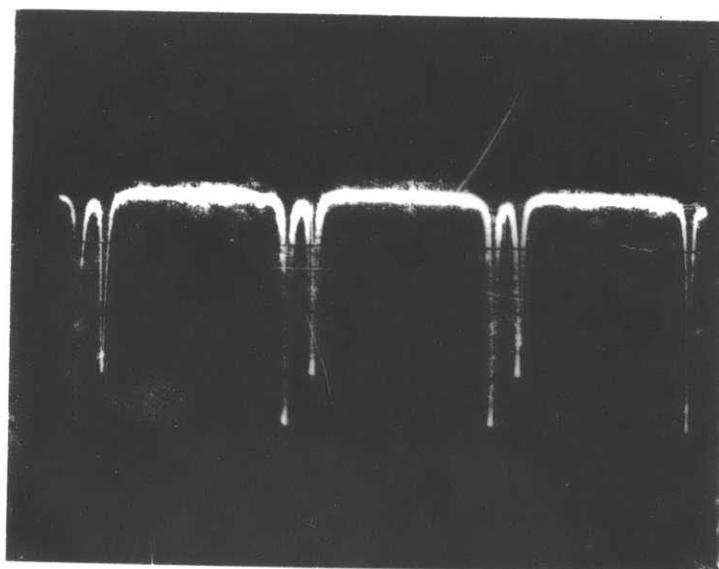


Figure 38b

Appendix B : Sample Cell and High Pressure System

This appendix details the construction and components of the high pressure and vacuum system. A rough sketch of the window mounting of the monel sample cell is given in Figure 39. This design has the advantage that the high pressure is held in by the large outer bolts, and can only seat the sapphire window more firmly onto its O-ring. The plate and small screws need only hold the window against the one atmosphere pressure encountered when the cell is evacuated. (Both inner and outer screws should be tightened using a torque screwdriver for even compression of the O-rings and to avoid cracking a window.)

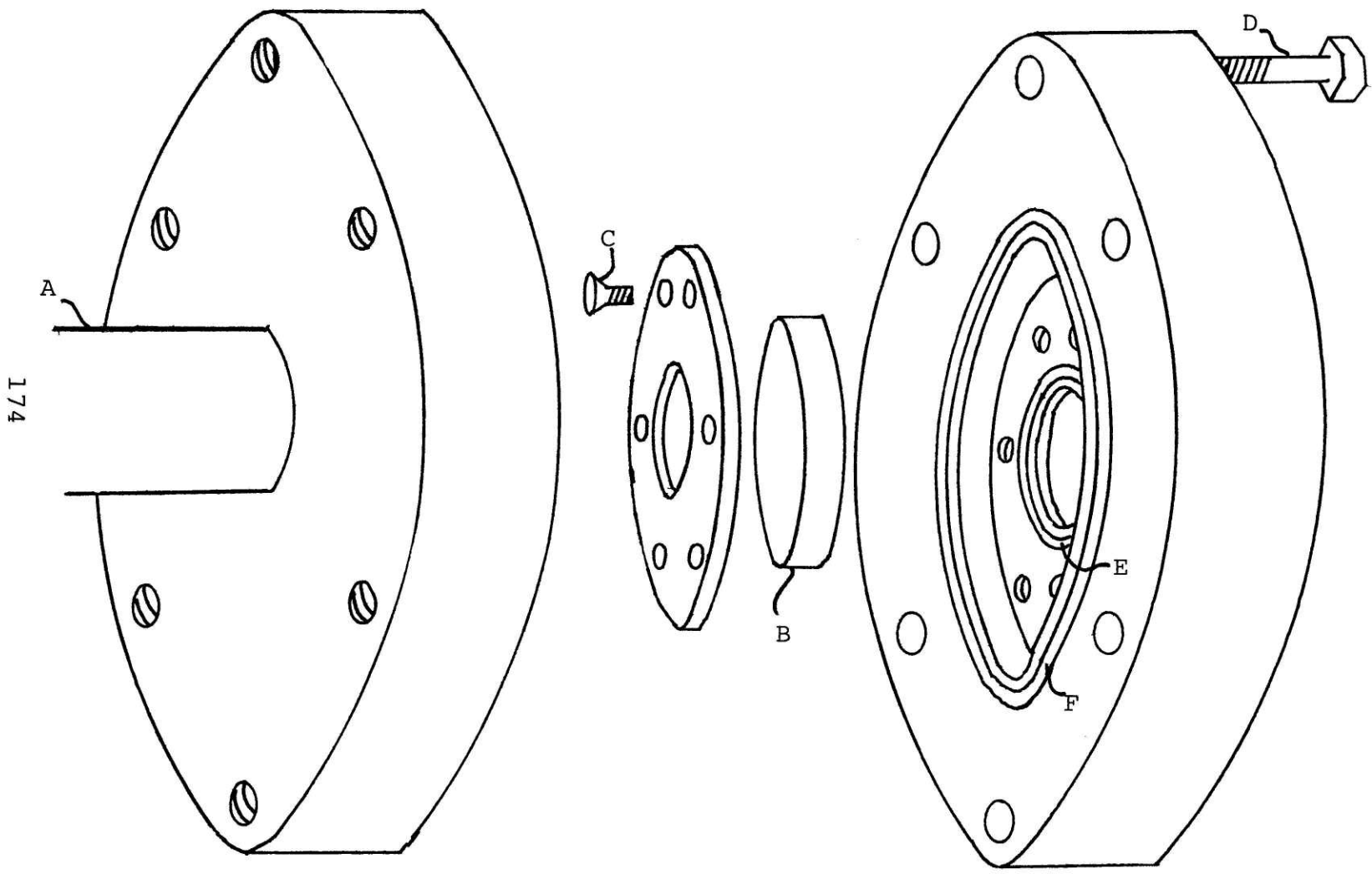
Figure 40 is a schematic diagram of the metal part of the high pressure and vacuum system. High pressures, up to 2000 pounds per square inch of argon, are measured by a Heise stainless steel Bourdon gauge with 5 psi divisions, calibrated to within 2 psi. The sample pressures (typically a few torr) are measured with a U-tube manometer with one monel arm and one glass arm. It is filled with 13-21 Halocarbon oil (specific gravity 1.9).

In filling the cell, one normally takes the sample gas trapped between the two valves on the lecture bottle and expands it into the rest of the system. After measuring the pressure with the oil manometer, the valve to the cell is closed and the rest of the system is evacuated through a liquid nitrogen trap in the glass system. (Alternatively,

after the cell valve is closed most of the remaining sample gas can be frozen out into the stainless steel trap marked N in Figure 40, for reuse.) The high pressure argon is first put into the system up to the cell valve. Then the valve is opened, causing argon to fill the cell to the desired pressure on the gauge, without allowing the sample gas to escape.

Figure 39: A sketch of the window assembly of the monel sample cell. A parts list is given in Table 10.

Figure 40: A block diagram of the high pressure system. A parts list is given in table 11.



174

Figure 39

175

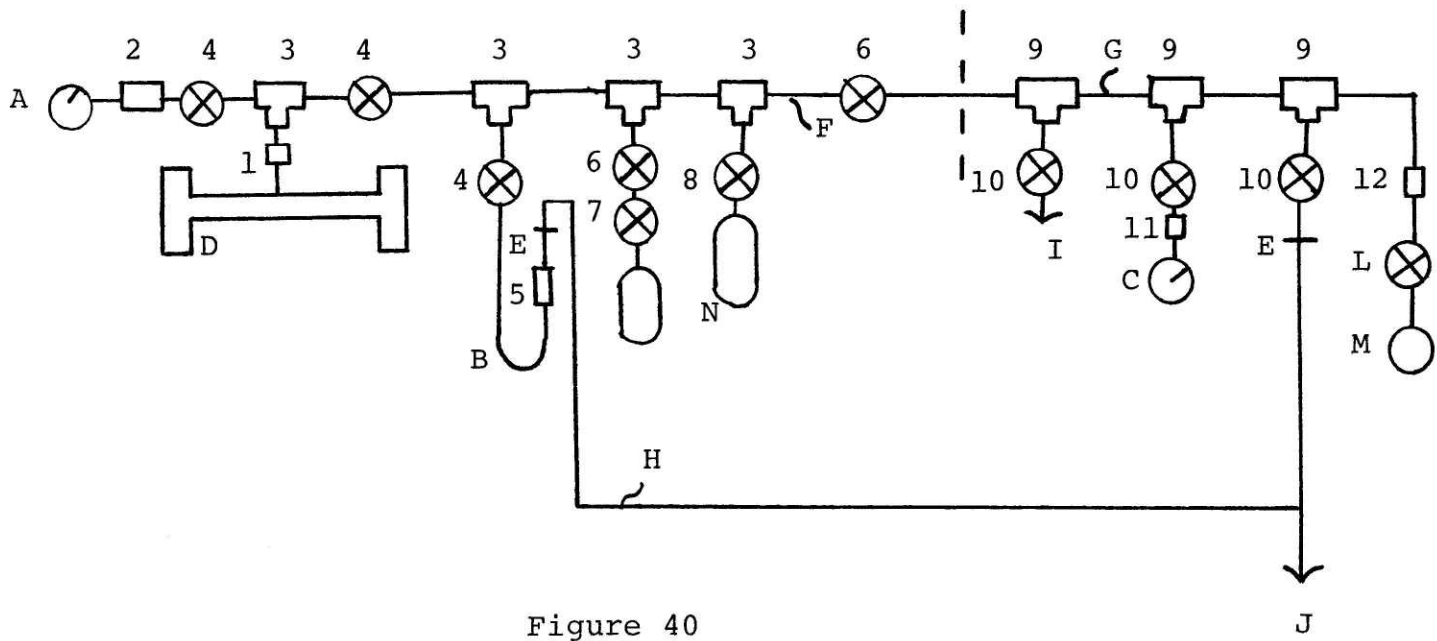


Figure 40

Table 10: Parts List for Figure 39, Monel Sample Cell

- A. 20" by 1/2" schedule 40 monel pipe
- B. 1" diameter, 1/4" thick sapphire windows (Adolf Meller)
- C. 6-32 3/8" flat head monel screws
- D. 1/4-20 1 1/2" hex head steel bolts
- E. Teflon 018 O-ring, 3/4" i.d., 1/16" width
- F. Teflon 226 O-ring, 2" i.d., 1/8" width

Table 11: Parts List for Figure 40, High Pressure System

1. M-400-6 Swagelock monel union
2. 400-1-4-316 Swagelock stainless steel 1/4" male
pipe thread connector
3. M-400-3 Swagelock monel union tee joint
4. 1VS4-M Whitey monel valve
5. 400-6-316 Swagelock stainless steel union
6. 1RS4-M Whitey monel regulating valve
7. Matheson 60L monel valve
8. 1VS4-M4-A-316 Whitey stainless steel angle valve
9. 400-3-316 Swagelock stainless steel union tee joint
10. 1VS4-316 Whitey stainless steel valve
11. 810-6-4-316 Swagelock stainless steel reducing union
12. B-400-1-4 Swagelock brass 1/4" male pipe thread connector

Table 11: (continued)

- A. Heise 8 1/2" Bourdon gauge with 1/4" female pipe thread fitting
- B. Oil manometer with 1/4" o.d. monel and 3/16" o.d. glass tubing
- C. Consolidated Electrodynamics GP-140 vacuum gauge with GP-001 Pirani tube
- D. Monel sample cell
- E. Glass to metal seal
- F. 1/4" o.d. by .049" wall monel tubing
- G. 1/4" o.d. stainless steel tubing
- H. 5/16" o.d. glass tubing
- I. Tygon tubing leading to hood
- J. Glass vacuum manifold and mechanical pump
- K. Sample lecture bottle
- L. Matheson 4-580 high pressure regulator
- M. Argon cylinder
- N. Trap, Matheson 6-635-2520 500 ml stainless steel sampling cylinder with 1/4" female pipe thread fitting

Appendix C : Integrator Description and Operation

In order to do absorption spectroscopy using a pulsed laser it is necessary to transform the size of a voltage pulse on the order of 100 nsec in width into a form whose amplitude can be measured, in our case by the analog to digital converter of the PDP-8/L computer. This could be done by integration using a simple RC circuit. Indeed, this was originally attempted, but there was found to be a complication. Just before the laser pulse there occurs a large pulse of electrical noise, which when integrated contributes the larger part of the total signal.

In order to reject this noise, a switch is placed in front on the integrator, here a very fast FET switch which can be opened just long enough to admit the laser pulse. This type of switch means that the integration must be done by an operational amplifier integrator circuit, a block diagram of which was given in Figure 2. In this circuit, with its extremely long decay time, integration results in a nearly constant voltage on the integrating capacitor. This voltage is read by the computer and then returned to zero by a second switch across the capacitor.

This appendix describes the operation of the op-amp integrator, referring to the schematic drawing of the front and back panels in Fig 41. The detailed integrator circuitry is shown in Figure 42, the triggering circuitry in Figure 43, and the physical placement of the components in Figure 44.

A list of the potentiometers and capacitors involved in the adjustments on the front and back panels is given in Table 12.

The laser power supply produces two types of trigger pulses, one associated with the discharging of the flashlamp and one synchronized with the windows in the Q-switch RF. However, the actual laser pulse occurs at varying times after the lamp trigger. And the Q-switch is free-running with a reset before each lamp flash, meaning that there are many Q-switch windows, only one of which contains the laser pulse.

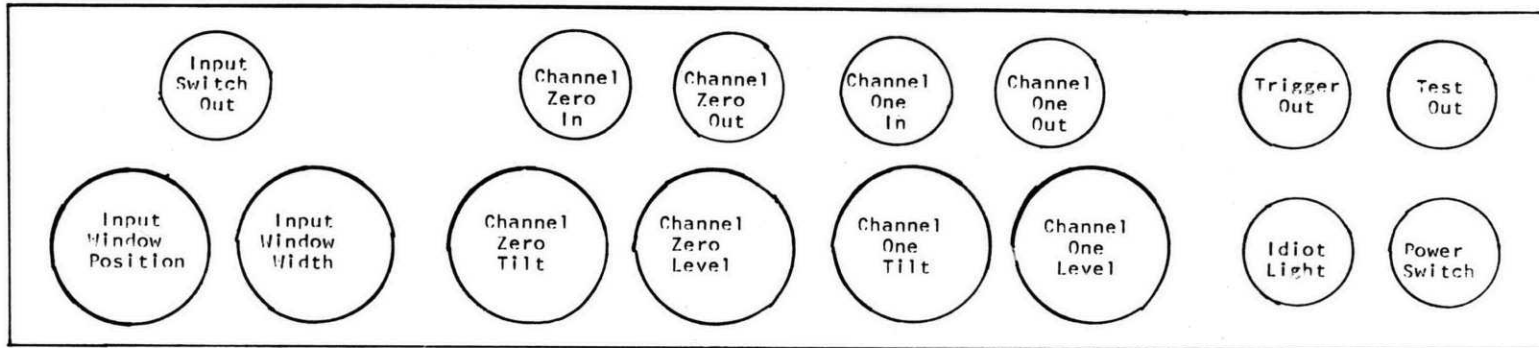
The problem of positioning the input switch window in time so that it falls directly on the laser pulse is solved by using an integrated circuit known as a 74107 JK flip-flop. Briefly, this is an integrated circuit whose output voltage will change state upon receiving a certain sequence of pulses. Here, the lamp trigger pulse from the laser power supply (connected from Lamp Sync Out on the laser power supply to the lamp trigger input on the integrator box) gives rise to a longer voltage pulse referred to as the stretched lamp pulse. The length of this pulse can be adjusted so that it drops to zero just before the chosen Q-switch pulse, the one before that containing the laser pulse. (This lamp trigger stretch adjustment, monitored by the stretched lamp trigger output, can be useful in maximizing the stability of the triggering circuitry, which is touchy and not well understood.) At the trailing edge of this pulse the output voltage of the JK flip-flop (monitored at the Q-switch trigger output on the

Figure 41: Location of adjustment potentiometers and BNC connectors on integrator box panels.

Figure 42: Operational amplifier integrator and post-amplifier circuit diagram.

Figure 43: Input and integrator switch trigger circuit.

Front Panel



Back Panel

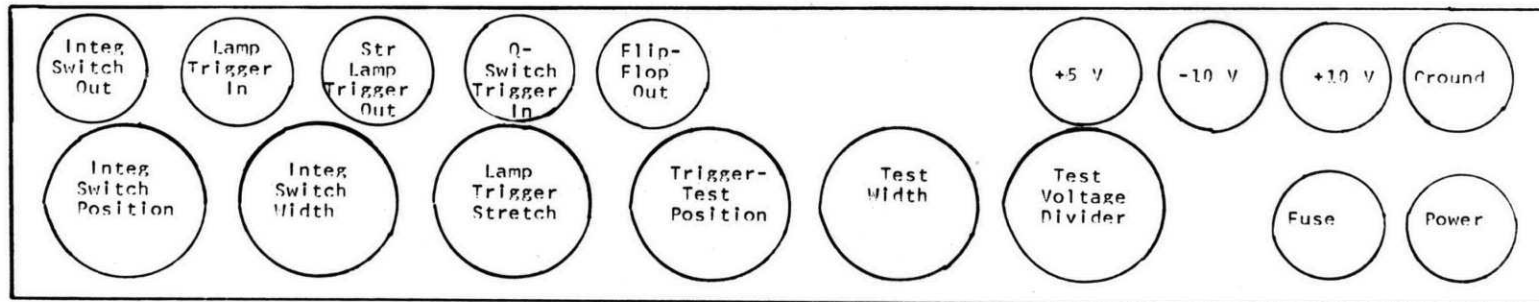
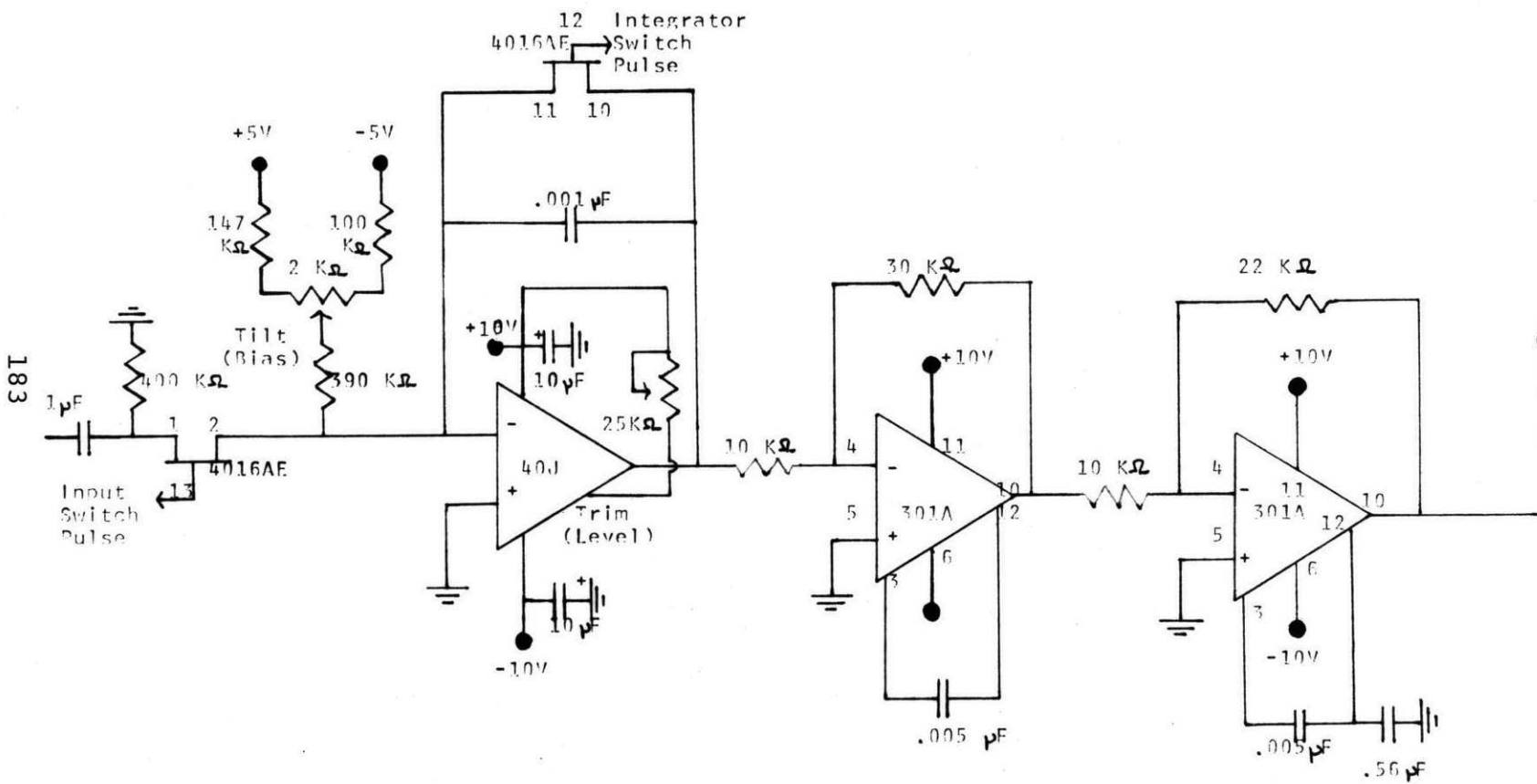


Figure 41



183

Figure 42

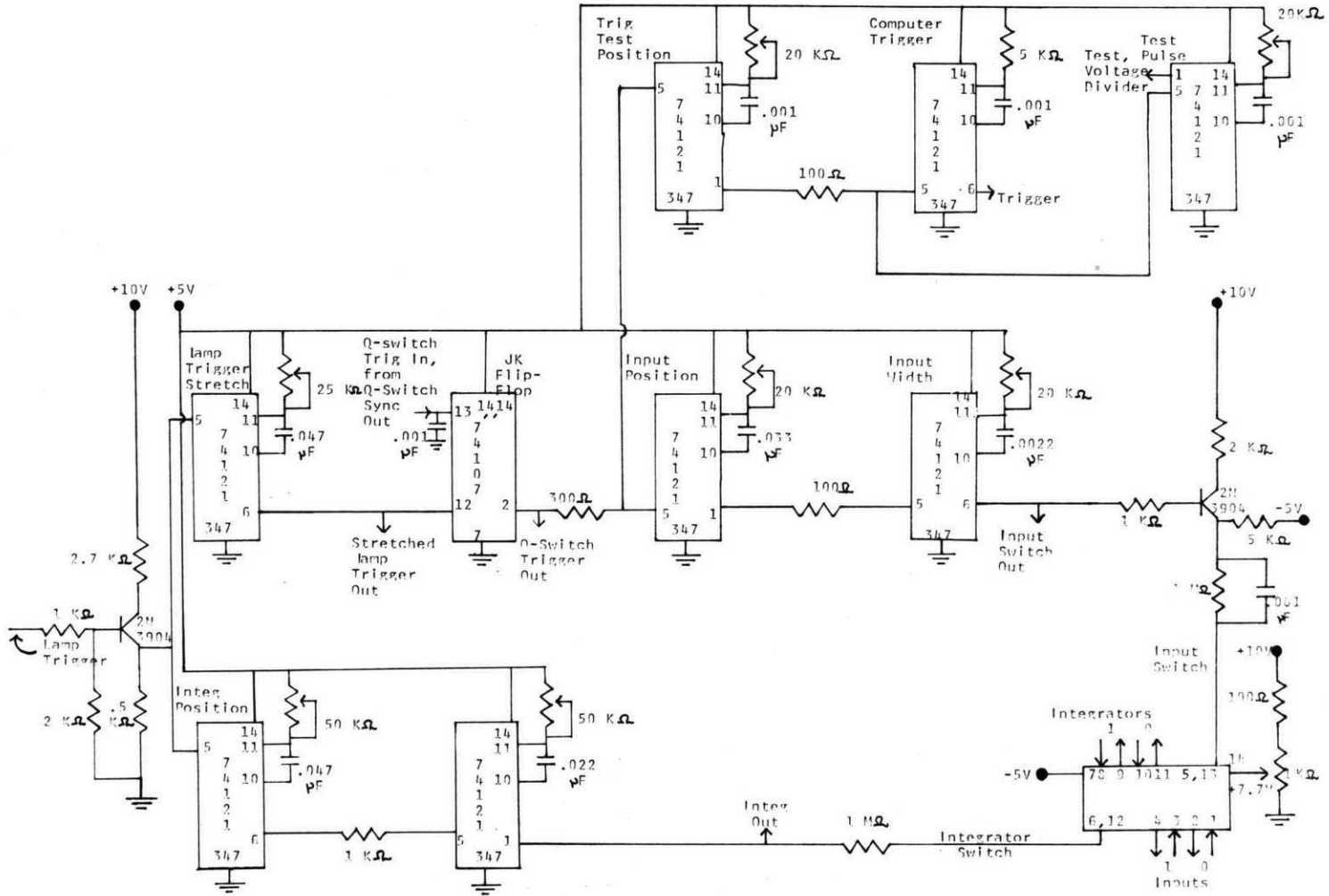
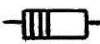



Figure 43

Figure 44: In this drawing, components of the operational amplifier integrator are represented by boxes of the appropriate size and shape rather than by conventional circuit diagram symbols. In addition, resistors are denoted by , and zener diodes by . The notation "Wiper" on one resistor in the biasing network on the front side of the input switch indicates that it is attached to the center post of the bias potentiometer on the front panel, while the other two resistors are attached to each side. The two boxes labeled "Transistor" actually include a number of resistors, as shown in the circuit diagram Figure 43. Also, the resistors and capacitors associated with the trigger integrated circuits are omitted. The wiring is color coded, with the signal represented by red (- - - in the drawing) as much as possible. The logic connections are gray wire, ground is green, and the +5 V power supply for the logic is blue. The plus and minus 10 V from the dual power supplies are purple and black, and the plus and minus 5 V obtained through the zener network are yellow and white, respectively.

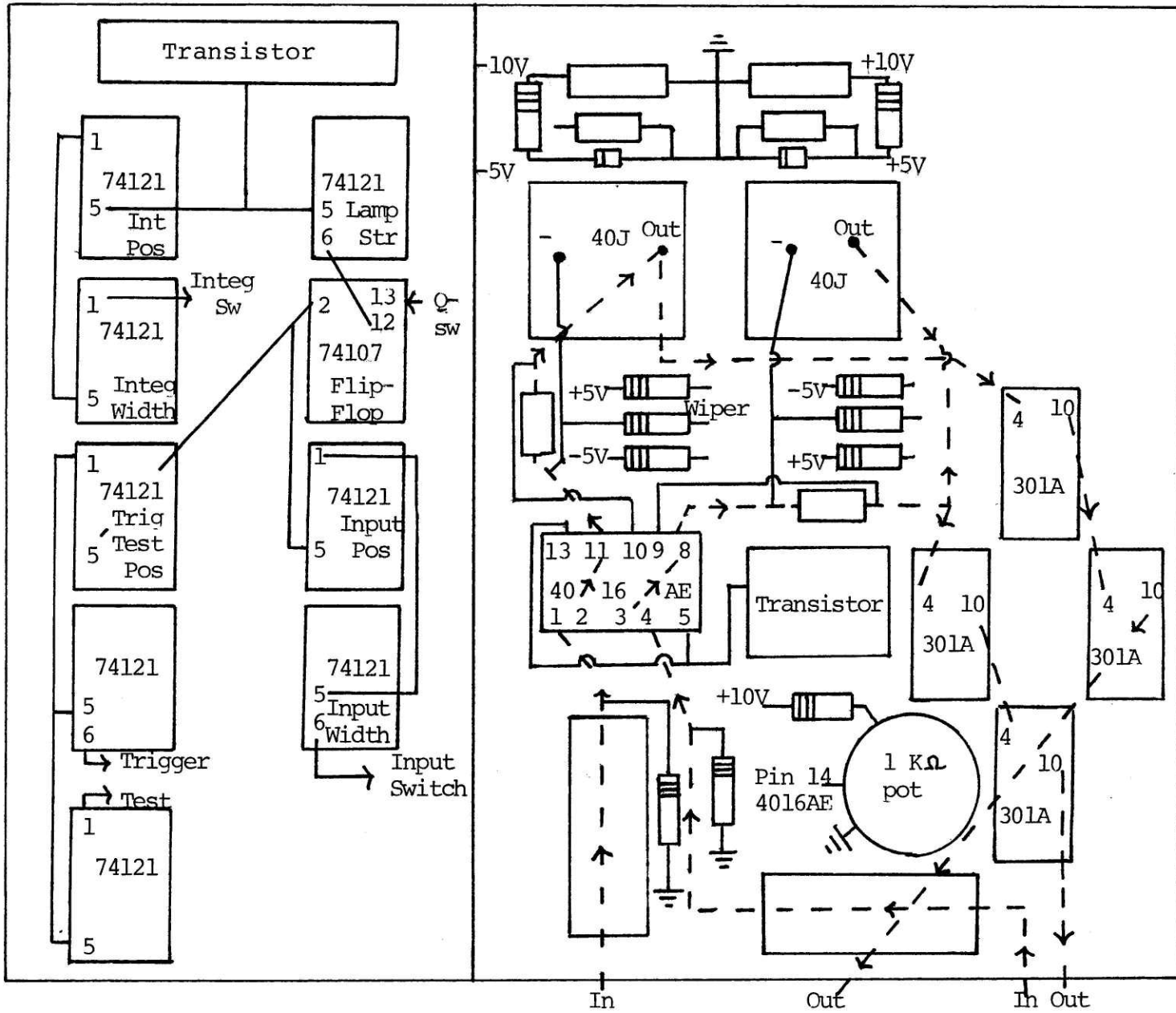
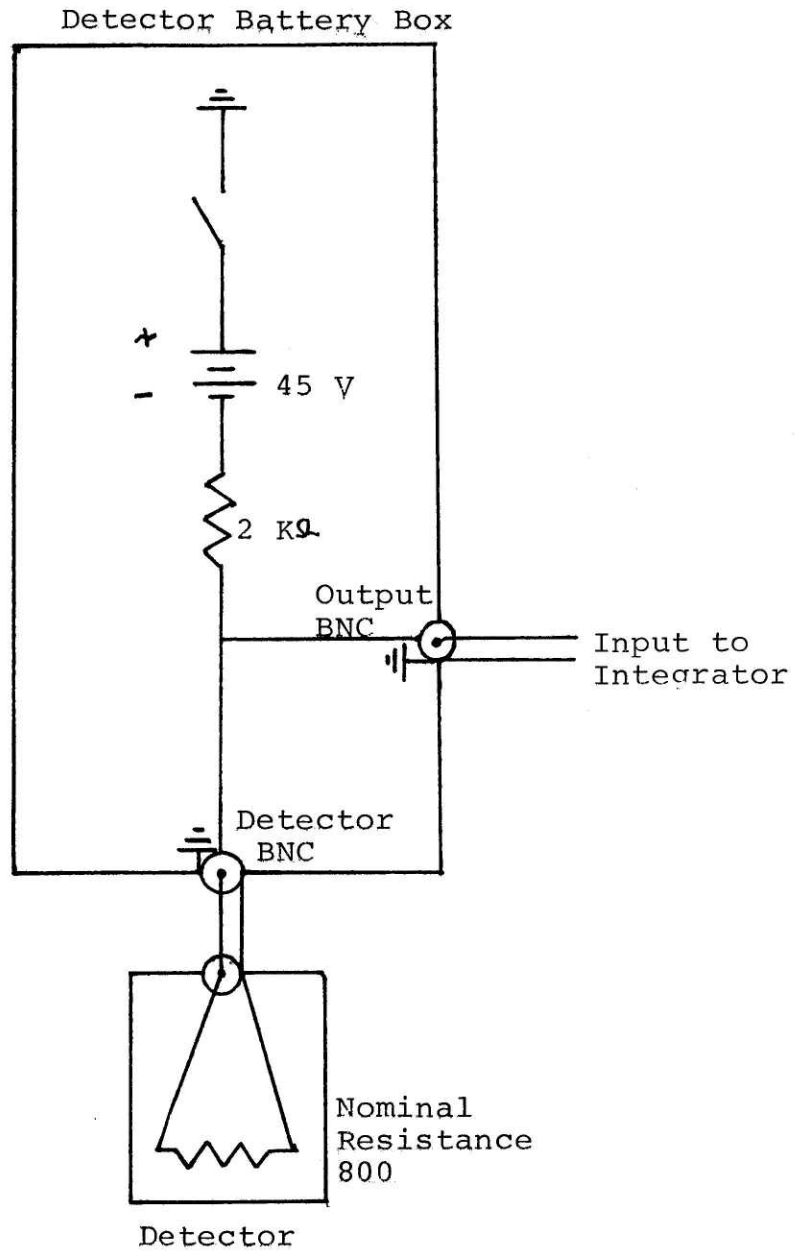


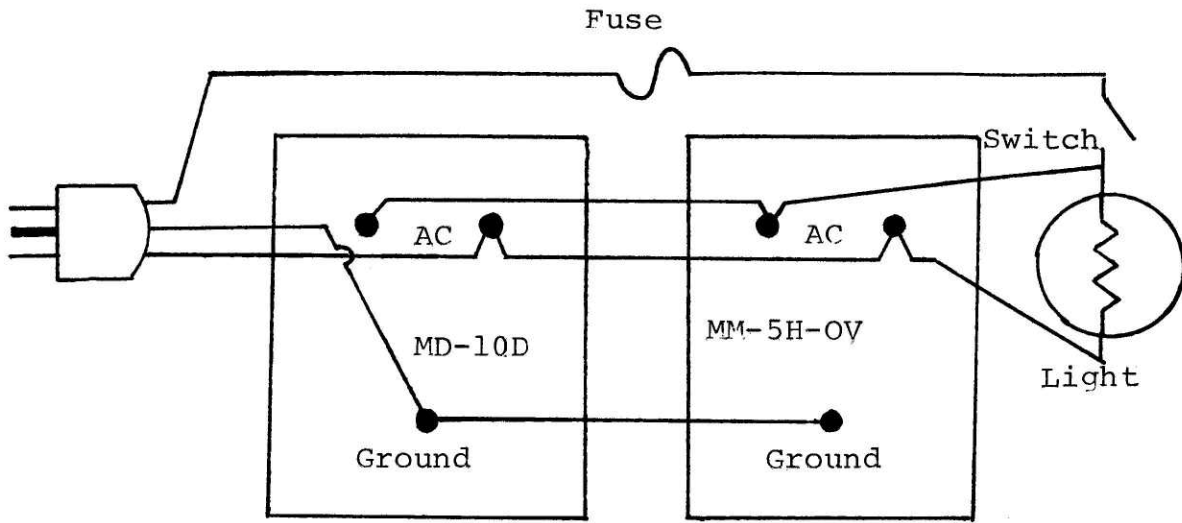
Figure 44

Figure 45: Bias circuit used for Mullard RPY77 InSb infrared detector. A somewhat different circuit was used for the Ge:Au detectors (nominal resistance $70\text{ K}\Omega$ at liquid nitrogen temperature). The detector and a $100\text{ K}\Omega$ bias resistor are connected from the two posts of a 22.5 V battery in parallel to ground. The oscilloscope monitors the voltage across the bias resistor.

Figure 46: (a) Wiring diagram for power supplies.
(b) Zener diode circuit. The zener diodes are 5 V, 1N 4733.

Figure 45





Power Supplies

Figure 46a

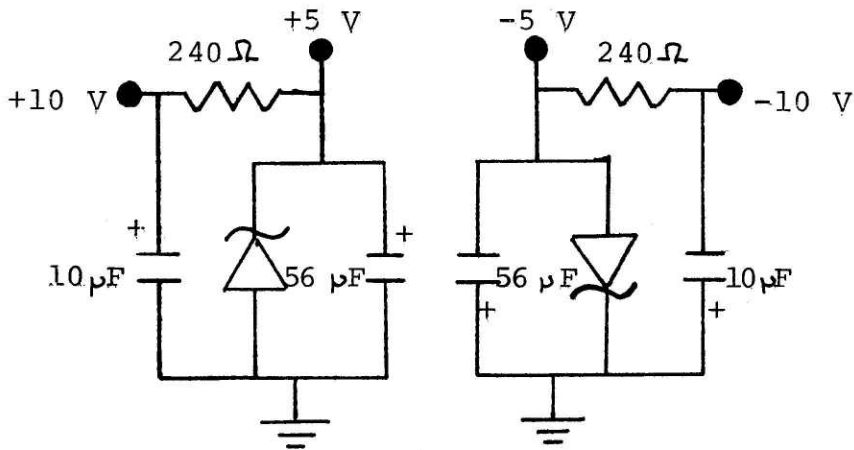


Figure 46b

Table 12: Trigger Circuit Potentiometers and Capacitors

<u>Adjustment</u>	<u>Potentiometer</u>	<u>Capacitor</u>	<u>Nominal Time</u>	<u>Nominal Resistance</u>	<u>Maximum Time</u>
Integrator Position	50 K	.047 F	60 sec	2 K	1400 sec
Integrator Width	50	.022	500	35	600
Lamp Stretch	25	.047	150	4.5	900
Trig Test Position	20	.033	250	10	500
Test Width	20	.001	-	0.8	0.2 to 10
190 Input Width	20	.0022	2	1.3	0.2 to 40
Input Position	20	.033	250	11	500
Trigger Width	-	.001	3	5.1	3

back of the integrator box) becomes negative. It is returned to zero by the trailing edge of the Q-switch pulse preceding that containing the laser. (The connection for Q-switch trigger pulses is from Q-switch Sync Out on the laser power supply to the Q-switch input on the integrator box.) Thus the trailing edge of this pulse is synchronized with the Q-switch pulses, and therefore with the laser pulse (to within some tens of nsec) and is used to trigger the position of the input switch window.

The laser pulse and the input switch output can be superimposed using a dual beam scope and the input window position adjustment. The width can then be adjusted to eliminate as much noise as possible without cutting out the laser pulse. There are similar position and width adjustments for the integrator switch, but they are less critical, since it only need be opened before the laser pulse and closed after the computer has read the voltage.

Before the computer can read the voltage levels, the A/D converter must receive a positive trigger pulse, which can be obtained from the trigger output on the front of the box. Its position can be adjusted so that the A/D reads at some time while the integrator switch is open. (The reading process can be seen as a small disturbance on the oscilloscope trace of the of the integrator output.)

The trigger positioning logic also controls a negative test voltage pulse which can be used to model the laser pulse. Its width can be adjusted, as can its height through a voltage

divider also located on the back of the box.

When a detector, such as that diagrammed in Figure 45, or its output through an amplifier is plugged into the input of either integrator channel, it has an effect on the integrated voltage level, whether the detector is receiving the laser or not. There are two adjustments which allow normalization with the laser blocked. The tilt adjustment can change the voltage level at the input side of the integrating capacitor so that with the input switch closed it will not integrate a DC voltage level and produce a ramp form. The level adjustment is a trim potentiometer on the integrating operational amplifier. In normal operation, it is used to set the integrator level with the laser blocked to several tenths of a volt, (while using the tilt to produce a horizontal level.) This is done so that small fluctuations in the level do not carry it negative, where it cannot be read by the A/D converter.

The power supplies are a Power-Mate MM-5H-0V supplying a positive 5 volts to the logic board, and a Power-Mate MD-10D giving plus and minus 10 volts. (These outputs and ground can be accessed at banana plugs on the back of the box.) The plus 10 volts is cut down to around 7.7 volts using a voltage divider before powering the FET switch, to prevent leakage of current into the integrating capacitor. The plus and minus 10 volts are also reduced to plus and minus 5 volts by a zener diode network, in order to power the bias adjustment on the integrating operational amplifier. Figure 46 shows the power

supply wiring and the zener diode circuit.

Appendix D : Computer Programs

In the following pages we reproduce a listing of the machine language program Ratio Averager which reads the integrated outputs of the cell and reference detectors through the analog to digital converter, then ratios and stores them. We also list modifications which periodically output the ratio into the digital to analog converter and a chart recorder, or onto punched tape. The original program was written and commented by Paul Houston. Here we present additional remarks on the functions of the various subroutines, after which we will demonstrate its operation by example. A flow chart is given in Figure 47.

The subroutine COMP compares two binary numbers. It is used to see if the integrated voltages are within the upper and lower acceptable limits. If QB is greater than QS it exits with 1 in the accumulator, while if QB is less than QS it exits with zero. CALIB is a subroutine to set up the calibrate mode, which sets MODE to 1, SLOPE0 and SLOPE1 to 1, and INT1 and INT0 to zero. The initialization subroutine INIT gets and stores the run number, slopes, intercepts, and minimum and maximum voltages, then sets MODE equal to zero. INTEG is a subroutine to convert a floating point number in the floating point accumulator (FLAC) into a binary number in the AC. It is used to convert maximum and minimum voltages into numbers that can be compared with the reading of the A/D converter.

AVRG does the averaging upon receiving an interrupt by the

Figure 47 : Ratio Averager program
flow chart.

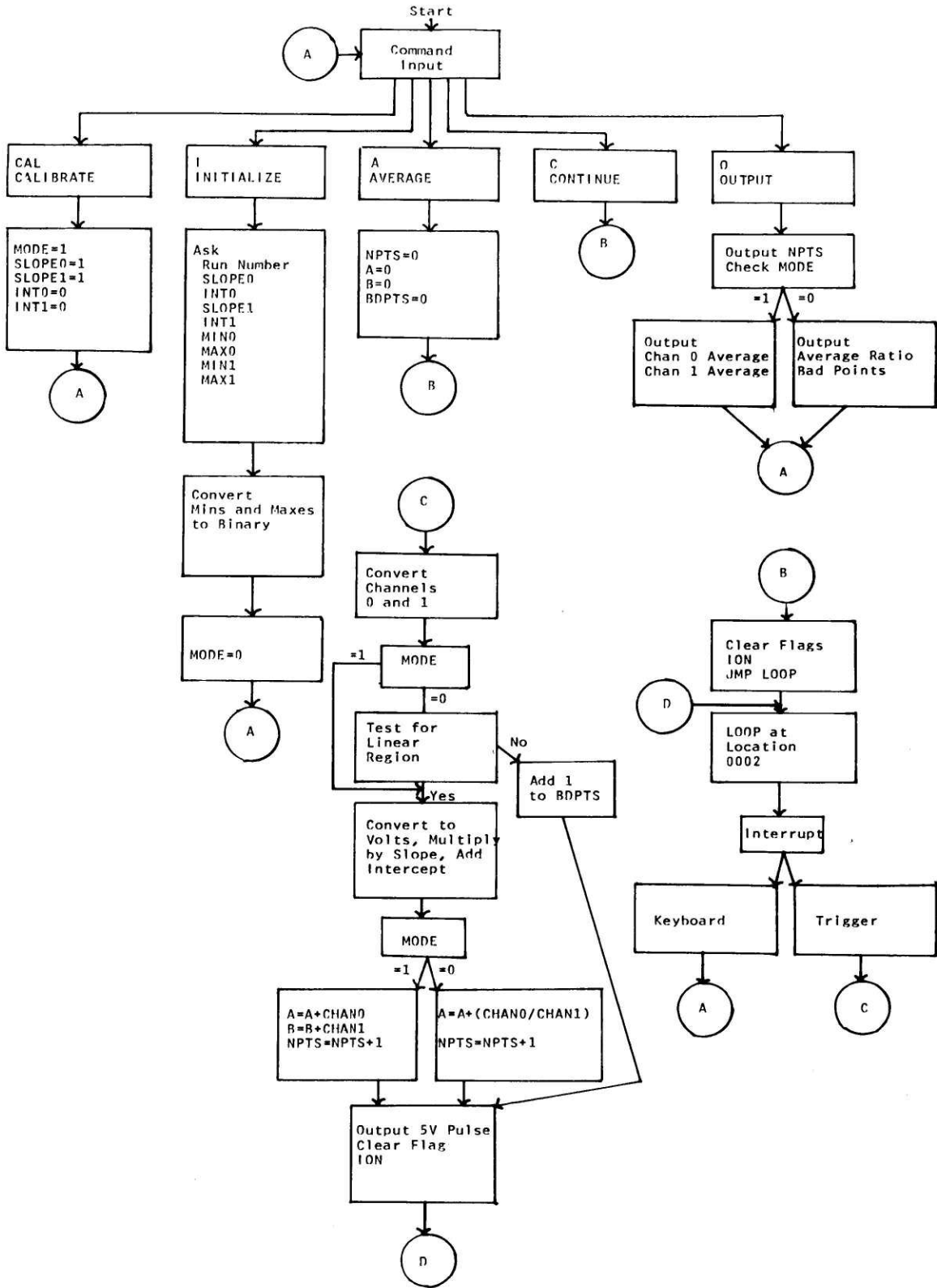


Figure 47

(Text resumes on page 220.)

```
ORIGINAL RATIO AVERAGER TAPE 1

*0000
0000 0000 0
0001 5531 JMP I SSERV
0002 5002 LØØP, JMP .
*0007
0007 5600 5600 /PØINTER TØ FP PKG 3

*0044
0044 0000 FLAC, 0
0045 0000 0
0046 0000 0

*0055
0055 0001 0001 /FØR CR AFTER ØUTPUT
0056 7777 7777 /FØR LF AFTDR ØUTPUT
0057 0000 0
0060 0000 0
0061 0000 0

*70
0070 0000 AC, 0
0071 0000 L, 0
0072 0000 BØFF, 0
0073 0200 TRØN, 200
0074 4000 TEXT, 4000
0075 0240 TSLØØØ, 240
0076 0300 TINTØ, 300
0077 0340 TSLØØØ1, 340
0100 0400 TINT1, 400
0101 0000 RUN, 0
0102 0000 0
0103 0000 0
0104 0000 SLØØØ, 0
0105 0000 0
0106 0000 0
0107 0000 INTO, 0
0110 0000 0
0111 0000 0
0112 0000 SLØØØ1, 0
0113 0000 0
0114 0000 0
0115 0000 INT1, 0
0116 0000 0
0117 0000 0
0120 0000 NPTS, 0
0121 0000 0
0122 0000 0
0123 0000 A, 0
0124 0000 0
0125 0000 0
0126 3400 SCØMP, CØMP
0127 1000 SØUT, ØUT
0130 3000 SINIT, INIT
0131 1200 SSERV, SERV
0132 1400 SINPT, INPT
0133 3600 SAVRG, AVRG
0134 1022 SCRLF, CRLF
0135 1300 SSTRT, STRT
0136 2400 SFINI, FINI
0137 1030 STYPE, TYPE
0140 2200 SCLEAR, CLEAR
0141 2600 SCALIB, CALIB
0142 0000 MINØ, 0
0143 0000 MIN1, 0
0144 0000 MAXØ, 0
0145 0000 MAX1, 0
```

0146	3200	SINTEG,	INTEG	
0147	0000	QB,	0	
0150	0000	QS,	0	
0151	0440	TMINO,	440	
0152	0600	TMIN1,	600	
0153	0640	TMAXO,	640	
0154	0700	TMAX1,	700	
0155	0740	TCHO,	740	
0156	1000	TCH1,	1000	
0157	1040	TBDPT,	1040	
0160	0000	BDPTS,	0	
0161	0000		0	
0162	0000		0	
0163	0540	TAV,	540	
0164	0500	TPTS,	500	
0165	0000	MØDE,	0	
0166	0001	ØNE,	0001	
0167	2000		2000	
0170	0000		0000	
0171	0000	B,	0	
0172	0000		0	
0173	0000		0	
0174	0000	ZERØ,	0	
0175	0000		0	
0176	0000		0	
		*200		
0200	7300	CLA CLL		/PROGRAM STARTS HERE
0201	6046	TLS		/T3 SET PRINTER FLAG
0202	5603	JMP I SCF		
0203	1604	SCF,	INPT+204	

ORIGINAL RATIO AVERAGER TAPE 2

```

*JIT
1000 0000  JIT,  0          /SUBROUTINE TO OUTPUT TEXT
1001 7300          CLA CLL
1002 7000          N3P
1003 1072          TAD BUFP
1004 3236          DCA BUFPPT
1005 4222          JMS CRLF
1006 1636  CHRTYP, TAD I BUFPPT
1007 1241          TAD MD2LAR
1010 7450          SNA
1011 5217          JMP .+6
1012 7300          CLA CLL
1013 1636          TAD I BUFPPT  /GET A NON-$ CHAR
1014 4230          JMS TYPE    /TYPE IT
1015 2236          ISZ BUFPPT
1016 5206          JMP CHRTYP  /GET ANOTHER CHAR
1017 7300          CLA CLL    /HERE IF $
1020 7300          CLA CLL
1021 5600          JMP I JIT
1022 0000  CRLF,  0
1023 1237          TAD K215
1024 4230          JMS TYPE
1025 1240          TAD K212
1026 4230          JMS TYPE
1027 5622          JMP I CRLF
1030 0000  TYPE,  0
1031 6041          TSF
1032 5231          JMP .-1
1033 6046          TLS
1034 7200          CLA
1035 5630          JMP I TYPE
1036 0000  BUFPPT, 0
1037 0215          K215,  215
1040 0212          K212,  212
1041 7534          MD2LAR, 7534
*SERV
1200 3070  SERV,  DCA AC    /SERVICE SUBROUTINE
1201 7004          RAL
1202 3071          DCA L
1203 6031          KSF      /KEYBOARD?
1204 7410          SKP      /NO
1205 4532          JMS I SINPT /YES
1206 6301          SLTF     /TRIGGER
1207 7410          SKP      /NO
1210 4533          JMS I SAVRG /YES
1211 7410          SKP
1212 7777  K7777, 7777
1213 1212          TAD K7777  /A HALT SHOWING 7777
1214 6041          TSF      /INDICATES ILLEGAL INTERRUPT
1215 7410          SKP
1216 7402          HLT
1217 6021          PSF
1220 7410          SKP
1221 7402          HLT
1222 6011          RSF
1223 7410          SKP

```

1224	7402		HLT	
1225	6531		ADSF	
1226	7410		SKP	
1227	7402		HLT	
1230	7402		HLT	/ROOM FOR OTHER FLAG TESTS BELOW
		*STRT		
1300	0000	STRT,	0	
1301	7300		CLA CLL	
1302	4407		FENT	
1303	5174		FGET ZERO	
1304	6120		FPUT NPTS	
1305	6123		FPUT A	
1306	6171		FPUT B	
1307	6160		FPUT BDPTS	
1310	0000		FEXT	
1311	5700		JMP I STRT	
		*INPT		
1400	0000	INPT,	0	/SERVICES INTERRUPT BY KEYBOARD
1401	7300		CLA CLL	
1402	6046		TLS	/TO SET PRINT FLAG
1403	1074		TAD TEXT	
1404	3222		DCA TXTPT	
1405	6211		CDF +10	
1406	6031	CRLA,	KSF	
1407	5206		JMP --1	
1410	6036		KRB	
1411	6046		TLS	
1412	3622		DCA I TXTPT	/READS CHARACTER PRINTS IT
1413	1622		TAD I TXTPT	/AND STORES IT
1414	1221		TAD MCR	/TEST FOR CR
1415	7450		SNA	
1416	5223		JMP .+5	
1417	2222		ISZ TXTPT	/GET MORE
1420	5206		JMP CRLA	
1421	7563	MCR,	7563	
1422	0000	TXTPT,	0	
1423	4534		JMS I SCRLF	/INPUT TERMINATED
1424	7300		CLA CLL	
1425	1222		TAD TXTPT	
1426	3245		DCA TXTEND	
1427	1074		TAD TEXT	
1430	3222		DCA TXTPT	
1431	3246		DCA C3MND	
1432	1622		TAD I TXTPT	
1433	1246		TAD C3MND	
1434	3246		DCA C3MND	/EVALUATING C3MND
1435	1245		TAD TXTEND	
1436	7041		CIA	
1437	2222		ISZ TXTPT	
1440	1222		TAD TXTPT	
1441	7450		SNA	
1442	5247		JMP .+5	
1443	7300		CLA CLL	
1444	5232		JMP --12	/GET MORE OF C3MND
1445	0000	TXTEND,	0	
1446	0000	C3MND,	0	
1447	7300		CLA CLL	/EXECUTE C3MND
1450	6201		CDF +00	
1451	1246		TAD C3MND	/INITIALIZE ?
1452	7041		CIA	
1453	1347		TAD CINIT	
1454	7440		SZA	
1455	5260		JMP .+3	
1456	4530		JMS I SINIT	

1457	5760	JMP I SCMT	
1460	7300	CLA CLL	
1461	1246	TAD CØMND	
1462	7041	CIA	
1463	1350	TAD CI	
1464	7440	SZA	
1465	5270	JMP .+3	
1466	4530	JMS I SINIT	
1467	5760	JMP I SCMT	
1470	7300	CLA CLL	/AVERAGE ?
1471	1246	TAD CØMND	
1472	7041	CIA	
1473	1352	TAD CA	
1474	7440	SZA	
1475	5300	JMP .+3	
1476	4535	JMS I SSTRT	
1477	5361	JMP BACK	
1500	7300	CLA CLL	
1501	1246	TAD CØMND	
1502	7041	CIA	
1503	1351	TAD CAVER	
1504	7440	SZA	
1505	5310	JMP .+3	
1506	4535	JMS I SSTRT	
1507	5361	JMP BACK	
1510	7300	CLA CLL	/OUTPUT ?
1511	1246	TAD CØMND	
1512	7041	CIA	
1513	1354	TAD CØ	
1514	7440	SZA	
1515	5320	JMP .+3	
1516	4536	JMS I SFINI	
1517	5760	JMP I SCMT	
1520	7300	CLA CLL	
1521	1246	TAD CØMND	
1522	7041	CIA	
1523	1353	TAD CØUT	
1524	7440	SZA	
1525	5330	JMP .+3	
1526	4536	JMS I SFINI	
1527	5760	JMP I SCMT	
1530	7300	CLA CLL	/CONTINUE ?
1531	1246	TAD CØMND	
1532	7041	CIA	
1533	1356	TAD CC	
1534	7440	SZA	
1535	5337	JMP .+2	
1536	5361	JMP BACK	
1537	7300	CLA CLL	
1540	1246	TAD CØMND	
1541	7041	CIA	
1542	1355	TAD CCØNT	
1543	7440	SZA	
1544	5346	JMP .+2	
1545	5361	JMP BACK	
1546	5757	JMP I CPGE	/NO MORE CØMMANDS, GET ØN NEXT PAGE
1547	3762	CINIT,	3762
1550	0311	CI,	311
1551	2573	CAVER,	2573
1552	0301	CA,	301
1553	2361	CØUT,	2361
1554	0317	CØ,	317
1555	3145	CCØNT,	3145
1556	0303	CC,	303
1557	1600	CPGE,	1600
			/SUM ØF LETTERS IN INITIALIZE

1560	1604	SCMT,	SCMX	
1561	7300	BACK,	CLA CLL	
1562	6041		TSF	
1563	5362		JMP .-1	/HAVE TO MAKE SURE PRINTER WAS
1564	4540		JMS I SCLEAR	/BEFORE WE TRY TO CLEAR ITS FLAG
1565	6001		I0N	
1566	5002		JMP LOOP	
		*INPT+200		
1600	5215		JMP BEL0	/FOR MORE COMMANDS
1601	7300	XT,	CLA CLL	
1602	1211		TAD CQ	
1603	4537		JMS I STYPE	
1604	7300	SCMX,	CLA CLL	
1605	1212		TAD CC0	
1606	4537		JMS I STYPE	
1607	5610		JMP I CRD	
1610	1403	CRD,	INPT+3	
1611	0277	CQ,	277	
1612	0272	CC0,	272	
1613	1120	CAL,	1120	
1614	3407	CCAL,	3407	
1615	7300	BEL0,	CLA CLL	
1616	1636		TAD I CMND	
1617	7041		CIA	
1620	1213		TAD CAL	
1621	7440		SZA	
1622	5225		JMP .+3	
1623	4541		JMS I SCALIB	
1624	5204		JMP SCMX	
1625	7300		CLA CLL	
1626	1636		TAD I CMND	
1627	7041		CIA	
1630	1214		TAD CCAL	
1631	7440		SZA	
1632	5235		JMP .+3	
1633	4541		JMS I SCALIB	
1634	5204		JMP SCMX	
1635	5201		JMP XT	
1636	1446	CMND,	CMND	

ORIGINAL RATIO AVERAGER TAPE 3

```

                *CLEAR
2200 0000 CLEAR, 0
2201 6022 PCF /HSP
2202 6032 KCC /TTY
2203 6302 CLTF /TRIGGER
2204 6534 ADRB /AD CONV
2205 6042 TCF /TTY
2206 6012 RRB /HSR
2207 7300 CLA CLL
2210 5600 JMP I CLEAR

                *FINI
2400 0000 FINI, 0 /SUBROUTINE TO OUTPUT ANSWERS
2401 7300 CLA CLL
2402 6046 TLS /TO SET PRINTER FLAG
2403 1164 TAD TPTS
2404 3072 DCA BUFF
2405 6211 CDF +10
2406 4527 JMS I SOUT
2407 6201 CDF +00
2410 4407 FENT
2411 5120 FGET NPTS
2412 0014 OUTPUT
2413 0000 FEXT
2414 7300 CLA CLL
2415 1165 TAD MØDE /CHECK FOR MØDE
2416 7650 SNA CLA /CALIBRATE?
2417 5221 JMP .+2 /NO
2420 5251 JMP X1 /YES
2421 1163 TAD TAV
2422 3072 DCA BUFF
2423 6211 CDF +10
2424 4527 JMS I SOUT
2425 6201 CDF +00
2426 4407 FENT
2427 5123 FGET A
2430 4120 FDIV NPTS
2431 7000 FNØR
2432 0014 OUTPUT
2433 0000 FEXT
2434 7300 CLA CLL
2435 1157 TAD TØDPT
2436 3072 DCA BUFF
2437 6211 CDF +10
2440 4527 JMS I SOUT
2441 6201 CDF +00
2442 4407 FENT
2443 5160 FGET ØDPTS
2444 7000 FNØR
2445 0014 OUTPUT
2446 0000 FEXT
2447 7300 CLA CLL
2450 5600 JMP I FINI /DONE
2451 7300 X1, CLA CLL /HERE IF CALIBRATE MØDE
2452 1155 TAD TCHO
2453 3072 DCA BUFF
2454 6211 CDF +10
2455 4527 JMS I SOUT
2456 6201 CDF +00
2457 4407 FENT

```

2460	5123	FGET A	
2461	4120	FDIV NPTS	
2462	7000	FNØR	
2463	0014	ØUTPIJT	
2464	0000	FEXT	
2465	7300	CLA CLL	
2466	1156	TAD TCH1	
2467	3072	DCA BUFF	
2470	6211	CDF +10	
2471	4527	JMS I SØUT	
2472	6201	CDF +00	
2473	4407	FENT	
2474	5171	FGET B	
2475	4120	FDIV NPTS	
2476	7000	FNØR	
2477	0014	ØUTPUT	
2500	0000	FEXT	
2501	7300	CLA CLL	
2502	5600	JMP I FINI	/DØNE

ORIGINAL RATIO AVERAGER TAPE 4

```

*CALIB
2600 0000 CALIB, 0 /HANDLES CALIBRATE COMMAND
2601 7300 CLA CLL
2602 7001 IAC
2603 3165 DCA M0DE /SET M0DE=1 INDICATING CALIBRATE M0DE
2604 4407 FENT
2605 5166 FGET 0NE
2606 6104 FPUT SL0P0
2607 6112 FPUT SL0P1
2610 5174 FGET ZER0
2611 6107 FPUT INTO
2612 6115 FPUT INT1
2613 0000 FEXT
2614 5600 JMP I CALIB

*INIT
INIT,
3000 0000 0 /INITIALIZATION SUBROUTINE
3001 7300 CLA CLL /T0 GET RUN NUMBER SL0PES
3002 6046 TLS /AND INTERCEPTS
3003 1073 TAD TRUN /TLS SETS TTY FLAG
3004 3072 DCA BUFF
3005 6211 CDF +10 /TEXT IS IN UPPER 4K
3006 4527 JMS I S0UT /ASK FOR RUN NUMBER
3007 6201 CDF +00
3010 4407 FENT
3011 0013 INPUT /GET RUN NUM AND STORE
3012 7000 FN0R
3013 6101 FPUT RUN
3014 0000 FEXT
3015 7300 CLA CLL
3016 1075 TAD TSL0P0 /GET SL0P0
3017 3072 DCA BUFF
3020 6211 CDF +10
3021 4527 JMS I S0UT
3022 6201 CDF +00
3023 4407 FENT
3024 0013 INPUT
3025 7000 FN0R
3026 6104 FPUT SL0P0
3027 0000 FEXT
3030 7300 CLA CLL /GET INTO
3031 1076 TAD TINT0
3032 3072 DCA BUFF
3033 6211 CDF +10
3034 4527 JMS I S0UT
3035 6201 CDF +00
3036 4407 FENT
3037 0013 INPUT
3040 7000 FN0R
3041 6107 FPUT INTO
3042 0000 FEXT
3043 7300 CLA CLL /GET SL0P1
3044 1077 TAD TSL0P1
3045 3072 DCA BUFF
3046 6211 CDF +10
3047 4527 JMS I S0UT
3050 6201 CDF +00
3051 4407 FENT
3052 0013 INPUT

```

3053	7000	FNØR	
3054	6112	FPUT SLØP1	
3055	0000	FEXT	
3056	7300	CLA CLL	/GET INT1
3057	1100	TAD TINT1	
3060	3072	DCA BUFF	
3061	6211	CDF +10	
3062	4527	JMS I SØUT	
3063	6201	CDF +00	
3064	4407	FENT	
3065	0013	INPUT	
3066	7000	FNØR	
3067	6115	FPUT INT1	
3070	0000	FEXT	
3071	7300	CLA CLL	/GET MINS AND MAXS
3072	1151	TAD TMIN0	
3073	3072	DCA BUFF	
3074	6211	CDF +10	
3075	4527	JMS I SØUT	
3076	6201	CDF +00	
3077	4407	FENT	
3100	0013	INPUT	
3101	7000	FNØR	
3102	3364	FMPY F4095	
3103	4367	FDIV FTEN	
3104	7000	FNØR	
3105	0000	FEXT	
3106	4546	JMS I SINTEG	
3107	3142	DCA MIN0	
3110	1153	TAD TMAX0	
3111	3072	DCA BUFF	
3112	6211	CDF +10	
3113	4527	JMS I SØUT	
3114	6201	CDF +00	
3115	4407	FENT	
3116	0013	INPUT	
3117	7000	FNØR	
3120	3364	FMPY F4095	
3121	4367	FDIV FTEN	
3122	7000	FNØR	
3123	0000	FEXT	
3124	4546	JMS I SINTEG	
3125	3144	DCA MAX0	
3126	1152	TAD TMIN1	
3127	3072	DCA BUFF	
3130	6211	CDF +10	
3131	4527	JMS I SØUT	
3132	6201	CDF +00	
3133	4407	FENT	
3134	0013	INPUT	
3135	7000	FNØR	
3136	3364	FMPY F4095	
3137	4367	FDIV FTEN	
3140	7000	FNØR	
3141	0000	FEXT	
3142	4546	JMS I SINTEG	
3143	3143	DCA MIN1	
3144	1154	TAD TMAX1	
3145	3072	DCA BUFF	
3146	6211	CDF +10	
3147	4527	JMS I SØUT	
3150	6201	CDF +00	
3151	4407	FENT	

3152	0013		INPUT	
3153	7000		FNØR	
3154	3364		FMPY F4095	
3155	4367		FDIV FTEN	
3156	7000		FNØR	
3157	0000		FEXT	
3160	4546		JMS I SINTEG	
3161	3145		DCA MAX1	
3162	3165		DCA MØDE	/FØR REGULAR MØDE
3163	5600		JMP I INIT	/DØNE
3164	0012	F4095,	0012	
3165	3777		3777	
3166	4000		4000	
3167	0004	FTEN,	0004	
3170	2400		2400	
3171	0000		0000	
		*INTEG		
3200	0000	INTEG,	0	/CØNVERTS NUMBER IN FLAC TØ
3201	7300		CLA CLL	/AN INTEGER IN THE AC
3202	1044		TAD FLAC	
3203	7510		SPA	
3204	5242		JMP NEG	/THE FL PT EXPØNENT IS NEG
3205	7300		CLA CLL	
3206	1046		TAD FLAC+2	
3207	0244		AND K4000	/GET LEFT BIT
3210	7450		SNA	
3211	5213		JMP .+2	
3212	7020		CML	
3213	1045		TAD FLAC+1	
3214	7004		RAL	
3215	7100		CLL	
3216	3246		DCA INT	
3217	1044		TAD FLAC	
3220	1250		TAD M12	
3221	7540		SMA SZA	
3222	5237		JMP XY	/LARGER THAN 2**12
3223	7500		SMA	
3224	5234		JMP XX	/=0
3225	3247		DCA SHFT	
3226	1246		TAD INT	
3227	7100		CLL	
3230	7010		RAR	
3231	2247		ISZ SHFT	
3232	5227		JMP .-3	
3233	5600		JMP I INTEG	
3234	7300	XX,	CLA CLL	
3235	1246		TAD INT	
3236	5600		JMP I INTEG	
3237	7300	XY,	CLA CLL	
3240	1245		TAD K7777	
3241	5600		JMP I INTEG	
3242	7300	NEG,	CLA CLL	
3243	5600		JMP I INTEG	
3244	4000	K4000,	4000	
3245	7777	K7777,	7777	
3246	0000	INT,	0	
3247	0000	SHFT,	0	
3250	7766	M12,	7766	
		*CØMP		
3400	0000	CØMP,	0	
3401	7300		CLA CLL	/DØES ABSØLUTE CØMPARISØN,
3402	1147		TAD ØB	/IE: 4000>3777
3403	7700		SMA CLA	
3404	5210		JMP .+4	
3405	7240		CLA CMA	/ØB IS MINUS

3671	7012	RTR	
3672	3045	DCA 45	
3673	3046	DCA 46	
3674	1342	TAD C13	
3675	3044	DCA 44	
3676	4407	FENT	
3677	7000	FNØR	
3700	3335	FMPY TØVØLTS	
3701	3104	FMPY SLØP0	
3702	1107	FADD INTO	
3703	7000	FNØR	
3704	6327	FPUT CHAN0	
3705	0000	FEXT	
3706	7300	CLA CLL	
3707	1343	TAD STR1	
3710	7012	RTR	/THIS CHANGES DIGITAL
3711	3045	DCA 45	/INFORMATION TO ACTUAL
3712	3046	DCA 46	/VØLTS. SAME AS ABOVE
3713	1342	TAD C13	/IT ALSO MULTIPLIES BY
3714	3044	DCA 44	/SLOPE AND ADDS INT.
3715	4407	FENT	
3716	7000	FNØR	
3717	3335	FMPY TØVØLTS	
3720	3112	FMPY SLØP1	
3721	1115	FADD INT1	
3722	7000	FNØR	
3723	6332	FPUT CHAN1	
3724	0000	FEXT	
3725	7300	CLA CLL	
3726	5747	JMP I XY	
3727	0000	CHAN0,	0
3730	0000		0
3731	0000		0
3732	0000	CHAN1,	0
3733	0000		0
3734	0000		0
3735	7772	TØVØLTS,	7772
3736	2401		2401
3737	2005		2005
3740	7772		7772
3741	2401		2401
3742	0013	C13,	0013
3743	0000	STR1,	0
3744	0000	STRO,	0
3745	0001	K0001,	0001
3746	4042	ØØT,	ØIT
3747	4000	XY,	XZ
		*AVRG+200	
4000	7300	XZ,	CLA CLL
4001	1165		TAD MØDE
4002	7650		SNA CLA
4003	5205		JMP RAT
4004	5222		JMP CBRAT
4005	7300	RAT,	CLA CLL
4006	4407		FENT
4007	5120		FGET NPTS
4010	1166		FADD ØNE
4011	7000		FNØR
4012	6120		FPUT NPTS
4013	5652		FGET I CH0
4014	4653		FDIV I CH1
4015	1123		FADD A
4016	7000		FNØR
4017	6123		FPUT A
4020	0000		FEXT
4021	5242		JMP ØIT

3406	3244		DCA SB	
3407	5212		JMP .+3	
3410	7201		CLA IAC	/QB IS POS OR ZERO
3411	3244		DCA SB	
3412	1150		TAD QS	
3413	7700		SMA CLA	
3414	5226		JMP .+12	
3415	1244		TAD SB	/QS IS MINUS
3416	7700		SMA CLA	
3417	5242		JMP N0	
3420	1150		TAD QS	
3421	7041		CIA	
3422	1147		TAD QB	
3423	7700		SMA CLA	
3424	5240		JMP YES	
3425	5242		JMP N0	
3426	1244		TAD SB	/QS IS PLUS OR ZERO
3427	7700		SMA CLA	
3430	5232		JMP .+2	
3431	5240		JMP YES	
3432	1150		TAD QS	
3433	7041		CIA	
3434	1147		TAD QB	
3435	7700		SMA CLA	
3436	5240		JMP YES	
3437	5242		JMP N0	
3440	7201	YES,	CLA IAC	/QB>QS AC=1
3441	5600		JMP I COMP	
3442	7300	N0,	CLA CLL	/QB<QS AC=0
3443	5600		JMP I COMP	
3444	0000	SB,	0	

ORIGINAL RATIO AVERAGER TAPE 5

```

*AVRG
3600 0000 AVRG, 0
3601 7300 CLA CLL /HERE IN 29.3 MICROSEC
3602 6542 ADSC /SELECT CHANNEL 0
3603 7300 CLA CLL /AND CONVERT
3604 6531 ADSF /SKIP WHEN DONE
3605 5204 JMP .-1
3606 6534 ADRB /READ INTO AC
3607 3344 DCA STRO
3610 1345 TAD K0001
3611 6542 ADSC /SELECT CHANNEL 1
3612 7300 CLA CLL
3613 6531 ADSF
3614 5213 JMP .-1
3615 6534 ADRB
3616 3343 DCA STR1 /VOLTAGES ARE STORED
3617 1165 TAD M0DE /CHECK M0DE
3620 7650 SNA CLA /CALIBRATE?
3621 5223 JMP .+2
3622 5267 JMP C0N /YES
3623 1344 TAD STRU /NO
3624 3150 DCA QS
3625 1144 TAD MAX0 /CHANO<MAX0?
3626 3147 DCA QB
3627 4526 JMS I SC0MP
3630 7650 SNA CLA
3631 5260 JMP BAD /NO
3632 1344 TAD STRO /YES; CHANO>MIN0?
3633 3147 DCA QB
3634 1142 TAD MIN0
3635 3150 DCA QS
3636 4526 JMS I SC0MP
3637 7650 SNA CLA
3640 5260 JMP BAD /NO
3641 1343 TAD STR1 /YES; CHAN1<MAX1?
3642 3150 DCA QS
3643 1145 TAD MAX1
3644 3147 DCA QB
3645 4526 JMS I SC0MP
3646 7650 SNA CLA
3647 5260 JMP BAD /NO
3650 1343 TAD STR1 /YES; CHAN1>MIN1?
3651 3147 DCA QB
3652 1143 TAD MIN1
3653 3150 DCA QS
3654 4526 JMS I SC0MP
3655 7650 SNA CLA
3656 5260 JMP BAD /NO
3657 5267 JMP C0N
3660 7300 BAD, CLA CLL /HERE IF NOT ON LINEAR REGION
3661 4407 FENT /OF VOLTAGE CURVE
3662 5160 FGET BDPTS /INCREMENT BDPTS
3663 1166 FADD 0NE
3664 6160 FPUT BDPTS
3665 0000 FEXT
3666 5746 JMP I 00T
3667 7300 C0N, CLA CLL
3670 1344 TAD STRO

```

3671	7012	RTR	
3672	3045	DCA 45	
3673	3046	DCA 46	
3674	1342	TAD C13	
3675	3044	DCA 44	
3676	4407	FENT	
3677	7000	FNØR	
3700	3335	FMPY TØVØLTS	
3701	3104	FMPY SLØPO	
3702	1107	FADD INTO	
3703	7000	FNØR	
3704	6327	FPUT CHANO	
3705	0000	FEXT	
3706	7300	CLA CLL	
3707	1343	TAD STR1	
3710	7012	RTR	/THIS CHANGES DIGITAL
3711	3045	DCA 45	/INFORMATION TØ ACTUAL
3712	3046	DCA 46	/VØLTS. SAME AS ABOVE
3713	1342	TAD C13	/IT ALSØ MULTIPLIES BY
3714	3044	DCA 44	/SLOPE AND ADDS INT.
3715	4407	FENT	
3716	7000	FNØR	
3717	3335	FMPY TØVØLTS	
3720	3112	FMPY SLØP1	
3721	1115	FADD INT1	
3722	7000	FNØR	
3723	6332	FPUT CHAN1	
3724	0000	FEXT	
3725	7300	CLA CLL	
3726	5747	JMP I XY	
3727	0000	CHANO, 0	
3730	0000	0	
3731	0000	0	
3732	0000	CHAN1, 0	
3733	0000	0	
3734	0000	0	
3735	7772	TØVØLTS, 7772	
3736	2401	2401	
3737	2005	2005	
3740	7772	7772	
3741	2401	2401	
3742	0013	C13, 0013	
3743	0000	STR1, 0	
3744	0000	STRO, 0	
3745	0001	KØØØ1, 0001	
3746	4042	ØØT, ØIT	
3747	4000	XY, XZ	
		*AVRG+200	
4000	7300	XZ, CLA CLL	
4001	1165	TAD MØDE	/CHECK MØDE
4002	7650	SNA CLA	
4003	5205	JMP RAT	/NØRMAL MØDE; GET .RATIØ
4004	5222	JMP CBRAT	
4005	7300	RAT, CLA CLL	
4006	4407	FENT	
4007	5120	FGET NPTS	
4010	1166	FADD ØNE	
4011	7000	FNØR	
4012	6120	FPUT NPTS	
4013	5652	FGET I CHO	
4014	4653	FDIV I CH1	
4015	1123	FADD A	
4016	7000	FNØR	
4017	6123	FPUT A	
4020	0000	FEXT	
4021	5242	JMP ØIT	

4022	7300	CBRAT,	CLA CLL	/CALIBRATE MODE
4023	4407		FENT	
4024	5120		FGET NPTS	
4025	1166		FADD ONE	
4026	7000		FNOR	
4027	6120		FPUT NPTS	
4030	5652		FGET I CH0	
4031	1123		FADD A	
4032	7000		FNOR	
4033	6123		FPUT A	
4034	5653		FGET I CH1	
4035	1171		FADD B	
4036	7000		FNOR	
4037	6171		FPUT B	
4040	0000		FEXT	
4041	5242		JMP BIT	
4042	7300	BIT,	CLA CLL	
4043	6551		6551	/OUTPUT +5 VOLTS TO CHAN1
4044	1254		TAD K4000	
4045	6551		6551	/OUTPUT 0 VOLTS
4046	7300		CLA CLL	
4047	6302		CLTF	/NEED ONLY CLEAR FLAG CAUSING INTRPT
4050	6001		IEN	
4051	5002		JMP LOOP	
4052	3727	CH0,	CHAN0	
4053	3732	CH1,	CHAN1	
4054	4000	K4000,	4000	

ORIGINAL RATIO AVERAGER TAPE 6

		FIELD=1	
		*200	
0200	0322	322	/R
0201	0325	325	/U
0202	0316	316	/N
0203	0240	240	/
0204	0316	316	/N
0205	0325	325	/U
0206	0315	315	/M
0207	0302	302	/B
0210	0305	305	/E
0211	0322	322	/R
0212	0272	272	/:
0213	0244	244	/S
		*240	
0240	0323	323	/S
0241	0314	314	/L
0242	0317	317	/J
0243	0320	320	/P
0244	0305	305	/E
0245	0260	260	/O
0246	0272	272	/:
0247	0244	244	/S
		*300	
0300	0311	311	/I
0301	0316	316	/N
0302	0324	324	/T
0303	0305	305	/E
0304	0322	322	/R
0305	0303	303	/C
0306	0305	305	/E
0307	0320	320	/P
0310	0324	324	/T
0311	0260	260	/O
0312	0272	272	/:
0313	0244	244	/S
		*340	
0340	0323	323	/S
0341	0314	314	/L
0342	0317	317	/J
0343	0320	320	/P
0344	0305	305	/E
0345	0261	261	/I
0346	0272	272	/:
0347	0244	244	/S
		*400	
0400	0311	311	/I
0401	0316	316	/N
0402	0324	324	/T
0403	0305	305	/E
0404	0322	322	/R
0405	0303	303	/C
0406	0305	305	/E
0407	0320	320	/P
0410	0324	324	/T
0411	0261	261	/I
0412	0272	272	/:
0413	0244	244	/S

		*500		
0500	0316		316	/N
0501	0325		325	/U
0502	0315		315	/M
0503	0302		302	/B
0504	0305		305	/E
0505	0322		322	/R
0506	0240		240	/
0507	0317		317	/B
0510	0306		306	/F
0511	0240		240	/
0512	0320		320	/P
0513	0317		317	/B
0514	0311		311	/I
0515	0316		316	/N
0516	0324		324	/T
0517	0323		323	/S
0520	0275		275	/=
0521	0244		244	/S
		*540		
0540	0301		301	/A
0541	0326		326	/V
0542	0305		305	/E
0543	0322		322	/R
0544	0301		301	/A
0545	0307		307	/G
0546	0305		305	/E
0547	0240		240	/
0550	0322		322	/R
0551	0301		301	/A
0552	0324		324	/T
0553	0311		311	/I
0554	0317		317	/B
0555	0275		275	/=
0556	0244		244	/S
		*440		
0440	0303		303	/C
0441	0310		310	/H
0442	0301		301	/A
0443	0316		316	/N
0444	0316		316	/N
0445	0305		305	/E
0446	0314		314	/L
0447	0240		240	/
0450	0260		260	/O
0451	0240		240	/
0452	0315		315	/M
0453	0311		311	/I
0454	0316		316	/N
0455	0272		272	/!
0456	0244		244	/S
		*600		
0600	0303		303	/C
0601	0310		310	/H
0602	0301		301	/A
0603	0316		316	/N
0604	0316		316	/N
0605	0305		305	/E
0606	0314		314	/L
0607	0240		240	/
0610	0261		261	/!
0611	0240		240	/
0612	0315		315	/M
0613	0311		311	/I
0614	0316		316	/N
0615	0272		272	/!

0616	0244		244	/S
		*640		
0640	0303		303	/C
0641	0310		310	/H
0642	0301		301	/A
0643	0316		316	/N
0644	0316		316	/N
0645	0305		305	/E
0646	0314		314	/L
0647	0240		240	/
0650	0260		260	/O
0651	0240		240	/
0652	0315		315	/M
0653	0301		301	/A
0654	0330		330	/X
0655	0272		272	/:
0656	0244		244	/S
		*700		
0700	0303		303	/C
0701	0310		310	/H
0702	0301		301	/A
0703	0316		316	/N
0704	0316		316	/N
0705	0305		305	/E
0706	0314		314	/L
0707	0240		240	/
0710	0261		261	/I
0711	0240		240	/
0712	0315		315	/M
0713	0301		301	/A
0714	0330		330	/X
0715	0272		272	/:
0716	0244		244	/S
		*740		
0740	0301		301	/A
0741	0326		326	/V
0742	0305		305	/E
0743	0322		322	/R
0744	0301		301	/A
0745	0307		307	/G
0746	0305		305	/E
0747	0240		240	/
0750	0317		317	/Q
0751	0306		306	/F
0752	0240		240	/
0753	0303		303	/C
0754	0310		310	/H
0755	0301		301	/A
0756	0316		316	/N
0757	0316		316	/N
0760	0305		305	/E
0761	0314		314	/L
0762	0240		240	/
0763	0260		260	/O
0764	0240		240	/
0765	0275		275	/=
0766	0244		244	/S
		*1000		
1000	0301		301	/A
1001	0326		326	/V
1002	0305		305	/E
1003	0322		322	/R
1004	0301		301	/A
1005	0307		307	/G
1006	0305		305	/E
1007	0240		240	/

1010	0317		317	/Ø
1011	0306		306	/F
1012	0240		240	/
1013	0303		303	/C
1014	0310		310	/H
1015	0301		301	/A
1016	0316		316	/N
1017	0316		316	/N
1020	0305		305	/E
1021	0314		314	/L
1022	0240		240	/
1023	0261		261	/1
1024	0240		240	/
1025	0275		275	/=
1026	0244		244	/S
		*1040		
1040	0316		316	/N
1041	0325		325	/H
1042	0315		315	/M
1043	0302		302	/B
1044	0305		305	/E
1045	0322		322	/R
1046	0240		240	/
1047	0317		317	/Ø
1050	0306		306	/F
1051	0240		240	/
1052	0302		302	/B
1053	0301		301	/A
1054	0304		304	/D
1055	0240		240	/
1056	0320		320	/P
1057	0317		317	/Ø
1060	0311		311	/I
1061	0316		316	/N
1062	0324		324	/T
1063	0323		323	/S
1064	0275		275	/=
1065	0244		244	/S

RATIO AVERAGER WITH CHART TAPE 5

```

*AVRG
3600 0000  AVRG,  0
3601 7300          CLA CLL      /HERE IN 29.3 MICROSEC
3602 6542          ADSC         /SELECT CHANNEL 0
3603 7300          CLA CLL      /AND CONVERT
3604 6531          ADSF         /SKIP WHEN DONE
3605 5204          JMP  .-1
3606 6534          ADRB         /READ INTO AC
3607 3344          DCA STRO
3610 1345          TAD K0001
3611 6542          ADSC         /SELECT CHANNEL 1
3612 7300          CLA CLL
3613 6531          ADSF
3614 5213          JMP  .-1
3615 6534          ADRB
3616 3343          DCA STR1     /VOLTAGES ARE STORED
3617 1165          TAD M0DE     /CHECK M0DE
3620 7650          SNA CLA      /CALIBRATE?
3621 5223          JMP  .+2
3622 5267          JMP  C0N     /YES
3623 1344          TAD STRO     /NO
3624 3150          DCA 05
3625 1144          TAD MAX0     /CHANO<MAX0?
3626 3147          DCA 08
3627 4526          JMS I SC0MP
3630 7650          SNA CLA
3631 5260          JMP  BAD     /NO
3632 1344          TAD STRO     /YES; CHANO>MIN0?
3633 3147          DCA 08
3634 1142          TAD MIN0
3635 3150          DCA 05
3636 4526          JMS I SC0MP
3637 7650          SNA CLA
3640 5260          JMP  BAD     /NO
3641 1343          TAD STR1     /YES; CHAN1<MAX1?
3642 3150          DCA 05
3643 1145          TAD MAX1
3644 3147          DCA 08
3645 4526          JMS I SC0MP
3646 7650          SNA CLA
3647 5260          JMP  BAD     /NO
3650 1343          TAD STR1     /YES; CHAN1>MIN1?
3651 3147          DCA 08
3652 1143          TAD MIN1
3653 3150          DCA 05
3654 4526          JMS I SC0MP
3655 7650          SNA CLA
3656 5260          JMP  BAD     /NO
3657 5267          JMP  C0N
3660 7300  BAD,   CLA CLL      /HERE IF NOT ON LINEAR REGION
3661 4407          FEXT        /OF VOLTAGE CURVE
3662 5160          FGET BDPTS   /INCREMENT HDPTS
3663 1166          FADD 0NE
3664 6160          FPUT BDPTS
3665 0000          FEXT
3666 5746          JMP I 00T
3667 7300  C0N,   CLA CLL
3670 1344          TAD STRO
3671 7012          RTR
3672 3045          DCA 45

```

3673	3046		DCA 46	
3674	1342		TAD C13	
3675	3044		DCA 44	
3676	4407		FENT	
3677	7000		FNØR	
3700	3335		FMPY TØVØLTS	
3701	3104		FMPY SLØPO	
3702	1107		FADD INTO	
3703	7000		FNØR	
3704	6327		FPUT CHANO	
3705	0000		FEXT	
3706	7300		CLA CLL	
3707	1343		TAD STR1	
3710	7012		RTR	/THIS CHANGES DIGITAL
3711	3045		DCA 45	/INFØRMATION TØ ACTUAL
3712	3046		DCA 46	/VØLTS. SAME AS ABOVE
3713	1342		TAD C13	/IT ALSO MULTIPLIES BY
3714	3044		DCA 44	/SLØPE AND ADDS INT.
3715	4407		FENT	
3716	7000		FNØR	
3717	3335		FMPY TØVØLTS	
3720	3112		FMPY SLØPI	
3721	1115		FADD INT1	
3722	7000		FNØR	
3723	6332		FPUT CHANI	
3724	0000		FEXT	
3725	7300		CLA CLL	
3726	5747		JMP I XY	
3727	0000	CHANO,	Ø	
3730	0000		Ø	
3731	0000		Ø	
3732	0000	CHANI,	Ø	
3733	0000		Ø	
3734	0000		Ø	
3735	7772	TØVØLTS,	7772	
3736	2401		2401	
3737	2005		2005	
3740	7772		7772	
3741	2401		2401	
3742	0013	C13,	0013	
3743	0000	STR1,	Ø	
3744	0000	STRØ,	Ø	
3745	0001	KØØØ1,	ØØØ1	
3746	4063	ØØT,	ØIT	
3747	4000	XY,	XZ	
			*AVRG+2ØØ	
4000	7300	XZ,	CLA CLL	
4001	1165		TAD MØDE	/CHECK MØDE
4002	7650		SNA CLA	
4003	5205		JMP RAT	/NØRMAL MØDE; GET RATIØ
4004	5243		JMP CBRAT	
4005	7300	RAT,	CLA CLL	
4006	4407		FENT	
4007	5120		FGET NPTS	
4010	1166		FADD ØNE	
4011	7000		FNØR	
4012	6120		FPUT NPTS	
4013	5672		FGET I CHØ	
4014	4673		FDIV I CH1	
4015	1123		FADD A	
4016	7000		FNØR	
4017	6123		FPUT A	
4020	0000		FEXT	
4021	2274		ISZ NBPTS	
4022	5263		JMP ØIT	
4023	4407		FENT	

4024	5123		FGET A	
4025	3267		FMPY FK40	
4026	0000		FEXT	
4027	4546		JMS I SINTEG	
4030	1276		TAD K4000	
4031	6551		6551	
4032	7300		CLA CLL	
4033	1275		TAD NCPTS	
4034	3274		DCA NBPTS	
4035	4407		FENT	
4036	5174		FGET ZERØ	
4037	6123		FPUT A	
4040	6120		FPUT NPTS	
4041	0000		FEXT	
4042	5263		JMP ØIT	
4043	7300	ØBRAT,	CLA CLL	/CALIBRATE MØDE
4044	4407		FENT	
4045	5120		FGET NPTS	
4046	1166		FADD ØNE	
4047	7000		FNØR	
4050	6120		FPUT NPTS	
4051	5672		FGET I CHØ	
4052	1123		FADD A	
4053	7000		FNØR	
4054	6123		FPUT A	
4055	5673		FGET I CH1	
4056	1171		FADD B	
4057	7000		FNØR	
4060	6171		FPUT B	
4061	0000		FEXT	
4062	5263		JMP ØIT	
4063	7300	ØIT,	CLA CLL	
4064	6302		CLTF	
4065	6001		IØN	
4066	5002		JMP LØØP	
4067	0003	FK40,	0003	
4070	2000		2000	
4071	0000		0000	
4072	3727	CHØ,	CHANO	
4073	3732	CH1,	CHAN1	
4074	7720	NBPTS,	7720	
4075	7720	NCPTS,	7720	
4076	4000	K4000,	4000	

trigger flag. First it converts channels 0 and 1 to digital values. If in calibrate mode it adds CHAN0 to A, CHAN1 to B, and 1 to NPTS. If in normal mode, it checks that voltages read are within the specified region, and if so adds CHAN0/CHAN1 to A and 1 to NPTS. If not it simply adds 1 to BDPTS. In any case, it then clears the trigger flag and turns the interrupt facility on, and jumps back into the waiting loop, line 0002.

The subroutine STRT gets ready for averaging by setting NPTS, A, B, and BDPTS equal to zero. CLEAR clears all flags, FINI outputs information, and INPT interprets and directs commands. SERV services an interrupt and determines where an interrupt came from. TYPE types a character, CRLF types a carriage return and a line feed, and OUT outputs text starting at the location given in BUFF and ending when a \$ is encountered.

We now discuss the operation of the Ratio Averager programs with the help of the flow chart in Figure 47 and the sample dialog in Figure 48. To begin, one normally types CAL and then A, to read the voltage levels on channels 0 and 1. These are adjusted on the integrator while the laser is running but blocked from the detectors, commonly to around 0.4 volts so that fluctuations in the integrator level do not carry it negative. Then during the initialization step the negative of these levels are input as the intercepts for each channel. The minimum voltages are chosen around 0.15 volt larger, again so that fluctuations in the integrator levels do not cause a value which is actually zero to be read. The slope values can be used to

Figure 48: Sample Ratio Averager
initializing dialog. Since the laser
was fluctuating when the example was
taken, the average ratio calculated
from the voltage levels taken after
returning to CAL mode is .66 as compared
with .64 taken during ratio averaging,
when pulses below the minimum level
were being rejected.

```

CAL
:A
0
NUMBER OF POINTS=+0.1635000E+04
AVERAGE OF CHANNEL 0 =+0.6334226E+00
AVERAGE OF CHANNEL 1 =+0.4445503E+00
:I
RUN NUMBER:1
SLOPE0:1.
INTERCEPT0:-.63
SLOPE1:1.
INTERCEPT1:-.44
CHANNEL 0 MIN:.78
CHANNEL 0 MAX:9.
CHANNEL 1 MIN:.59
CHANNEL 1 MAX:9.
ARDS PLOT MAX:8.
:A
0
NUMBER OF POINTS=+0.4800000E+03
AVERAGE RATIO=+0.6396517E+00
NUMBER OF BAD POINTS=+0.2000000E+01
:CAL
:A
0
NUMBER OF POINTS=+0.6559998E+03
AVERAGE OF CHANNEL 0 =+0.4304985E+01
AVERAGE OF CHANNEL 1 =+0.6009995E+01
:

```

Figure 48

compensate for differences in amplification, but they are normally set to 1. The maximum voltage levels are set 1 or 2 volts below 10 volts, which is the limit of the A/D converter and also the point where the integrator amplifiers saturate.

In the original program, typing 0 causes the average ratio, the number of points contributing, and the number of points outside the voltage limits to be typed out. In the chart modification, the average of every 48 points (a number specified by the NBPTS counter) is output through channel 1 of the D/A converter through the command 6551. The amplitude scale of the chart trace is set by the variable FK40, usually adjusted by changing line 4070 (or 4104 in the modification with the punch) using the switch register.

To operate the Ratio Averager modification which periodically outputs the ratio through the high speed punch as well as onto a chart recorder is more difficult, because changes must be made in the floating point package so that output is punched rather than typed. (All versions of the Ratio Averager program contain the Floating Point Package 3, which is not listed here but in its own DEC manual.) Here the problem of changing over to the punch is handled rather inelegantly, as follows. The original program is loaded and initialized using the teletype. Then the computer is stopped, the punch is turned on, and the modified tape 5 is loaded. The modification to punched output is made by changing line 7345 to 6021 and line 7347 to 6026. Also, to speed up output only three significant

(Text continues on page 227)
 RATIO AVERAGER WITH PUNCH TAPE 5

```

*AVRG
3600 0000  AVRG,  0
3601 7300      CLA CLL      /HERE IN 29.3 MICROSEC
3602 6542      ADSC        /SELECT CHANNEL 0
3603 7300      CLA CLL      /AND CONVERT
3604 6531      ADSF        /SKIP WHEN DONE
3605 5204      JMP .-1
3606 6534      ADRB        /READ INTO AC
3607 3344      DCA STRO
3610 1345      TAD K0001
3611 6542      ADSC        /SELECT CHANNEL 1
3612 7300      CLA CLL
3613 6531      ADSF
3614 5213      JMP .-1
3615 6534      ADRB
3616 3343      DCA STR1    /VOLTAGES ARE STORED
3617 1165      TAD M0DE    /CHECK MODE
3620 7650      SNA CLA     /CALIBRATE?
3621 5223      JMP .+2
3622 5267      JMP C0N     /YES
3623 1344      TAD STRO    /NO
3624 3150      DCA QS
3625 1144      TAD MAX0    /CHANO<MAX0?
3626 3147      DCA QB
3627 4526      JMS I SC0MP
3630 7650      SNA CLA
3631 5260      JMP BAD     /NO
3632 1344      TAD STRO    /YES; CHANO>MINO?
3633 3147      DCA QB
3634 1142      TAD MINO
3635 3150      DCA QS
3636 4526      JMS I SC0MP
3637 7650      SNA CLA
3640 5260      JMP BAD     /NO
3641 1343      TAD STR1    /YES; CHAN1<MAX1?
3642 3150      DCA QS
3643 1145      TAD MAX1
3644 3147      DCA QB
3645 4526      JMS I SC0MP
3646 7650      SNA CLA
3647 5260      JMP BAD     /NO
3650 1343      TAD STR1    /YES; CHAN1>MIN1?
3651 3147      DCA QB
3652 1143      TAD MIN1
3653 3150      DCA QS
3654 4526      JMS I SC0MP
3655 7650      SNA CLA
3656 5260      JMP BAD     /NO
3657 5267      JMP C0N
3660 7300      BAD,  CLA CLL /HERE IF NOT ON LINEAR REGION
3661 4407      FENT        /OF VOLTAGE CURVE
3662 5160      FGET BDPTS  /INCREMENT BDPTS
3663 1166      FADD 0NE
3664 6160      FPUT BDPTS
3665 0000      FEXT
3666 5746      JMP I 00T
3667 7300      C0N,  CLA CLL
3670 1344      TAD STRO
3671 7012      RTR
3672 3045      DCA 45
  
```


3673	3046		DCA 46	
3674	1342		TAD C13	
3675	3044		DCA 44	
3676	4407		FENT	
3677	7000		FNØR	
3700	3335		FMPY TØVØLTS	
3701	3104		FMPY SLØPD	
3702	1107		FADD INTO	
3703	7000		FNØR	
3704	6327		FPUT CHANO	
3705	0000		FEXT	
3706	7300		CLA CLL	
3707	1343		TAD STR1	
3710	7012		RTR	/THIS CHANGES DIGITAL
3711	3045		DCA 45	/INFØRMATION TØ ACTUAL
3712	3046		DCA 46	/VØLTS. SAME AS ABOVE
3713	1342		TAD C13	/IT ALSØ MULTIPLIES BY
3714	3044		DCA 44	/SLØPE AND ADDS INT.
3715	4407		FENT	
3716	7000		FNØR	
3717	3335		FMPY TØVØLTS	
3720	3112		FMPY SLØP1	
3721	1115		FADD INT1	
3722	7000		FNØR	
3723	6332		FPUT CHAN1	
3724	0000		FEXT	
3725	7300		CLA CLL	
3726	5747		JMP I XY	
3727	0000	CHANO,	0	
3730	0000		0	
3731	0000		0	
3732	0000	CHAN1,	0	
3733	0000		0	
3734	0000		0	
3735	7772	TØVØLTS,	7772	
3736	2401		2401	
3737	2005		2005	
3740	7772		7772	
3741	2401		2401	
3742	0013	C13,	0013	
3743	0000	STR1,	0	
3744	0000	STRO,	0	
3745	0001	K0001,	0001	
3746	4042	ØØT,	ØIT	
3747	4000	XY,	XZ	
			*AVRG+200	
4000	7300	XZ,	CLA CLL	
4001	1165		TAD MØDE	/CHECK MØDE
4002	7650		SNA CLA	
4003	5205		JMP RAT	/NØRMAL MØDE; GET RATIØ
4004	5222		JMP CBRAT	
4005	7300	RAT,	CLA CLL	
4006	4407		FENT	
4007	5120		FGET NPTS	
4010	1166		FADD ØNE	
4011	7000		FNØR	
4012	6120		FPUT NPTS	
4013	5706		FGET I CHO	
4014	4707		FDIV I CHI	
4015	1123		FADD A	
4016	7000		FNØR	
4017	6123		FPUT A	
4020	0000		FEXT	
4021	5242		JMP ØIT	
4022	7300	CBRAT,	CLA CLL	/CALIBRATE MØDE
4023	4407		FENT	

4024	5120		FGET NPTS
4025	1166		FADD ONE
4026	7000		FNOR
4027	6120		FPUT NPTS
4030	5706		FGET I CHO
4031	1123		FADD A
4032	7000		FNOR
4033	6123		FPUT A
4034	5707		FGET I CH1
4035	1171		FADD B
4036	7000		FNOR
4037	6171		FPUT B
4040	0000		FEXT
4041	5242		JMP BIT
4042	7300	BIT,	CLA CLL
4043	6302		CLTF
4044	2310		ISZ NBPTS
4045	6001		ION
4046	1310		TAD NBPTS
4047	7440		SZA
4050	5002		JMP LOOP
4051	7300		CLA CLL
4052	6026		6026
4053	4407		FENT
4054	5123		FGET A
4055	4120		FDIV NPTS
4056	7000		FNOR
4057	0014		OUTPUT
4060	5123		FGET A
4061	3303		FMPI FK40
4062	0000		FEXT
4063	4546		JMS I SINTEG
4064	1312		TAD K4000
4065	6551		6551
4066	6022		6022
4067	7300		CLA CLL
4070	1311		TAD NCPTS
4071	3310		DCA NBPTS
4072	4407		FENT
4073	5174		FGET ZERO
4074	6123		FPUT A
4075	6120		FPUT NPTS
4076	0000		FEXT
4077	7300		CLA CLL
4100	6302		CLTF
4101	6001		ION
4102	5002		JMP LOOP
4103	0003	FK40,	0003
4104	2000		2000
4105	0000		0000
4106	3727	CHO,	CHAN0
4107	3732	CH1,	CHAN1
4110	7720	NBPTS,	7720
4111	7720	NCPTS,	7720
4112	4000	K4000,	4000

figures are retained, by changing memory location 7325 to 7776. Then to run the program, load address 3601 and start.

Finally, we make some explanatory comments on the Ratio Averager modification which plots points on the ARDS graphics display terminal whose x and y coordinates are the integrated outputs of the two detectors. This modification was originally carried out by Bruce Garetz. We refer to the listings on following pages.

In tape 1, there are some additional floating point memory locations. AMAX is the maximum value of the ARDS plot, typed in during the initial dialogue. SCALE is the number of ARDS display points along the entire x or y axis, while SHIFT is half that and is used to move the zero of the plot from the center of the screen to the lower left corner. SPLOT is an added subroutine reference, and the definition of TAMAX gives the address of the text for the plot maximum question on tape 6.

The only change in tape 4 is to draw the axes after the initial dialogue. In line 3162 we go to the subroutine AXES, on tape 4.5. The subroutine takes through line 2633 to ask for the maximum of the ARDS scale. Then the instruction 6312 clears the ARDS flag. The character KERASE, which is zero, is read by the ARDS on the command 6314. There is a loop which checks to see if the ARDS is done reading, including the command 6311 to skip the following statement if done. Lines 2643 through 2646 are a delay to give the ARDS time to erase. Lines 2651 through 2655 put the ARDS into set point

(Text continues on page 245.)

HATIØ AVERAGER WITH ARDS TAPE 1

```

*0000
0000 0000 0
0001 5531 JMP I SSERV
0002 5002 LØØP, JMP .
*0007
0007 5600 5600 /PØINTER TØ FP PKG 3
*0015
0015 0000 AMAX, 0000
0016 0000 0000
0017 0000 0000
*0023
0023 0012 SHIFT, 0012
0024 2070 2070
0025 0000 0000
0026 0013 SCALE, 0013
0027 2070 2070
0030 0000 0000
0031 2730 SPLØT, PLØT
0032 1100 TAMAX, 1100
*0044
0044 0000 FLAC, 0
0045 0000 0
0046 0000 0
*0055
0055 0001 0001 /FØR CR AFTER ØUTPUT
0056 7777 7777 /FØR LF AFTDR ØUTPUT
0057 0000 0
0060 0000 0
0061 0000 0
*70
0070 0000 AC, 0
0071 0000 L, 0
0072 0000 BUFF, 0
0073 0200 TRIN, 200
0074 4000 TEXT, 4000
0075 0240 TSLØPO, 240
0076 0300 TINTO, 300
0077 0340 TSLØPI, 340
0100 0400 TINTI, 400
0101 0000 RUN, 0
0102 0000 0
0103 0000 0
0104 0000 SLØPO, 0
0105 0000 0
0106 0000 0
0107 0000 INTO, 0
0110 0000 0
0111 0000 0
0112 0000 SLØPI, 0
0113 0000 0
0114 0000 0
0115 0000 INTI, 0
0116 0000 0
0117 0000 0
0120 0000 NPTS, 0
0121 0000 0
0122 0000 0
0123 0000 A, 0
0124 0000 0
0125 0000 0
0126 3400 SCØMP, CØMP
```

0127	1000	SØUT,	ØUT	
0130	3000	SINIT,	INIT	
0131	1200	SSERV,	SERV	
0132	1400	SINPT,	INPT	
0133	3600	SAVRG,	AVRG	
0134	1022	SCRLF,	CRLF	
0135	1300	SSTRT,	STRT	
0136	2400	SFINI,	FINI	
0137	1030	STYPE,	TYPE	
0140	2200	SCLEAR,	CLEAR	
0141	2600	SCALIB,	CALIB	
0142	0000	MINO,	0	
0143	0000	MINI,	0	
0144	0000	MAXO,	0	
0145	0000	MAXI,	0	
0146	3200	SINTEG,	INTEG	
0147	0000	QB,	0	
0150	0000	QS,	0	
0151	0440	TMINO,	440	
0152	0600	TMINI,	600	
0153	0640	TMAXO,	640	
0154	0700	TMAXI,	700	
0155	0740	TCHO,	740	
0156	1000	TCH1,	1000	
0157	1040	TBDPT,	1040	
0160	0000	BDPTS,	0	
0161	0000		0	
0162	0000		0	
0163	0540	TAV,	540	
0164	0500	TPTS,	500	
0165	0000	MØDE,	0	
0166	0001	ØNE,	0001	
0167	2000		2000	
0170	0000		0000	
0171	0000	B,	0	
0172	0000		0	
0173	0000		0	
0174	0000	ZERØ,	0	
0175	0000		0	
0176	0000		0	
		*200		
0200	7300	CLA CLL		/PROGRAM STARTS HERE
0201	6046	TLS		/TØ SET PRINTER FLAG
0202	5603	JMP I SCF		
0203	1604	SCF,	INPT+204	

RATIO AVERAGER WITH ARDS TAPE 4

```

*CALIB
2600 0000 CALIB, 0 /HANDLES CALIBRATE COMMAND
2601 7300 CLA CLL
2602 7001 IAC
2603 3165 DCA MØDE /SET MØDE=1 INDICATING CALIBRATE MØDE
2604 4407 FENT
2605 5166 FGET ØNE
2606 6104 FPUT SLØPO
2607 6112 FPUT SLØP1
2610 5174 FGET ZERO
2611 6107 FPUT INTO
2612 6115 FPUT INT1
2613 0000 FEXT
2614 5600 JMP I CALIB

*INIT
3000 0000 INIT, 0 /INITIALIZATION SUBROUTINE
3001 7300 CLA CLL /TO GET RUN NUMBER SLØPES
3002 6046 TLS /AND INTERCEPTS
3003 1073 TAD TRUN /TLS SETS TTY FLAG
3004 3072 DCA BUFF
3005 6211 CDF +10 /TEXT IS IN UPPER 4K
3006 4527 JMS I SØUT /ASK FOR RUN NUMBER
3007 6201 CDF +00
3010 4407 FENT
3011 0013 INPUT /GET RUN NUM AND STORE
3012 7000 FNØR
3013 6101 FPUT RUN
3014 0000 FEXT
3015 7300 CLA CLL
3016 1075 TAD TSLØPO /GET SLØPO
3017 3072 DCA BUFF
3020 6211 CDF +10
3021 4527 JMS I SØUT
3022 6201 CDF +00
3023 4407 FENT
3024 0013 INPUT
3025 7000 FNØR
3026 6104 FPUT SLØPO
3027 0000 FEXT
3030 7300 CLA CLL /GET INTO
3031 1076 TAD TINTU
3032 3072 DCA BUFF
3033 6211 CDF +10
3034 4527 JMS I SØUT
3035 6201 CDF +00
3036 4407 FENT
3037 0013 INPUT
3040 7000 FNØR
3041 6107 FPUT INTO
3042 0000 FEXT
3043 7300 CLA CLL /GET SLØP1
3044 1077 TAD TSLØP1
3045 3072 DCA BUFF
3046 6211 CDF +10
3047 4527 JMS I SØUT
3050 6201 CDF +00
3051 4407 FENT
3052 0013 INPUT
3053 7000 FNØR

```

3054	6112	FPUT SLØPI	
3055	0000	FEXT	
3056	7300	CLA CLL	/GET INT1
3057	1100	TAD TINT1	
3060	3072	DCA BUFF	
3061	6211	CDF +10	
3062	4527	JMS I SØUT	
3063	6201	CDF +00	
3064	4407	FENT	
3065	0013	INPUT	
3066	7000	FNØR	
3067	6115	FPUT INT1	
3070	0000	FEXT	
3071	7300	CLA CLL	/GET MINS AND MAXS
3072	1151	TAD TMIN0	
3073	3072	DCA BUFF	
3074	6211	CDF +10	
3075	4527	JMS I SØUT	
3076	6201	CDF +00	
3077	4407	FENT	
3100	0013	INPUT	
3101	7000	FNØR	
3102	3366	FMPY F4095	
3103	4371	FDIV FTEN	
3104	7000	FNØR	
3105	0000	FEXT	
3106	4546	JMS I SINTEG	
3107	3142	DCA MIN0	
3110	1153	TAD TMAX0	
3111	3072	DCA BUFF	
3112	6211	CDF +10	
3113	4527	JMS I SØUT	
3114	6201	CDF +00	
3115	4407	FENT	
3116	0013	INPUT	
3117	7000	FNØR	
3120	3366	FMPY F4095	
3121	4371	FDIV FTEN	
3122	7000	FNØR	
3123	0000	FEXT	
3124	4546	JMS I SINTEG	
3125	3144	DCA MAX0	
3126	1152	TAD TMIN1	
3127	3072	DCA BUFF	
3130	6211	CDF +10	
3131	4527	JMS I SØUT	
3132	6201	CDF +00	
3133	4407	FENT	
3134	0013	INPUT	
3135	7000	FNØR	
3136	3366	FMPY F4095	
3137	4371	FDIV FTEN	
3140	7000	FNØR	
3141	0000	FEXT	
3142	4546	JMS I SINTEG	
3143	3143	DCA MIN1	
3144	1154	TAD TMAX1	
3145	3072	DCA BUFF	
3146	6211	CDF +10	
3147	4527	JMS I SØUT	
3150	6201	CDF +00	
3151	4407	FENT	
3152	0013	INPUT	
3153	7000	FNØR	
3154	3366	FMPY F4095	
3155	4371	FDIV FTEN	

3156	7000		FNØR	
3157	0000		FEXT	
3160	4546		JMS I SINTEG	
3161	3145		DCA MAX1	
3162	4774		JMS I SAXES	
3163	7300		CLA CLL	
3164	3165		DCA MØDE	/FØR REGULAR MØDE
3165	5600		JMP I INIT	/DØNE
3166	0012	F4095,	0012	
3167	3777		3777	
3170	4000		4000	
3171	0004	FTEN,	0004	
3172	2400		2400	
3173	0000		0000	
3174	2620	SAXES,	AXES	
		*INTEG		
3200	0000	INTEG,	0	/CØNVERTS NUMBER IN FLAC TØ
3201	7300		CLA CLL	/AN INTEGER IN THE AC
3202	1044		TAD FLAC	
3203	7510		SPA	
3204	5242		JMP NEG	/THE FL PT EXPØNENT IS NEG
3205	7300		CLA CLL	
3206	1046		TAD FLAC+2	
3207	0244		AND K4000	/GET LEFT BIT
3210	7450		SNA	
3211	5213		JMP .+2	
3212	7020		CML	
3213	1045		TAD FLAC+1	
3214	7004		RAL	
3215	7100		CLL	
3216	3246		DCA INT	
3217	1044		TAD FLAC	
3220	1250		TAD M12	
3221	7540		SMA S/A	
3222	5237		JMP XY	/LARGER THAN 2**12
3223	7500		SMA	
3224	5234		JMP XX	/=0
3225	3247		DCA SHFT	
3226	1246		TAD INT	
3227	7100		CLL	
3230	7010		RAR	
3231	2247		ISZ SHFT	
3232	5227		JMP .-3	
3233	5600		JMP I INTEG	
3234	7300	XX,	CLA CLL	
3235	1246		TAD INT	
3236	5600		JMP I INTEG	
3237	7300	XY,	CLA CLL	
3240	1245		TAD K7777	
3241	5600		JMP I INTEG	
3242	7300	NEG,	CLA CLL	
3243	5600		JMP I INTEG	
3244	4000	K4000,	4000	
3245	7777	K7777,	7777	
3246	0000	INT,	0	
3247	0000	SHFT,	0	
3250	7766	M12,	7766	
		*CØMP		
3400	0000	CØMP,	0	
3401	7300		CLA CLL	/DØES ABSØLUTE CØMPARISØN,
3402	1377		TAD Q	/IÈ: 4000>3777
3403	7700		SMA CLA	
3404	5210		JMP .+4	
3405	7240		CLA CMA	/QB IS MINUS
3406	3244		DCA SB	
3407	5212		JMP .+3	

3410	7201		CLA IAC	/QB IS POS OR ZERO
3411	3244		DCA SB	
3412	1150		TAD QS	
3413	7700		SMA CLA	
3414	5226		JMP .+12	
3415	1244		TAD SB	/QS IS MINUS
3416	7700		SMA CLA	
3417	5242		JMP NØ	
3420	1150		TAD QS	
3421	7041		CIA	
3422	1147		TAD QB	
3423	7700		SMA CLA	
3424	5240		JMP YES	
3425	5242		JMP NØ	
3426	1244		TAD SB	/QS IS PLUS OR ZERO
3427	7700		SMA CLA	
3430	5232		JMP .+2	
3431	5240		JMP YES	
3432	1150		TAD QS	
3433	7041		CIA	
3434	1147		TAD QB	
3435	7700		SMA CLA	
3436	5240		JMP YES	
3437	5242		JMP NØ	
3440	7201	YES,	CLA IAC	/QB>QS AC=1
3441	5600		JMP I COMP	
3442	7300	NØ,	CLA CLL	/QB<QS AC=0
3443	5600		JMP I COMP	
3444	0000	SB,	0	

RATIO AVERAGER WITH ARDS TAPE 4.5

		*AXES	
2620	0000	AXES,	0
2621	7300		CLA CLL
2622	1032		TAD TAMAX
2623	3072		DCA BUFF
2624	6211		CDF +10
2625	4527		JMS I SOUT
2626	6201		CDF +00
2627	4407		FENT
2630	0013		INPUT
2631	7000		FNOR
2632	6015		FPUT AMAX
2633	0000		FEXT
2634	7300		CLA CLL
2635	6312		6312
2636	1321		TAD KERASE
2637	6314		6314
2640	6311		6311
2641	5240		JMP.-1
2642	7300		CLA CLL
2643	1312		TAD K4000
2644	7001		IAC
2645	7510		SPA
2646	5244		JMP.-2
2647	6312		6312
2650	7300		CLA CLL
2651	1320		TAD GSS
2652	6314		6314
2653	6311		6311
2654	5253		JMP.-1
2655	6312		6312
2656	7300		CLA CLL
2657	1313		TAD M540
2660	4431		JMS I SPL0T
2661	1314		TAD K480
2662	4431		JMS I SPL0T
2663	1311		TAD RSS
2664	6314		6314
2665	6311		6311
2666	5265		JMP.-1
2667	6312		6312
2670	7300		CLA CLL
2671	1317		TAD KO
2672	4431		JMS I SPL0T
2673	1316		TAD M1020
2674	4431		JMS I SPL0T
2675	1315		TAD K1020
2676	4431		JMS I SPL0T
2677	1317		TAD KO
2700	4431		JMS I SPL3T
2701	7300		CLA CLL
2702	1320		TAD GSS
2703	6314		6314
2704	6311		6311
2705	5304		JMP.-1
2706	6312		6312
2707	7300		CLA CLL
2710	5620		JMP I AXES
2711	0036	RSS,	0036

2712	4000	K4000,	4000
2713	6744	M540,	6744
2714	0740	K480,	0740
2715	1774	K1020,	1774
2716	6004	M1020,	6004
2717	0000	K0,	0000
2720	0035	GSS,	0035
2721	0000	KERASE,	0000
2722	3300	SFLØT,	FLØT
		*PLØT	
2730	0000	PLØT,	0
2731	7500		SMA
2732	5335		JMP.+3
2733	7040		CMA
2734	1360		TAD K4001
2735	3357		DCA TEMP
2736	1357		TAD TEMP
2737	7004		RAL
2740	7200		CLA
2741	1357		TAD TEMP
2742	0356		AND MASK37
2743	7004		RAL
2744	1361		TAD K1000
2745	4762		JMS I SØAT
2746	1357		TAD TEMP
2747	7012		RTR
2750	7012		RTR
2751	7010		RAR
2752	0356		AND MASK37
2753	1361		TAD K1000
2754	4762		JMS I SØAT
2755	5730		JMP I PLØT
2756	0037	MASK37,	0037
2757	0000	TEMP,	0000
2760	4001	K4001,	4001
2761	0100	K1000,	0100
2762	2770	SØAT,	ØAT
		*ØAT	
2770	0000	ØAT,	0
2771	6314		6314
2772	6311		6311
2773	5372		JMP.-1
2774	6312		6312
2775	7300		CLA CLL
2776	5770		JMP I ØAT

RATIO AVERAGER WITH ARDS TAPE 4.7

		*FLØT	
3300	0000	FLØT,	0
3301	3045		DCA 45
3302	3046		DCA 46
3303	1311		TAD C13
3304	3044		DCA 44
3305	4407		FENT
3306	7000		FNØR
3307	0000		FEXT
3310	5700		JMP I FLØT
3311	0013	C13,	0013
		*FFIX	
3320	0000	FFIX,	0
3321	7200		CLA
3322	1044		TAD 44
3323	7540		SZA SNA
3324	5327		JMP.+3
3325	7200		CLA
3326	5344		JMP DØNE+1
3327	1345		TAD M13
3330	7450		SNA
3331	5343		JMP DØNE
3332	3044		DCA 44
3333	7100	GJ,	CLL
3334	1045		TAD 45
3335	7510		SPA
3336	7020		CML
3337	7010		RAR
3340	3045		DCA 45
3341	2044		ISZ 44
3342	5333		JMP GJ
3343	1045	DØNE,	TAD 45
3344	5720		JMP I FFIX
3345	7765	M13,	-13

RATIO AVERAGER WITH ARDS TAPE 5

```

*AVRG
3600 0000 AVRG, 0
3601 7300 CLA CLL /HERE IN 29.3 MICROSEC
3602 6542 ADSC /SELECT CHANNEL 0
3603 7300 CLA CLL /AND CONVERT
3604 6531 ADSF /SKIP WHEN DONE
3605 5204 JMP .-1
3606 6534 ADRB /READ INTO AC
3607 3344 DCA STRO
3610 1345 TAD K0001
3611 6542 ADSC /SELECT CHANNEL 1
3612 7300 CLA CLL
3613 6531 ADSF
3614 5213 JMP .-1
3615 6534 ADRB
3616 3343 DCA STR1 /VOLTAGES ARE STORED
3617 1165 TAD M0DE /CHECK M0DE
3620 7650 SNA CLA /CALIBRATE?
3621 5223 JMP .+2
3622 5267 JMP C0N /YES
3623 1344 TAD STRO /NO
3624 3150 DCA Q5
3625 1144 TAD MAX0 /CHANO<MAX0?
3626 3147 DCA Q6
3627 4526 JMS I SC0MP
3630 7650 SNA CLA
3631 5260 JMP BAD /NO
3632 1344 TAD STRO /YES; CHANO>MIN0?
3633 3147 DCA Q6
3634 1142 TAD MIN0
3635 3150 DCA Q5
3636 4526 JMS I SC0MP
3637 7650 SNA CLA
3640 5260 JMP BAD /NO
3641 1343 TAD STR1 /YES; CHAN1<MAX1?
3642 3150 DCA Q5
3643 1145 TAD MAX1
3644 3147 DCA Q6
3645 4526 JMS I SC0MP
3646 7650 SNA CLA
3647 5260 JMP BAD /NO
3650 1343 TAD STR1 /YES; CHAN1>MIN1?
3651 3147 DCA Q6
3652 1143 TAD MIN1
3653 3150 DCA Q5
3654 4526 JMS I SC0MP
3655 7650 SNA CLA
3656 5260 JMP BAD /NO
3657 5267 JMP C0N
3660 7300 BAD, CLA CLL /HERE IF NOT 3N LINEAR REGION
3661 4407 FENT /3F VOLTAGE CURVE
3662 5160 FGET BDPTS /INCREMENT BDPTS
3663 1166 FADD 0NE
3664 6160 FPUT BDPTS
3665 0000 FEXT
3666 5746 JMP I 00T
3667 7300 C0N, CLA CLL
3670 1344 TAD STRO
3671 7012 RTR

```

3672	3045	DCA 45	
3673	3046	DCA 46	
3674	1342	TAD C13	
3675	3044	DCA 44	
3676	4407	FENT	
3677	7000	FNØR	
3700	3335	FMPY TØVØLTS	
3701	3104	FMPY SLØPO	
3702	1107	FADD INTO	
3703	7000	FNØR	
3704	6327	FPUT CHANO	
3705	0000	FEXT	
3706	7300	CLA CLL	
3707	1343	TAD STR1	
3710	7012	RTR	/THIS CHANGES DIGITAL
3711	3045	DCA 45	/INFORMATION TO ACTUAL
3712	3046	DCA 46	/VØLTS. SAME AS ABOVE
3713	1342	TAD C13	/IT ALSØ MULTIPLIES BY
3714	3044	DCA 44	/SLØPE AND ADDS INT.
3715	4407	FENT	
3716	7000	FNØR	
3717	3335	FMPY TØVØLTS	
3720	3112	FMPY SLØP1	
3721	1115	FADD INT1	
3722	7000	FNØR	
3723	6332	FPUT CHAN1	
3724	0000	FEXT	
3725	7300	CLA CLL	
3726	5747	JMP I XY	
3727	0000	CHANO, 0	
3730	0000	0	
3731	0000	0	
3732	0000	CHAN1, 0	
3733	0000	0	
3734	0000	0	
3735	7772	TØVØLTS, 7772	
3736	2401	2401	
3737	2005	2005	
3740	7772	7772	
3741	2401	2401	
3742	0013	C13, 0013	
3743	0000	STR1, 0	
3744	0000	STR0, 0	
3745	0001	K0001, 0001	
3746	4072	ØØT, ØIT	
3747	4000	XY, XZ	
		*AVRG+200	
4000	7300	XZ, CLA CLL	
4001	1165	TAD MØDE	/CHECK MØDE
4002	7650	SNA CLA	
4003	5205	JMP RAT	/NØRMAL MØDE; GET RATIO
4004	5252	JMP CBRAT	
4005	7300	RAT, CLA CLL	
4006	4407	FENT	
4007	5120	FGET NPTS	
4010	1166	FADD ØNE	
4011	7000	FNØR	
4012	6120	FPUT NPTS	
4013	5702	FGET I CHO	
4014	4703	FDIV I CH1	
4015	1123	FADD A	
4016	7000	FNØR	
4017	6123	FPUT A	
4020	5702	FGET I CHO	
4021	3026	FMPY SCALE	
4022	4015	FDIV AMAX	

4023	2023		FSUB SHIFT	
4024	7000		FNØR	
4025	0000		FEXT	
4026	4705		JMS I SFFIX	
4027	3702		DCA I CHO	
4030	4407		FENT	
4031	5703		FGET I CH1	
4032	3026		FMPY SCALE	
4033	4015		FDIV AMAX	
4034	2023		FSUB SHIFT	
4035	7000		FNØR	
4036	0000		FEXT	
4037	4705		JMS I SFFIX	
4040	3703		DCA I CH1	
4041	7300		CLA CLL	
4042	1702		TAD I CHO	
4043	4431		JMS I SPLØT	
4044	7300		CLA CLL	
4045	1703		TAD I CH1	
4046	4431		JMS I SPLØT	
4047	4320		JMS DRAW	
4050	7300		CLA CLL	
4051	5272		JMP ØIT	
4052	7300	CBRAT,	CLA CLL	/CALIBRATE MØDE
4053	4407		FENT	
4054	5120		FGET NPTS	
4055	1166		FADD ØNE	
4056	7000		FNØR	
4057	6120		FPUT NPTS	
4060	5702		FGET I CHO	
4061	1123		FADD A	
4062	7000		FNØR	
4063	6123		FPUT A	
4064	5703		FGET I CH1	
4065	1171		FADD B	
4066	7000		FNØR	
4067	6171		FPUT B	
4070	0000		FEXT	
4071	5272		JMP ØIT	
4072	7300	ØIT,	CLA CLL	
4073	6551		6551	/ØOUTPUT +5 VØLTS TØ CHAN1
4074	1304		TAD K4000	
4075	6551		6551	/ØOUTPUT 0 VØLTS
4076	7300		CLA CLL	
4077	6302		CLTF	/NEED ØNLY CLEAR FLAG CAUSING INTRPT
4100	6001		IØN	
4101	5002		JMP LØØP	
4102	3727	CHO,	CHANO	
4103	3732	CH1,	CHAN1	
4104	4000	K4000,	4000	
4105	3320	SFFIX,	FFIX	
		*DRAW		
4120	0000	DRAW,	0	
4121	7300		CLA CLL	
4122	1343		TAD RSK	
4123	6314		6314	
4124	6311		6311	
4125	5324		JMP.-1	
4126	6312		6312	
4127	7300		CLA CLL	
4130	1345		TAD K1	
4131	4431		JMS I SPLØT	
4132	1345		TAD K1	
4133	4431		JMS I SPLØT	
4134	1344		TAD GSK	
4135	6314		6314	

4136	6311		6311
4137	5336		JMP.-1
4140	6312		6312
4141	7300		CLA CLL
4142	5720		JMP I DRAW
4143	0036	RSK,	0036
4144	0035	GSK,	0035
4145	0001	K1,	0001

BAD	3660
CBRAT	4052
CHANO	3727
CHAN1	3732
CHO	4102
CH1	4103
C0N	3667
C13	3742
GSK	4144
K0001	3745
K1	4145
K4000	4104
JIT	4072
J0T	3746
RAT	4005
RSK	4143
SFFIX	4105
STRO	3744
STR1	3743
T3V0LT	3735
XY	3747
XZ	4000

RATIO AVERAGER WITH ARDS, GRID TAPE 4.5

		*AXES	
2620	0000	AXES,	0
2621	7300		CLA CLL
2622	1032		TAD TAMAX
2623	3072		DCA BUFF
2624	6211		CDF +10
2625	4527		JMS I SOUT
2626	6201		CDF +00
2627	4407		FEXT
2630	0013		INPIT
2631	7000		FNOR
2632	6015		FPJT AMAX
2633	0000		FEXT
2634	7300		CLA CLL
2635	1324		TAD GSS
2636	6314		6314
2637	6311		6311
2640	5237		JMP.-1
2641	6312		6312
2642	7300		CLA CLL
2643	1322		TAD M540
2644	4431		JMS I SPL0T
2645	1320		TAD K540
2646	4431		JMS I SPL0T
2647	1321		TAD RSS
2650	6314		6314
2651	6311		6311
2652	5251		JMP.-1
2653	6312		6312
2654	7300		CLA CLL
2655	1323		TAD KO
2656	4431		JMS I SPL0T
2657	1322		TAD M540
2660	4431		JMS I SPL0T
2661	1323		TAD KO
2662	4431		JMS I SPL0T
2663	1322		TAD M540
2664	4431		JMS I SPL0T
2665	1320		TAD K540
2666	4431		JMS I SPL0T
2667	1323		TAD KO
2670	4431		JMS I SPL0T
2671	1320		TAD K540
2672	4431		JMS I SPL0T
2673	1323		TAD KO
2674	4431		JMS I SPL0T
2675	1323		TAD KO
2676	4431		JMS I SPL0T
2677	1320		TAD K540
2700	4431		JMS I SPL0T
2701	1323		TAD KO
2702	4431		JMS I SPL0T
2703	1320		TAD K540
2704	4431		JMS I SPL0T
2705	1322		TAD M540
2706	4431		JMS I SPL0T
2707	1323		TAD KO
2710	4431		JMS I SPL0T
2711	1322		TAD M540

2712	4431		JMS I SPLØT
2713	1323		TAD KO
2714	4431		JMS I SPLØT
2715	4717		JMS I SGRID
2716	5620		JMP I AXES
2717	3450	SGRID,	GRID
2720	1034	K540,	1034
2721	0036	RSS,	0036
2722	6744	M540,	6744
2723	0000	K0,	0000
2724	0035	GSS,	0035
		*PLØT	
2730	0000	PLØT,	0
2731	7500		SMA
2732	5335		JMP.+3
2733	7040		CMA
2734	1360		TAD K4001
2735	3357		DCA TEMP
2736	1357		TAD TEMP
2737	7004		RAL
2740	7200		CLA
2741	1357		TAD TEMP
2742	0356		AND MASK37
2743	7004		RAL
2744	1361		TAD K1000
2745	4762		JMS I SØAT
2746	1357		TAD TEMP
2747	7012		RTR
2750	7012		RTR
2751	7010		RAR
2752	0356		AND MASK37
2753	1361		TAD K1000
2754	4762		JMS I SØAT
2755	5730		JMP I PLØT
2756	0037	MASK37,	0037
2757	0000	TEMP,	0000
2760	4001	K4001,	4001
2761	0100	K1000,	0100
2762	2770	SØAT,	ØAT
		*ØAT	
2770	0000	ØAT,	0
2771	6314		6314
2772	6311		6311
2773	5372		JMP.-1
2774	6312		6312
2775	7300		CLA CLL
2776	5770		JMP I ØAT

RATIO AVERAGER WITH ARDS, GRID TAPE 4.7

		*FLØT	
3300	0000	FLØT,	0
3301	3045		DCA 45
3302	3046		DCA 46
3303	1311		TAD C13
3304	3044		DCA 44
3305	4407		FENT
3306	7000		FNØR
3307	0000		FEXT
3310	5700		JMP I FLØT
3311	0013	C13,	0013
		*FFIX	
		FFIX,	0
3320	0000		CLA
3321	7200		TAD 44
3322	1044		SZA SMA
3323	7540		JMP.+3
3324	5327		CLA
3325	7200		JMP DØNE+1
3326	5344		TAD M13
3327	1345		SMA
3330	7450		JMP DØNE
3331	5343		DCA 44
3332	3044		GØ,
3333	7100		CLL
3334	1045		TAD 45
3335	7510		SPA
3336	7020		CML
3337	7010		RAR
3340	3045		DCA 45
3341	2044		ISZ 44
3342	5333		JMP GØ
3343	1045	DØNE,	TAD 45
3344	5720		JMP I FFIX
3345	7765	M13,	-13
		*GRID	
		GRID,	0
3450	0000		CLA CLL
3451	7300		TAD M648
3452	1357		DCA X
3453	3365		TAD M648
3454	1357		DCA Y
3455	3366		TAD M11
3456	1364		DCA M
3457	3367		CLA CLL
3460	7300	BEG1,	TAD X
3461	1365		TAD K108
3462	1360		DCA X
3463	3365		TAD M11
3464	1364		DCA N
3465	3370		CLA CLL
3466	7300	BEG2,	TAD Y
3467	1366		TAD K108
3470	1360		DCA Y
3471	3366		TAD GSS
3472	1355		6314
3473	6314		6311
3474	6311		JMP.-1
3475	5274		6312
3476	6312		CLA CLL
3477	7300		TAD X
3500	1365		

3501	4431		JMS I SPLØT
3502	1366		TAD Y
3503	4431		JMS I SPLØT
3504	1356		TAD RSS
3505	6314		6314
3506	6311		6311
3507	5306		JMP.-1
3510	6312		6312
3511	7300		CLA CLL
3512	1362		TAD K2
3513	4431		JMS I SPLØT
3514	1361		TAD KØ
3515	4431		JMS I SPLØT
3516	1363		TAD M4
3517	4431		JMS I SPLØT
3520	1361		TAD KØ
3521	4431		JMS I SPLØT
3522	1362		TAD K2
3523	4431		JMS I SPLØT
3524	1361		TAD KØ
3525	4431		JMS I SPLØT
3526	1361		TAD KØ
3527	4431		JMS I SPLØT
3530	1362		TAD K2
3531	4431		JMS I SPLØT
3532	1361		TAD KØ
3533	4431		JMS I SPLØT
3534	1363		TAD M4
3535	4431		JMS I SPLØT
3536	2370		ISZ N
3537	5266		JMP BEG2
3540	7300		CLA CLL
3541	1357		TAD M648
3542	3366		DCA Y
3543	2367		ISZ M
3544	5260		JMP BEG1
3545	7300		CLA CLL
3546	1355		TAD GSS
3547	6314		6314
3550	6311		6311
3551	5350		JMP.-1
3552	6312		6312
3553	7300		CLA CLL
3554	5650		JMP I GRID
3555	0035	GSS,	0035
3556	0036	RSS,	0036
3557	6570	M648,	6570
3560	0154	K108,	0154
3561	0000	KØ,	0000
3562	0002	K2,	0002
3563	7774	M4,	7774
3564	7765	M11,	7765
3565	0000	X,	0
3566	0000	Y,	0
3567	0000	M,	0
3570	0000	N,	0

mode. Then putting up first M540 and then K480 and going to the PLOT subroutine (discussed below) sets the ARDS beam at the upper left corner of the screen. Lines 2663 through 2667 put the ARDS into long vector mode. The ARDS is given the projections of the vector on the x and y axes and draws a line of that length from the point previously set. So giving it 0 and M1020 and then K1020 and 0 means it draws first a y and then an x axis.

The program arrives at the subroutine PLOT with an argument character (coordinate) in the accumulator. This is then operated on to recast it in the form accepted by the ARDS, as described in the ARDS operating manual, page 4-10. Here we take as an example the coordinate M540 which sets a point at the extreme left of the screen. Line 2731 checks for a negative argument. M540, which is 6744 in octal or 110 111 100 100 in binary, is negative. So it is complemented, producing 001 000 011 100, the last ten bits of which (bits 10 through 1) add up to 540. Then adding 4001 puts the negative sign in bit 12, and ensures that the complement of 7777 is 1 rather than 0. The sum is stored in TEMP. The left rotation i line 2737 puts the sign bit in the link. Then retrieving the argument from TEMP, using the AND command with MASK37 leaves the last five bits (bits 1-5, the least significant). Another left rotation puts the sign in bit 1, and adding 0100 puts a 1 in bit 7, signifying that this is an argument character. At this point this first argument character

is in correct form to be given to the ARDS for plotting through the subroutine OAT. Taking the argument out of TEMP again, five right rotations and the use of MASK37 give the other five digits. After adding 0100 again this too is output through OAT.

In tape 4.7, the subroutines FFIX and FLOT are analagous to the decimal-binary conversion routines of the Floating Point Package, DECON and DECONV.

In tape 5, the subroutine DRAW plots the data points by the method already discussed. It operates in long vector mode, where a point is the shortest possible vector of length 1,1. Also reproduced here are modifications of tapes 4.5 and 4,7 which draw a grid along with the axes.

Having discussed the machine language programs which produce lineshape data, we now turn to the FOCAL programs used in processing that data. An example of the treatment of data tapes to produce an averaged absorption lineshape is given in Section I C. In following pages we give a listing of the FOCAL program Alpha Reader used to do that, and begin this portion of the appendix with some comments on the functions of various sections.

Sections 2, 3, and 4 form a loop which adds in tapes, storing the data points in the array SUM. In section 7 these ratios are operated on (in line 7.21) to obtain absorbances. The initial baseline and its slope are estimated from values in the wings of the line or from recent vacuum baselines, and

Alpha Reader Program

```

01.10 ERASE
01.90 A "HOW MANY POINTS ARE YOU CONSIDERING ?",MAX,!

02.05 A "DO YOU WISH TO ADD ANOTHER TAPE ?",AN,!
02.10 IF (AN-OYES)7.01,3.01,7.01

03.01 SET N = N+1
03.05 A "HOW MANY POINTS DO YOU WISH TO THROW AWAY ?",TA,!
03.06 IF (TA)3.50,3.7,3.5
03.50 FOR I=1,TA; DO 3.6
03.51 GT 3.7
03.60 *; ASK X;*
03.70 FOR I=1,MAX; DO 4.05
03.71 GT 2.05

04.05 *;A X;A Y;*;S SUM(I)=SUM(I)+(X+Y)/2

05.05 F I=1,MAX; IF (SUM(I))5.10,5.10,5.20
05.10 SET SUM(I)=0
05.20

07.01 A !, "BASELINE ? ",M,!!
07.02 A "SLOPE? ",SL,!!
07.03 A "END LINE? ",EL,!!
07.05 T " I ALPHA",!!
07.10 F I=1,EL,MAX; D 7.20; T !
07.12 A !!!!!"WANT A * PL0T? ",ANS,!
07.13 IF (ANS-OYES)7.14,8.01,7.14
07.14 A !!!!!"WANT AN XY PL0T? ",ANT,!
07.15 IF (ANT-OYES)12.01,9.05,12.01
07.20 F J=1,EL; D 7.21; D 7.22;
07.21 S SUM(I+J-1)=1.8519*FL0G(SUM(I+J-1)/N*M); S M=M+SL
07.22 T %4.0 I+J-1, %5.03 SUM(I+J-1)

08.01 A "POINTS PER * ? ",SP,!
08.02 A "PEAK VALUE? ",PV,!
08.03 A "MAXIMUM SPACES? ",MS,!!
08.04 S SMX=SP*PV/MS
08.10 F I=1,SP,MAX; S XX=0; T "*" ,!; D 8.11; D 8.12
08.11 F K=1,SP; SET XX=XX+SUM(I+K-1)
08.12 FOR J=0,XX/SMX; T " "
08.30 GT 7.14

09.05 A "XF? ",XF,!
09.06 A "YF? ",YF,!
09.07 A "INX? ",INX,!
09.08 A "IMY? ",IMY,!
09.09 F I=2,MAX; D 9.11; D 9.13
09.10 GT 9.20
09.11 F IX=0,INX; D 9.12
09.12 S Z=FDIS(XF*(I-1+(IX/INX)),YF*SUM(I-1));
09.13 F IY=0,SG/(FABS(SUM(I-1)-SUM(I))+.01),IMY;D 9.14
09.14 S Z=FDIS(XF*I,YF*(SUM(I-1)+IY*((SUM(I)-SUM(I-1))/IMY)))
09.16 A "ANOTHER XY? ",RAT,!
09.18 IF (RAT-OYES)9.20,9.05,9.20
09.20 A "WANT A L0RENTZIAN FIT? ",ANR,!
09.21 IF (ANR-OYES)9.22,12.02,9.22
09.22 QUIT
09.30 SET L=FDIS(0,0)

```

```

10.10 S Z=FDIS(O,YF*SJM(1))
10.20 F I=1,1000;C
10.30 G 9.09

12.02 A "YF? ",YF,!
12.04 A "HOW MANY PKS? ",L,!
12.05 A "NUMBER OF DIVISIONS? ",MX,!
12.06 A "SC? ",SC
12.20 F K=1,L; DØ 12.3
12.21 GT 12.5
12.30 T X1, !"FOR PEAK ",K; GØTØ 12.32
12.32 A !"LOCATION ",W(K)," ABSORBANCE ",R(K)," WIDTH ",P(K)
12.50 T ! "GIVE THE INITIAL AND FINAL POINTS, AND INCREMENT YØ!" !
12.60 A "WISH EVALUATED. ",M,N,J
12.90 T !!!" H W 100*A"!!

13.10 F H=1,MX; D 13.20; D 13.25
13.15 GT 13.30
13.20 F W=M+(H-1)*(N-M)/MX,J,M+H*(N-M)/MX; D 14
13.25 T X3,H+1," ",%6.03,(W-W(1))*SC," ",%5.03,100*T,!
13.30 QUIT

14.10 S T=0
14.20 F K=1,L; D 15
14.30 S Z=FDIS(W,YF*T*100)

15.10 SET S=R(K)/((W-W(K))*SC/P(K))^2+1)
15.20 SET T=T+S;R

16.30 S SJM(I)=1.8519*FLØG(FEXP(SJM(I)/1.8519)*MI/MT)
16.40 S MI=MI+SL
16.50 S MT=MT+ST

29.10 S Z=FNEW(2);T SJM(I);S Z=FNEW(3,1);S Z=FNEW(1)

31.10 S Z=FNEW(2);S Z=FNEW(3,300)
31.20 W A
31.30 S Z=FNEW(3,300); S Z=FNEW(1)
*
```


SHORT ALPHA READER

```

03.10 F I=1,MAX; IF (SUM(I))3.30,3.30,3.50
03.30 S SUM(I)=0
03.50

04.05 F I=1,MAX; *A X;A Y;*; S SUM(I)=SUM(I)+(X+Y)/2

07.10 F I=1,EL,MAX; D 7.20; T !
07.20 F J=1,EL; D 7.21; D 7.22
07.21 S SUM(I+J-1)=1.8519*FL2G(SUM(I+J-1)/N*M); S M=M+SL
07.22 T %4.0 I+J-1,%5.03 SUM(I+J-1)

09.09 F I=2,MAX; D 9.11; D 9.13
09.11 F IX=0,INX; D 9.12
09.12 S Z=FDIS(XF*(I-1+(IX/INX)),YF*SUM(I+SH-1))
09.13 F IY=0,IMY; D 9.14
09.14 S Z=FDIS(XF*I,YF*(SUM(I+SH-1)+IY*((SUM(I+SH)-SUM(I+SH-1))/IMY)))

16.30 S SUM(I)=1.8519*FL2G(FEXP(SUM(I)/1.8519)*MI/MT)
16.40 S MI=MI+SL
16.50 S MT=MT+ST

30.10 S Z=FNEW(2); T SUM(I); S Z=FNEW(3,1); S Z=FNEW(1)

31.10 S Z=FNEW(2)
31.20 W A
31.30 S Z=FNEW(1)
*
```

then adjusted to best fit a Lorentzian. This section also prints out each point as it is calculated, and the value given the "END LINE?" question specifies how many points will be printed on a line before a carriage return- usually 5. This printing out is useful in finding reader errors before plotting, in finding the peak value for scaling, and in checking for negative values in the wings. These last are unavoidable when fitting a baseline through a noisy zero absorption trace. Yet they cannot be plotted, since the x-y recorder only accepts positive values. Once the final baseline is chosen, section 5 is used to set these small negative values to zero.

Section 8 is a simple plotting routine for the teletype, helpful in superimposing tapes with no original chart trace since the data points are easy to count.

Section 9 plots the lineshape on the x-y recorder, given the scaling factors XF and YF which convert data point number and absorbance amplitude into x-y recorder points. The granularities INX and IMY are the number of divisions in traveling from one point to the next, used to reduce pen overshoot. In this particular version, the y plotting loop 9.14 contains an automatically varying step size, where SG should be set to between .01 and .02. Section 10 positions the pen before x-y plotting begins.

Sections 12 through 15 calculate Lorentzian lineshapes and plot them on the x-y recorder for comparison with experiment. The number of divisions, MX, determines how many

points on the Lorentzian are typed out. The calculation of the scaling factor SC is discussed in Section I C. The location of the Kth line $W(K)$ is measured in chart recorder points, as are the initial and final points and increment to be evaluated, M,N, and J. The half width at half maximum $P(K)$ is measured in cm^{-1} . The peak absorbance $R(K)$ is input in true absorbance units, cm^{-1} , although in section 7 the amplitudes calculated and output are 100 times larger.

Section 16 allows changes in baseline and slope for a set of data already operated on. Section 29 outputs an averaged line onto punched tape.

An elaborate program such as that described above allows room for only a little over 500 data points. To process longer scans, a short version of the Alpha Reader program is used, in which the variables must be defined by equations. This is listed following the longer program.

We also give a listing of the deconvolution program, a modification of one used by J. Logan and C. Mims. Its dialog has been written out in detail so that its operation should be self-explanatory.

DECORVOLUTION PROGRAM

```

01.04 S C0=0
01.05 A "NUMBER OF ITERATIONS? ",CN,!!
01.06 A "SCALING FACTOR? ",SB,!
01.20 A "MAXIMUM POINTS (BINS) OF CORV ",TC
01.22 F I=1,TC; D 1.24
01.23 G 1.25
01.24 S H(I)=0; S M(I)=0; S N(I)=0
01.25 T !
01.26 A "DATA ON TAPE? ",C,!
01.28 I (C-OYES) 1.30,5.0,1.30
01.30 A "LORENTZIAN? ",D,!
01.31 I (D-OYES) 1.40,1.36,1.40
01.32 F I=1,TC; D 5.0
01.34 G 1.49
01.36 F I=1,TC; D 7.0
01.38 G 1.49
01.40 F I=1,TC; D 1.48
01.44 G 1.49
01.48 T "H(",%3.00,I,")= ";A H(I)
01.49 T %6.02 !," I NORM CORV",!!
01.50 F I=1,TC;D 1.58
01.54 G 1.59
01.58 T %3.0,I, %6.03 H(I),!; S M(I)=H(I)
01.59 T !
01.60 A "INSTRUMENT FUNCTION WIDTH (BINS) ",NS,!
01.64 F I=-((NS-1)/2,1,(NS+1)/2-1; D 1.70
01.66 G 1.80
01.70 *; A SH(I); *;
01.80 S Z=FNEW(1)
01.82 IF (C0-CN+2) 1.90,1.84,1.84
01.84 T !!,"BIN FREQ DECORV RECORV",!
01.90 F I=1,TC; D 2.0
01.94 G 4.04

02.10 S X=0; F J=-((NS-1)/2,1,(NS+1)/2-1; D 3
02.20 S N(I)=M(I)*H(I)/X
02.25 IF (C0-CN+2) 2.35,2.30,2.30
02.30 T !,%2.00,I,%6.03,(1-W(1))*SC,N(I),X
02.35

03.10 S K=I+J; I (K) 3.2,3.2,3.25
03.20 S K=K+TC; G 3.30
03.25 I (K-TC) 3.3,3.30,3.28
03.28 S K=K-TC
03.30 S X=X+M(K)*SH(J)

04.04 S C0=C0+1
04.05 IF (C0-CN)4.20,4.10,4.10
04.10 A !!,"MORE ITERATIONS? ",CM,!
04.12 IF (CM-ON0) 4.14,4.30,4.14
04.14 S CN=CN+CM; GT 4.20
04.20 F A=1,TC; D 4.26
04.22 G 1.82
04.26 S M(A)=N(A); S N(A)=0
04.30 A !!,"PLOT ORIG CORVOL? ",Q; I (Q-OYES)9.16,9.05,9.16
04.40 T !
04.41 Q
04.50 S Z=FNEW(2); F I=1,TC; T N(I),!,0,!
04.55 S Z=FNEW(1)
04.60 Q

```

```

05.10 *; A H(I),E; *; I (H(I))5.3
05.20 S SB=SB+H(I); R
05.30 S H(I)=0

06.01 F I=1,40; T !,%2.00,I,%6.02,H(I)

07.04 A "HOW MANY PKS? ",L;!
07.06 A "SC? ",SC
07.20 F K=1,L; D 7.3
07.21 G 7.6
07.30 T %1,!"FOR PEAK ",K; G 7.32
07.32 A !"LÖCATIÖN ",W(K)," ABSÖRBANCE ",R(K)," WIDTH ",P(K)
07.60 F I=1,TC; D 7.64
07.62 R
07.64 F K=1,L; D 7.66
07.66 S H(I)=H(I)+R(K)/(((I-W(K))*SC/P(K))+2+1)

09.05 A "XF? ",XF,!,"YF? ",YF,!
09.06 A "INX? ",INX,!,"IMY? ",IMY,!
09.08 F J=1,200; S Z=FDIS(0,YF*H(I))
09.09 F I=2,TC; D 9.11; D 9.13
09.10 G 9.16
09.11 F IX=0,INX; D 9.12
09.12 S Z=FDIS(XF*(I-1+(IX/INX)),YF*H(I-1));
09.13 F IY=0,IMY; D 9.14
09.14 S Z=FDIS(XF*I,YF*(H(I-1)+IY*((H(I)-H(I-1))/IMY)))
09.16 A !,"PLÖT DECÖNV? ",RT; I (RT-ÖYES)9.50,9.18,9.50
09.18 A !,"PEAK RATIO? ",RA; S YF=YF/RA
09.19 F J=1,200; S Z=FDIS(0,YF*N(I))
09.20 F I=2,TC; D 9.24; D 9.26
09.22 G 9.50
09.24 F IX=0,INX; D 9.25
09.25 S Z=FDIS(XF*(I-1+(IX/INX)),YF*N(I-1));
09.26 F IY=0,IMY; D 9.27
09.27 S Z=FDIS(XF*I,YF*(N(I-1)+IY*((N(I)-N(I-1))/IMY)))
09.50 A !,"PLÖT INST FÖNCT? ",TR; I (TR-ÖYES)9.8,9.51,9.8
09.51 A !,"PEAK RATIO? ",RB; S YF=YF/RB
09.52 F J=1,200; S Z=FDIS(0,SH(I))
09.53 F I=-((NS-1)/2,1,(NS+1)/2-1; D 9.56; D 9.58
09.54 G 9.8
09.56 F IX=0,INX; D 9.57;
09.57 S Z=FDIS(XF*(I+(NS-1)/2+(IX/INX)),YF*SH(I-1))
09.58 F IY=0,IMY; D 9.59;
09.59 S Z=FDIS(XF*(I+(NS+1)/2),YF*(SH(I-1)+IY*((SH(I)-SH(I-1))/IMY)))
09.80 Q

31.10 S Z=FNEW(2); S Z=FNEW(3,300)
31.20 W A
31.30 S Z=FNEW(3,300); S Z=FNEW(1)
*
```

Appendix E : The Tunable Diode Laser

This appendix on the tunable diode laser has two objectives. One is to show by example that though the diode laser has its own very different characteristics as a spectroscopic tool compared with those of the parametric oscillator discussed in Section I C, it also has possibly serious problems in the measurement of its frequency and amplitude. The other object is to present, as measures of performance, some very preliminary lineshape data for ammonia lines, both for Doppler broadening and pressure broadening by ammonia and air. These indicate that with more measurements and some improvement in technique, interesting experiments can be done.

The theory and operation of the Arthur D. Little diode laser used in these studies has already been described in detail in Reference 127. Additional general information on diode lasers can be found in References 128-130. We will simply repeat here that the laser output, in the 4.6 and 10.6 micron regions, is very weak, extremely narrow in frequency, and is easily and continuously tunable by changing the current passing through the diode.

However, a major problem is the existence of several laser modes at one current, as shown in Figures 49 through 52. Figures 49-51 show the diode output at several current settings as a function of monochromator setting and so frequency. Data from these measurements and from line overlaps went into making

Figure 49: Scanning monochromator at constant diode laser current for the 4.6 micron diode. (Since the monochromator is scanned manually the frequency scale is actually irregular.) One can follow the progress of individual modes toward higher frequency with increasing current. One can also compare this set of scans with one taken an hour later, shown in Figures 50 and 51. Comparison at -1.55 A or -1.575 A shows similar mode structure but different intensities.

Figure 50: More diode laser monochromator scans, taken soon after Figure 49.

Figure 51: More diode laser monochromator scans- a continuation of Figure 50.

Figure 49

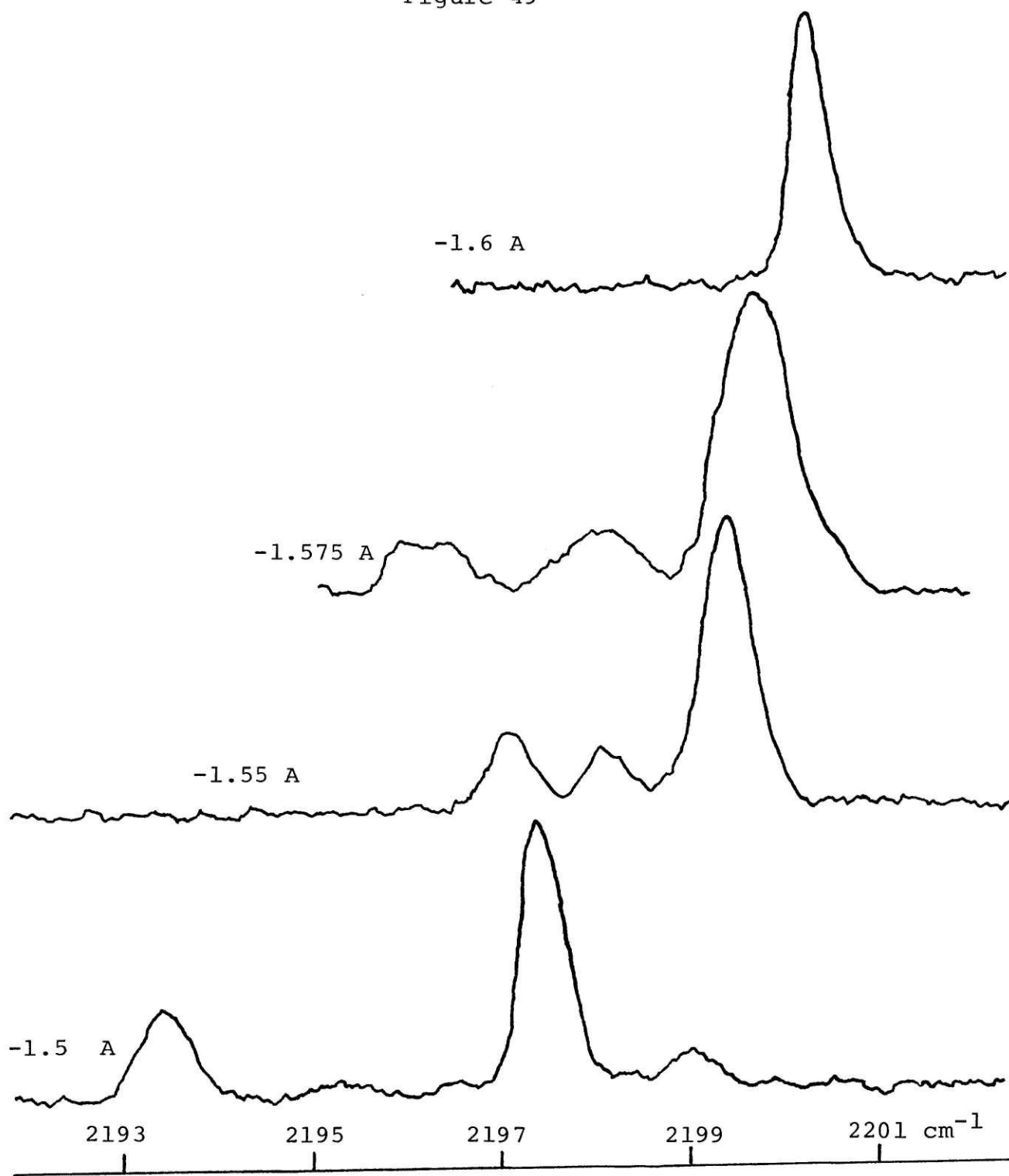


Figure 50

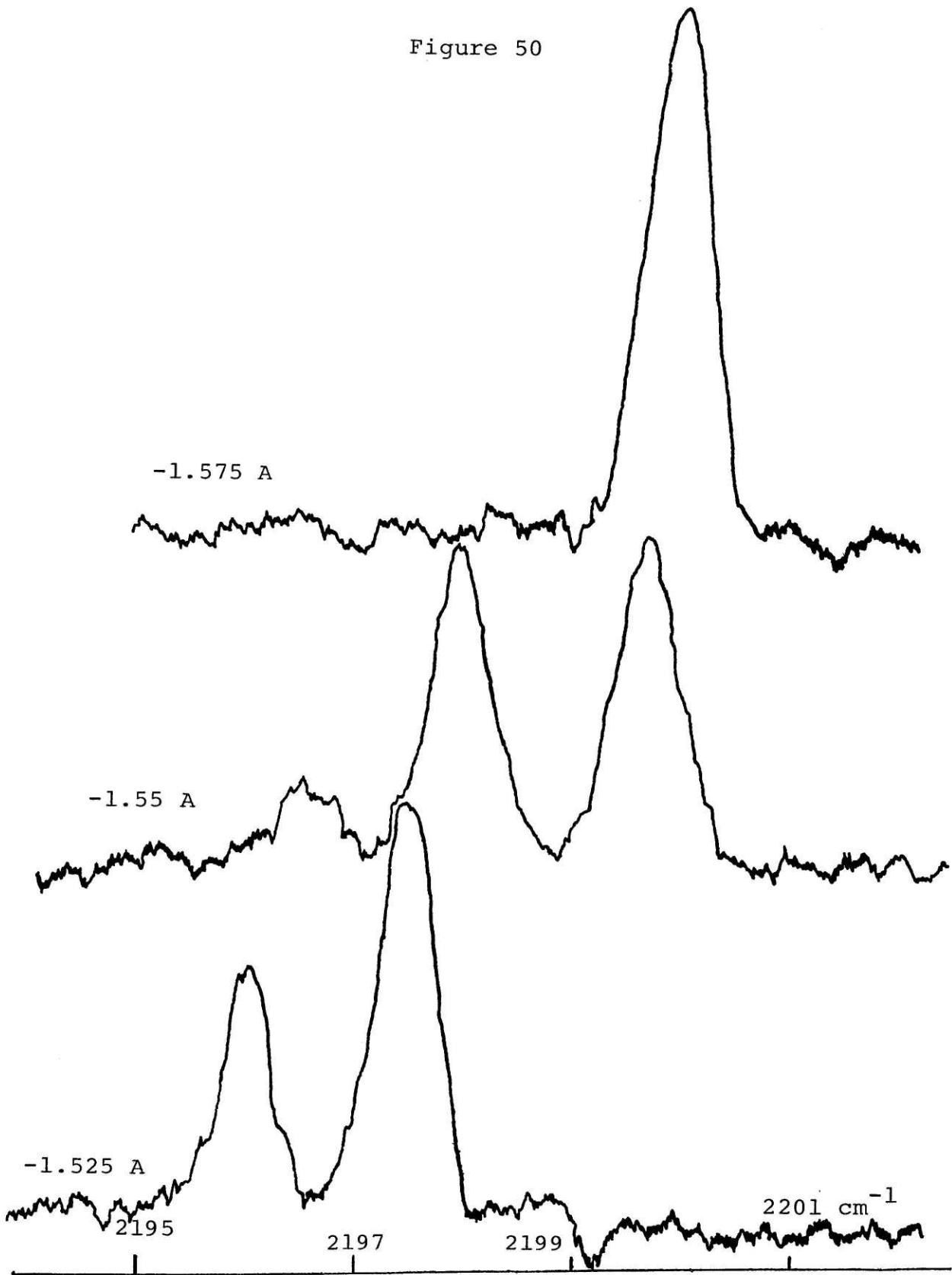


Figure 51

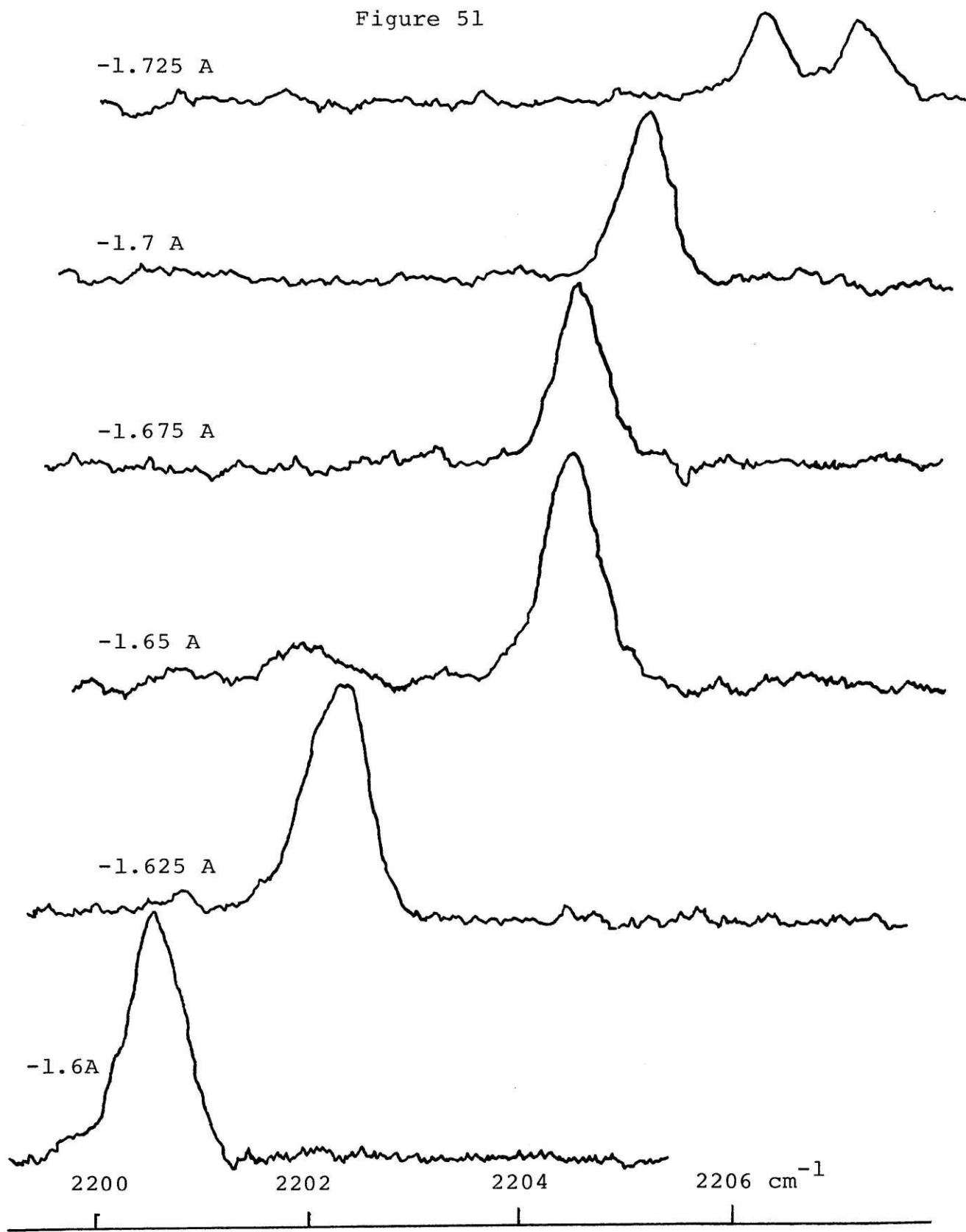


Figure 52: Graph of frequency of output of the 4.6 micron diode laser as a function of diode current. (Since diode characteristics change over time, the graph is no longer accurate.) The dots are diode laser output observed a fixed frequency by scanning the monochromator. The diagonal lines represent an attempt to organize the points into modes. The solid horizontal lines show positions of CO absorption lines, the long and short dashed lines the positions of DCI³⁵ and DCI³⁷ lines, and the two dot-dash lines are HI lines. Most overlaps of the diode laser modes with absorption lines predicted by this graph were actually observed. The modes marked A, B, and C are discussed in the caption to Figure 53.

260

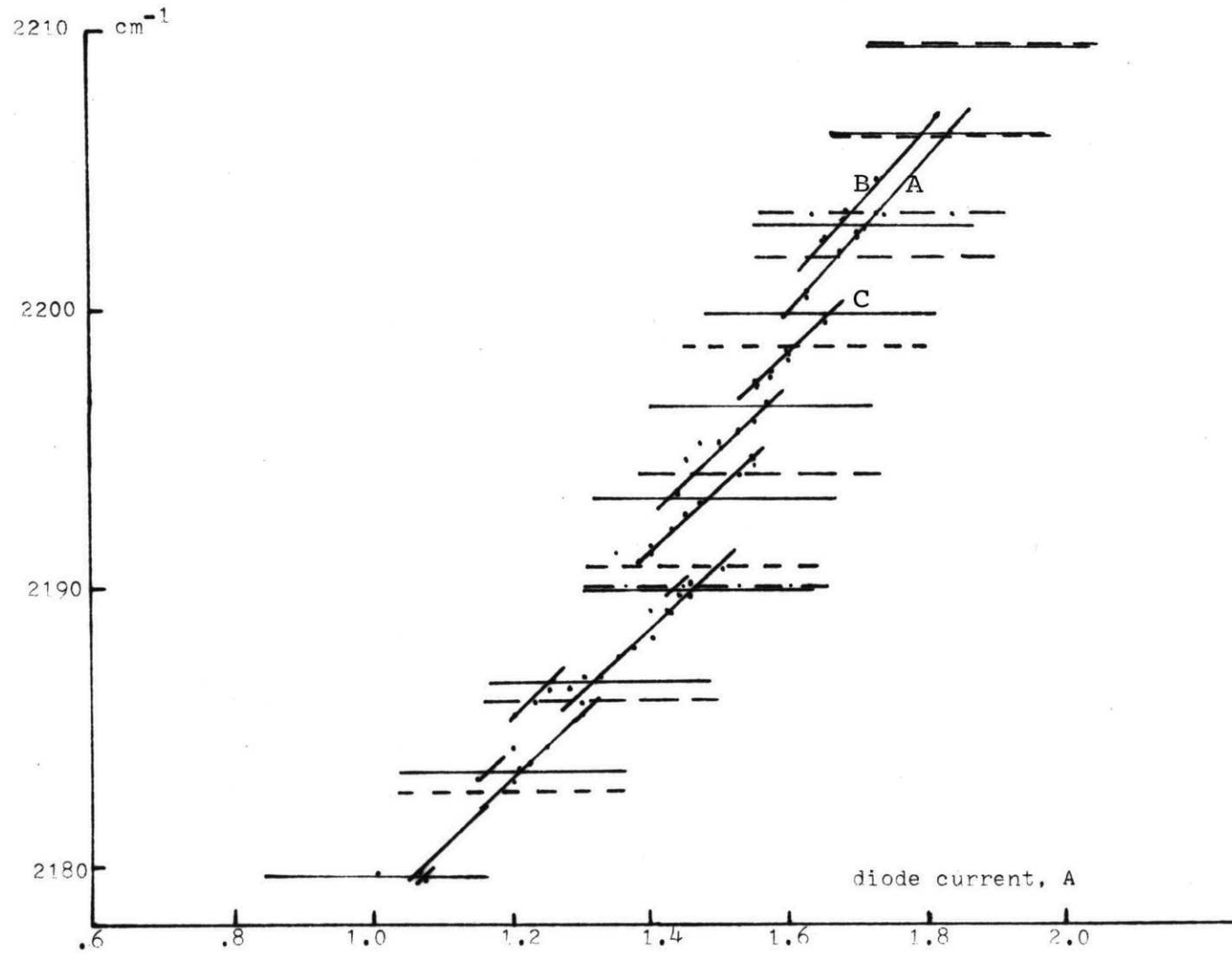


Figure 52

Figure 52, showing output in the 4.6 micron region as a function of current and making an attempt to sort it into modes. Also Figure 53 gives an example of overlaps with absorption lines, in which some lines appear more than once because of parallel modes.

Next we exhibit some results to show that the diode laser can give plausible results for low density linewidths. For ammonia at room temperature, the Doppler width is 42 MHz.¹³¹ Figure 54 shows a number of lines at ammonia pressures of 100 to 560 mtorr, most of which are around 47 MHz wide, while the narrowest is 41 MHz.

From references 132 and 133, common self-broadened microwave linewidths are between 20 and 25 MHz/torr. Dividing the increase in ammonia pressure into the increase in linewidth for the lines in Figure 55 gives values from 15 to 21 MHz/torr. (Figure 56 shows two of those lines and an etalon scan, which must always be used to set the frequency scale.)

Finally, References 132-134 give nitrogen broadened microwave linewidths of 3.1 to 5.1 MHz/torr for the 1,1 to 12,12 inversions, while oxygen broadened lines are smaller. Figure 57 shows one of a set of traces taken with around 1 torr NH_3 and one of several with 10.9 torr of added air. The difference between the averages gives 2.7 MHz/torr. (Another line studied gave 1.8 MHz/torr.)

These linewidths are measured without converting to absorbance, and with only an estimate of where the true base-

Figure 53: A series of diode laser traces showing overlaps with absorption lines of CO, HI, and DC1. The monochromator was at 934 drum setting, corresponding to 2204 cm^{-1} , and had 1 mm entrance and exit slits. The lock-in amplifier was set at 1 mV sensitivity and 1 second time constant. The diode current scan rate was .0005 A/sec. In the lowest trace, involving CO lines and the germanium etalon, the etalon was deliberately misaligned so the fringes would not obscure the lines. Referring to Figure 52, a possible interpretation is that the overlaps are first mode C with the CO line at 2200 cm^{-1} , then mode B with the 2203 cm^{-1} CO line, mode A with the 2202 cm^{-1} DC1 line, mode B with the HI line, mode A with the 2203 cm^{-1} CO line and then the HI line, and finally mode B with the CO line around 2206 cm^{-1} . This interpretation assumes that mode B had a somewhat steeper tuning rate than that drawn (so that the last CO overlap will appear close to that of mode A with HI) and that mode B did not extend down far enough on that day to overlap the 2202 cm^{-1} DC1 line.

Figure 53

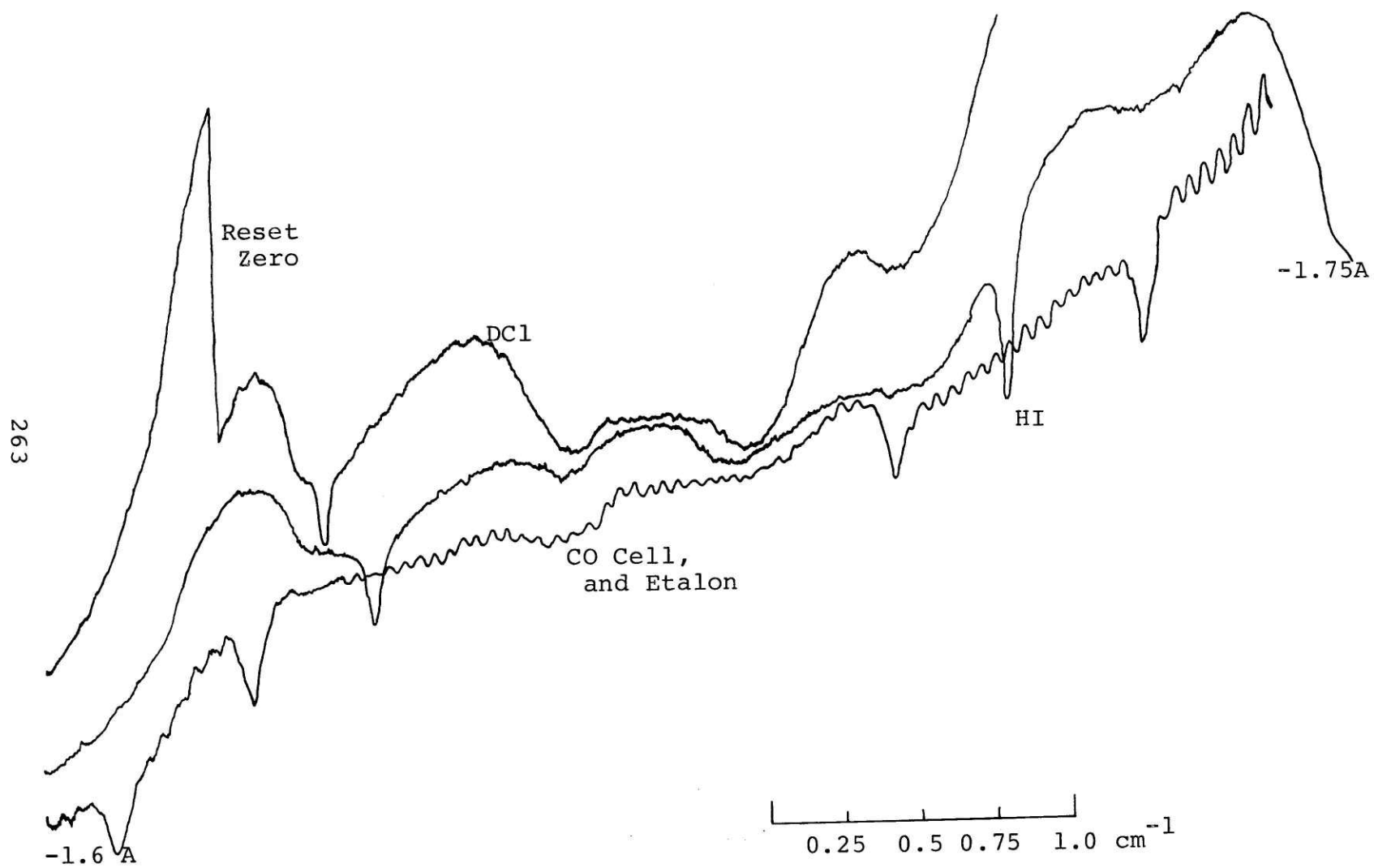


Figure 54: From top to bottom, traces are of an absorption line due to 107, 195, 288, 400, and 560 mtorr of ammonia, showing the Doppler limit.

Figure 55: From top to bottom, traces are of an absorption line due to 2.3, 4.6, 5.8, 7.9, 9.2, and 11.5 torr of pure ammonia, illustrating self broadening.

Figure 56: The same ammonia lines at 2.3 and 4.6 torr as shown in Figure 55, and a trace due to the germanium etalon, which must always be used to set the frequency scale. The distance between etalon peaks is 0.05 cm^{-1} .

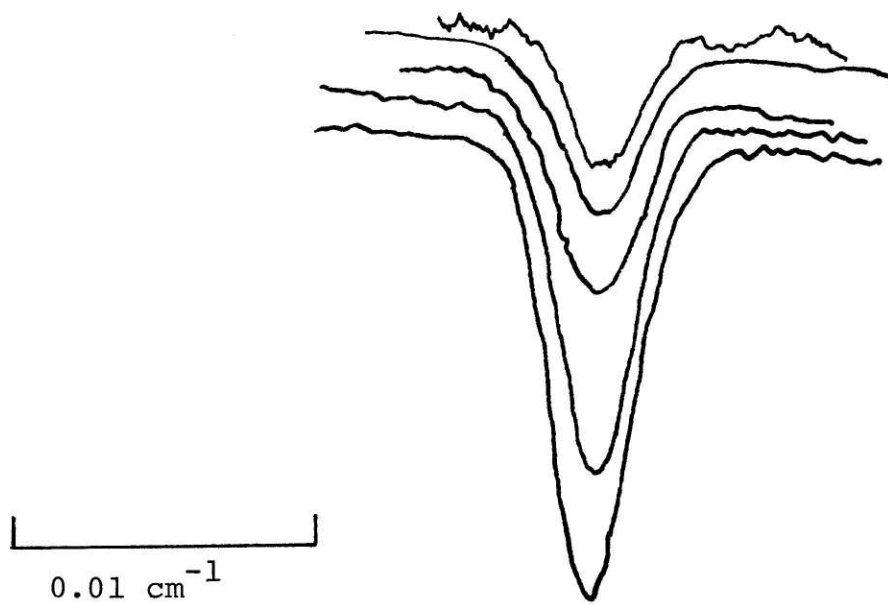


Figure 54

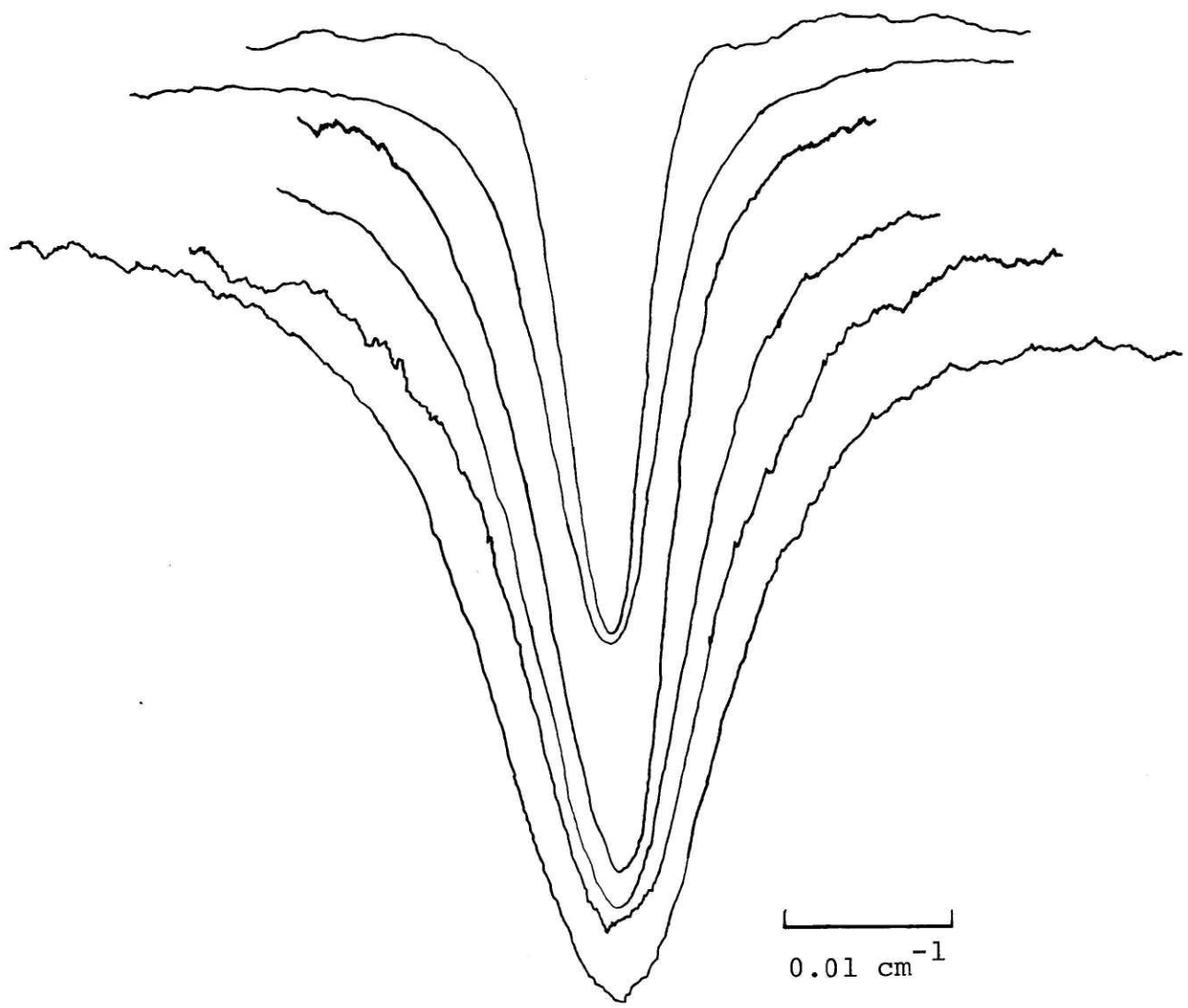
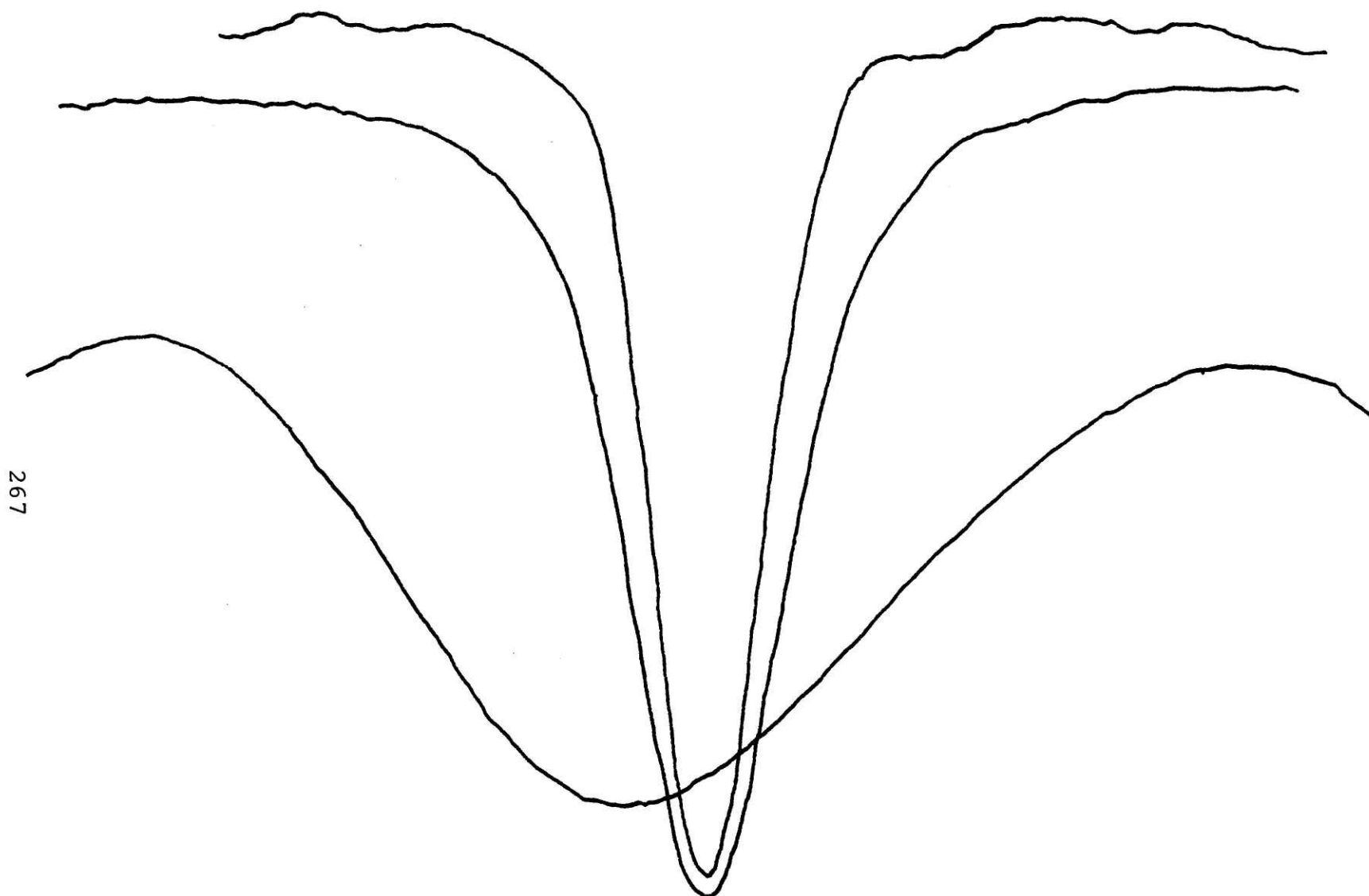


Figure 55

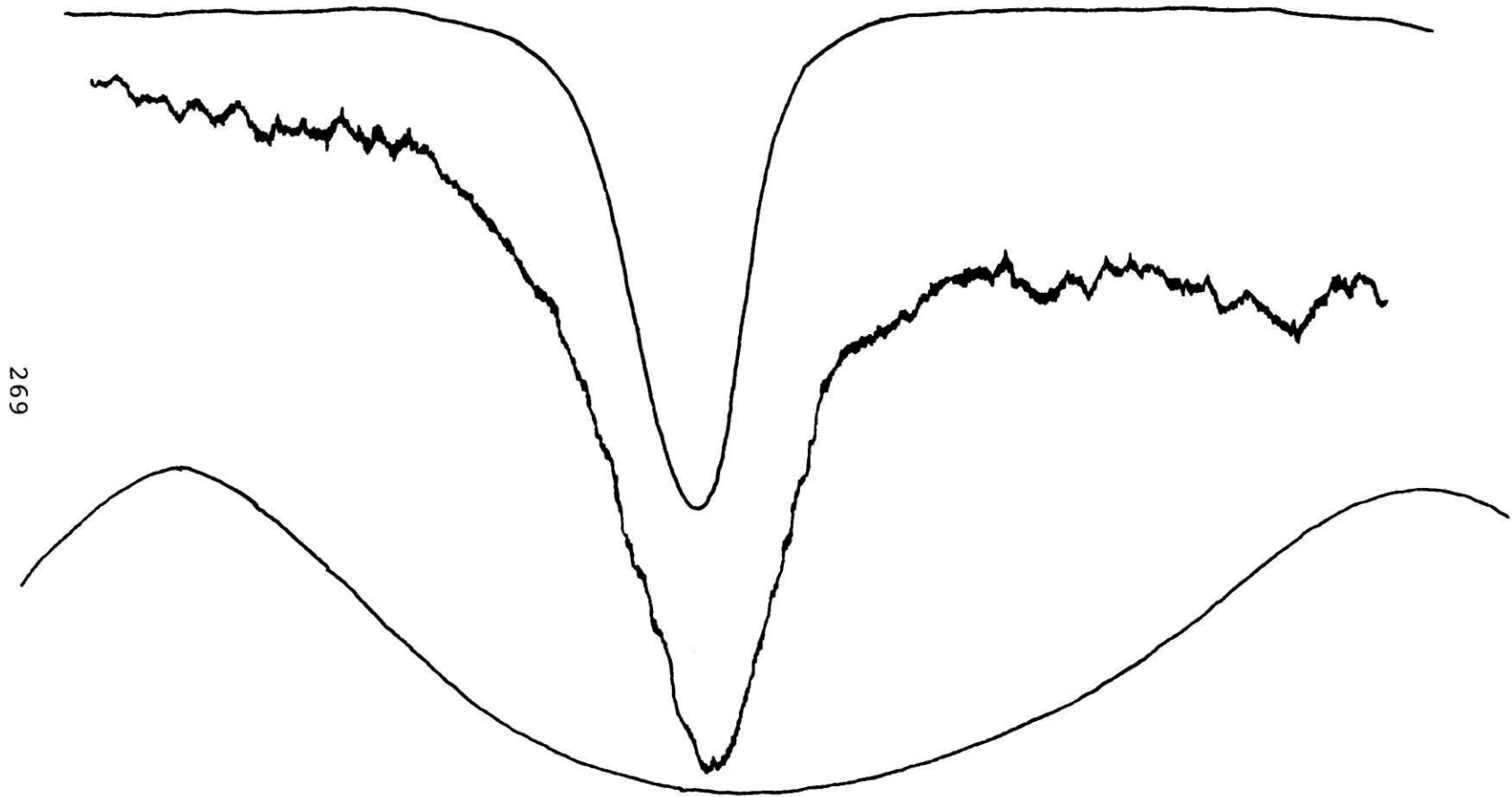


267

Figure 56

Figure 57: The upper trace is an absorption line due to around 1 torr of ammonia only, while the lower is the same line broadened by 10.9 torr of added air. The upper trace was taken with the Cu:Ge detector, the lower with the HgCdTe detector, which here was much noisier. The difference was not always so striking, and the fact that the HgCdTe detector operates at liquid nitrogen temperature rather than liquid helium makes it more attractive to operate.

Figure 57



line is, so the 10 to 20 per cent scatter in repeated linewidth measurements is not unexpected. Uncertainties in pressure measurement could contribute to twenty per cent differences observed in measuring identical samples on different days. But there are other disturbing observations. One is shown in Figure 58. The broader trace is one of five measurements on 150 mtorr of NH_3 alone, all giving 62 MHz to within a few per cent. The lower trace is one of five more taken with .77 torr of added air, giving an average width of only 51 MHz. These experiments were done in order to find just such an effect, which could be due to Dicke narrowing of the Doppler linewidth.¹³⁵⁻¹³⁶ But this seems to be the wrong pressure regime for Dicke narrowing, and subsequent attempts under similar conditions could never uncover any more clear evidence for the effect.

Even if the tuning rate stability and spectral purity of the tunable diode laser were satisfactory, there are problems with amplitude measurement. Since the tuning range of the diode laser will obviously not allow choosing a baseline by looking at the absorption far in the wings of the lines, intensity measurement must also be accurate and reproducible. In practice, this means a double beam setup must be used, because although over short periods of time the amplitude may be fairly reproducible, over the time needed to record absorption traces and evacuate the cell the single beam intensity can change by 20 and 30 per cent. Yet considering

Figure 58: The lower trace was taken with 150 mtorr of ammonia only, while the upper (and narrower) trace had .77 torr added air.

Figure 59: Two successive scans of the same 100 mtorr pure ammonia line, showing irreproducibility found when using the diode laser in a single beam configuration.

Figure 58

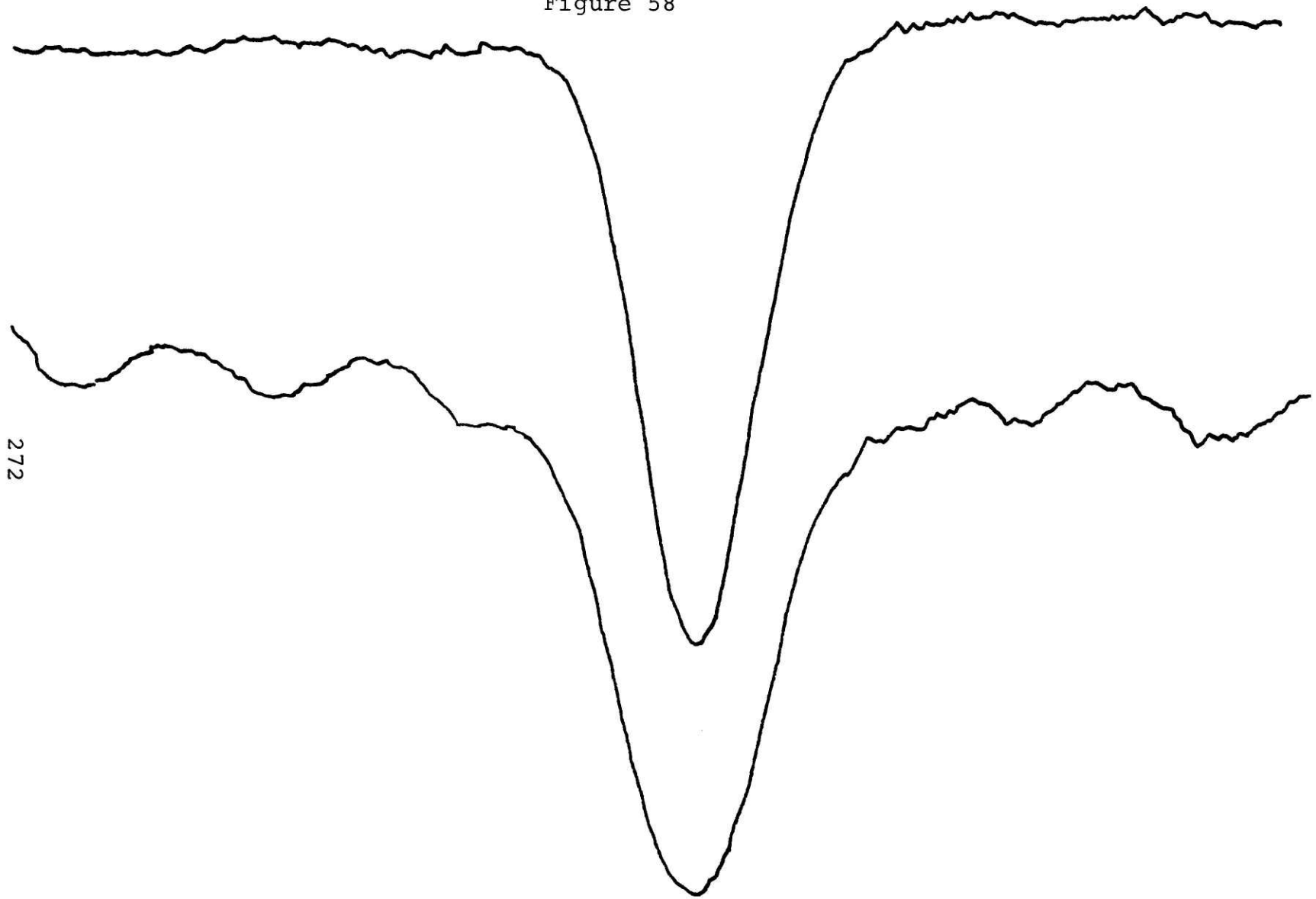
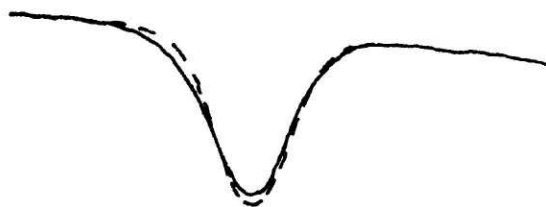


Figure 59



the low output power of the diode laser, a double beam setup would be very difficult to achieve. So even if one diode laser mode could be tuned without interference over several wavenumbers, obtaining lineshapes and linewidths at high pressures would be a difficult task. (Figure 59 is another example of non-reproducibility.)

Yet there is a type of higher order density effect which could be studied using the diode laser, with its high signal-to-noise ratio and narrow bandwidth over short tuning ranges. Indeed, perhaps this proposed experiment could be done in a single beam arrangement, making it easier to set up. As mentioned in Section II A, the logarithmic density dependence of the lineshape is expected to occur only close to the zero density resonance frequency, causing some sort of irregularity on the order of 0.1 cm^{-1} wide. Since the line shifts with pressure, the above point would be rather far out on one wing. So one would look for some lump or dip in the high pressure absorption scan of one wing which did not appear in the other. The diode laser, with its sensitivity to small spectral features might still prove useful in setting an upper limit on possible logarithmic terms.

Appendix F : Relation of the Binary Collision Operator to Widths and Shifts

In the following we discuss the scattering tetradic T as we define it here in relation to the T operators used by Fano¹³⁷, T_F , and Albers³⁷, T_A . Then we will give examples of how the T operator is related to Lorentzian widths and shifts.

The following discussion is given in order to arrive at a definition for the width and shift operator $\mathcal{L}(\omega) = \text{Tr}_2 T_{12} \tilde{\rho}(2)$ such that in the denominator of the lineshape expression it appears with a positive sign with respect to $i\omega$. As a preliminary we note that Equation (3) of Fano for the absorption coefficient is

$$\text{Re} \int_0^{\infty} e^{i\omega t} \text{Tr}(\rho \rho(t) \rho) dt$$

while Equations (3.1) and (3.2) of Albers give

$$\text{Re} \int_0^{\infty} \text{Tr} \rho e^{-i\omega t} e^{-\lambda t} \rho \rho dt$$

so the ω of Fano is $-\omega$ in Albers. Therefore Equation (40) of Fano becomes

$$(91) \quad T_F = K' + K' \frac{1}{-\omega - \omega_0} T_F = K' - K' \frac{1}{\omega + \omega_0} T_F$$

To get appropriate definitions of the width and shift we will want $T = iT_F$. But if we substitute this ($T = iT_F$) into Equation (91) we obtain not Equation (2.18) of Albers³⁷,

$$T_A = -iK' + iK' G_0 T_A$$

but rather $-iT = K' + iK' \frac{1}{i\omega + \omega_0} iT = K' - K' G_0 T$ or

$$(92) \quad T = iK' - iK' G_0 T$$

which we take as our definition.

We now quickly run through the binary collision expansion and resummation process to show that Equation (92) gives the desired result. With α denoting a pair of particles, $T_\alpha = iK_\alpha - iK'_\alpha G_0 T_\alpha$ says

$$T_\alpha G_0 = \frac{iK'_\alpha G_0}{(1 + iK'_\alpha G_0)} = iK'_\alpha G_\alpha,$$

and by $\frac{1}{A+B} = \frac{1}{A} - \frac{1}{A} B \frac{1}{A+B}$,

$$(iK_0 + iK'_\alpha)^{-1} = \frac{1}{iK_0} - \frac{1}{iK_0} iK'_\alpha \frac{1}{iK_0 + iK'_\alpha}$$

$$= G_0 - G_0 iK'_\alpha G_\alpha = G_0 + G_0 T_\alpha G_0$$

So we can write $G = G_0 - \sum_\alpha G_0 iK'_\alpha G_\alpha$ and

$$G = G_R - \sum_{\beta \text{ not } R} G_R iK'_\beta G_\beta = G_R - \sum_{\beta \text{ not } R} G_0 T_\beta G_0$$

and use the second equation to iterate the first, obtaining

$$G = G_0 - \sum_\alpha G_0 T_\alpha G_0 + \sum_{\alpha \text{ not } \beta} G_0 T_\alpha G_0 T_\beta G_0 + \dots$$

So eventually after averaging we get

$$\text{Tr } \rho (R(1) - R(1) \rho \mathcal{L}(1) R(1) + R(1) \rho^2 \mathcal{L}(1) R(1) \mathcal{L}(1) R(1) - \dots) \tilde{\rho}(1) \rho$$

where $R(1) = (\epsilon + i\omega + iK_{int}(1))^{-1}$ and resumming gives us

$$(93) \quad \text{Tr } \rho (i\omega + iK_{int}(1) + \rho \mathcal{L}(1))^{-1} \tilde{\rho} \rho$$

where the linewidth operator $\rho \mathcal{L}(1)$ does indeed appear with a positive sign.

If we use Equation (55) of Fano for the scattering tetradic we can obtain the analog of Equation (A.8) of Albers,³⁸ or of Equation (D.18) of Reference 39, (writing the volume normalization of the t matrices explicitly),

$$(94) \quad T_{abcd} \Rightarrow \frac{1}{V^2} (t_{ac}(E_b - \omega) \Delta_{bd} - t_{bd}^*(E_c + \omega) + i\pi \delta(E_a + \hbar\omega - E_c) t_{ac} \frac{1}{V^4} + t_{ac}^*(E_a) t_{bd}^*(E_d) + i\pi \delta(E_b - \hbar\omega - E_d) t_{ac} \frac{1}{V^4} + t_{bd}^*(E_b))$$

There are more terms in the expression for the T operator

given by Fano. In the discussion following his Equation (55) he explains that they describe transient, or duration of collision effects, and can be ignored in the impact approximation. Also in Appendix D of Reference 39 it is shown that this ignoring of terms not in Equation (94) corresponds to the $\vec{k} \rightarrow 0$ limit of $\frac{1}{\sqrt{2}} (\vec{p}_1 \vec{p}_2 \vec{p}'_1 \vec{p}'_2 \vec{p}''_1 \vec{p}''_2)$ where $\vec{k} = \vec{p}_1' - \vec{p}_1''$.

If we look at T_{abab} , and make the approximation $\omega = \omega_{ba}$ Equation (94) becomes

$$(95) \quad i \left(\frac{\gamma_{aa}}{\gamma^2} - \frac{\gamma_{bb}^*}{\gamma^2} + 2\pi i \delta(E_b - E_a) \frac{\gamma_{aa} \gamma_{bb}^*}{\gamma^4} \right)$$

We now want to look at the consequences of our definition of T on its relation to line widths and shifts. First the presence of the weighting factor $\tilde{\rho}_a$ or $\frac{e^{-\beta E_a}}{\sum_i e^{-\beta E_i}}$ in the lineshape expression tells us that in $L(abab)$ or $L_{ab} a$ is the initial state, and so in absorption it is the lower state. We want $\omega_{ba} = \frac{\epsilon_b - \epsilon_a}{\hbar}$ to be greater than zero, and if ϵ_a and ϵ_b are negative, we want $|\epsilon_a| > |\epsilon_b|$, or ϵ_a should indeed be the ground state energy. (In Anderson theory³¹ the frequency is also ω_{ξ_f} .)

The Anderson theory lineshift appearing in the Lorentzian (for instance in Equation (78) of Reference 138), $\gamma \gamma \delta_i$, is proportional to $V_i - V_f$, or $V_a - V_b$, and $\Delta \nu$, the experimentally observed shift is $-\gamma \gamma \delta_i \propto V_b - V_a$. So looking at the first Born approximation to Equation (94), $\text{Im } L \propto \text{Im} (i(\gamma_{aa} - \gamma_{bb}^*)) = \gamma_a - \gamma_b \propto \delta_i$. To check against Fano, since his ω is $-\omega$ of Albers, his Equation (1) has a perturbed frequency of $i\omega_{ba} - i\delta_{ba} - \omega_{ba}$ so

that his shift $d \propto \epsilon_i$ (and his Equation (57)) is $d \propto V_a - V_b$. Fano says that in $(\omega_F - \omega_{ab} - \langle M_c \rangle_{abab})^{-1}$ the shift $d = \text{Re} \langle M_c \rangle$. So by $-i\mathcal{L} = \langle M_c \rangle$, $d = \text{Im} \mathcal{L}$, so again $\text{Im} \mathcal{L} \propto \epsilon_i$.

In absorption, most shifts of HCl and HF lines due to collisions with rare gas atoms are experimentally observed to be negative (red), meaning that ϵ_i is positive.^{12,13,19,24} Now $\epsilon_i \propto \text{Im} \mathcal{L}_{ab} \propto V_{aa} - V_{bb}$, and since $\epsilon_i > 0$, $V_{aa} > V_{bb}$. But V_{aa} and V_{bb} are negative if attractive, so $|V_{aa}| < |V_{bb}|$, when averaged over those collisions which contribute to shifts. This is plausible if we ascribe shifts primarily to long range collisions where forces are attractive. One might indeed expect the upper state to be more attractive because of its greater average size due to vibrational excitation and therefore its greater polarizability. Thus with the upper state shifted down more by this weighted average than the lower state, a red shift results. (There are also rotational effects which for low J can increase the importance of the repulsive part of the potential, which one would expect to be higher at a given intermolecular distance for the larger upper state, and even lead to a blue shift.

Fano¹³⁷ says that in $(\omega - \omega_0 - \langle M_c \rangle)^{-1}$ the Lorentzian width w corresponding to the Anderson theory³¹ width $\gamma V \epsilon_i$ is $-\text{Im} \langle M_c \rangle$, which is $\text{Re} \mathcal{L}$ by $-i\mathcal{L} \propto \langle M_c \rangle$. (Also in Cattani,⁶³ his \bar{H} is our \mathcal{L} , and his shift term $s \propto -\text{Im} \bar{H}$ is the experimentally reported shift.) And indeed from Equation (93) we see that $\text{Re} \rho \mathcal{L}_{ab}$ is the theoretical quantity corresponding to the observed half

width $\Delta\nu_{1/2}$.

That $\rho \mathcal{L}_{ab}$ is itself positive can be seen using a version of the optical theorem,¹³⁹ for instance as in Equation (19.74) of Reference 98,

$$\text{Im}(\tau_{aa} - \tau_{aa}^*) = -2\text{Im} \tau_{aa} = 2\pi \sum_c \nu(E_c - E_a) \tau_{ca}^* \tau_{ca}$$

Then the first two terms of Equation (95) become

$$(96) \quad \pi \sum_c (|\tau_{ac}|^2 \nu(E_c - E_a) + |\tau_{bc}|^2 \nu(E_c - E_b))$$

an expression which is manifestly positive. Especially in the limit that V_b is very much like V_a , one can just as easily see that the third term of Equation (95) is negative. However in this limit it is related to the elastic cross section, while Equation (96) is related in the same way to the larger total scattering cross section, so that the difference is positive.

So in summary in the approximations of Anderson theory \mathcal{L} will become $\nu(\epsilon_r + i\epsilon_i)$, and from Equation (21) of Fano, $-(i\omega_F - i\omega_{ab} - i\langle M_c \rangle)^{-1}$ with $-\omega_F = \omega$ and $\langle M_c \rangle \Rightarrow -i\rho\mathcal{L}$ we obtain $(i(\omega - \omega_{ba}) + \rho\mathcal{L})^{-1}$ in our lineshape expression.

A final word of caution is in order. When our \mathcal{L} is reduced to a number, in the Lorentzian function $\gamma / ((\omega - \omega_{ba})^2 + \gamma^2)$ when the distance from line center squared, $(\omega - \omega_{ba})^2$ equals γ^2 , the value of the function is 1/2. So theoretically we are computing the half width at half maximum (HWHM). The full width at half maximum (FWHM) is twice that, and either may be reported in experimental papers.

Appendix G : Determination of Cutoff k_0 for a Square Well

In this appendix we wish to gain an estimate of the upper limit cutoff wave vector k_0 by approximating the \vec{k} dependence of the T operators in the simplest possible way. We use the first Born approximation and simply look at $V(-\vec{k}, 0) = \int d\vec{r} e^{i\vec{k}\cdot\vec{r}_{12}} V(r_{12})$.

We first take a step function for our potential, $V(r_{12}) = \epsilon_w$ for $0 \leq r_{12} \leq r_w$ and 0 for $r_{12} > r_w$. Then by $\int_{-1}^1 du e^{iku} = 2 \frac{\sin Kr}{Kr}$ and $\int x \sin ax dx = \frac{1}{a^2} \sin ax - \frac{x}{a} \cos ax$,

$$V(-\vec{k}, 0) = 4\pi/K (\epsilon_w/K^2 \sin Kr_w - \epsilon_w/K r_w \cos Kr_w),$$

$$\text{while } V(0, 0) = 4\pi \epsilon_w r_w^3/3.$$

To determine the effective k_0 due to two k dependent T_{12} factors, we solve

$$(97) \int_0^\infty dK \left(\frac{\sin Kr_w}{K^3} - \frac{r_w}{K^2} \cos Kr_w \right)^2 = \int_0^{K_0} dK \left(\frac{r_w^3}{3} \right)^2 = K_0 \left(\frac{r_w^3}{3} \right)^2$$

or, changing to a dimensionless K by $R_w = \bar{p}_{12} r_w / \hbar$, Equation (97) becomes

$$(98) \frac{\hbar^5}{\bar{p}_{12}^5} \int_0^\infty dK \left(\frac{\sin KR_w}{K^3} - \frac{R_w}{K^2} \cos KR_w \right)^2 = K_0 \left(\frac{\hbar}{\bar{p}_{12}} \right)^6 \left(\frac{R_w^3}{3} \right)^2$$

For \bar{p}_{12} being the thermal average momentum and r_w on the order of 3 A, R_w is 100. We can note that since $J_1(z) = \frac{\sin z}{z^2} - \frac{\cos z}{z}$ and

$J_1(KR_w) = (\pi/2KR_w)^{1/2} J_{3/2}(KR_w)$ the integral in Equation (98) is

$$(99) R_w^4 \int_0^\infty dK \frac{1}{K^2} \left(\frac{\sin KR_w}{(KR_w)^2} - \frac{\cos KR_w}{(KR_w)} \right)^2 = R_w^4 \frac{\pi}{2} \int_0^\infty \frac{dK}{R_w K^3} \left(J_{3/2}(KR_w) \right)^2$$

On page 331 of Volume 1 of Reference 140 we find that Mellin

transform (33) is $\int_0^\infty J_\mu(ax) J_\nu(ax) x^{s-1} dx$, $a > 0$

$$= 2^{s-1} a^{-s} B(1-s, \frac{1}{2}\mu + \frac{1}{2}\nu + \frac{1}{2}s)$$

$$\Gamma(\frac{1}{2}\nu - \frac{1}{2}\mu - \frac{1}{2}s + 1) \Gamma(\frac{1}{2}\mu - \frac{1}{2}\nu - \frac{1}{2}s + 1)$$

for $-\text{Re}(\mu + \nu) < \text{Re}(s) < 1$

where the beta function $B(x, y) = \frac{\Gamma(x)\Gamma(y)}{\Gamma(x+y)}$, $\Gamma(n-1) = \frac{\Gamma(n)}{(n-1)}$, and $\Gamma(n) = (n-1)!$

So Equation (99) becomes $\frac{\pi}{15} R_w^5$. (The same result is also

obtained using the Hankel transform 8.11 (4) on page 4 of Volume 2 of Reference 140.) This means that k_0 is $9\pi/15r_w$ or approximately $1/1.7A$ for r_w around 3 A.

We can also investigate more complicated step function potentials, such as one for which $V(r_{12})$ is ϵ_b for $0 \leq r_{12} \leq r_b$, ϵ_a for $r_b \leq r_{12} \leq r_a$, and 0 for $r_{12} > r_a$. For this, k_0 is

$$\begin{aligned} & \text{defined by } \int_0^\infty ((\epsilon_b - \epsilon_a) R_b^{3/2} J_{3/2}(KR_b) + \epsilon_a R_a^{3/2} J_{3/2}(KR_a))^2 dK / K^3 \\ &= (\epsilon_b - \epsilon_a)^2 \frac{\pi}{15} R_b^5 + 2(\epsilon_b - \epsilon_a) \epsilon_a \frac{\pi}{12} \frac{R_a^3 R_b^3}{(R_a + R_b)} {}_2F_1 \left(\frac{1}{2}, 2, 4, \frac{4R_a R_b}{(R_a + R_b)^2} \right) + \epsilon_a^2 \frac{\pi}{15} R_a^5 \\ &\equiv \chi_0 ((\epsilon_b - \epsilon_a) (R_b^3) + \epsilon_a (R_a^3))^2 \end{aligned}$$

But the hypergeometric function ${}_2F_1$ is difficult to evaluate, so numerical integration was used for several examples. For this potential the results depend on the relative sizes of ϵ_a and ϵ_b , where in the simplest case the value of k_0 was independent of ϵ_w . So for instance for the choices $\epsilon_b = 4$, $\epsilon_a = -1$, $r_b = 3$ A, and $r_a = 6$ A, k_0 is around $1/2.1$ A, while for $\epsilon_b = 4$, $\epsilon_a = 1$, $r_b = 3$ A and $r_a = 6$ A, k_0 is around $1/3A$. In the estimates made in Section II we will take r_0 , the reciprocal of k_0 , to be 3 A, but this is obviously only an order of magnitude guess.

Appendix H : The Jacobian between \hat{p}_{13}'' and \hat{p}_{12}''

From T_{13} we have an integration over the angles of \hat{p}_{13}'' , the momentum after the 1-3 collision, but we would rather integrate over the angles of \hat{p}_{12}'' , which appears in the G_0 denominator. So in two dimensions we need the Jacobian $J = \partial \theta_{13}'' / \partial \theta_{12}''$.

By momentum conservation, $\vec{p}_1' + \vec{p}_3 = \vec{p}_1'' + \vec{p}_3'$, or
 $\vec{p}_1' - \vec{p}_1'' = \vec{p}_3' - \vec{p}_3$, so that $\vec{p}_{12}'/m - \vec{p}_{12}''/m = \vec{p}_1'/m_1 - \vec{p}_1''/m_1$ is
 $m_1/m_1 (\vec{p}_1'/m_1 + \vec{p}_1/m_3 - \vec{p}_1''/m_1 - \vec{p}_1''/m_3) = m_1/m_1 (\vec{p}_1'/m_1 - \vec{p}_3/m_3 - \vec{p}_1''/m_1 + \vec{p}_3'/m_3)$
 $= m_1/m_1 (\vec{p}_{13}'/m - \vec{p}_{13}''/m)$

Therefore,

$$(100) \quad P_{13}''x = P_{13}' \cos \theta_{13}' - \left(\frac{m_1}{m}\right) (P_{12}' \cos \theta_{12}' - P_{12}'' \cos \theta_{12}'')$$

and

$$(101) \quad P_{13}''y = P_{13}' \sin \theta_{13}' - \left(\frac{m_1}{m}\right) (P_{12}' \sin \theta_{12}' - P_{12}'' \sin \theta_{12}'')$$

so that

$$(102) \quad \partial P_{13}''y / \partial \theta_{12}'' = \left(\frac{m_1}{m}\right) P_{12}'' \cos \theta_{12}'' = \left(\frac{m_1}{m}\right) P_{12}''x$$

and so on. So with $\theta_{13}'' = \tan^{-1} P_{13}''y / P_{13}''x$,

$$(103) \quad \frac{\partial \theta_{13}''}{\partial \theta_{12}''} = \left(1 + \left(\frac{P_{13}''y}{P_{13}''x}\right)^2\right) \left(\frac{m_1}{m}\right) \frac{P_{12}''x}{P_{13}''x} + P_{13}''x \frac{\left(\frac{m_1}{m}\right) P_{12}''y}{P_{13}''x^2}$$

$$\left(\frac{m_1}{m}\right) \frac{(P_{12}''x P_{13}''x + P_{12}''y P_{13}''y)}{(P_{13}''x)^2 + (P_{13}''y)^2} = \left(\frac{m_1}{m}\right) \frac{\vec{p}_{12}'' \cdot \vec{p}_{13}''}{P_{13}''^2}$$

In three dimensions, we can shorten our path to the

Jacobian by first transforming dp_{13}'' into $\left(\frac{m_1}{m}\right)^3 dp_{12x}'' dp_{12y}'' dp_{12z}''$

and into $\left(\frac{m_1}{m}\right)^3 P_{12}''^2 dP_{13}'' \partial P_{12}'' \partial P_{13}'' \sin \theta_{12}'' d\theta_{12}'' d\phi_{12}''$. Then $\vec{p}_{12}'' = \left(\frac{m_1}{m_1}\right) (\vec{p}_{13}' - \vec{p}_{13}'') + \vec{p}_{12}'$

means that $P_{12}'' = \left(\left(\frac{m_1}{m_1}\right)^2 |\vec{p}_{13}' - \vec{p}_{13}''|^2 + P_{12}'^2 + 2\left(\frac{m_1}{m_1}\right) \vec{p}_{12}' \cdot (\vec{p}_{13}' - \vec{p}_{13}'')\right)^{1/2}$. So using

$\partial P_{13}'' / \partial P_{13}'' = P_{13}'' / P_{13}''$ and so on, we find

$$(104) \quad \partial P_{12}'' / \partial P_{13}'' = \frac{1}{P_{12}''} \left(\left(\frac{m_1}{m_1}\right)^2 (\vec{p}_{13}' - \vec{p}_{13}'') \cdot \frac{\vec{p}_{13}''}{P_{13}''} + \left(\frac{m_1}{m_1}\right) \frac{\vec{p}_{12}' \cdot \vec{p}_{13}''}{P_{13}''} \right) = \frac{1}{P_{12}''} \left(\frac{m_1}{m_1}\right) \frac{\vec{p}_{12}' \cdot \vec{p}_{13}''}{P_{13}''}$$

so that

$$(105) \quad J = \frac{\partial(\cos\theta_3'' \phi_{13}'')}{\partial(\cos\theta_{12}'' \phi_{12}'')} = \left(\frac{m_1}{m}\right) \frac{P_{12}''^2}{P_{13}''^2} \frac{\vec{P}_{12}'' \cdot \vec{P}_{13}''}{P_{12}'' P_{13}''}$$

Since this is an important result, it is worth while to also obtain it straightforwardly. We use

$$(106) \quad \begin{aligned} P_{13}'' x &= P_{13}' \sin\theta_{13}' \cos\phi_{13}' - \left(\frac{m_1}{m}\right) (P_{12}' \sin\theta_{12}' \cos\phi_{12}' - P_{12}'' \sin\theta_{12}'' \cos\phi_{12}'') \\ P_{13}'' y &= P_{13}' \sin\theta_{13}' \sin\phi_{13}' - \left(\frac{m_1}{m}\right) (P_{12}' \sin\theta_{12}' \sin\phi_{12}' - P_{12}'' \sin\theta_{12}'' \sin\phi_{12}'') \end{aligned}$$

$$P_{13}'' z = P_{13}' \cos\theta_{13}' - \left(\frac{m_1}{m}\right) (P_{12}' \cos\theta_{12}' - P_{12}'' \cos\theta_{12}'')$$

with $\theta_{13}'' = \tan^{-1}((P_{13}'' x^2 + P_{13}'' y^2)^{1/2} / P_{13}'' z)$, $\phi_{13}'' = \tan^{-1} P_{13}'' y / P_{13}'' x$, $\cos\theta_{13}'' = P_{13}'' z / P_{13}''$, and $\partial \sin\theta / \partial \cos\theta = -\cos\theta / \sin\theta$.

We will want¹⁴¹ the difference of

$$(107) \quad \begin{aligned} \frac{\partial \cos\theta_{13}''}{\partial \cos\theta_{12}''} &= \left[\left(\frac{m_1}{m}\right) \frac{P_{12}''}{P_{13}''} - \frac{P_{13}'' z}{P_{13}''^3} \frac{1}{2} (2 P_{13}'' z \left(\frac{m_1}{m}\right) P_{12}'') \right] \\ &\quad - \left[\frac{P_{13}'' z}{P_{13}''^3} (2 P_{13}'' x (-\left(\frac{m_1}{m}\right) P_{12}'' \frac{\cos\theta_{12}''}{\sin\theta_{12}''} \cos\phi_{12}'' + 2 P_{13}'' y (-\left(\frac{m_1}{m}\right) P_{12}'' \frac{\cos\theta_{12}''}{\sin\theta_{12}''} \sin\phi_{12}'')) \right] \end{aligned}$$

times

$$(108) \quad \frac{\partial \phi_{13}''}{\partial \phi_{12}''} = \frac{P_{13}''^2}{(P_{13}'' x^2 + P_{13}'' y^2)} \left(\frac{P_{13}'' x P_{12}'' y \left(\frac{m_1}{m}\right)}{(P_{13}'' x)^2} + \frac{\left(\frac{m_1}{m}\right) P_{12}'' x P_{13}'' y}{(P_{13}'' y)^2} \right)$$

and

$$(109) \quad \frac{\partial \cos\theta_{13}''}{\partial \phi_{12}''} = -\frac{1}{2} \frac{P_{13}'' z}{P_{13}''^3} (-2 P_{13}'' x \left(\frac{m_1}{m}\right) P_{12}'' y + 2 P_{13}'' y \left(\frac{m_1}{m}\right) P_{12}'' x)$$

times

$$(110) \quad \frac{\partial \phi_{13}''}{\partial \cos\theta_{12}''} = \frac{P_{13}''^2}{(P_{13}'' x^2 + P_{13}'' y^2)} \left(\frac{-P_{13}'' y}{(P_{13}'' x)^2} \left(\left(\frac{m_1}{m}\right) P_{12}'' \frac{\cos\theta_{12}''}{\sin\theta_{12}''} \cos\phi_{12}'' - \left(\frac{m_1}{m}\right) \frac{P_{12}'' \cos\theta_{12}'' \sin\phi_{12}''}{P_{13}'' x \sin\theta_{12}''} \right) \right)$$

We denote the two terms in square brackets in Equation (107)

as A and B, and first look at $B \frac{\partial \phi_{13}''}{\partial \phi_{12}''} - \frac{\partial \cos\theta_{13}''}{\partial \phi_{12}''} \frac{\partial \phi_{13}''}{\partial \cos\theta_{12}''}$

$$(111) \quad \begin{aligned} &= \frac{1}{2} \frac{P_{13}'' z}{P_{13}''^3} \frac{P_{13}''^2}{(P_{13}'' x^2 + P_{13}'' y^2)} \frac{P_{12}''}{(P_{13}'' x)^2} \left(\frac{m_1}{m}\right) \frac{\cos\theta_{12}''}{\sin\theta_{12}''} \left(\frac{m_1}{m}\right) \\ &\quad \times \left[2 P_{13}'' x \cos\phi_{12}'' (P_{13}'' y P_{12}'' y + P_{12}'' x P_{13}'' x) + 2 P_{13}'' y \cos\phi_{12}'' (2 P_{13}'' x P_{12}'' y - 2 P_{13}'' y P_{12}'' x) \right. \\ &\quad \left. + 2 P_{13}'' y \sin\phi_{12}'' (P_{13}'' y P_{12}'' y + P_{12}'' x P_{13}'' x) + 2 P_{13}'' x \sin\phi_{12}'' (2 P_{13}'' x P_{12}'' y - 2 P_{13}'' y P_{12}'' x) \right] \end{aligned}$$

The terms in the square bracket in Equation (111) reduce to

$$2P_{12}'' \sin \Theta_{12}'' (P_{13}'' x^2 + P_{13}'' y^2),$$

so that the entire contribution is

$$\left(\frac{m_1}{m}\right)^2 P_{12}'' / P_{13}'' P_{13}'' x^2 P_{12}'' / P_{13}'' y^2.$$

Then $A \partial \phi_{13}'' / \partial \phi_{12}''$ is

$$\frac{1}{(P_{13}'' x^2 + P_{13}'' y^2)} \left(\frac{m_1}{m}\right) (P_{13}'' y P_{12}'' + P_{12}'' x P_{13}'' y) \left(\frac{m_1}{m}\right) \frac{P_{12}''}{P_{13}''} \frac{1}{P_{13}''} (P_{13}'' x^2 - P_{13}'' z^2) = \left(\frac{m_1}{m}\right)^2 \frac{P_{12}''}{P_{13}''} (P_{13}'' y P_{12}'' y + P_{12}'' x P_{13}'' x)$$

So J is indeed $\left(\frac{m_1}{m}\right)^2 P_{12}'' / P_{13}'' P_{13}'' x^2 P_{12}'' / P_{13}'' y^2$

It is interesting to compare the result, $2(\lambda\pi)^3 \pi^2$, of integrating $\int \sin \Theta_{13}' d\Theta_{13}' d\phi_{13}' \sin \Theta_{12}'' d\Theta_{12}'' d\phi_{12}'' \sin \Theta_{12}'' d\Theta_{12}'' d\phi_{12}''$ over two "delta plus" functions, $(\pi d(u-u_0) - 9P(\frac{1}{u-u_0}))$, with u being $\cos \Theta_{12}'$ and $\cos \Theta_{12}''$, with that obtained by including $\left(\frac{m_1}{m}\right)^2 P_{13}'' \cdot P_{12}'' / P_{13}'' P_{12}''$ in the integration.

First we do the ϕ integrals, using Equations (106) and

$$\int_0^{2\pi} \sin \phi d\phi = 0 = \int_0^{2\pi} \cos \phi d\phi, \quad \int_0^{2\pi} \sin^2 \phi d\phi = \pi = \int_0^{2\pi} \cos^2 \phi d\phi.$$

We obtain

$$(112) \quad \frac{1}{P_{13}''} (\lambda\pi)^2 \left(\frac{m_1}{m}\right)^2 (\lambda\pi \sin^2 \Theta_{12}'' \left(\frac{m_1}{m}\right) + \lambda\pi \cos \Theta_{12}'' (P_{13}'' - \left(\frac{m_1}{m}\right) (P_{12}' \cos \Theta_{12}' - P_{12}'' \cos \Theta_{12}'')))$$

The delta functions say that $\sin \Theta_{12}''$ in the first term goes to 1, while $\cos \Theta_{12}''$ goes to zero. But the second term has a contribution from

$$P \int \frac{\cos \Theta_{12}'' \sin \Theta_{12}'' d\Theta_{12}''}{((\omega - \omega_{00}) + K v_{12}'' \cos \Theta_{12}'')} \rightarrow \int_{-1}^1 \frac{u du}{(u - u_0)} = 2$$

and from the same integration over Θ_{12}' . So with a factor of

two from the Θ_{13}' integration, we obtain $2(\lambda\pi)^3 \left(\frac{m_1}{m}\right)^3 (\pi^2 - P_{12}' / P_{13}''^2)$

If we say P_{12}' / P_{13}'' averages to around one, and choose the case of equal masses, so $(m_1/m) = 2$, then this is about $80(\lambda\pi)^3$, so comparing with around $20(\lambda\pi)^3$ without integrating over J, we might conclude that J is worth about 4. But there are enough

considerations which have been left out of the calculation that we are as well justified in simply ignoring J , that is, taking it to be 1, as we are in assuming some other effective value.

REFERENCES

1. S. E. Harris, Proc. IEEE 57, 2096 (1969).
2. A. Yariv, Introduction to Optical Electronics, (Holt, Rinehart and Winston, New York, 1971).
3. R. L. Byer, in Quantum Electronics IB, Eds. H. Rabin and C. L. Tang (Academic Press, New York, 1975).
4. M. Garbuny, in Laser Photochemistry, Tunable Lasers, and Other Topics, Physics of Quantum Electronics 4, Ed. S. F. Jacobs (Addison Wesley, Reading, 1976), p. 271
5. R. G. Smith, in Lasers, A Series of Advances 4, Eds. A. K. Levine and A. J. DeMaria (Marcel Dekker, New York, 1976), p. 190.
6. R. W. Terhune and P. D. Maker, in Lasers, A Series of Advances 2, Ed. A. K. Levine (Marcel Dekker, New York, 1968), p. 295.
7. P. A. Jansson, R. H. Hunt and E. K. Plyler, J. Opt. Soc. Am. 60, 596 (1970).
8. P. E. Siska, J. Chem. Phys. 59, 6052 (1973).
9. J. Pourcin and R. Romanetti, Infrared Physics 13, 161 (1973).
10. W. F. Herget, W. E. Deeds, N. M. Gailar, R. J. Lovell and A. H. Nielsen, J. Opt. Soc. Am. 52, 1113 (1962).
11. R. M. Talley, H. M. Kaylor and A. H. Nielsen, Phys. Rev. 77, 529 (1950).
12. A. Ben-Reuven, S. Kimel, M. A. Hirshfeld, and J. H. Jaffe, J. Chem Phys. 35, 955 (1961).

13. J. H. Jaffe, A. Rosenberg, M. A. Hirshfeld, and N. M. Gailar, *J. Chem. Phys.* 43, 1525 (1965).
14. E. K. Plyler and E. D. Tidwell, *Z. Elektrochemie* 64, 717 (1960).
15. W. S. Benedict and E. K. Plyler, *J. Res. NBS* 46, 246 (1951).
16. R. J. Lovell and W. F. Herget, *J. Opt. Soc. Am.* 52, 1374 (1962).
17. P. Varanasi, S. K. Sarangi and G. D. T. Tejwani, *J. Quant. Spectry. Rad. Transfer* 12, 857 (1972).
18. E. Whalley and W. Schneider, *J. Chem. Phys.* 23, 1644 (1955).
19. T. A. Wiggins, N. C. Griffen, E. M. Arlin, and D. L. Kerstetter, *J. Mol. Spec.* 36, 77 (1970).
20. J. Jarecki and R. M. Herman, *J. Quant. Spectry. Rad. Transfer* 15, 707 (1975).
21. G. Bachet, *C. R. Acad. Sci. Paris* 226B, 307 (1973).
22. B. Oksengorn, *Spectrochim. Acta* 19, 541 (1963).
23. M. Atwood and H. Vu, *C. R. Acad. Sci. Paris* 260, 4969 (1965).
24. D. H. Rank, D. F. Eastman, B. S. Rao and T. A. Wiggins, *J. Mol. Spec.* 10, 34 (1963).
25. A. Levy, E. Piollet-Mariel and C. Boulet, *J. Quant. Spectry. Rad. Transfer* 13, 673 (1973).
26. J.-P. Houdeau, M. Larvor, and C. Haeusler, *J. Quant. Spectry. Rad. Transfer* 16, 457 (1976).

27. D. Williams, D. C. Wenstrand, R. J. Brockman and B. Curnutte, *Mol. Phys.* 20, 769 (1971).
28. S.-Y. Ch'en and M. Takeo, *Rev. Mod. Phys.* 29, 20 (1957).
29. R. H. Tipping and R. M. Herman, *J. Quant. Spectry. Rad. Transfer* 10, 881 (1970).
30. C. Boulet, P. Isnard, and A Levy, *J. Quant. Spectry. Rad. Transfer* 13, 897 (1973).
31. P. W. Anderson, *Phys. Rev.* 76, 647 (1949).
32. D. E. Fitz and R. A. Marcus, *J. Chem. Phys.* 62, 3788 (1975).
33. W. B. Neilsen and R. G. Gordon, *J. Chem. Phys* 58, 4149 (1973).
34. H. A. Gebbie and N. W. B. Stone, *Proc. Phys. Soc.* 82, 309 (1963).
35. R. M. Van Aalst, J. A. Schuurman and J. Van der Elsken, *Chem. Phys. Lett.* 35, 558 (1975).
36. P. A. Bonczyk, *Phys. Rev.* 13, 251 (1976).
37. J. Albers and I. Oppenheim, *Physica* 59, 161 (1972).
38. J. Albers and I. Oppenheim, *Physica* 59, 187 (1972).
39. J. Albers, Doctoral Thesis, Dept. of Chemistry M. I. T. (1970)
40. J. T. Bartis and I. Oppenheim, *Physica* 74, 1 (1974)
41. K. Kawasaki and I. Oppenheim, in Statistical Mechanics, Ed. T. Bak (Benjamin, New York, 1966)
42. K. Kawasaki and I. Oppenheim, *Phys. Rev.* 136, A1519 (1964)

43. K. Kawasaki and I. Oppenheim, *Phys. Rev.* 139, A649 (1965)
44. K. Kawasaki and I. Oppenheim, *Phys. Rev.* 139, A1763 (1965)
45. E. W. Smith, J. Cooper, W. R. Chappell, and T. Dillon,
J. Quant. Spectry. Rad. Trans. 11, 1547 (1971)
46. M Cattani, *Lett. Nuovo Cimento* 4, 346 (1970)
47. I. I. Sobel'man, *Introduction to the Theory of Atomic Spectra*, (Pergamon Press, New York, 1972)
48. R. Kubo, in *Lectures in Theoretical Physics I*, Ed.
W. E. Brittin, (Gordon and Breach, New York, 1958)
49. R. Zwanzig, *Phys. Rev.* 129, 486 (1963)
50. M. H. Ernst, L. K. Haines, and J. R. Dorfman, *Rev.*
Mod. Phys. 41, 296 (1969)
51. J. Kestin, *Proc. of the Fourth International Conference on High Pressure*, Kyoto, November 1974, (Special Issue of *Rev. Phys. Chem. Japan*, 1975)
52. D. Ronis and I. Oppenheim, *Physica*, to be published
53. A. Gervois, C. Normand-Alle, and Y. Pomeau, *Phys Rev.*
12, 1570 (1975)
54. M. Baranger, *Phys. Rev.* 111, 494 (1958)
55. R. G. Gordon, *J. Chem. Phys.* 46, 448 (1967)
56. S. Chapman and T. G. Cowling, *The Mathematical Theory of Nonuniform Gases* (Cambridge University Press, London, 1970)
57. H. Mori, *Phys. Rev.* 111, 694 (1958)
58. R. C. Desai and J. Ross, *J. Chem. Phys.* 49, 3754 (1968)
59. J. E. Reissner and W. A. Steele, *J. Stat. Phys.* 13,
283 (1975)

60. F. Reif, Fundamentals of Statistical and Thermal Physics,
(McGraw-Hill, New York, 1965)
61. C. Boulet, P. Isnard, and A. Levy, C. R. Acad. Sci.
Paris, 272B, 324 (1971)
62. R. D. Sharma and R. H. Picard, J. Chem. Phys. 62, 3340
(1970)
63. M. Cattani, Can. J. Phys. 51, 1388 (1973)
64. A. Ben-Reuven, in Advances in Chemical Physics 33,
Eds. I. Prigogine and S. A. Rice (John Wiley, New York,
1975)
65. P. R. Berman, Appl. Phys. 6, 283 (1975)
66. P. R. Berman, Phys. Rev. 6, 2157 (1972)
67. S. G. Rautian and I. I. Sobel'man, Sov. Phys. Uspekhi 9,
701 (1965)
68. M. Nelkin and A. Ghatak, Phys. Rev. 135, 4 (1964)
69. J. I. Gersten and H. M. Foley, J. Opt. Soc. Am. 58,
933 (1968)
70. S. Hess, Physica 61, 80 (1972)
71. H. R. Zaidi, Can. J. Phys. 50, 2792 (1972)
72. J. Keilson and J. E. Storer, Quart. Appl. Math. 10,
243 (1952)
73. P. L. Bhatnagar, E. P. Gross, and M. Krook, Phys. Rev.
94, 511 (1954)
74. E. P. Gross, Phys. Rev. 97, 395 (1955)
75. J. Schmidt, P. R. Berman, and R. G. Brewer, Phys. Rev.
Lett. 31, 1103 (1973)

76. L. Galatry, Phys. Rev. 122, 1218 (1961)
77. M. I. Podgoretskii and A. V. Stepanov, Sov. Phys. JETP 13, 393 (1961)
78. K. S. Singwi and A. Sjolander, Phys. Rev. 120, 1093 (1960)
79. U. Fano, Phys. Rev. 131, 259 (1963)
80. M. Baranger, Phys. Rev. 111, 481 (1958)
81. M. Baranger, Phys. Rev. 112, 855 (1958)
82. M. Baranger, in Atomic and Molecular Processes, Ed. D. R. Bates (Academic Press, New York, 1962)
83. R. P. Futrelle, Phys. Rev. 5, A2162 (1972)
84. A. Royer, Phys. Rev. 4, 499 (1971)
85. J. Szudy, Acta Physica Polonica A40, 361 (1971)
86. W. Baylis and J. Szudy, J. Quant. Spectry. Rad. Transfer 15, 641 (1975)
87. P. W. Anderson and J. D. Talman, Proceedings of Conference on Broadening of Spectral Lines, U. of Pittsburgh, July 1956, (Bell System Technical Monograph 3117)
88. A. T. Mattick, N. A. Kurnit and A. Javan, Chem. Phys. Lett. 38, 176 (1976)
89. P. Varanasi and S. Sarangi, J. Quant. Spectry. Rad. Transfer 14, 845 (1974)
90. P. R. Berman, J. Quant. Spectry. Rad. Transfer 12, 1331, (1972)
91. W. Peticolas, in Ann. Rev. Phys. Chem. 18, 233 (1967)
92. G. Nienhuis, Physica 66, 245 (1973)

93. G. Nienhuis, *Physica* 74, 157 (1974)
94. C. Trindle and K. Illinger, *J. Chem. Phys.* 48, 4415 (1968)
95. L. K. Haines, J. R. Dorfman, and M. H. Ernst, *Phys. Rev.* 144, 207 (1966)
96. J. Weinstock, *Phys. Rev.* 140, A460 (1965)
97. J. Weinstock, *Phys. Rev.* 132, 470 (1963)
98. E. Merzbacher, Quantum Mechanics (John Wiley, New York, 1970)
99. T. L. Hill, Statistical Mechanics, (McGraw-Hill, New York, 1956)
100. H. C. Longuet-Higgins and J. A. Pople, *J. Chem. Phys.* 25, 884 (1956)
101. J. V. Sengers and E. G. D. Cohen, *Physica* 27, 230 (1961)
102. J. V. Sengers, *Acta Physica Austriaca*, Supplement X, pp. 177-208 (1973)
103. J. V. Sengers, in Kinetic Equations, Eds. R.L. Liboff and N. Rostoker (Gordon and Breach, New York, 1971)
104. G. F. Mazenko, *Phys. Rev.* 7, 209 and 222 (1973)
105. G. F. Mazenko, *Phys. Rev.* 9, 360 (1974)
106. H. Hanley, J. McCarty and E. G. D. Cohen, *Physica* 60, 322 (1972)
107. W. Kauzmann, Kinetic Theory of Gases, (Benjamin, New York, 1966)
108. T. R. Mifflin and C. O. Bennett, *J. Chem. Phys.* 29, 975 (1958)
109. L. Durbin and R. Kobayashi, *J. Chem. Phys.* 37, 1643 (1962)
110. W. L. Robb and H. G. Drickamer, *J. Chem. Phys.* 19, 1504 (1951)

111. P. Carelli, I. Modena, and F. P. Ricci, *Phys. Rev.* 7, 298 (1973)
112. P. Carelli, A. DeSantis, I. Modena, and F. P. Ricci, *Phys. Rev.* 13, 1131 (1976)
113. S. Takahashi, *Bull. Chem. Soc. Japan* 41, 1573 (1968)
114. C.-H. Chou and J. J. Martin, *Ind. Eng. Chemistry* 49, 758 (1957)
115. H. A. O'Hern and J. J. Martin, *Ind. Eng. Chemistry* 47, 2081 (1955)
116. S. Takahashi and H. Iwasaki, *Bull. Chem. Soc. Japan* 39, 2105 (1966)
117. K. D. Timmerhaus and H. G. Drickamer, *J. Chem. Phys.* 19, 1242 (1951)
118. E. W. Becker, W. Vogell, and F. Zigan, *Z. Naturforschung* 8a, 686 (1953)
119. J. M. H. Levelt-Sengers, M. Klein and J. S. Gallagher in American Institute of Physics Handbook (McGraw-Hill, New York, 1972) p. 4-204
120. A. Levy, E. Piollet-Mariel, and C. Haeusler, *C. R. Acad. Sci. Paris* 269B, 427 (1969)
121. A. Levy, E. Piollet-Mariel, J.-P. Bouanich and C. Haeusler, *J. Quant. Spectry. Rad. Transfer* 10, 203 (1970)
122. R. Beaume and R. Coulon, *C. R. Acad. Sci. Paris* 266B, 1024 (1968)

123. E. U. Franck, M. Brose and K. Mangold, in Progress in International Research on Thermodynamic and Transport Properties, Eds. J. F. Masi and D. H. Tsai (Academic Press, New York, 1962)
124. E. U. Franck and W. Spalthoff, *Z. Elektrochem.* 61, 48 (1957)
-]25. J. O Hirschfelder, C. F. Curtiss, and R. B. Bird, Molecular Theory of Gases and Liquids, (Wiley, New York, 1954)
-]26. L. Monchick and E. A. Mason, *J. Chem. Phys.* 36, 2746 (1962)
127. B. D. Green, Doctoral Thesis, Department of Chemistry, M. I. T., 1976
128. E. D. Hinkley, K. W. Nill and F. A. Blum, *Laser Focus* 12 (4), 47 (1976)
129. I. Melngailis and A. Mooradian, in Laser Applications to Optics and Spectroscopy, Physics of Quantum Electronics 2, Eds. S. F. Jacobs, M. Sargent III, J. F. Scott and M. O. Scully (Addison-Wesley, Reading, 1975)
130. M. J. Colles and C. R. Pidgeon, *Reports on Progress in Physics* 38, 329 (1975)
131. C. H. Townes and A. L. Schawlow, Microwave Spectroscopy (McGraw-Hill, New York, 1955) p. 337
132. R. L. Legan, J. A. Roberts, E. A. Rinehart and C. C. Lin, *J. Chem. Phys.* 43, 4337 (1965)
133. J. S. Murphy and J. E. Boggs, *J. Chem. Phys.* 50, 3320 (1969)

134. Krishnaji, J. *Scient. Ind. Res.* 32, 168 (1973)
135. R. H. Dicke, *Phys. Rev.* 89, 472 (1953)
136. R. S. Eng, A. R. Calawa, T. C. Harman, P. L. Kelley, and A. Javan, *Appl Phys. Lett.* 21, 303 (1972)
137. U. Fano, *Phys. Rev.* 131, 259 (1963)
138. C. J. Tsao and B. Curnutte, *J. Quant. Spectry. Rad. Transfer* 2, 45 (1962)
139. P. Roman, *Advanced Quantum Theory*, (Addison-Wesley, Reading, 1965)
140. Bateman Manuscript Project, *Tables of Integral Transforms*, Ed. A. Erdelyi (McGraw-Hill, New York, 1954)
141. H. Margenau and G. M. Murphy, *The Mathematics of Physics and Chemistry* (Van Nostrand, Princeton, 1964)

BIOGRAPHICAL NOTE

The author was born on June 14, 1952 in St. Cloud, Minnesota. In January of 1972 he received the Bachelor of Science degree from the University of Iowa and entered the doctoral program in the Department of Chemistry at M.I.T.